ISBN 978-82-326-0734-1 (printed version)
ISBN 978-82-326-0735-8 (electronic version)
ISSN 1503-8181

NTNU – Trondheim
Norwegian University of
Science and Technology

Doctoral Thesis

Bjørn Austbø

Doctoral theses at NTNU, 2015:33

Bjørn Austbø

Use of Optimization in Evaluation and Design of Liquefaction Processes for Natural Gas

NTNU
Norwegian University of
Science and Technology
Faculty of Engineering
Science and Technology
Department of Energy and
Process Engineering

NTNU – Trondheim
Norwegian University of
Science and Technology

Doctoral theses at NTNU, 2015:33

NTNU

Bjørn Austbø

Use of Optimization in Evaluation and Design of Liquefaction Processes for Natural Gas

Thesis for the degree of Philosophiae Doctor

Trondheim, February 2015

Norwegian University of Science and Technology
Faculty of Engineering Science and Technology
Department of Energy and Process Engineering

NTNU – Trondheim
Norwegian University of
Science and Technology

NTNU
Norwegian University of Science and Technology

Thesis for the degree of Philosophiae Doctor

Faculty of Engineering Science and Technology
Department of Energy and Process Engineering

ISBN 978-82-326-0734-1 (printed version)
ISBN 978-82-326-0735-8 (electronic version)
ISSN 1503-8181

Doctoral theses at NTNU, 2015:33

Printed by Skipnes Kommunikasjon as

Abstract

Liquefied natural gas (LNG) is a fast growing energy carrier suitable for transport of natural gas when the distance from source to market is long and/or the volumes are moderate. In order to liquefy the natural gas, and thereby reduce its volume, energy demanding low-temperature refrigeration over a wide temperature range is required. Hence, energy efficient designs depend on small temperature differences in heat transfer.

Over the years, many process concepts have been proposed for liquefaction of natural gas, with different advantages and disadvantages. While development of LNG processes for a long time was concerned primarily with increased capacity and energy efficiency, the emergence of new applications such as remote gas and floating operations have put focus also on properties such as safety, environmental impact, compactness, operability and flexibility.

For all applications, optimization is essential for fair comparison of different process concepts, in order to minimize cost, energy use and environmental impact. Due to characteristics of the liquefaction processes and the rigorous thermodynamic models required for practical feasibility of the design, optimization of LNG processes is a complex problem. In order to accommodate this challenge, the focus of this work has been to improve the optimization problem formulation through use of thermodynamic analysis and insight, with the objective of enabling rigorous and robust optimization of both simple and complex process concepts.

In this work, the refrigeration processes have been modelled with a commercial process simulation tool using cubic equations of state. Optimization has been performed using a sequential quadratic programming algorithm. A stochastic search algorithm (simulated annealing) has also been tested. The observed performance was, however, better for the deterministic search method. Processes studied in this project include single mixed-refrigerant process, single and dual nitrogen expander processes, pure-refrigerant cascade processes and a dual mixed-refrigerant process.

Optimization studies of nitrogen expander processes have been carried out both with a simplified process model assuming perfect gas behaviour of the refrigerant and a rigorous process model using a cubic equation of state. Comparison of the results indicated agreement between the models only for a limited number of cases. In the majority of the case studies, a better solution was found for the rigorous model accounting for the non-idealities of the refrigerant.

The intermediate pressure levels in multi-stage compression with intercooling have been optimized for the case of perfect gas behaviour and constant isentropic efficiency. For the case of different suction temperatures in the different compression stages, the results indicate that the optimal intermediate pressure levels are characterized by uniform discharge temperatures for the compression stages rather than uniform pressure ratios. A heuristic rule for the optimal intermediate pressure in multi-stage real gas compression has also been proposed. For a single mixed-refrigerant cycle this was proven to generally provide high accuracy.

The influence of the choice of decision variables and bounds on the optimization search performance has been illustrated for optimization of pure-refrigerant cascade processes. Compared to a fairly obvious choice of variables, a set of decision variables based on process characteristics was found to give significant improvement in the success rate of the optimization search.

Exergy analysis of cascade refrigeration processes have been used to illustrate the interaction between the different refrigeration cycles in a cascade. The results demonstrate that the solution that provides the smallest compression power in a single cycle not necessarily coincides with the solution that gives the smallest power consumption for the overall process.

Based on these findings, an approach for design and optimization of complex cascade processes has been proposed as an alternative to simultaneous optimization of all variables. In the suggested approach, the load distribution between the different cycles in the cascade is optimized in an outer loop, while the different refrigeration cycles are optimized sequentially in an inner loop starting from the lowest temperature level. The principles of the procedure have been illustrated for a dual mixed-refrigerant process.

Studies on the influence of constraint formulations for optimal trade-off between operating and investment costs in LNG process design have proven the inadequacy of the common approach with a minimum temperature difference constraint. A case study presented for a single mixed-refrigerant process illustrated that significant savings in energy use could be realized by optimal distribution of heat transfer driving forces.

Preface

This thesis is the result of my PhD project carried out at the Department of Energy and Process Engineering at the Norwegian University of Science and Technology (NTNU) between August 2011 and December 2014.

The work has been performed within the project "Enabling Low-Emission LNG Systems", led by SINTEF Energy Research under the PETROMAKS programme. The project partners; Statoil and GDF Suez, and the Research Council of Norway (193062/S60) are gratefully acknowledged for the support. Statoil is also acknowledged for a travel grant enabling conference participation.

A special thanks goes to my main supervisor, Professor Truls Gundersen. His always motivating and challenging feedback has been essential for the progress of my work. Despite his busy schedule, he has always found time for thorough proofreading and helpful and inspiring discussions.

My co-supervisor Per Eilif Wahl and Sigurd Weidemann Løvseth (SINTEF Energy Research) have also been important discussion partners. Per Eilif Wahl has developed the simulation-optimization framework used in this work, and I am very grateful for all his help with the use of this software.

I would also like to thank Professor Paul I. Barton and his research group in the Chemical Engineering Department at the Massachusetts Institute of Technology (MIT) for allowing me to visit. My eight-month stay in Cambridge was very inspiring and gave me valuable insight into the field of global optimization. Support from "Hans Mustad og Robert og Ella Wenzins legat ved Norges teknisk-naturvitenskaplige universitet" and "Forsknings- og undervisningsfondet i Trondheim", enabling this research stay abroad, is gratefully acknowledged.

The administrative staff at the Department of Energy and Process Engineering is gratefully acknowledged for all their help with different forms and applications.

I would also like to thank my fellow PhD candidates and colleagues at NTNU for the many coffee breaks and Friday lunches.

Finally, I would like to thank my parents, Grete and Oddvar, my sister Ingrid and my brother Knut for all their support and motivation.

Trondheim, December 2014
Bjørn Austbø

Contents

List of Figures

List of Tables

Nomenclature

Abbreviations

ABC	Artificial bee colony optimization
ACO	Ant colony optimization
ASA	Adaptive simulated annealing
C1	Methane
C2	Ethane
C3	Propane
C3MR	Propane-precooled mixed-refrigerant process
CFD	Computational fluid dynamics
CNG	Compressed natural gas
COMP	Compressor
COOL	Cooler
COP	Coefficient of performance
CV	Control volume
DMR	Dual mixed-refrigerant process
ES	Evolutionary search
EXP	Expander-based processes
GA	Genetic algorithms
GDSRK	Groborski and Daubert's modification of SRK
GTL	Gas to liquids
GTS	Gas to solids
iC4	Iso-butane
iC5	Iso-pentane
IEA	The International Energy Agency

HS	Harmony search
HX	Heat exchanger
LB	Lower bound
LNG	Liquefied natural gas
LP	Linear program
MEG	Monoethylene glycol
MFC	Mixed-refrigerant cascade process
MILP	Mixed-integer linear program
MINLP	Mixed-integer nonlinear program
N2	Nitrogen
nC4	Normal-butane
nC5	Normal-pentane
NG	Natural gas
NGL	Natural gas liquids
NLP	Nonlinear program
NMSS	Nelder-Mead simple search
PR	Peng-Robinson
PSO	Particle swarm optimization
SA	Simulated annealing
SMR	Single mixed-refrigerant process
SQP	Sequential quadratic programming
SRK	Soave-Redlich-Kwong
TS	Tabu search
UB	Upper bound
VAR	Variable
VLV	Valve

Greek

β	Penalty exponent
γ	Penalty exponent
Δ	Difference
$\dot{E}$	Exergy flow rate (kW)
η	Efficiency (-)
κ	Isentropic exponent (-)

φ	Modified objective function
ψ	Rational exergy efficiency (-)

Roman

A	Area (m^2)
a	Heat exchanger unit cost (USD/m^2)
b	Constant
C	Constant
c	Constant / penalty factor
c_p	Specific heat capacity (kJ/kgK)
e	Exergy unit cost (USD/kW)
f	Function / correction factor (-)
g	Inequality constraint
$\dot{H}$	Enthalpy flow (kW)
h	Equality constraint
h	Heat transfer coefficient (W/m^2K)
h	Specific enthalpy (kJ/kg)
$\dot{I}$	Irreversibility rate (kW)
L	Phenomenological heat transfer coefficient (kWK/m^2)
$\dot{m}$	Mass flow rate (kg/s)
$\dot{n}$	Molar flow rate (kmol/s)
p	Pressure (bar)
PR	Pressure ratio (-)
$\dot{Q}$	Heat flow rate (kW)
$\dot{q}$	Heat flux (kW/m^2)
R	Gas constant (kJ/kmolK)
r	Penalty factor
$\dot{S}$	Entropy production rate (kW)
s	Specific entropy (kJ/kg)
T	Temperature (K)
T'	Dimensionless temperature (-)
TR	Temperature ratio (-)
U	Overall heat transfer coefficient (kW/ m^2K)
UA	Heat exchanger conductance (kW/K)

$\dot{V}$	Volumetric flow rate (m^3/s)
$\dot{W}$	Power (kW)
w	Specific work (kJ/kg)
x	Variable / Vapor fraction (-)
x	Vector of variables
y	Molar composition (-)
y	Vector of variables
Z	Compressiblity (-)
z	Variable

Subscript/superscript

*	Optimal
0	Ambient
best	Best known solution
C	Cold
cb	Cricondenbar
cold	Cold end
COMP	Compressor
comp	Compressor
cond	Condensation and de-superheating
cool	Cooling
crit	Critical
dew	Dew point
ENT	Entropy
EXP	Expander
GEO	Geometric
H	Hot
hot	Hot end
HX	Heat exchanger
i	Index
in	In
inverse	With a constant temperature driving force $\Delta(1/T)$
j	Index
linear	With a temperature difference proportional to the absolute temperature

LM	Logarithmic mean
M	Intermediate
max	Maximum
min	Minimum
MR	Mixed refrigerant
net	Net
NG	Natural gas
OPT	Optimal
out	Out
p	Polytropic
pen	Penalty
prod	Produced
R	Refrigerant
s	Dimension
s	Isentropic
sat	Saturation
small	Smallest
span	Difference between high and low
square	With a temperature difference proportional to the square of the absolute temperature
sub	Sub-cooling
sup	Superheating
t	Dimension
target	Target
tot	Total
uniform	With a uniform temperature difference ΔT
v	Volume
valve	Throttle valve
vap	Vapour

1 Introduction

This PhD thesis investigates the use of optimization in evaluation and design of liquefaction processes for natural gas.

1.1 Background and motivation

During the past decades, liquefied natural gas (LNG) has been a fast growing energy carrier, projected to account for an even larger part of the global natural gas trade in the future. By liquefaction, large volumes can be transferred across wide distances. Liquefaction of natural gas does, however, require energy demanding cooling over a wide temperature range and at low temperature levels. Hence, over the years, many process concepts have been proposed in order to meet the requirements of small temperature driving forces for heat transfer in a cost-effective manner.

For a long time, the development in LNG process design was focused mainly on increased capacity and improved energy efficiency. With the increasing interest in remote gas production and floating operations, other aspects such as process safety, environmental impact, compactness, operability and flexibility have also been given more attention. These are often conflicting objectives, increasing the complexity of the design task.

For fair comparison of different process concepts, optimization is required. Even though natural gas liquefaction processes are fairly simple in nature, with no chemical reaction or separation required, complicated trade-offs and several degrees of freedom complicates the design and evaluation of LNG processes. In addition, rigorous thermodynamic models are required in modelling to make sure that the process design is applicable in practice.

Optimization studies available in literature have mainly been concerned with relatively simple process concepts. As the complexity of the process flowsheet increases, so does the optimization problem. In order to enable optimization of more complex process

concepts, the optimization methods and/or the problem formulations should be improved.

1.2 Scope

This study is limited to optimization of liquefaction processes. Other processes in the LNG plant such as pre-treatment and conditioning have not been not been considered. Optimization has been used for design and evaluation of liquefaction process concepts. Optimal start-up, operation and shut-down has been excluded from the scope of this project. Experimental work has also been left outside the scope of this project. Evaluation and design of LNG processes have been based on process modelling and simulation.

Development of optimization methods has not been the focus of this work. The scope has rather been to improve the problem formulation, so that the optimization problem can be solved with existing algorithms and software. The work has been performed using a commercial process simulator for modelling and simulation, connected with external optimization algorithms. Thermodynamic tools, such as exergy analysis, have been used to facilitate the optimization and evaluation of different process concepts.

1.3 Objectives

The main objective of the work has been to enable rigorous and robust optimization of LNG processes. An evaluation and design approach should be able to handle both simple and complex process concepts in order to enable fair comparison and optimal process performance. In this work, the objective has been to make this possible by use thermodynamic analysis and insight.

1.4 Contributions

The main contributions from the PhD project are the following:

- An extensive review of literature related to optimization of LNG processes has been carried out in order to determine the current status of the field. This review has taken the form of an annotated bibliography. In addition to optimization of liquefaction processes for natural gas, the review also covers optimization of other relevant low-temperature processes, applications of optimization in other parts of the LNG value chain and alternative approaches for LNG process improvement.
- Sensitivity analyses and parameter studies have been used to visualize the characteristics of the optimization problem and to reveal possible challenges for the optimization search.

- Studies on the influence of constraint formulations for optimal balance between investment and operating costs have both illustrated and explained why a minimum temperature difference specification is an inadequate trade-off parameter. For optimization of LNG processes, such a constraint does neither take into account the optimal distribution of heat transfer driving forces with respect to temperature and nonlinearities of the composite curves nor the trade-off between refrigerant flow rate and pressure ratio. Considerable savings in energy use have been indicated by use of other trade-off parameters, including a maximum specification for the heat exchanger conductance.
- A design strategy has been proposed for optimization of cascade refrigeration processes. The increased difficulty of solving the optimization problem when the process complexity is increased could be counteracted by instead solving a series of simpler optimization problems. If the load distribution between the different cycles in a cascade is optimized in an outer optimization problem, the different refrigeration cycles could be optimized sequentially in an inner loop. A case study of a dual mixed-refrigerant process has been used to illustrate the importance of accounting for the interaction between the refrigeration cycles in the cascade. The cycles should be optimized sequentially starting at the lowest temperature level and with the objective of minimizing irreversibilities rather than compression power. The suggested approach could simplify optimization of complex process concepts, by confining the variable bounds and providing a good starting point for overall simultaneous optimization.
- The influence of the choice of decision variables has been documented through optimization of pure-refrigerant cascade processes. By use of process insight, a set of decision variables was proposed that for the given operating conditions gave feasible solutions for all combinations. Compared with the fairly intuitive choice of decision variables, considerable improvement was observed for the optimization performance.
- An expression for optimal intermediate pressure levels in multi-stage compression with intercooling has been deduced for perfect gas compression with constant isentropic efficiency. Rather than uniform pressure ratios, the isentropic discharge temperature of all compression stages should be equal in order to minimize power consumption. This is of importance when the suction temperatures of the different compression stages are different.
- Based on the optimality condition for intermediate pressure levels in perfect gas compression, a heuristic design rule for optimal intermediate pressure levels in real gas compression has been suggested. As long as the intercooling temperature is not limited by the superheating requirements of the compressors, the suggested design guidelines prove very high accuracy. By use

of this heuristic rule, the number of decision variables in optimization of complex process concepts with instances of multi-stage compression can be reduced (at least in the initial phase of the optimization search) with the result of reduced computational times.

- Comparisons have been made between a simplified and a rigorous thermodynamic model for optimization of nitrogen expander processes. Even though the behaviour of nitrogen for some operating conditions is close to ideal gas behaviour, the results indicate that better solutions can be found when the non-idealities of the refrigerant are taken into account.
- From thermodynamic analysis of cascade processes, the impact of interaction between the different refrigeration cycles has been demonstrated. The solution that gives the smallest power consumption for the overall process does not necessarily coincide with the solution that gives the smallest power consumption in a given refrigeration cycle.
- The stochastic search algorithm simulated annealing has been tested for optimization of a single mixed-refrigerant process. Based on the characteristics of the process, an approach for constraint handling has been proposed. The influence of different options in the search algorithms has also been tested in order to improve the performance of the search. The solutions found are of similar quality as the ones obtained for the deterministic search method otherwise used in this project, yet the search time is significantly increased.

1.5 Thesis structure

The main part of this thesis has been divided into eight chapters. The content of each chapter is indicated below:

- **Chapter 2** gives an introduction to relevant topics for LNG, followed by a literature review on LNG process optimization.
- **Chapter 3** introduces the simulation-optimization framework used in this study. In order to get a better view of the problem characteristics, sensitivity analyses and parameter studies are performed for a single mixed-refrigerant process.
- **Chapter 4** presents results obtained using the stochastic search algorithm Adaptive Simulated Annealing for optimization of a single mixed-refrigerant process. Different constraint handling techniques are also compared.
- **Chapter 5** gives results from optimization of a single and a dual nitrogen expander process. The performance of a simplified thermodynamic model assuming perfect gas behaviour for the refrigerant is compared with a rigorous model using a cubic equation of state. In addition, optimal intermediate pressure levels in dual-stage compression are discussed.

- **Chapter 6** discusses the influence of the choice of decision variables and bounds for optimization of pure-refrigerant cascade processes. Optimal load distribution between the refrigeration cycles and the influence of interaction between the refrigeration cycles is also discussed.
- **Chapter 7** presents a discussion on the influence of constraint formulations for the optimal trade-off between power consumption and heat exchanger size in LNG process optimization. A literature review on optimal distribution of driving forces in heat transfer is followed by case studies of a simple heat exchanger and a single mixed-refrigerant process.
- **Chapter 8** presents an approach suggested for optimization of cascade refrigerant processes based on sequential optimization of the different refrigeration cycles. A case study is presented for a dual mixed-refrigerant process in order to illustrate the methodology. In addition, heuristic guidelines for optimal intermediate pressure levels in multi-stage compression are presented and tested.
- **Chapter 9** provides a summary of the work done in the PhD project and suggestions for future work.

1.6 Publications

Papers published, accepted or submitted during the PhD project are listed in the following, sorted according to the type of publication.

Journal publications:

- Austbø B, Løvseth SW, Gundersen T. Annotated bibliography – Use of optimization in LNG process design and operation. *Computers and Chemical Engineering* 2014;71:391-414.
- Austbø B, Gundersen T. Impact of problem formulation on LNG process optimization. Submitted to *AIChE Journal*, November 2014.

Conference papers published in journals:

- Austbø B, Wahl PE, Gundersen T. Constraint handling in stochastic optimization algorithms for natural gas liquefaction processes. *Computer Aided Chemical Engineering* 2013;32:445-450.
- Austbø B, Gundersen T. Using thermodynamic insight in the optimization of LNG processes. *Computer Aided Chemical Engineering* 2014;33:1273-1278.
- Austbø B, Gundersen T. Optimization of a single expander LNG process. Accepted for publication in *Energy Procedia*.

Conference proceedings:

- Austbø B, Gundersen T. Thermodynamic analysis in LNG process optimization. In: Zevenhoven R, editor. Proceedings of the 27th International Conference on Efficiency, Cost, Optimization, Simulation and Environmental Impact of Energy Systems (ECOS 2014), Turku, Finland, 2014.

Conferences presentations:

- Austbø B, Wahl PE, Gundersen T. Constraint handling in stochastic optimization algorithms for natural gas liquefaction. 23rd European Symposium on Computer Aided Process Engineering, 9-12 June 2013, Lappeenranta, Finland. Poster presentation.
- Austbø B, Gundersen T. The impact of problem formulation on LNG process optimization. 2013 AIChE Annual Meeting, 3-8 November 2013, San Francisco, USA. Oral presentation.
- Austbø B, Gundersen T. Optimization of a single expander LNG process. 3rd Trondheim Gas Technology Conference, 4-5 June 2014, Trondheim, Norway. Oral presentation.
- Austbø B, Gundersen T. Using thermodynamic insight in the optimization of LNG processes. 24th European Symposium on Computer Aided Process Engineering, 15-18 June 2014, Budapest, Hungary. Oral presentation.
- Austbø B, Gundersen T. Thermodynamic analysis in LNG process optimization. ECOS 2014. 27th International Conference on Efficiency, Cost, Optimization, Simulation and Environmental Impact of Energy Systems, 15-19 June 2014, Turku, Finland. Oral presentation.

2 Background

In this chapter, a short introduction to the field of natural gas liquefaction and surrounding topics is provided. First, a general overview on the global energy situation is given, centred around natural gas. Second, a short introduction to the characteristics of liquefied natural gas (LNG) and alternative energy carriers is presented. This is followed by an outline of the different activities in an LNG plant, paying especially attention to the liquefaction process itself.

In the end, a review of literature related to LNG process optimization is provided. This is used to illustrate the current status of the field, with respect to the processes that have been studied and methodologies that have been used for process simulation and optimization.

This chapter is partly based on the following publication:

- Austbø B, Løvseth SW, Gundersen T. Annotated bibliography – Use of optimization in LNG process design and operation. *Computers and Chemical Engineering* 2014;71:391-414.

2.1 Introduction

Due to an increasing world population and rapidly growing emerging economies, the global primary energy use is expected to increase with 1.5 % per annum on average between 2012 and 2035 according to estimates by BP (2014a). For the same period, energy use from natural gas is expected to grow by 1.9 % per year (BP, 2014a). In 2013, the global energy use grew 2.3 % and the natural gas consumption 1.4 % (BP, 2014b). Natural gas accounted for 23.7 % of the global energy use in 2013 (BP, 2014b) and is expected to account for around 27 % in 2035 (BP, 2014b). According to the International Energy Agency (IEA) (2012), global gas consumption is expected to continue growing through 2035, regardless of the development in government policies.

Liquefied natural gas (LNG) accounted for 31.4 % of global gas trade in 2013 after a rebound by 0.6 % (BP, 2014b). An average growth of 3.9 % per annum in LNG trade

is, however, estimated from 2012 to 2035 according to BP (2014a). By 2035, LNG is projected to account for more than 46 % of the global natural gas trade. Hence, pipeline transport is expected to remain the primary method for natural gas trade despite a decline in share of consumption. The total natural gas trade grew by 1.8 % in 2013 (BP, 2014b).

2.2 Liquefied natural gas

Liquefied natural gas (LNG) is an energy carrier suitable for transport of natural gas of small to moderate volumes and/or over long distances. At atmospheric pressure, liquefied natural gas occupies about 1/600 of its volume at standard conditions (15 °C and 1 atm), which enables efficient transport of large quantities in specialized vessels. Liquefaction of natural gas requires energy intensive refrigeration. Compared with pipeline transmission, both capital and operating costs of the facilities are larger for LNG, while the cost of additional transport distance is smaller.

2.2.1 Alternatives to LNG

Liquefaction is not the only alternative for increasing the energy density of natural gas. Compressed natural gas (CNG) is an alternative technology for enhanced energy density, based on compressing the natural gas to 125-250 bar. Coselle is a CNG concept where the natural gas is compressed to about 210 bar and transported in in a large coil of small-diameter pipe. In the Votrans concept, the natural gas is both compressed and cooled, before being transported stored in insulated large-diameter pipe sections (Thomas and Dawe, 2003; Economides et al., 2006).

Since the natural gas is not liquefied, CNG production is less energy intensive than LNG. LNG ships can, however, transport 2-3 times more gas (Economides et al., 2006). Overall, CNG is a simpler alternative than LNG, but as the energy density is smaller larger cargo sizes are required (Khalilpour and Karimi, 2012).

Alternatively, natural gas can be converted into synthetic liquid fuels using a Fischer-Tropsch process or an oxygenation method (Thomas and Dawe, 2003). Due to its high energy density, gas to liquids (GTL) is an attractive fuel alternative (Khalilpour and Karimi, 2012). As opposed to LNG and CNG, GTL shipping does not require specialized vessels (Khalilpour and Karimi, 2012). GTL is a product ready for use, hence there is no need for a special facility at the import terminal (Khalilpour and Karimi, 2012).

The natural gas can also be transported as a solid (GTS). Gas hydrates can be formed by mixing natural gas with liquid water around 80-100 bar and 2-10 °C. Since decomposition at atmospheric pressure is very slow around -15 °C, hydrates can be transported in simple insulated bulk carriers that are significantly less expensive than

LNG carriers. As the volumetric density is smaller than for LNG, however, the transport cost is higher (Thomas and Dawe, 2003). In addition to the above given alternatives, the energy in natural gas can be transferred to other forms prior to transport, either as electricity or as a commodity (Thomas and Dawe, 2003).

Based on a techno-economical evaluation, Khalilpour and Karimi (2012) found CNG to be the most profitable alternative for remote gas production when the distance from source to market is relatively short, irrespective of the reservoir capacity. For longer transport distances, LNG was found to provide the highest net present value for relatively small reservoirs, while GTL provided the best alternative for larger reservoirs. Thomas and Dawe (2003) and Economides et al. (2006) also concluded that CNG, at the time being, was considered to be an alternative to LNG only for short transport distances.

2.3 LNG plant

Prior to liquefaction, pretreatment of the natural gas is required. Impurities such as water, acid gases and mercury must be removed from the natural gas in order to prevent freezing, corrosion and depositions in process equipment (Bahadori, 2014). Natural gas conditioning is also required to meet given specifications for the LNG product. Different requirements on heating value and Wobbe index apply to different markets (Mokhatab et al., 2010). A flow diagram of typical activities in an LNG plant is given in Fig. 2.1 (Bahadori, 2014; Mokhatab et al., 2014).

Upon arrival at the LNG production plant, large liquid slugs in the natural gas feed stream from the field can be removed in a slug catcher. Both hydrocarbon liquids (condensate) and an aqueous phase are separated from the gas. For the former, condensate stabilization is required to allow storage at atmospheric pressure. Monoethylene glycol (MEG) used to prevent hydrate formation in the well stream can be separated from the aqueous phase and returned to the production field (Mokhatab et al., 2014).

In the acid gas removal unit, CO_2 and H_2S are removed from the natural gas stream in order to meet criteria for the LNG product stream. According to Mokhatab et al. (2014), the CO_2 content must be reduced to 50-100 ppmv in order to avoid freezing in the cryogenic heat exchangers in the liquefaction process, while the H_2S content typically must be less than 4 ppmv to meet product specifications. Other sulphuric species contributing to sulphur emissions must also be removed. Acid gases are typically removed by use of an absorption process (Mokhatab et al., 2014).

Water can be removed from the natural gas stream by adsorption in molecular sieves. Removal of mercury can also be accomplished through adsorption. In addition to being

a potential environmental and safety hazard, traces of mercury can result in severe aluminium corrosion in heat exchangers (Mokhatab et al., 2014). As indicated in Fig. 2.1, acid gas removal, dehydration and mercury removal must be carried out prior to liquefaction.

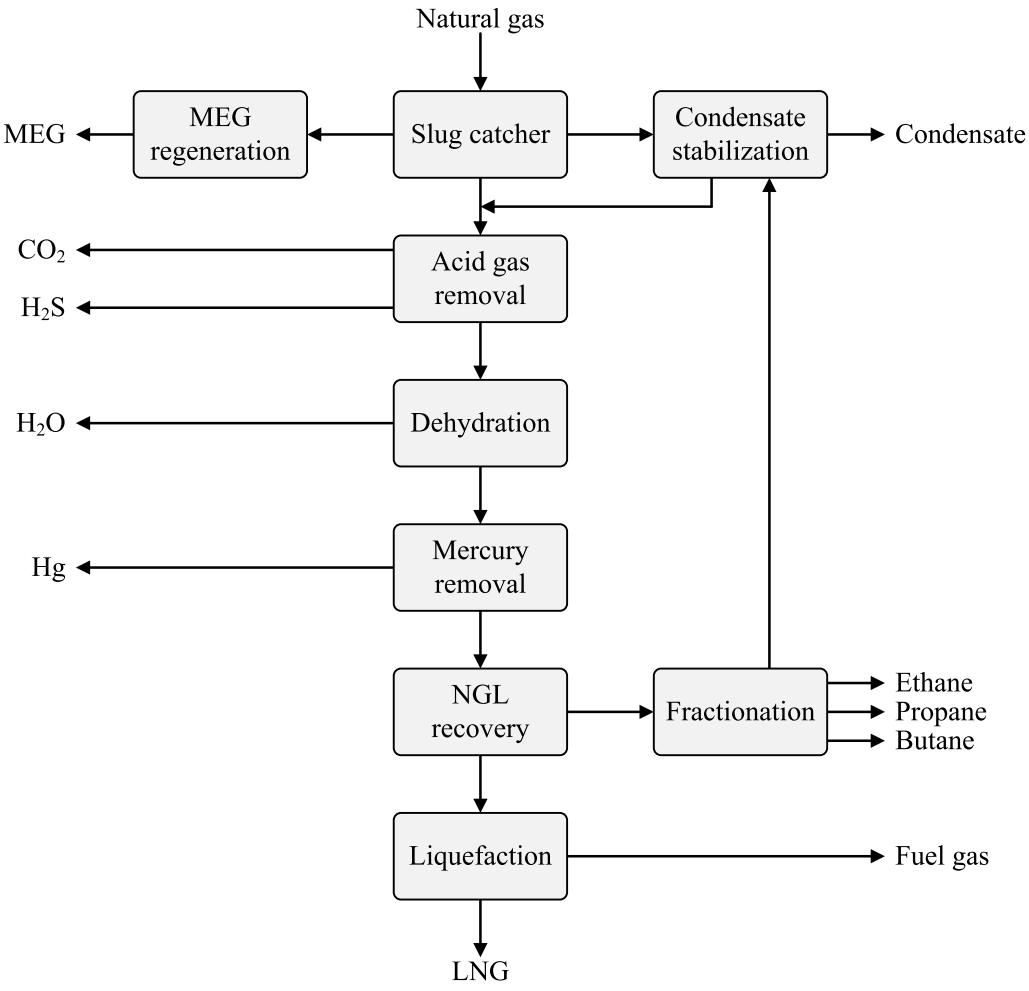

Figure 2.1. Typical LNG plant flow diagram (Bahadori, 2014; Mokhatab et al., 2014).

In order to avoid waxing at cryogenic temperatures, the amount of heavier hydrocarbons in the natural gas must be reduced. Less volatile components are separated from the main stream and sent to the condensate stabilization unit. The condensate can be sold as a valuable liquid product (Mokhatab et al., 2014). The natural gas liquids (NGL) can both be sold as separate products (ethane, propane and butane) and used for refrigerant makeup (Bahadori, 2014). In Fig. 2.1, removal of

heavier hydrocarbons is done prior to liquefaction. This could, however, also be integrated with the liquefaction process.

Liquefying a lean natural gas mixture is less energy demanding than liquefying a rich mixture. Hence, according to Mokhatab et al. (2014), less power would be required in the liquefaction process if the heavier hydrocarbons are removed prior to liquefaction. In addition, the reliability and availability of the plant would be higher if the two processes (NGL recovery and liquefaction) are performed independently (Mokhatab et al., 2014).

Integrated NGL recovery would, however, enable cost reductions. Duplicate heat exchangers can be avoided, and the pressure drops thereby reduced compared to separated processes (Mokhatab et al., 2014). Potential energy savings could be realized by integrating heating and cooling demands within the LNG plant.

After liquefaction, the condensed natural gas stream is expanded to the desired transport or storage pressure (close to atmospheric pressure). Vapour potentially formed in this process (rich in methane and nitrogen) is separated from the liquid. This also enables removal of excess nitrogen (Bahadori, 2014). The flash gas produced is typically used as fuel within the LNG plant. In-depth details on natural gas pretreatment and alternative processing technologies are provided by Bahadori (2014) and Mokhatab et al. (2014).

2.4 Exergy

Exergy is a measure of energy quality, providing a target for the maximum work that can be extracted from a system when brought to equilibrium with its surroundings (or alternatively, the minimum work that must be supplied to bring a system in equilibrium with the surroundings to a given state). A process in which the exergy is conserved is reversible. In this case, both the system and its environment can be restored to their initial states without any residual effects in either (Kotas, 1995). Irreversibilities are, however, present in all real processes.

All process irreversibilities lead to exergy loss or destruction. From the Gouy-Stodola relation, the irreversibility rate of a process is given as the product of the entropy production rate and the temperature of the environment (Kotas, 1995). Based on irreversibilities, the exergy efficiency of a process can be used as a measure for thermodynamic performance. As discussed by Marmolejo-Correa and Gundersen (2012), many different exergy efficiency parameters have been defined.

The rational efficiency of a system can be defined as the ratio of exergy of output to exergy input (Kotas, 1995):

$$\psi = \frac{\sum \Delta \dot{\mathrm{E}}_{\mathrm{out}}}{\sum \Delta \dot{\mathrm{E}}_{\mathrm{in}}} = \frac{\sum \Delta \dot{\mathrm{E}}_{\mathrm{out}}}{\sum \Delta \dot{\mathrm{E}}_{\mathrm{out}} + \dot{I}}. \tag{2.1}$$

Here, $\sum \Delta \dot{\mathrm{E}}_{\mathrm{in}}$ is the sum of exergy input and $\sum \Delta \dot{\mathrm{E}}_{\mathrm{out}}$ the sum of exergy output. The sum of irreversibilities $\dot{I}$ is equal to the difference between exergy input and output. For all real processes, the rational efficiency is less than unity.

Of particular importance for natural gas liquefaction is the exergy of heat. The exergy available in a heat flow $\dot{Q}_{\mathrm{i}}$ is given as

$$\dot{\mathrm{E}}\left(\dot{Q}_{\mathrm{i}}\right) = \dot{Q}_{\mathrm{i}} \cdot \left(1 - \frac{T_0}{T_{\mathrm{i}}}\right), \tag{2.2}$$

where T_0 is the ambient temperature and T_{i} is the temperature at which the heat is transferred (Kotas, 1995). By definition, a heat flow is positive when heat is transferred to a system. Hence, heat transfer to a system would lead to increased exergy above ambient temperature but reduced exergy below ambient temperature (Kotas, 1995). In Fig. 2.2, the exergy of heat per unit of heat is plotted as function of the absolute temperature relative to the ambient temperature.

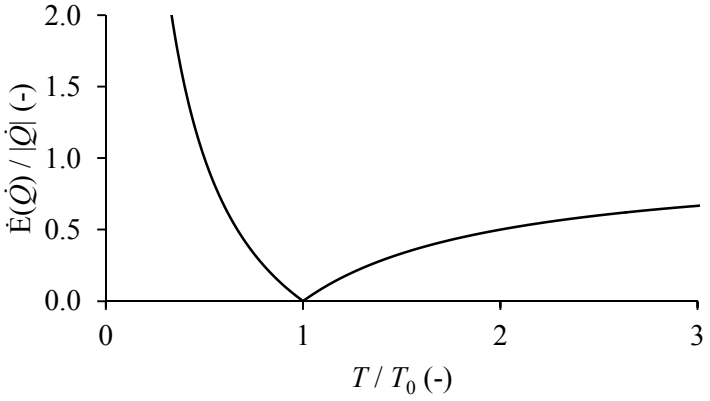

Figure 2.2. Exergy of heat as a function of temperature relative to the ambient.

At ambient temperature, a system would be in equilibrium with its surroundings, thus heat contains no exergy. As the temperature increases above ambient, the exergy of heat increases monotonically, asymptotically approaching unity. For temperatures below ambient, the exergy of heat grows asymptotically towards infinity when the

temperature approaches zero. At a temperature equal to half the ambient temperature, the exergy content is equal to the heat. The exergy of heat indicates that, in order to minimize irreversibilities associated with heat transfer, more attention should be paid to keeping the driving forces small at low temperature levels.

From Eq. (1.2), the irreversibilities associated with heat transfer between a source with temperature T_H and a sink with temperature T_C can be expressed as

$$\dot{I} = \dot{Q} \cdot T_0 \cdot \left(\frac{1}{T_C} - \frac{1}{T_H} \right) = \dot{Q} \cdot T_0 \cdot \frac{\Delta T}{T_H \cdot (T_H - \Delta T)}, \tag{2.3}$$

where ΔT is the temperature difference between the source and the sink. One may observe that for the same temperature difference, the irreversibilities associated with heat transfer increase with decreasing temperature level. Hence, for energy efficient liquefaction of natural gas, which involves heat transfer at low temperature level, the temperature difference in the refrigeration process should be kept small. Due to the fact that the cooling load in natural gas liquefaction processes is distributed over a wide temperature span, this is a challenging task.

2.5 Refrigeration

The purpose of a refrigeration process is to transfer heat from a source to a sink, in a system where the temperature of the sink is higher than the temperature of the source. From the second law of thermodynamics, this cannot be done without addition of work. In vapour-compression refrigeration processes, heat is absorbed by an evaporating refrigerant with temperature lower than the heat source and rejected by condensation of the same refrigerant with temperature higher than the heat sink.

2.5.1 Classification

Based on the terminology used by Barnés and King (1974) and Cheng and Mah (1980), a refrigeration cycle may be defined as a closed sub-system within a refrigeration process. A refrigeration cycle may contain branches and/or loops, enabling sub-cycles to operate at different pressure levels and thereby evaporation at different temperature levels. According to the terminology, a simple refrigeration cycle would only contain one level of condensation and one level of evaporation. A complex refrigeration cycle, however, would be divided into intermediate pressure levels (Barnés and King, 1974; Cheng and Mah, 1980).

When the temperature difference between the source and the sink is large, such as for liquefaction of natural gas, cascade refrigeration systems may be installed to improve energy efficiency. In cascade refrigeration processes, two or more refrigeration cycles are combined in series. Instead of transferring all heat directly from the source to the

sink, as would be the case for single-stage refrigeration, at least part of the heat is transferred to the sink via other refrigeration cycles.

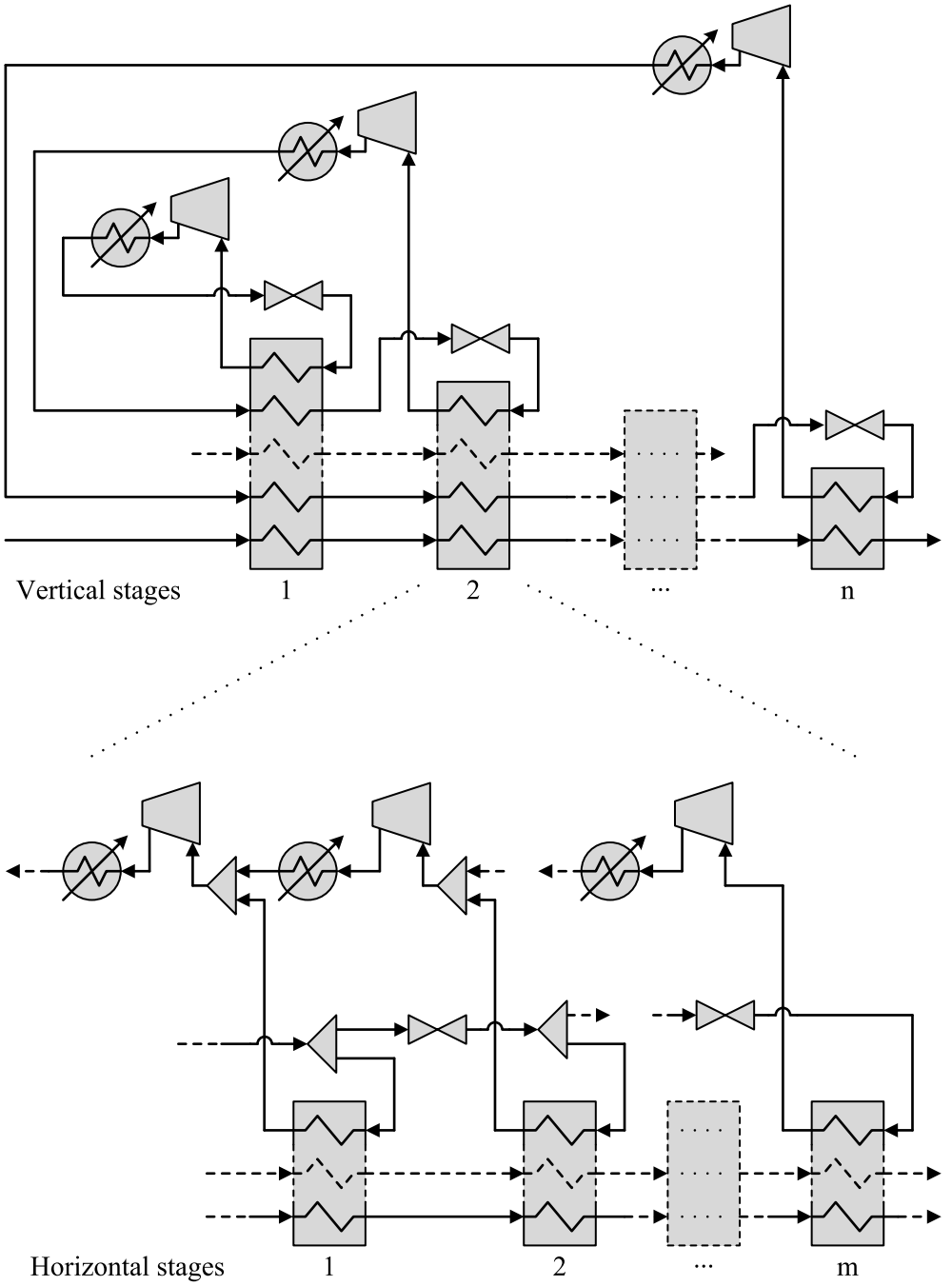

Figure 2.3. Refrigeration process with vertical and horizontal stages.

Using the terminology of Vaidyaraman and Maranas (2002), each refrigeration cycle in a refrigeration process can be defined as a vertical stage, while each sub-cycle in a refrigeration cycle can be defined as a horizontal stage. Hence, a simple refrigeration cycle is equivalent to a vertical stage with only one horizontal stage, while a complex refrigeration cycle involves two or more horizontal stages. A process with n vertical stages is illustrated in the upper part of Fig. 2.3.

Each of the vertical stages can be divided into horizontal stages, as illustrated in the lower part of Fig. 2.3. Here, the refrigeration cycle contains m evaporation levels. Each evaporation level in a vertical stage represents a horizontal stage. One the one hand, there is only one horizontal stage in each vertical stage in a simple cascade. In a complex cascade, on the other hand, at least one of the vertical stages is divided into two or more horizontal stages.

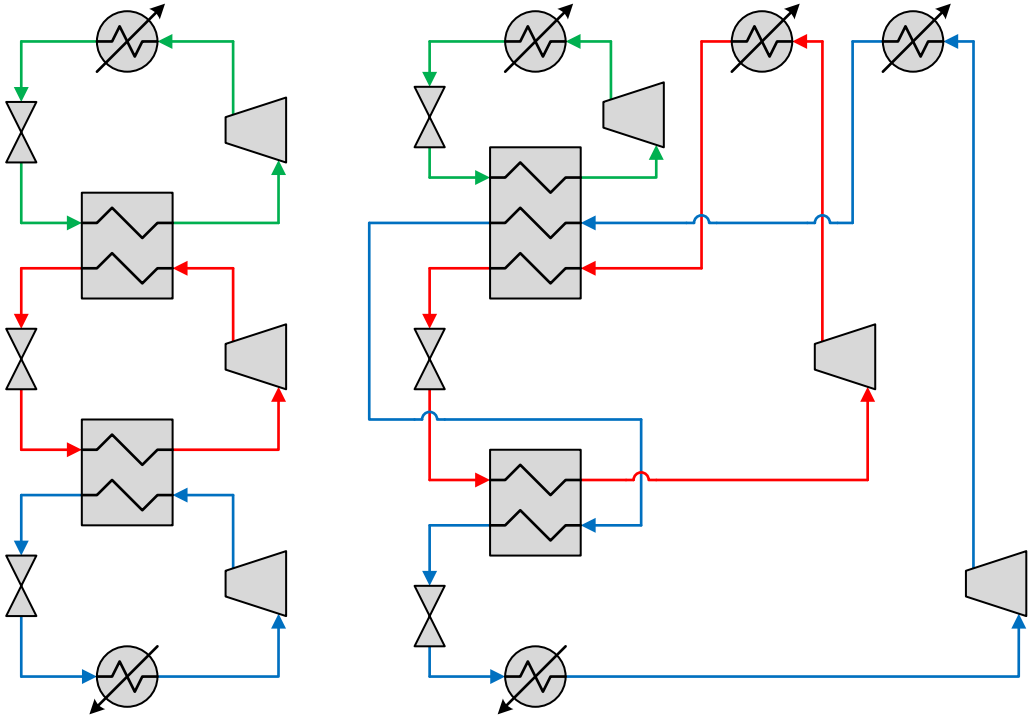

Figure 2.4. (a) Full cascade; (b) Partial cascade.

The arrangement of the different refrigeration cycles in a cascade would depend on the use. In the work by Quack (2012), cascade processes were categorized according to the way heat is transferred from the source to the sink. In a full cascade, all heat absorbed in a vertical stage is transferred to the preceding vertical stage in the cascade (a

refrigeration cycle operating at higher temperature). Thus, all heat is transferred to the sink in the refrigeration cycle operating at the highest temperature level. Such a cascade process is illustrated in Fig. 2.4 (a).

In a partial cascade, each refrigeration cycle deliver at least part of the heat absorbed directly to the sink. The remaining heat is transferred to the sink via other refrigeration cycles (Quack, 2012). A partial cascade is illustrated in Fig. 2.4 (b). The choice of cascade system is closely related to the compressor discharge temperatures, which determine the temperature level at which the heat can be rejected. This would depend on operating conditions such as temperature span between source and sink, number of refrigeration cycles and choice of refrigerants.

2.6 LNG process concepts

Being a mixture, isobaric condensation of natural gas takes place at gliding temperature. Hence, as already mentioned, cooling must be provided over a wide temperature range in order to liquefy natural gas. From the perspective of exergy of heat, this heat transfer should be provided with small temperature driving forces, especially at low temperature levels. In order to accommodate this challenge in an economic manner, a large variety of process concepts have been proposed.

2.6.1 Classification

Most LNG processes are based on vapour-compression refrigeration systems, with the addition of reverse Brayton processes (also known as expander processes). An obvious classification criterion for LNG processes would be based on the choice of refrigerant used in the process:

- Evaporating pure-refrigerant
- Evaporation multi-component refrigerant
- Vapour-phase refrigerant

One the one hand, assuming the pressure is constant, evaporation and condensation of a single-component refrigerant takes place at constant temperature. A mixed-refrigerant, on the other hand, evaporates and condenses at gliding temperature. For LNG purposes, the mixed-refrigerant is usually composed of different hydrocarbons and nitrogen. When a vapour-phase refrigerant all heat transfer is based on sensible heat, as the refrigerant is kept as a gas throughout the refrigeration cycle.

The different process concepts may also be categorized according to their structure. For improved efficiency and increased capacity, refrigeration cycles may be combined in series (vertical stages) or divided into sub-cycles (horizontal stages). The optimal process design is given by the optimal trade-off between capital and operating costs.

Increasing the number of stages may improve the energy efficiency (reduced operating cost), while increasing the equipment count and thereby also the capital cost and complexity of the process.

The optimal balance between capital and operating costs depends on the application. Hence, a large variety of LNG process concepts, with different strengths and weaknesses, has been developed over the years. In Fig. 2.5, a selection of common process concepts have been classified according to refrigerants used and the process structure.

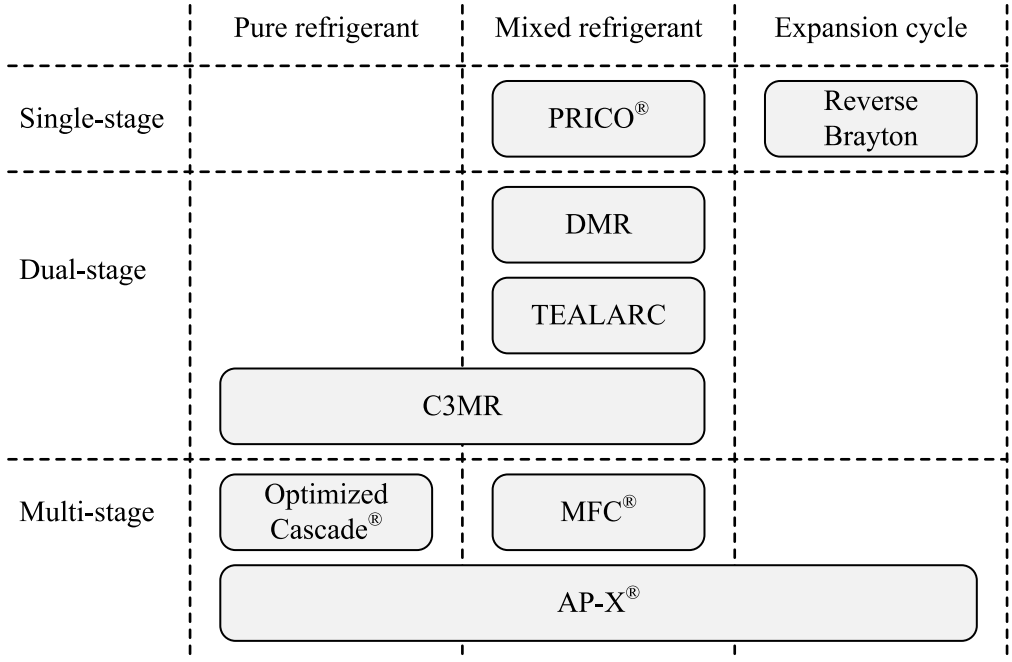

Figure 2.5. Classification of a selection of LNG process concepts.

2.6.2 Pure-refrigerant cascade processes

Evaporation at constant temperature leads to large temperature differences in heat transfer between refrigerant and natural gas. Hence, in a pure-refrigerant process different refrigerants must be combined in a cascade. Different refrigerants are operated at different temperature levels in each vertical stage in a cascade. A typical simple pure-refrigerant cascade process with three vertical stages is illustrated in Fig. 2.6. According to the classification presented in Section 2.5.1, the process is modelled as a partial cascade.

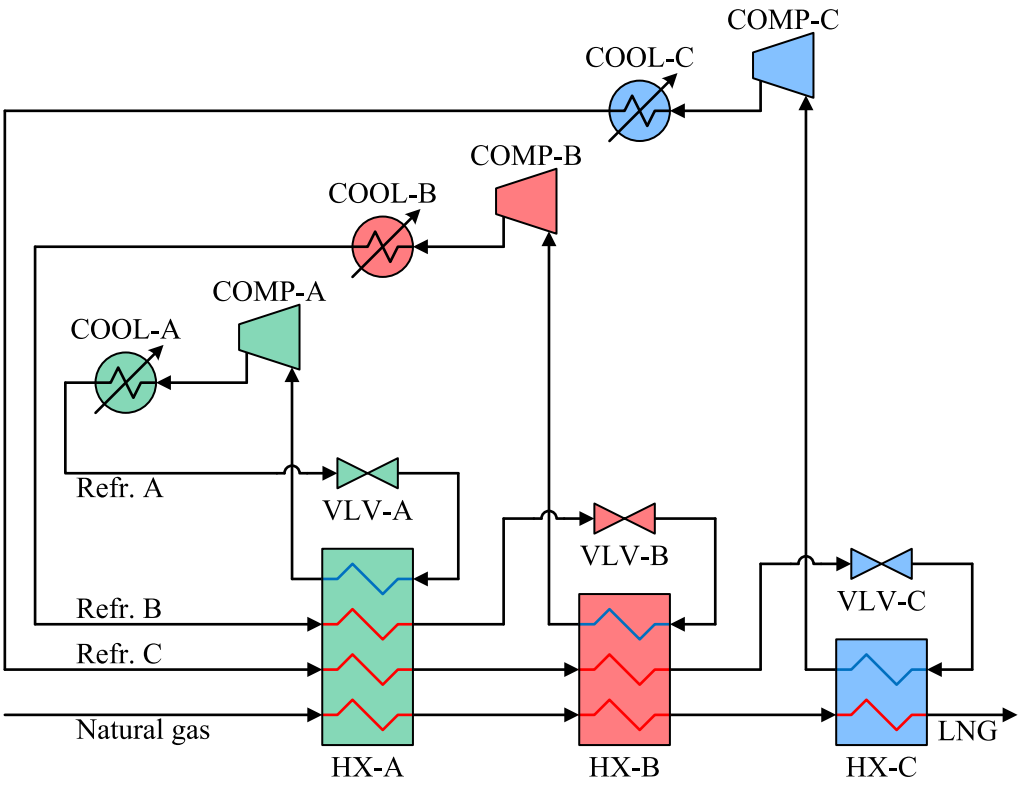

Figure 2.6. Pure-refrigerant cascade process for liquefaction of natural gas.

Further improvement in energy efficiency is obtained by dividing each vertical stage into horizontal stages operating at different pressure levels, and thereby proving refrigeration at different evaporating temperatures. Typically, three different refrigerants are combined to cover the temperature range of the natural gas cooling load: propane in cycle A, ethene (ethylene) in cycle B and methane in cycle C. Alternatively, ethane could be used as refrigerant in cycle B. In the ConocoPhillips Optimized Cascade®, the methane stage is replaced by an open loop system (Ransbarger, 2007; Venkatarathnam, 2008).

2.6.3 Mixed-refrigerant processes

With a mixed-refrigerant, the entire cooling range of the natural gas can be covered in a single stage with reasonable efficiency. This is done in the PRICO® process (Swenson, 1977), which is one of the simplest practical LNG process. As indicated in the flowsheet given in Fig. 2.7, both the natural gas and the refrigerant itself is cooled in the main heat exchanger. Hence, the heat capacity of the refrigerant cold stream must be larger than for the refrigerant hot stream, in order to provide cooling both to the natural gas stream and the refrigerant hot stream.

Slightly more complex processes can be designed by dividing this mixed refrigerant cycle in horizontal stages by introducing phase separators at intermediate points in the cooling range. Due to the fact that the liquid and vapour composition of a two-phase mixture will be different, sub-streams of different composition are then created. Hence, sub-cycles with different refrigerant composition can be designed even with a single vertical stage. Such processes are also referred to as auto-cascade processes (Gong et al., 2001; Wang et al., 2013b).

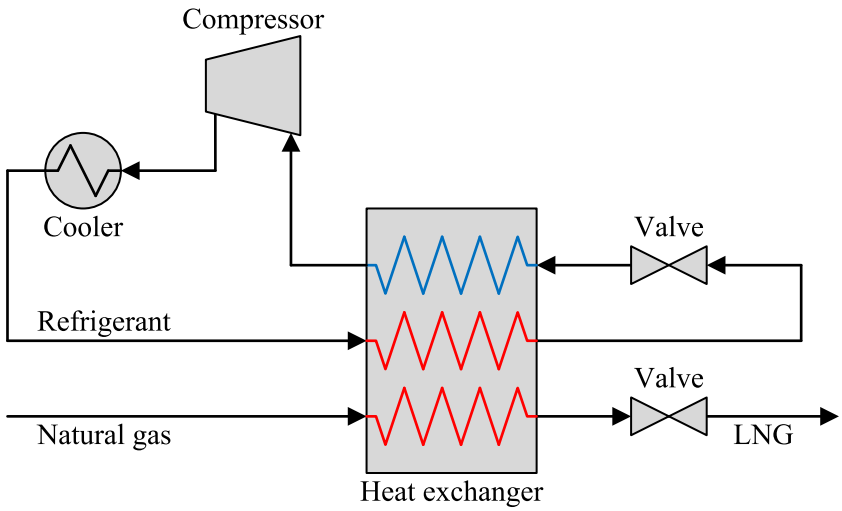

Figure 2.7. Single mixed-refrigerant process for natural gas liquefaction.

Improved energy efficiency is possible by combining two or more mixed-refrigerant cycles in a cascade. In dual mixed-refrigerant processes (DMR) two vertical stages are used (Liu and Pervier, 1985; Newton, 1985; Grootjans et al., 2002). Two mixed-refrigerant cycles are used also in the TEALARC process. Here, however, one of the cycles is dedicated to precooling the other mixed-refrigerant cycle. Details on the TEALARC process can be found in work presented by Michelsen et al. (2010a, 2010b, 2010c) and Morin et al. (2011).

In the mixed fluid cascade process (MFC®) (Stockmann et al., 2001) three mixed-refrigerant cycles are combined in a cascade. The simplified layout of the process is therefore similar to the pure-refrigerant cascade process illustrated in Fig. 2.6, except for the fact that mixed refrigerants are used in all cycles. With increasing number of refrigeration cycles, the energy efficiency is in general improved, but at the expense of greater complexity (Finn et al., 1999). The energy savings resulting from adding additional vertical stages decrease with the number of stages, while the complexity and capital cost keep increasing.

2.6.4 Expansion cycles

In reverse Brayton processes (expander cycles), the refrigerant is typically nitrogen, methane or a mixture of the two. In addition to the fact that the refrigerant is kept in gas phase throughout the process, expansion cycles are characterized by the turbines are used for expansion, as it provides a larger temperature drop and enables extraction of work. A simple single-expander process for liquefaction of natural gas is illustrated in Fig. 2.8.

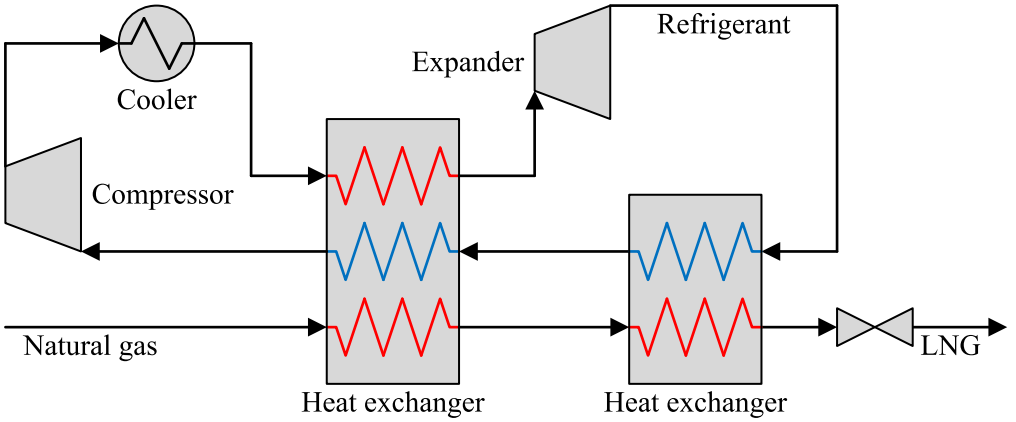

Figure 2.8. Single expander process for liquefaction of natural gas.

More energy efficient expander processes can be obtained by introducing a second stage of expansion. Despite relatively high energy use compared to other process concepts, nitrogen expander processes possess other qualities that useful in niche applications such as remote gas production (Castillo and Dorao, 2010).

2.6.5 Hybrid processes

The different refrigeration concepts may also be combined to take advantage of their different qualities. In the propane-precooled mixed-refrigerant process (C3MR), a propane cycle and a mixed-refrigerant cycle are combined in a cascade. The AP-X® process (Roberts and Agrawal, 2001) also includes a nitrogen expander cycle for sub-cooling of the natural gas stream. Other hybrid concepts have also been proposed in the literature. Different LNG process concepts have also been discussed by Venkatarathnam (2008) and Lim et al. (2013). In addition to improved energy efficiency, combined process concepts may also enable increased plant capacities.

2.6.6 Alternative liquefaction technologies

There are also some applications of other refrigeration technologies available in the literature, such as absorption refrigeration (Kalinowski et al., 2009; Mortazavi et al., 2010; Rodgers et al., 2012) and thermoacoustic refrigeration (Backhaus and Swift,

1999). Absorption refrigeration has been proposed as an alternative for precooling of natural gas, by either replacing or enhancing propane precooling.

According to Venkatarathnam (2008), mixed-refrigerant cycles are used in more than 95 % of all base-load LNG plants, while pure-refrigerant cascade processes are used in the remaining. Propane-precooled mixed-refrigerant processes are by far the most popular process in base-load LNG. An overview of LNG technology market shares was also given by Barclay and Denton (2005).

2.7 Remote gas production

For a long time, the development of LNG plants has been focused on increasing the train size in order to utilize the economy of scale (Avidan et al., 2002). Today, however, there is also an increasing interest in new applications such as utilization of remote gas resources. These resources are often too marginal to justify the cost of developing a fixed infrastructure (Tangen and Mølnvik, 2009), and offshore floating LNG production has emerged as a cost-effective alternative (Finn et al., 1999). In remote gas production, the premises are different from those of onshore base-load LNG plants, and therefore also the criteria for LNG process technology selection.

While energy efficiency arguably is the most important selection criterion for large-scale onshore natural gas liquefaction processes, other factors become more important in offshore projects (Barclay and Denton, 2005). Yet still an important criterion, energy efficiency must be weighed against criteria such as compactness, safety. modularity, operability, equipment count and availability (Finn et al., 1999; Barclay and Denton, 2005; Castillo and Dorao, 2010). The process must also be able to handle effects of a marine environment, such as vessel motion (Castillo and Dorao, 2010).

Despite high specific compression power, Castillo and Dorao (2010) found nitrogen expander processes to be suitable for floating operations. These processes are extremely compact, inherently safe (inert refrigerant) and largely independent of feed gas properties. In addition they provide a low equipment count. A disadvantage is, however, the high presence of rotating equipment (Castillo and Dorao, 2010).

Li and Ju (2010) found nitrogen expander processes to be a better option for offshore LNG than a single mixed-refrigerant process and a propane-precooled mixed-refrigerant process. Mixed-refrigerant processes are sensitive to changes in feed gas composition as it requires adjustments of the refrigerant composition to maintain efficient operation (Finn et al., 1999).

Different process concepts have different strengths and weaknesses, and the choice of technology would vary with the applications. In order to make a fair comparison of

different process alternatives and in order to achieve an energy-efficient, environmentally friendly and economical process design, optimization is required.

2.8 Optimization

A general mathematical optimization problem can be formulated as

$$\begin{aligned} \min_{\mathbf{x},\mathbf{y}} \quad & f(\mathbf{x},\mathbf{y}) \\ s.t. \quad & g_i(\mathbf{x},\mathbf{y}) \le 0, \qquad i = 1,...,n \\ & h_j(\mathbf{x},\mathbf{y}) = 0, \qquad j = 1,...,p \\ & \mathbf{x} \in \mathbb{R}^s, \mathbf{y} \in \{0,1\}^t. \end{aligned} \tag{2.4}$$

Here, $f(\mathbf{x},\mathbf{y})$ is the objective function which is to be minimized for a vector $\mathbf{x}$ of continuous variables and a vector $\mathbf{y}$ of discrete variables, subject to n inequality constraints $g_i(\mathbf{x},\mathbf{y})$ and p equality constraints $h_j(\mathbf{x},\mathbf{y})$. Maximization of the objective $f(\mathbf{x},\mathbf{y})$ is equivalent to minimizing $-f(\mathbf{x},\mathbf{y})$ (Nocedal and Wright, 2006; Biegler, 2010).

The general optimization problem in Eq. (2.4) corresponds to a mixed integer nonlinear program (MINLP). If all objective and constraint functions are linear functions, the optimization problem will be a mixed integer linear program (MILP). In nonlinear programs (NLP) only continuous variables are present. If, in addition, all functions are linear, the optimization problem will be a linear program (LP) (Nocedal and Wright, 2006; Biegler, 2010).

If discrete decision are considered, for instance in a superstructure model, the optimization problem could be formulated as an MINLP. More commonly, however, the optimization problems encountered in LNG process optimization can be formulated as nonlinear programs. An important factor regarding optimization of nonlinear programs is convexity. If the objective function or any of the constraint functions in Eq. (2.4) is a nonconvex function, the optimization problem will be nonconvex (Biegler, 2010).

A simple example of convex and nonconvex objective functions is given in Fig. 2.9. In the case of a convex optimization problem, any local optimum (better than all neighbouring points) is also a global optimum. For a nonconvex optimization problem, however, multiple local optima may be present as illustrated in Fig. 2.9 (b). Identifying a local optimal solution may therefore not mean that the global optimal solution has been found. For this reason, nonconvex optimization problems are hard to solve. A review of status and development in optimization relevant for chemical engineering applications was provided by Biegler and Grossmann (2004) and Grossmann and Biegler (2004).

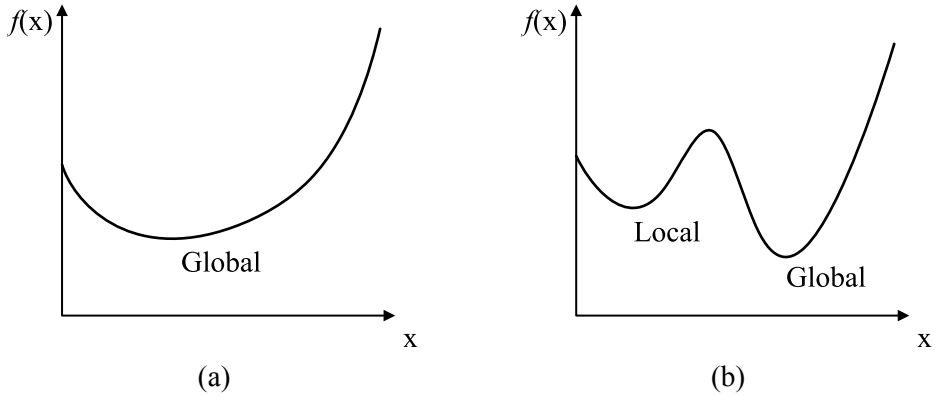

Figure 2.9. (a) Convex objective function; (b) Nonconvex objective function.

2.8.1 Sequential quadratic programming

Sequential quadratic programming (SQP) methods are very popular for optimization of nonlinear optimization problems, mainly due to their fast convergence properties inherited from Newton methods and their wide range of applicability (Biegler, 2010). More details on sequential quadratic programming and a review of different SQP codes were provided by Biegler (2010).

2.8.2 Global optimization

By use of sequential quadratic programming and other local optimization methods, localization of the global optimal solution can never be guaranteed for nonconvex optimization problems (Grossmann and Biegler, 2004). In this case, global optimization algorithms are required. In global optimization, convex optimization problems are constructed by use of underestimators and relaxations. The solution of these convex optimization problems provides a lower bound on the global optimization problem.

By gradually improving the objective of the original optimization problem and the accuracy of the underestimators (e.g. through branch and bound or cutting planes), the global optimization search will try to reduce the gap between the best solution found for the function to be optimized and the lower bound given by the relaxed optimization problem. A status review for global optimization was provided by Floudas and Gounaris (2009).

2.8.3 Stochastic search methods

As an alternative to deterministic global optimization, stochastic search methods are often used to solve nonconvex optimization problems. One the one hand, deterministic methods utilize analytical properties of the optimization problem to generate a sequence of solutions that converge to an optimum. In stochastic search methods, however, probabilistic elements are utilized in the search for the global optimum.

Most stochastic search methods have been developed based on processes in nature. Stochastic elements are included in order to avoid getting trapped in local optima. Due to its probabilistic nature, a stochastic search method would need an infinite number of iterations to guarantee convergence to the global optimum. In practice, however, acceptable solutions close to the global optimum can often be obtained relatively fast (Rangaiah, 2010).

Stochastic search methods may be divided into two main categories; point-to-point based algorithms and population based algorithms. Simulated annealing (SA) (Kirkpatrick et al., 1983) and tabu search (TS) (Glover, 1986; Glover et al., 1993) are commonly used search methods belonging to the former category. A very much applied population based search method is genetic algorithms (GA), for which more information is provided by Rangaiah (2010).

Other stochastic search methods inspired by nature include ant colony optimization (ACO) (Dorigo et al., 1997), particle swarm optimization (PSO) (Kennedy and Eberhart, 1995), artificial bee colony optimization (ABC) (Karaboga and Basturk, 2008) and harmony search (HS) (Lee and Geem, 2005). A review of stochastic search methods used in chemical engineering optimization was provided by Rangaiah (2010).

2.9 Modelling

Due to the small temperature driving forces necessary for energy efficient LNG process design, rigorous thermodynamic models are required in design and simulation. Inaccurate modelling may result in designs that are infeasible in practice. Rigorous thermodynamic models do, however, also lead to increased complexity in the optimization problem.

The Soave-Redlich-Kwong (SRK) (Soave, 1972) and Peng-Robinson (PR) (Peng and Robinson, 1976) cubic equations of state, or different modifications of these, are often used in natural gas process modelling. According to Nasrifar and Bolland (2006) these are relatively simple, yet also reasonably accurate. The introduction of the Soave-Redlich-Kwong equation of state enabled prediction of vapour-liquid equilibria for non-polar and slightly polar components (Kamath et al., 2010). The Peng-Robinson equation of state has a superior accuracy near the critical region and a better prediction of liquid density for most materials (Kamath et al., 2010).

More accurate equations of state have also been proposed. Nasrifar and Moshfeghian (1998) proposed an equation of state for prediction of liquid densities, while Dauber and Span (2011) presented GERG-2008 for accurate modelling of LNG. Among other studies on LNG process modelling, Stringari et al. (2014) pointed out the importance of accurate modelling CO_2 solubility in design of natural gas purification units.

Melaaen and Owren (1996) studied the influence of inaccuracies in vapour-liquid equilibrium calculations in LNG plant design by comparing the cubic equations of state PR, SRK and GDSRK (Groboski and Daubert's modification of SRK (Groboski and Daubert, 1978a, 1978b) with experimental data. The results indicated no significant difference between the different equations of state neither for prediction of equilibrium K-values nor for enthalpy calculations, yet the former was found to be generally underestimated (Melaaen and Owren, 1996). Nasrifar and Bolland (2006) compared the accuracy of 10 equations of state with respect to prediction of various thermo-physical properties of natural gas mixtures.

Due to their simplicity of application and low computational overhead, the cubic equations of state have remained widespread despite the fact that more theoretically based equations of state have been developed (Kamath et al., 2010).

2.9.1 Process modelling

The thermodynamic modelling of the LNG process can be performed either in a sequential modular approach or in an equation oriented approach. Even though both methods have their advantages and disadvantages, the former approach is dominant in the literature on LNG process optimization.

In a sequential modular approach, the different unit operations in a flowsheet are calculated sequentially by iteration. Biegler and Hughes (1982), Biegler (1985) and Biegler and Cuthrell (1985) have presented algorithms for optimization in sequential modular simulators without need for repeatedly convergence of the process flowsheet in every iteration. By use of infeasible path optimization the convergence of the flowsheet is handled by the optimization algorithm rather than the process simulator. An approach for global optimization of modular process flowsheets was proposed by Byrne and Bogle (2000).

In an equation-oriented simulation approach, the equations for all (or most) unit operations are solved simultaneously. Hence, the equations can be incorporated within the optimization problem and exact derivatives can be calculated directly (Kamath et al., 2010). According to Kamath et al. (2010), an equation-oriented simulation-optimization approach would require more careful problem formulation and initialization, and use of a robust general purpose nonlinear solver.

2.9.2 Heat exchanger modelling

A key component in any LNG process is the main cryogenic heat exchanger, and the choice of heat exchanger model is essential both for the model accuracy and the complexity of the optimization problem. The common approach taken in LNG process modelling and simulation is based on enthalpy balances, generally disregarding the

effects of heat transfer properties and pressure drop. As was discussed by Chang et al. (2012), homogeneous temperature profiles for all hot and cold streams are challenging to obtain in practical heat exchangers.

More rigorous heat exchanger models taking geometry into account have been proposed and used for LNG process design by Skaugen et al. (2010, 2013). Hasan et al. (2009a) used global optimization techniques to predict the operational performance of a multi-stream heat exchanger with phase changes, based on operational data. Afrianto et al. (2014) used computational fluid dynamics (CFD) to study the heat transfer characteristics of a multi-stream heat exchanger used for LNG regasification.

Kamath et al. (2012) proposed an equation-oriented approach to multi-stream heat exchanger modelling where the heat exchanger was modelled as a heat exchanger network problem with the different process streams divided into sub-streams with constant heat capacity.

The optimal choice of process models is given by a trade-off between accuracy and complexity. While a simple model is more likely to be solved to global optimality, the optimal solution of a simplified process model may not correspond to the optimal solution of a more complex process model.

2.10 Optimization in LNG value chain

Due to the challenges apparent in LNG process design and operation, a growing interest in optimization within the LNG value chain has been observed in the literature the past decades. Due to its significant influence on the overall economic performance, most of these studies have been concerned with the liquefaction process. While Finn et al. (1999) found the liquefaction to make up 25-50 % of the total capital cost in LNG production and storage, Shukri (2004) stated that the liquefaction process typically accounts for 30-40 % of the capital cost of LNG plant. In addition, the liquefaction process contribute to a significant share of the operating cost, due to the power consumption in the refrigeration process.

2.10.1 LNG process design optimization

A selection of late studies on LNG process design optimization is given in Table 2.1, with information on processes studied and optimization methods used. The majority of the optimization studies conducted are concerned with single mixed-refrigerant processes (SMR) such as PRICO®. A substantial amount of publications also treat propane-precooled mixed-refrigerant processes (C3MR). In many cases, however, only the precooling part (Lee et al., 2014) or the mixed-refrigerant part (Hatcher et al., 2012; Wang et al., 2012) is studied. Alabdulkarem et al. (2011) used a two-stage procedure where the mixed-refrigerant cycle was first optimized subject to a maximum cooling

load in the precooling cycle, before the propane cycle was optimized with the mixed refrigerant cycle fixed.

Other processes studied in the literature include different variations of the expander based process (reverse Brayton process) (EXP). In recent years, studies on dual mixed-refrigerant processes (DMR) have also been presented (Del Nogal et al., 2008; Morin et al., 2011; Hwang et al., 2013a, 2013b). No design optimization studies have been observed for more complex processes.

Table 2.1. A selection of recent studies on of LNG process design optimization.

Study	Processes	Optimization method
Alabdulkarem et al. (2011)	C3MR	GA
Aspelund et al. (2010)	SMR	TS + NMSS
Castillo and Dorao (2012)	SMR	GA
Del Nogal et al. (2008)	SMR and DMR	GA
Hatcher et al. (2012)	C3MR	BOX
He and Ju (2014a)	EXP	GA
He and Ju (2014b)	SMR	GA
Hwang et al. (2013a)	DMR	GA + SQP
Hwang et al. (2013b)	DMR	GA + SQP
Jensen and Skogestad (2008)	SMR	-
Kamath et al. (2012)	SMR	CONOPT
Khan and Lee (2013)	SMR	PSO
Khan et al. (2012)	SMR	SQP
Lee et al. (2012)	SMR	Mesh search
Lee et al. (2014)	C3MR	SQP
Morin et al. (2011)	SMR and DMR	SQP and ES
Shah et al. (2009)	EXP	GA
Shirazi and Mowla (2010)	SMR	GA
Skaugen et al. (2010)	SMR	SQP
Taleshbahrami and Saffari (2010)	C3MR	GA
Wahl et al. (2013)	SMR	SQP
Wang et al. (2013a)	C3MR	BOX
Wang et al. (2012)	C3MR	Branch-and-cut
Wang et al. (2011)	C3MR	SQP
Xu et al. (2013)	SMR	GA
Xu et al. (2014)	SMR	GA
Yoon et al. (2012)	SMR and EXP	GA

Stochastic search methods are employed in the majority of the optimization studies, and genetic algorithms are by far the most used. Among deterministic optimization methods, sequential quadratic programming algorithms have often been used. Other

optimization methods used include the built-in version of BOX (Box, 1965) in Aspen HYSYS® and Nelder-Mead simplex search (NMSS) (Nelder and Mead, 1965).

Different hybrid approaches, combining stochastic and deterministic search methods, have also been applied (Aspelund et al., 2010; Hwang et al., 2013a, 2013b). A stochastic search method is used to locate regions likely to contain the global optimal solution, while deterministic local search methods are used to refine solutions in these regions.

Optimization objective

Most optimization studies listed in Table 2.1 have been carried out with the objective of minimizing the power consumption (or alternatively maximizing the exergy efficiency) required to liquefy a given natural gas feed. The compression power is an important factor in the operating cost of an LNG process. Minimum irreversibilities profit from small temperature driving forces in heat transfer. This does, however, require vast heat exchanger areas. In order to accommodate the trade-off between investment cost and operating cost, a size limitation is given for the heat exchanger. This is most often done by requiring a minimum temperature driving force at all points in the heat transfer process.

Alternatively, investment and/or operating costs have typically been subject to minimization. Shah et al. (2009) performed optimization with the objective of minimizing hydrocarbon inventory. Multi-objective optimization in LNG process design has been performed by Shah et al. (2009) and Castillo and Dorao (2012). Other objective functions have, of course, been considered for optimal operation of LNG plants.

Process modelling

Modelling and simulation approaches used in the optimization studies listed in Table 2.1 are given in Table 2.2. For the cases where enough information is given, the thermodynamics models used are also indicated. One may observe that for the majority of studies listed in Table 2.2, the Peng-Robinson equation of state has been employed for modelling in LNG optimization studies. In the remaining studies listed in Table 2.2, the Soave-Redlich-Kwong equation of state has been used.

Commercial sequential modular simulation software such as Aspen HYSYS® (Aspen Technology, Inc.), UniSim® (Honeywell International Inc.), Aspen Plus® (Aspen Technology, Inc.) and PRO/II (Invensys Inc.) have been used in most studies. These simulators benefit from simple modelling, and all equality constraints related to mass and energy balances can be handled by the simulator. However, derivative information

is not readily available in commercial sequential modular simulators. Hence, derivatives are usually estimated by use of finite differences (Wahl et al, 2013).

In some cases, the use of sequential-modular simulators has been combined with other tools such as MATLAB (The MathWorks, Inc.) and GAMS (GAMS Development Corporation). Del Nogal et al. (2008) used in-house simulation software, WORK (The University of Manchester). The equation based process simulator gPROMS® (Process Systems Enterprise Limited) was used by Jensen and Skogestad (2008). However, little information is provided on the optimization approach.

Table 2.2. Modelling/simulation approach and equations of state used in recent studies on LNG process design optimization.

Study	Modelling/simulation	Equation of state
Alabdulkarem et al. (2011)	Aspen HYSYS®	PR
Aspelund et al. (2010)	Aspen HYSYS®	-
Castillo and Dorao (2012)	Aspen HYSYS®	-
Del Nogal et al. (2008)	WORK	PR, SRK
Hatcher et al. (2012)	Aspen HYSYS®	PR
He and Ju (2014a)	Aspen HYSYS®	PR
He and Ju (2014b)	Aspen HYSYS®	PR
Hwang et al. (2013a)	Aspen HYSYS®	PR
Hwang et al. (2013b)	Aspen HYSYS®	PR
Jensen and Skogestad (2008)	gPROMS®	-
Kamath et al. (2012)	GAMS	SRK
Khan and Lee (2013)	UniSim®	PR
Khan et al. (2012)	UniSim®	PR
Lee et al. (2012)	Aspen HYSYS®	PR
Lee et al. (2014)	Aspen HYSYS®	PR
Morin et al. (2011)	Aspen HYSYS®	-
Shah et al. (2009)	Aspen HYSYS®	PR
Shirazi and Mowla (2010)	MATLAB®/Aspen HYSYS®	PR
Skaugen et al. (2010)	Aspen HYSYS® / PRO/II	-
Taleshbahrami and Saffari (2010)	MATLAB® / Aspen HYSYS®	PR
Wahl et al. (2013)	Aspen HYSYS®	PR, SRK
Wang et al. (2013b)	Aspen HYSYS®	PR
Wang et al. (2012)	GAMS/Aspen Plus®	PR
Wang et al. (2011)	Aspen Plus®	PR
Xu et al. (2013)	Aspen Plus®	PR
Xu et al. (2014)	Aspen Plus®	PR
Yoon et al. (2012)	Aspen HYSYS®	PR

The study presented by Kamath et al. (2012) stands out in the sense that the process model has been modelled and optimized in GAMS. By use of an equation-oriented

process model, access to derivative information is enabled. The optimization problem was solved using CONOPT, which is based on the generalized reduced gradient method (Drud, 1985).

Another path that differs from the common approach was taken by Wang et al. (2012). Based on simulations in Aspen Plus®, linear and quadratic regression was used to create a simplified process model. This model was then optimized using the branch-and-cut optimization method LINDOGlobal in GAMS. In the end, the final results were validated and fine-tuned in the Aspen Plus® model.

Obviously, the complexity of the optimization problem increases with the complexity of the refrigeration cycles. Wahl et al. (2013) performed optimization of a PRICO® process modelled with cubic equations of state using a sequential quadratic programming method in a multi-start approach from randomly generated starting points. All solutions are found to be within 1 % of the best solution found. This indicates that for such simple processes, the non-convexity of the optimization problem may not be very prominent.

Neither stochastic search methods nor deterministic local search methods can provide any guarantee of finding the global optimal solution to the optimization problem. In general, a stochastic search requires many iterations and is therefore slower than the local search methods. With development in global optimization techniques and better modelling of the process, more and more process designs are likely to be optimized with high accuracy and confidence. Thermodynamic analysis and tool may also facilitate process optimization.

2.10.2 Alternative design strategies

As previously discussed, all practical processes are irreversible to some extent. By use of exergy analysis, these irreversibilities can be identified and quantified, so as to locate opportunities for improving the process. An introduction to exergy analysis is given by Kotas (1995).

Usually, exergy analysis is applied as a diagnostic tool, used for comparison of different process alternatives or in order to unveil the largest potentials for improvement. A selection of LNG process analysis using exergy analysis is given in Table 2.3. In addition, Rian and Ertesvåg (2012) presented an exergy analysis for a complete LNG plant where a mixed-refrigerant cascade process was used for liquefaction. A review of exergy analysis of heat exchangers was provided by Manjunath and Kaushik (2014).

Despite enabling allocation of energy saving opportunities, exergy is a tool focused on unit operations rather than the overall process (Aspelund et al., 2007). Hence, in order to apply exergy analysis for process design, different methodologies have been proposed where exergy analysis is combined with pinch analysis (Smith, 2005; Kemp, 2007), which is a systems oriented approach to process design.

Linnhoff and Dhole (1992) and Dhole and Linnhoff (1994) proposed design methods for low-temperature processes based on exergy analysis and pinch analysis. In the procedure proposed by Linnhoff and Dhole (1992), the exergy grand composite curve is used to estimate changes in shaftwork requirements without re-simulating the refrigeration system. Dhole and Linnhoff (1994) presented a systematic three-stage design methodology for shaftwork targeting, column targeting and refrigeration system design.

Table 2.3. Exergy analyses of LNG processes.

Process concept	Studies
Single mixed-refrigerant	Chiu and Newton (1980)
	Remeljej and Hoadley (2006)
	Marmolejo-Correa and Gundersen (2012)
Pure-refrigerant cascade	Kanoğlu (2002)
	Tsatsaronis and Morosuk (2010)
	Cipolato et al. (2012)
Reverse Brayton	Remeljej and Hoadley (2006)
Propane-precooled mixed-refrigerant	Chiu and Newton (1980)
	Vatani et al. (2014)
Dual mixed-refrigerant	Vatani et al. (2014)
Mixed-refrigerant cascade	Vatani et al. (2014)

Aspelund et al. (2007) proposed a methodology named ExPAnD for design of process operating at sub-ambient temperature. Also this approach was based on pinch analysis and exergy analysis. Heuristic guidelines were proposed for inclusion of pressure-based exergy transfer in heat exchanger network design below ambient temperature. The proposed methodology was used to derive the LNG process concept presented by Aspelund et al. (2009a, 2009b, 2009c, 2009d). Wechsung et al. (2011) implemented the methodology in a mathematical programming framework.

Marmolejo-Correa and Gundersen (2013) proposed a graphical approach for energy targeting in processes where both temperature and pressure are important design variables, such as low-temperature processes. Also this procedure combines features of exergy analysis and pinch analysis. In a case study, the methodology was used for design of a nitrogen expander process. Design methods based on pinch and exergy

analysis have also been proposed by Feng and Zhu (1997) and Anantharaman et al. (2006).

2.10.3 Optimal process operation

Operational degrees of freedom in a propane-precooled mixed-refrigerant process were identified by Jacobsen and Skogestad (2011). Jacobsen and Skogestad (2013) studied optimal operation of a single mixed-refrigerant process under disturbances in ambient conditions and discussed choice of control variables for different operation regimes.

Jensen and Skogestad (2006) discussed strategies of self-optimizing control (Skogestad, 2000a, 2000b) for optimal operation of a mixed-refrigerant cascade process. In yet another study, Jensen and Skogestad (2008) discussed differences in optimal design and optimal operation. Studies on optimal control of a dual mixed-refrigerant process (TEALARC) have been presented by Michelsen et al. (2010a, 2010b, 2010c). Singh et al. (2008) used self-optimizing control to maximize LNG production in a single mixed-refrigerant process. Also Husnil and Lee (2014) studied optimal operation of a mixed-refrigerant LNG process.

2.10.4 Optimization in the LNG plant

Despite the fact that most studied related to optimization in LNG plant have been dedicated to the liquefaction process itself, also other important operations in an LNG plant have been subject to study in the literature.

Since natural gas liquefaction is energy intensive, the power supply is also complex. Del Nogal et al. (2010) performed optimization of the power system in an LNG plant, in order to choose drivers and generators, and compressor arrangement. Optimal compressor operation in an LNG plant was also studied by Hasan et al. (2009b), with the objective of determining the optimal load distribution between different refrigeration cycles. Power system optimization was also performed by Manesh et al. (2009). Hasan et al. (2011) optimized the fuel network in an LNG plant.

Several studies on design and optimization of heavy hydrocarbon extraction in LNG plants have also been presented (Diaz et al., 1997; Madouri, 2004; Alfadala et al., 2005; Mehrpooya et al., 2006, 2009, 2010; Dimopoulos and Frangogoulos, 2008; Tahouni et al., 2010, 2011; Ghorbani et al., 2012).

2.10.5 Optimization elsewhere in the LNG value chain

Optimization has been applied also in other parts of the LNG value chain. Among these applications, Boulougouris and Papanikolaou (2008), Ku et al. (2014) and Hwang and Lee (2014) have presented optimization studies for design of a floating

LNG terminals. Zellouf and Portannier (2011), Lukaszewski et al. (2013) and Deshpande et al. (2011) all studied issues related to LNG storage.

Hasan et al. (2009c) minimized the boil-off losses in LNG transportation, while Shin et al. (2007), Park et al. (2010, 2011, 2012), Jang et al. (2011), Li and Chen (2012) and Li et al. (2012) studied LNG receiving terminals. Studies on cold exergy recovery in LNG regasification has been provided by, Dispenza et al. (2009a, 2009b, 2009c). Szargut and Szczygiel (2009) among others.

2.10.6 Optimization in LNG trade

The geographical mismatch between the location of resources and the location of demands drives an expansion of international trade (IEA, 2012). Traditionally, most gas in continental Europe has been traded under long-term contracts with oil-price indexation, but that is changing with a growing share of prices now being set by gas-to-gas competition (IEA, 2012).

Rising LNG supplies, increased short-term trading and greater operational flexibility are likely to lead to increasing price connectivity between regions and a degree of price convergence (IEA, 2012). Today, most international gas trade is organized under long-term contracts of 10-25 years coverage where the price has been indexed to the prices of competing fuels. A growing share of worldwide gas is traded on a spot basis. There is also a growing use of medium-term contracts of 2-4 years duration (IEA, 2012). In 2011, the spot market accounted for around one third of all LNG trade (IEA, 2012).

Models have been proposed for regional and global gas markets considering the whole gas value chain from producers to market (Egging et al., 2008, 2010; Egging, 2013). In these models different transmission options are considered. Khalilpour and Karimi (2011) optimized a natural gas value chain where LNG, CNG and GTL were considered as options for utilization of stranded gas.

More specific to the LNG market, Berle et al. (2013) presented an optimization model for a simplified LNG transportation network. Vessel routing and planning were optimized by Fodstad et al. (2010) for maximization of profit along LNG value chains from production to consumption. Optimization studies of an LNG value chain have also been presented by Furlonge (2008, 2011). Goel et al. (2012) optimized LNG transport schedules in order to minimize cost associated with lost production, stock-out and unmet contractual demands.

Grønhaug et al. (2010) maximized the profit of an LNG value chain by designing sailing routes and schedules. LNG vessel routing and scheduling were also subject to optimization in studies presented by Halvorsen-Weare and Fagerholt (2013) and

Halvorsen-Weare et al. (2013). In a study presented by Kuwahara et al. (2000), the cost of fulfilling contractual natural gas delivery requirements was minimized as a function of plant capacities, ship capacities and fleet size.

Massol and Tchung-Ming (2010) studied the possibility of cooperation between LNG exporters for maximization of collective profit. An LNG receiving terminal and vessel scheduling were optimized by Özelkan et al. (2008) for maximization of profit. Optimization models for LNG ship routing and scheduling were also proposed by Rakke et al. (2011) and Stålhane et al. (2012) taking into account the opportunity to sell excess LNG in the spot market. LNG value chain optimization was also subject to study by Uggen et al. (2013).

Natural gas liquefaction projects require very large investments. Hence, despite growing market for short- and medium-term contracts, Wood (2012) concluded that LNG trade will continue to be dominated by long-term contracts. According to Wood (2012), short-term contracts will still represent less than 20 % of LNG trade in 2022.

2.11 Conclusions

Most work related to applications of optimization in the LNG values chain has been concerned with the liquefaction process. In the majority of these studies, a commercial process simulator is used for modelling using a cubic equation of state connected to an external optimization algorithm. The optimization methods used have typically been stochastic search methods (especially genetic algorithms) or local deterministic search methods (typically sequential quadratic programming). Hybrid approaches combing the two have also been applied.

For the majority of the studies presented on LNG process optimization, relatively simple process concepts such as single mixed-refrigerant processes and propane-precooled mixed-refrigerant processes have been studied. In recent years, optimization studies have been presented also for slightly more complex process concepts such as the dual mixed-refrigerant process.

In order to enable optimization of more complex process concepts, both the problem formulation and the optimization methods should be improved.

2.12 References

Afrianto H, Tanshen MR, Munkhbayar B, Suryo UT, Chung H, Jeong H. A numerical investigation on LNG flow and heat transfer characteristic in heat exchanger. *International Journal of Heat and Mass Transfer* 2014;68:110-118.

Alabdulkarem A, Mortazavi A, Hwang Y, Radermacher R, Rogers P. Optimization of propane pre-cooled mixed refrigerant LNG plant. *Applied Thermal Engineering* 2011;31(6-7):1091-1098.

Alfadala HE, Ahmad BM, Warsame AF. A hierarchical approach to optimize LNG fractionation units. *Computer Aided Chemical Engineering* 2005;20:1279-1284.

Anantharaman R, Abbas OS, Gundersen T. Energy Level Composite Curves – A new graphical methodology for the integration of energy intensive processes. *Applied Thermal Engineering* 2006;26(13):1378-1384.

Aspelund A, Berstad DO, Gundersen T. An Extended Pinch Analysis and Design procedure utilizing pressure based exergy for subambient cooling. *Applied Thermal Engineering* 2007;27(16): 2633-2649.

Aspelund A, Gundersen T. A liquefied energy chain for transport and utilization of natural gas for power production with CO_2 capture and storage – Part 1. *Applied Energy* 2009a;86(6):781-792.

Aspelund A, Gundersen T. A liquefied energy chain for transport and utilization of natural gas for power production with CO_2 capture and storage – Part 2: The offshore and the onshore processes. *Applied Energy* 2009b;86(6):793-804.

Aspelund A, Gundersen T. A liquefied energy chain for transport and utilization of natural gas for power production with CO_2 capture and storage – Part 3: The combined carrier and onshore process. *Applied Energy* 2009c;86(6):805-814.

Aspelund A, Gundersen T. A liquefied energy chain for transport and utilization of natural gas for power production with CO_2 capture and storage – Part 3: The combined carrier and onshore process. *Applied Energy* 2009d;86(6):815-825.

Aspelund A, Gundersen T, Myklebust J, Nowak MP, Tomasgard A. An optimization-simulation model for a simple LNG process. *Computers and Chemical Engineering* 2010;34(10):1606-1617.

Avidan A, Messersmith D, Martinez B. LNG liquefaction technologies move toward greater efficiencies, lower emissions. *Oil and Gas Journal* 2002;100(33):60-68.

Backhaus S, Swift GW. A thermoacoustic Stirling heat engine. *Nature* 1999;399(6734):335-338.

Bahadori A. *Natural Gas Processing Technology and Engineering Design*. Oxford: Elsevier; 2014.

Barclay M, Denton N. Selecting offshore LNG processes. *LNG Journal* 2005;10(1):34-36.

Barnés FJ, King CJ. Synthesis of cascade refrigeration and liquefaction systems. *Industrial and Engineering Chemistry Process Design and Development* 1974;13(4):421-433.

Berle Ø, Norstad I, Asbjørnslett BE. Optimization, risk assessment and resilience in LNG transportation systems. *Supply Chain Management* 2013;18(3):253-264.

Biegler LT. Improved infeasible path optimization for sequential path optimization for sequential modular simulators – I: The interface. *Computers and Chemical Engineering* 1985;9(3):245-256.

Biegler LT. *Nonlinear Programming: Concepts, Algorithms, and Applications to Chemical Processes*. Philadelphia: Society for Industrial and Applied Mathematics; 2010.

Biegler LT, Cuthrell JE. Improved infeasible path optimization for sequential path optimization for sequential modular simulators – II: The optimization algorithm. *Computers and Chemical Engineering* 1985;9(3):257-267.

Biegler LT, Grossmann IE. Retrospective on optimization. *Computers and Chemical Engineering* 2004;28(8):1169-1192.

Biegler LT, Hughes RR. Infeasible path optimization with sequential modular simulators. *AIChE Journal* 1982;28(6):994-1002.

Boulougouris EK, Papanikolaou AD. Multi-objective optimisation of a floating LNG terminal. *Ocean Engineering* 2008;35(8-9):787-811.

Box MJ. A new method of constrained optimization and a comparison with other methods. *The Computer Journal* 1965;8(1):42-52.

BP plc. BP Energy Outlook 2035 [Internet]; 2014a [cited 2014 Sep 16]. Available from: http://www.bp.com/energyoutlook.

BP plc. BP Statistical Review of World Energy 2014 [Internet]; 2014b [cited 2014 Sep 16]. Available from: http://www.bp.com/statisticalreview.

Byrne RP, Bogle IDL. Global optimization of modular process flowsheets. *Industrial and Engineering Chemistry Research* 2000;39(11):4296-4301.

Castillo L, Dorao CA. Influence of the plot area in an economical analysis for selecting small scale LNG technologies for remote gas production. *Journal of Natural Gas Science and Engineering* 2010;2(6):302-309.

Castillo L, Dorao CA. Consensual decision-making model based on game theory for LNG processes. *Energy Conversion and Management* 2012;64:387-396.

Chang H-M, Lim HS, Choe KH. Effect of multi-stream heat exchanger on performance of natural gas liquefaction with mixed refrigerant. *Cryogenics* 2012;52(12):642-647.

Cheng WB, Mah RSH. Interactive synthesis of cascade refrigeration systems. *Industrial and Engineering Chemistry Process Design and Development* 1980;19(3):410-420.

Chiu C-H, Newton CL. Second law analysis in cryogenic processes. *Energy* 1980;5(8-9):899-904.

Cipolato L, Lirani MCA, Costa TV, Fábrega FM, d'Angelo JVH. Exergetic optimization of a refrigeration cycle for natural gas liquefaction. *Computer Aided Chemical Engineering* 2012;31:440-444.

Dauber F, Span R. Modelling liquefied-natural-gas processes using highly accurate property models. *Applied Energy* 2011;97:822-827.

Del Nogal F, Kim J-K, Perry S, Smith R. Optimal design of mixed refrigerant cycles. *Industrial and Engineering Chemistry Research* 2008;47(22):8724-8740.

Del Nogal FL, Kim J-K, Perry S, Smith R. Synthesis of mechanical driver and power generation configurations, Part 2: LNG applications. *AIChE Journal* 2010;56(9):2377-2389.

Deshpande KB, Zimmerman WB, Tennant MT, Webster MB, Lukaszewski MW. Optimization methods for real-time inverse problem posed by modelling of liquefied natural gas storage. *Chemical Engineering Journal* 170(1):44-52.

Dhole VR, Linnhoff B. Overall design of low temperature processes. *Computers and Chemical Engineering* 1994;18(Suppl. 1):S105-S111.

Diaz MS, Serrani A, Bandoni JA, Brignole EA. Automatic design and optimization of natural gas plants. *Industrial and Engineering Chemistry Research* 1997;36(7):2715-2724.

Dimopoulos GG, Frangopoulos CA. Synthesis, design and operation optimization of the marine energy system for a liquefied natural gas carrier. *International Journal of Thermodynamics* 2008;11(4):203-211.

Dispenza C, Dispenza G, La Rocca V, Panno G. Exergy recovery during LNG regasification: Electric energy production – Part one. *Applied Thermal Engineering* 2009a;29(2-3):380-387.

Dispenza C, Dispenza G, La Rocca V, Panno G. Exergy recovery during LNG regasification: Electric energy production – Part two. *Applied Thermal Engineering* 2009b;29(2-3):388-399.

Dispenza C, Dispenza G, La Rocca V, Panno G. Exergy recovery in regasification facilities – Cold utilization: A modular unit. *Applied Thermal Engineering* 2009c;29(17-18):3595-3608.

Dorigo M, Maniezzo V, Colorni A. Ant system: Optimization by a colony of cooperating agents. *IEEE Transactions on Systems, Man, and Cybernetics, Part B: Cybernetics* 1996;26(1):29-41.

Drud A. CONOPT: A GRG code for large sparse dynamic nonlinear optimization problems. *Mathematical Programming* 1985;31(2):153-191.

Economides MJ, Sun K, Subero G. Compressed natural gas (CNG): An alternative to liquefied natural gas (LNG). *SPE Production and Operations* 2006;21(2):318-324.

Egging R. Benders Decomposition for multi-stage stochastic mixed complementarity problems – Applied to a global natural gas market model. *European Journal of Operational Research* 2013;226(2):341-353.

Egging R, Gabriel SA, Holz F, Zhuang J. A complementarity model for the European natural gas market. *Energy Policy* 2008;36(7):2385-2414.

Egging R, Holz F, Gabriel SA. The World Gas Model. A multi-period mixed complementarity model for the global natural gas market. *Energy* 2010;35(10);4016-4029.

Feng X, Zhu XX. Combining pinch and exergy analysis for process modifications. *Applied Thermal Engineering* 1997;17(3):249-261.

Finn AJ, Johnson GL, Thomlinson TR. Developments in natural gas liquefaction. *Hydrocarbon Processing* 1999;78(4):47-59.

Floudas CA, Gounaris CE. A review of recent advances in global optimization. *Journal of Global Optimization* 2009;45(1):3-38.

Fodstad M, Uggen KT, Rømo F, Lium A-G, Stremersch G, Hecq S. LNGScheduler: a rich model for coordinating vessel routing, inventories and trade in the liquefied natural gas supply chain. *The Journal of Energy Markets* 2010;3(4):31-64.

Furlonge HI. Optimal distribution of economic value along the LNG chain from government and investor perspectives. *Energy Exploration and Exploitation* 2008;26(6):397-416.

Furlonge HI. A stochastic optimisation framework for analysing economic returns and risk distribution in the LNG business. *International Journal of Energy Sector Management* 2011;5(4):471-493.

Ghorbani B, Salehi GR, Ghaemmaleki H, Amidpour M, Hamedi MH. Simulation and optimization of refrigeration cycle in NGL recovery plants with exergy-pinch analysis. *Journal of Natural Gas Science and Engineering* 2012;7:35-43.

Glover F. Future paths for integer programming and links to artificial intelligence. *Computers and Operations Research* 1986;13(5):533-549.

Glover F, Taillard E, de Werra D. A user's guide to tabu search. *Annals of Operations Research* 1993;41(1):3-28.

Goel V, Furman KC, Song J-H, El-Bakry AS. Large neighbourhood search for LNG inventory routing. *Journal of Heuristics* 2012;18(6):821-848.

Gong MQ, Luo EC, Liang JT, Zhou Y, Wu JF. Thermodynamic analysis of a mixed-refrigerant auto-cascade J-T cryocooler with distributed heat loads. *Cryocoolers* 2001;11:523-530.

Groboski MS, Daubert TE. A modified Soave equation of state for phase equilibrium calculations. 1. Hydrocarbon systems. *Industrial and Engineering Chemistry Process Design and Development* 1978a;17(4):443-448.

Groboski MS, Daubert TE. A modified Soave equation of state for phase equilibrium calculations. 2. Systems containing CO_2, H_2S, N_2 and CO. *Industrial and Engineering Chemistry Process Design and Development* 1978b;17(4):448-454.

Grønhaug R, Christiansen M, Desaulniers G, Desrosiers J. A branch-and-price method for liquefied natural gas inventory routing problem. *Transportation Science* 2010;44(3):400-415.

Grootjans HF, Nagelvoort RK, Vink KJ. Liquefying a stream enriched in methane, US Patent 6370910. 2002.

Grossmann IE, Biegler LT. Part II. Future perspective on optimization. *Computers and Chemical Engineering* 2004;28(8):1193-1218.

Halvorsen-Weare EE, Fagerholt K. Routing and scheduling in a liquefied natural gas shipping problem with inventory and berth constraints. *Annals of Operations Research* 2013;203(1):167-186.

Halvorsen-Weare EE, Fagerholt K, Rönnqvist M. Vessel routing and scheduling under uncertainty in the liquefied natural gas business. *Computers and Industrial Engineering* 2013;64(1):290-301.

Hasan MMF, Karimi IA, Alfadala HE, Grootjans H. Operational modeling of multistream heat exchangers with phase changes. *AIChE Journal* 2009a;55(1):150-171.

Hasan MMF, Razib MS, Karimi IA. Optimization of compressor networks in LNG operations. *Computer Aided Chemical Engineering* 2009b;27:1767-1772.

Hasan MMF, Zheng AM, Karimi IA. Minimizing boil-off losses in liquefied natural gas transportation. *Industrial and Engineering Chemistry Research* 2009c;48(21):9571-9580.

Hasan MMF, Karimi IA, Avison CM. Preliminary synthesis of fuel gas networks to conserve energy and preserve the environment. *Industrial and Engineering Chemistry Research* 2011;50(12):7414-7427.

Hatcher P, Khalilpour R, Abbas A. Optimisation of LNG mixed-refrigerant processes considering operation and design objectives. *Computers and Chemical Engineering* 2012;41:123-133.

He T, Ju Y. A novel conceptual design of parallel nitrogen expansion liquefaction process for small-scale LNG (liquefied natural gas) plant in skid-mounted packages. *Energy* 2014a;75:349-359.

He T, Ju Y. Design and optimization of a novel mixed refrigerant cycle integrated with NGL recovery process for small-scale LNG plant. *Industrial and Engineering Chemistry Research* 2014b;53(13):5545-5553.

Husnil YA, Lee M. Control structures for operational optimization of mixed refrigerant processes for liquefied natural gas plant. *AIChE Journal* 2014;60(7):2428-2441.

Hwang J, Lee K-Y. Optimal liquefaction process cycle considering simplicity and efficiency for LNG FPSO at FEED stage. *Computers and Chemical Engineering* 2014;63:1-33.

Hwang J-H, Ku N-K, Roh M-I, Lee K-Y. Optimal design of liquefaction cycles of liquefied natural gas floating, production, storage, and offloading unit considering optimal synthesis. *Industrial and Engineering Chemistry Research* 2013a;52(15):5341-5356.

Hwang J-H, Roh M-I, Lee K-Y. Determination of the optimal operating conditions of the dual mixed refrigerant cycle for the LNG FPSO topside liquefaction process. *Computer and Chemical Engineering* 2013b;49:25-36.

IEA. World Energy Outlook 2012. [Internet]; 2012 [cited 2014 Sep 16]. Available from: http://www.worldenergyoutlook.org/publications/weo-2012/.

Jacobsen MG, Skogestad S. Optimization of LNG plants – challenges and strategies. *Computer Aided Chemical Engineering* 2011;29:1854-1858.

Jacobsen MG, Skogestad S. Active constraint regions for a natural gas liquefaction process. *Journal of Natural Gas Science and Engineering* 2013;10:8-13.

Jang N, Shin MW, Choi SH, Yoon ES. Dynamic simulation and optimization of boil-off gas compressors in a liquefied natural gas gasification plant. *Korean Journal of Chemical Engineering* 2011;28(5):1166-1171.

Jensen JB, Skogestad S. Optimal operation of a mixed fluid cascade LNG plant. *Computer Aided Chemical Engineering* 2006;21:1569-1574.

Jensen JB, Skogestad S. Problems with specifying ΔT_{min} in the design of processes with heat exchangers. *Industrial and Engineering Chemistry Research* 2008;47(9):3071-3075.

Kalinowski P, Hwang Y, Radermacher R, Al Hashimi S, Rodgers P. Application of waste heat powered absorption refrigeration system to the LNG recovery process. *International Journal of Refrigeration* 2009;32(4):687-694.

Kamath RS, Biegler LT, Grossmann IE. An equation-oriented approach for handling thermodynamics based on cubic equation of state in process optimization. *Computers and Chemical Engineering* 2010;34(12):2085-2096.

Kamath RS, Biegler LT, Grossmann IE. Modeling multistream heat exchangers with and without phase changes for simultaneous optimization and heat integration. *AIChE Journal* 2012;58(1):190-204.

Kanoğlu M. Exergy analysis of multistage cascade refrigeration cycle used for natural gas liquefaction. *International Journal of Energy Research* 2002;26(8):763-774.

Karaboga D, Basturk B. On the performance of artificial bee colony (ABC) algorithm. *Applied Soft Computing Journal* 2008;8(1):687-697.

Kemp IC. *Pinch Analysis and Process Integration: a user guide on process integration for the efficient use of energy*. 2nd ed. Oxford: Butterworth-Heinemann; 2007.

Kennedy J, Eberhart R. Particle Swarm Optimization. In: Proceedings of the IEEE International Conference on Neural Networks. Vol. 4. 1995. p. 1942-1948.

Khalilpour R, Karimi IA. Investment portfolios under uncertainty for utilizing natural gas resources. *Computers and Chemical Engineering* 2011;35(9):1827-1837.

Khalilpour R, Karimi IA. Evaluation of utilization alternatives for stranded natural gas. *Energy* 2012;40():317-328.

Khan MS, Lee M. Design optimization of single mixed refrigerant natural gas liquefaction process using the particle swarm paradigm with nonlinear constraints. *Energy* 2013;49(1):146-155.

Khan MS, Lee S, Lee M. Optimization of single mixed refrigerant natural gas liquefaction plant with nonlinear programming. *Asia-Pacific Journal of Chemical Engineering* 2012;7(Suppl. 1):S62-S70.

Kirkpatrick S, Gelatt Jr CD, Vecchi MP. Optimization by Simulated Annealing. *Science* 1983;220(4598):671-680.

Kotas TJ. *The Exergy Method of Thermal Plant Analysis*. Malabar: Krieger Publishing Company; 1995.

Ku N-K, Hwang J-H, Lee J-C, Roh M-I, Lee K-Y. Optimal module layout for generic offshore LNG liquefaction process of LNG-FPSO. *Ships and Offshore Structures* 2014;9(3):311-332.

Kuwahara N, Bajay SV, Castro LN. Liquefied natural gas supply optimisation. *Energy Conversion and Management* 2000;41(2):153-161.

Lee I, Tak K, Kwon H, Kim J, Ko D, Moon I. Design and optimization of a pure refrigerant cycle for natural gas liquefaction with subcooling. *Industrial and Engineering Chemistry Research* 2014;53(25):10397-10403.

Lee KS, Geem ZW. A new meta-heuristic algorithm for continuous engineering optimization: Harmony search theory and practice. *Computer Methods in Applied Mechanics and Engineering* 2005;194(36-38):3902-3933.

Lee S, Long NVD, Lee M. Design and optimization of natural gas liquefaction and recovery processes for offshore floating liquefied natural gas plants. *Industrial and Engineering Chemistry Research* 2012;51(30):10021-10030.

Lim W, Choi K, Moon I. Current status and perspectives of liquefied natural gas (LNG) plant design. *Industrial and Engineering Chemistry Research* 2013;52(9):3065-3088.

Li QY, Ju YL. Design and analysis of liquefaction process for offshore associated gas resources. *Applied Thermal Engineering* 2010;30(16):2518-2525.

Li Y, Chen X. Dynamic simulation for improving the performance of boil-off gas recondensation systems at LNG receiving terminals. *Chemical Engineering Communications* 2012;199(10):1251-1262.

Li Y, Chen X, Chein M-H. Flexible and cost-effective optimization of BOG (boil-off gas) recondensation process at LNG receiving terminals. *Chemical Engineering Research and Design* 2012;90(10):1500-1505.

Linnhoff B, Dhole VR. Shaftwork Targets for low-temperature process design. *Chemical Engineering Science* 1992;47(8):2081-2091.

Liu Y-N, Pervier JW. Dual mixed refrigerant natural gas liquefaction; US Patent 4545795. 1985.

Lukaszewski MW, Zimmerman WBJ, Tennant MT, Webster MB. Application of inverse methods based algorithms to Liquefied Natural Gas (LNG) storage management. *Chemical Engineering Research and Design* 2013;91(3):457-463.

Madouri A. Optimized LPG extraction improves LNG high heating value. *Oil and Gas Journal* 2004;102(35):53-55.

Manesh MHK, Mazhari V, Amidpour M. Power Plant Optimization Study in Iran LNG Project through MINLP Method. *Chemical Engineering Transactions* 2009;18:935-940.

Manjunath K, Kaushik SC. Second law thermodynamic study of heat exchangers: A review. *Renewable and Sustainable Energy Reviews* 2014;40:348-374.

Marmolejo-Correa D, Gundersen T. A comparison of exergy efficiency definitions with focus on low temperature processes. *Energy* 2012;44(1):477-489.

Marmolejo-Correa D, Gundersen T. New graphical representation of exergy applied to low temperature process design. *Industrial and Engineering Chemistry Research* 2013;52(22):7145-7156.

Massol O, Tchung-Ming S. Cooperation among liquefied natural gas suppliers: Is rationalization the sole objective? *Energy Economics* 2010;32(4):933-947.

Mehrpooya M, Gharagheizi F, Vatani A. Thermoeconomic analysis of a large industrial propane refrigeration cycle used in NGL recovery plant. *International Journal of Energy Research* 2009;33(11):960-977.

Mehrpooya M, Jarrahian A, Pishvaie MR. Simulation and exergy-method analysis of an industrial refrigeration cycle used in NGL recovery units. *International Journal of Energy Research* 2006;30(15):1336-1351.

Mehrpooya M, Vatani A, Mousavian SMA. Optimum design of integrated liquid recovery plants by variable population size genetic algorithm. *Canadian Journal of Chemical Engineering* 2010;88(6):1054-1064.

Melaaen IS, Owren G. How do the inaccuracies of enthalpy and vapour-liquid equilibrium calculations influence baseload LNG plant design? *Computers and Chemical Engineering* 1996;20(1):1-11.

Michelsen FA, Halvorsen IJ, Lund BF. The impact of process design decisions on operability and control of an LNG process. *Journal of Natural Gas Science and Engineering* 2010a;2(4):183-191.

Michelsen FA, Halvorsen IJ, Lund BF, Wahl PE. Modeling and simulation for control of the TEALARC liquified natural gas process. *Industrial and Engineering Chemistry Research* 2010b;49(16):7389-7397.

Michelsen FA, Lund BF, Halvorsen IJ. Selection of optimal, controlled variables for the TEALARC LNG process. *Industrial and Engineering Chemistry Research* 2010c;49(18):8624-8632.

Mokhatab S, Mak JY, Valappil JV, Wood DA. *Handbook of Liquefied Natural Gas*. Oxford: Elsevier; 2014.

Morin A, Wahl PE, Mølnvik M. Using evolutionary search to optimise the energy consumption for natural gas liquefaction. *Chemical Engineering Research and Desisgn* 2011;89(11):2428-2441.

Mortazavi A, Somers C, Alabdulkarem A, Hwang Y, Radermacher R. Enhancement of APCI cycle efficiency with absorption chillers. *Energy* 2010;35(9):3877-3882.

Nasrifar K, Bolland O. Prediction of thermodynamic properties of natural gas mixtures using 10 equations of state including a new cubic two-constant equation of state. *Journal of Petroleum Science and Engineering* 2006;51(3-4):253-266.

Nasrifar K, Moshfeghian M. A saturated liquid density equation in conjunction with the Predictive-Soave-Redlich-Kwong equation of state for pure refrigerants and LNG multicomponent systems. *Fluid Phase Equilibria* 1998;153(2):231-242.

Nelder JA, Mead R. A simplex method for function minimization. *The Computer Journal* 1965;7(4):308-313.

Newton CL. Dual mixed refrigerant natural gas liquefaction with stages compression, US Patent 4525185. 1985.

Nocedal J, Wright SJ. *Numerical Optimization*. 2nd ed. New York: Springer; 2006.

Özelkan EC, D'Ambrosio A, Teng SG. Optimizing liquefied natural gas terminal design for effective supply-chain operations. *International Journal of Production Economics* 2008;111(2):529-542.

Park C, Lee C-J, Lim Y, Lee S, Han C. Optimization of recirculation operating in liquefied natural gas receiving terminal. *Journal of the Taiwan Institute of Chemical Engineers* 2010;41(4):482-491.

Park C, Lim Y, Lee S, Han C. BOG handling method for energy saving in LNG receiving terminal. *Computer Aided Chemical Engineering* 2011;29:1829-1833.

Park C, Song K, Lee S, Lim Y, Han C. Retrofit design of a boil-off gas handling process in liquefied natural gas receiving terminals. *Energy* 2012;44(1):69-78.

Peng D-Y, Robinson DB. A new two-constant equation of state. *Industrial and Engineering Chemistry Fundamentals* 1976;15(1):59-64.

Quack H. Theory of cascade refrigeration. *AIP Conference Proceedings* 2012;1434(57):783-789.

Rakke JG, Stålhane M, Moe CR, Christiansen M, Andersson H, Fagerholt K, Norstad I. A rolling horizon heuristic for creating a liquefied natural gas annual delivery program. *Transportation Research Part C: Emerging Technologies* 2011;19(5):896-911.

Rangaiah GP, editor. *Stochastic Global Optimization: Techniques and Applications in Chemical Engineering*. Singapore: World Scientific; 2010.

Ransbarger W. A fresh look at LNG process efficiency. *Hydrocarbon Engineering* 2007;12(Suppl.):73-74,76-78,80.

Remeljej CW, Hoadley AFA. An exergy analysis of small-scale liquefied natural gas (LNG) liquefaction processes. *Energy* 2006;31(12):2005-2019.

Rian AB, Ertesvåg IS. Exergy evaluation of the arctic Snøhvit liquefied natural gas processing plant in northern Norway – Significance of ambient temperature. *Energy and Fuels* 2012;26(2):1259-1267.

Roberts MJ, Agrawal R. Hybrid cycle for the production of liquefied natural gas, US Patent 6308531. 2001.

Rodgers P, Mortazavi A, Eveloy V, Al-Hashimi S, Hwang Y, Radermacher R. Enhancement of LNG plant propane cycle through waste heat powered absorption cooling. *Applied Thermal Engineering* 2012;48:41-53.

Shah NM, Hoadley AFA, Rangaiah GP. Inherent safety analysis of a propane precooled gas-phase liquified natural gas process. *Industrial and Engineering Chemistry Research* 2009;48(10):4917-4927.

Shin MW, Shin D, Choi SH, Yoon ES, Han C. Optimization of the operation of boil-off gas compressors at a liquified natural gas gasification plant. *Industrial and Engineering Chemistry Research* 2007;46(20):6540-6545.

Shirazi MMH, Mowla D. Energy optimization for liquefaction process of natural gas in peak shaving plant. *Energy* 2010;35(7):2878-2885.

Shukri T. LNG technology selection. *Hydrocarbon Engineering* 2004;9(2):71-76.

Singh A, Hovd M, Kariwala V. Controlled variables selection for liquefied natural gas plant. *IFAC Proceedings Volumes* 2008;17(1):13913-13918.

Skaugen G, Gjøvåg, GA, Nekså P, Wahl PE. Use of sophisticated heat exchanger simulation models for investigation of possible design and operational pitfalls in LNG processes. *Journal of Natural Gas Science and Engineering* 2010;2(5):235-243.

Skaugen G, Kolsaker K, Walnum HT, Wilhelmsen Ø. A flexible and robust modelling framework for multi-stream heat exchangers. *Computers and Chemical Engineering* 2013;49:95-104.

Skogestad S. Plantwide control: the search for the self-optimizing control structure. *Journal of Process Control* 2000a;10(5):487-507.

Skogestad S. Self-optimizing control: The missing link between steady-state optimization and control. *Computers and Chemical Engineering* 2000b;24(2-7):569-575.

Smith R. *Chemical Process Design and Integration*. Chichester: John Wiley & Sons; 2005.

Soave G. Equilibrium constants from a modified Redlich-Kwong equation of state. *Chemical Engineering Science* 1972;27(6):1197-1203.

Stålhane M, Rakke JG, Moe CR, Andersson H, Christiansen M, Fagerholt K. A construction and improvement heuristic for a liquefied natural gas inventory routing problem. *Computers and Industrial Engineering* 2012;62(1):245-255.

Stockmann R, Forg W, Bolt M, Steinbauer M, Pfeiffer C, Paurola P, Fredheim AO, Sorensen O. Method for liquefying a stream rich in hydrocarbons, US Patent 6253574. 2001.

Stringari P, Campestrini M, Coquelet C, Arpentinier P. An equation of state for solid-liquid-vapor equilibrium applied to gas processing and natural gas liquefaction. *Fluid Phase Equilibria* 2014;362:258-267.

Swenson LK. Single mixed refrigerant, closed loop process for liquefying natural gas, US Patent 4033735. 1977.

Szargut J, Szczygiel I. Utilization of the cryogenic exergy of liquid natural gas (LNG) for the production of electricity. *Energy* 2009;34(7):827-837.

Tahouni N, Panjeshahi MH, Ataei A. Comparison of sequential and simultaneous design and optimization in low-temperature liquefaction and gas separation processes. *Journal of the Franklin Institute* 2011;348(7):1456-1469.

Tahouni N, Smith R, Panjeshahi MH. Comparison of stochastic methods with respect to performance and reliability of low-temperature gas separation processes. *Canadian Journal of Chemical Engineering* 2010;88(2):256-267.

Taleshbahrami H, Saffari H. Optimization of the C3MR cycle with genetic algorithm. *Transactions of the Canadian Society for Mechanical Engineering* 2010;34(3-4):433-448.

Tangen G, Mølnvik MJ. Scenarios for remote gas production. *Applied Energy* 2009;86(12):2681-2689.

Thomas S, Dawe RA. Review of ways to transport natural gas energy from countries which do not need the gas for domestic use. *Energy* 2003;28(14):1461-1477.

Tsatsaronis G, Morosuk T. Advanced exergetic analysis of a refrigeration system for liquefaction of natural gas. *International Journal of Energy and Environmental Engineering* 2010;1(1):1-18.

Uggen KT, Fodstad M, Nørstebø VS. Using and extending fix-and-relax to solve maritime inventory routing problems. *TOP* 2013;21(2):355-77.

Vaidyaraman S, Maranas CD. Synthesis of mixed refrigerant cascade cycles. *Chemical Engineering Communications* 2002;13(4):421-433.

Vatani A, Mehrpooya M, Palizdar A. Advanced exergetic analysis of five natural gas liquefaction processes. *Energy Conversion and Management* 2014;78:720-737.

Venkatarathnam G. *Cryogenic Mixed Refrigerant Processes*. New York: Springer Science; 2008.

Wahl PE, Løvseth SW, Mølnvik MJ. Optimization of a simple LNG process using sequential quadratic programming. *Computers and Chemical Engineering* 2013;56:27-36.

Wang M, Khalilpour R, Abbas A. Operation optimization of propane precooled mixed refrigerant processes. *Journal of Natural Gas Science and Engineering* 2013a;15:93-105.

Wang M, Zhang J, Xu Q. Optimal design and operation of a C3MR refrigeration system for natural gas liquefaction. *Computers and Chemical Engineering* 2012;39:84-95.

Wang M, Zhang J, Xu Q, Li K. Thermodynamic-analysis-based energy consumption minimization for natural gas liquefaction. *Industrial and Engineering Chemistry Research* 2011;50(22):12630-12640.

Wang Q, Li DH, Wang JP, Sun TF, Han XH, Chen GM. Numerical investigations on the performance of a single-stage auto-cascade refrigerator operating with two vapour-liquid separators and environmentally benign binary refrigerants. *Applied Energy* 2013b;112:949-955.

Wechsung A, Aspelund A, Gundersen T, Barton PI. Synthesis of heat exchanger networks at subambient conditions with compression and expansion of process streams. *AIChE Journal* 2011;57(8):2090-2108.

Wood DA. A review and outlook for the global LNG trade. *Journal of Natural Gas Science and Engineering* 2012;9:16-27.

Xu X, Liu J, Cao L. Optimization and analysis of mixed refrigerant composition for the PRICO natural gas liquefaction process. *Cryogenics* 2014;59:60-69.

Xu X, Liu J, Jian C, Cao L. The correlation between mixed refrigerant composition and ambient conditions in the PRICO LNG process. *Applied Energy* 2013;102:1127-1136.

Yoon S, Cho H, Lim D-H, Kim J-K. Process design and optimization of natural gas liquefaction processes. *Chemical Engineering Transactions* 2012;29:1585-1590.

Zellouf Y, Portannier B. First step in optimizing LNG storages for offshore terminals. *Journal of Natural Gas Science and Engineering* 2011;3(5):582-590.

3 Problem Characteristics

In this chapter, the simulation-framework used in this work is presented. The commercial simulator Aspen HYSYS® has been used for process simulation, while the sequential quadratic programming algorithm NLPQLP has been used for optimization.

Using a single mixed-refrigerant process as example, characteristics of the optimization problem have been illustrated by use of sensitivity analyses around the best known solution. From this, non-differential points related to phase change was observed as the refrigerant composition or pressure levels were changed.

In addition, the influence of different process parameters on the solution of the optimization problem has been studied. The parameters studied include minimum compressor superheating, minimum temperature difference, ambient temperature, compressor efficiency and natural gas supply and target conditions.

3.1 Simulation-optimization framework

In this work, a simulation-optimization framework developed at SINTEF Energy Research has been used for optimization of natural gas liquefaction processes. The framework combines use of a commercial sequential modular process simulator with external optimization algorithms. In this work, optimization has primarily been carried out using a sequential quadratic programming algorithm.

Aspen HYSYS® (V7.3 and V8.2) has been used for process simulation with cubic equations of state for thermodynamic modelling. By use of a sequential modular process simulator, equality constraints in the optimization problem (e.g. material and energy balances) are handled by the simulator. Hence, only inequality constraints are left to be handled by the optimizer. These constraints typically include restrictions on temperature driving forces or heat exchanger sizes, in addition to requirements for compressor suction streams.

The process simulator can be viewed as a black-box model, which takes values of the decision variables as input and returns values for the objective function and the

inequality constraints as output. The optimization search is performed using an external optimization algorithm.

In this work, the sequential quadratic programming algorithm NLPQLP (Schittkowski, 2006) has been used for optimization. Since derivative information cannot be obtained from the Aspen HYSYS® process models, derivatives have been estimated by used of finite differences. The step length used for these estimates was typically 10^{-4}. In order to reduce the risk of ending up in a local optimum, a multi-start approach from randomly generated initial solutions was used (uniform distribution within the variable bounds).

The optimization studies in this work have been performed on a Dell Latitude E6420 with Intel® Core™ i7-2720QM 2.2 GHz CPU and 8 GB RAM using Windows 7.

More information on the simulation-optimization framework is given by Wahl et al. (2013).

3.2 Problem formulation

Due to the energy intensive nature of low-temperature refrigeration, and thereby significant influence of process energy efficiency on the total cost of an LNG plant, LNG process is optimization often carried out with the objective of minimizing power consumption for a given production rate (or equivalently maximizing the exergy efficiency). In order to account for the trade-off between operating and investment costs, a constraint is added to limit the size of the heat exchanger(s). This is often formulated as a minimum required temperature difference $\Delta T_{\mathrm{HX,min}}$ in the heat exchanger to bound the temperature driving forces. In addition, a minimum superheating $\Delta T_{\mathrm{dew,min}}$ of the compressor suction stream is often required as a safety measure to avoid liquid inflow in the compressor.

For a vector of decision variables **x**, the optimization can then be formulated as:

$$\begin{aligned} \min_{\mathbf{x}} \quad & \dot{W}_{\mathrm{net}}\left(\mathbf{x}\right) \\ s.t. \quad & \Delta T_{\mathrm{dew}}\left(\mathbf{x}\right) \geq \Delta T_{\mathrm{dew,min}} \\ & \Delta T_{\mathrm{HX},i}\left(\mathbf{x}\right) \geq \Delta T_{\mathrm{HX,min}} \qquad i = 1,\ldots,n \end{aligned} \tag{3.1}$$

Here, $\dot{W}_{\mathrm{net}}$ is the net power consumption of the process, ΔT_{dew} is the superheating of the compressor suction stream and $\Delta T_{\mathrm{HX},i}$ is the temperature difference between the composite curves at point i in a heat exchanger with n evaluation points in total. For a single mixed-refrigerant process, the decision variables are typically the pressure levels, composition and flow rate of the refrigerant.

The minimum power required to liquefy the natural gas is given by the exergy increase of the natural gas through the process $\Delta\dot{E}_{NG}$. The actual power consumption is equivalent to the sum of this minimum power and the process irreversibilities $\dot{I}$:

$$\dot{W}_{net} = \Delta\dot{E}_{NG} + \sum \dot{I} \,. \tag{3.2}$$

The exergy change for the natural gas stream is constant for given inlet and outlet conditions. Hence, minimizing the power consumption is equivalent to minimizing the sum of irreversibilities.

For an isentropic compression process between pressure levels, p_1 and p_2, the power consumption can be expressed as

$$\dot{W}_{comp} = \dot{n} \cdot f_s \cdot \frac{\kappa_v}{\kappa_v - 1} \cdot \frac{Z_1 \cdot R_0 \cdot T_1}{\eta_s} \cdot \left(\left(\frac{p_2}{p_1} \right)^{\frac{\kappa_v - 1}{\kappa_v}} - 1 \right), \tag{3.3}$$

where $\dot{n}$ is the flow rate, κ_v the average isentropic volume exponent, Z_1 the compressibility factor for the suction stream, R_0 the universal gas constant, η_s the isentropic efficiency and T_1 the suction temperature (Schultz, 1962). An isentropic head correction factor f_s is used to account for errors in the estimate of the average isentropic volume exponent. More information on polytropic compression was provided by Schultz (1962).

Assuming changes in κ_v and f_s to be small with variations in temperature, the power consumption grows linearly with the refrigerant flow rate and suction temperature. Hence, in order to minimize the compression power, these should be kept as small as possible. As can be observed from Eq. (3.3), the power consumption also increases with increasing pressure ratio. Typically for an LNG process, the pressure ratio must be increased in order to fulfil the process restrictions if the refrigerant flow rate is reduced, and vice versa. The minimum power consumption is therefore found for the optimal trade-off between refrigerant flow rate and pressure ratio.

3.2.1 Case study – single mixed-refrigerant process

In order to study the problem characteristics, a simple single mixed-refrigerant process (PRICO®) has been optimized with the objective of minimizing the power consumption subject to a minimum superheating of the compressor suction stream and a minimum temperature difference. A process flowsheet is illustrated in Fig. 3.1.

The case study is based on a process model presented by Aspelund et al. (2010), with process parameters for the base case given in Table 3.1. The outlet temperature of the

cooler was assumed to be equal to the temperature of the natural gas feed stream ($T_3 = T_I$), and the refrigerant hot stream was assumed to exit the cold end of the LNG heat exchanger with the same temperature as the natural gas stream ($T_4 = T_{II}$).

Table 3.1. Natural gas properties for base case.

Property	Unit	Value
Molar flow rate $\dot{n}_{NG}$	kmol/s	1.00
Feed temperature T_I	K	293.15
Feed pressure p_I	bar	60.00
Product pressure p_{III}	bar	1.05
Product vapour fraction x_{III}	-	0.00
Molar composition:		
Methane	-	0.9589
Ethane	-	0.0296
Propane	-	0.0072
N-butane	-	0.0006
Nitrogen	-	0.0037

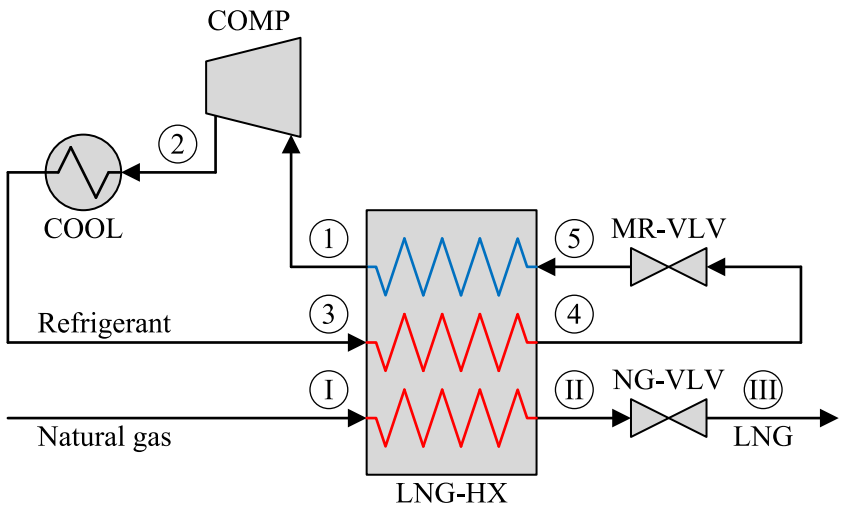

Figure 3.1. Flowsheet for single mixed-refrigerant LNG process.

In this study, pressure drop in heat transfer equipment was neglected, and limitations in compressor pressure ratio not considered. The process was simulated using the Peng-Robinson equation of state, and the heat exchanger was modelled with each stream discretized in 100 intervals of uniform enthalpy difference.

The base case was optimized subject to a minimum compressor superheating of 10 K and minimum temperature difference of 2 K in the heat exchanger. A constant isentropic efficiency $\eta_s = 0.80$ was assumed for the compressors.

Table 3.2. Decision variables with bounds and best solution found for simple PRICO® process.

Variable	Unit	LB	UB	Best
p_L	bar	1.0	8.0	3.867
p_H	bar	8.0	50.0	14.100
$\dot{n}_{C1}$	kmol/s	0.0	2.0	1.034
$\dot{n}_{C2}$	kmol/s	0.0	2.5	1.413
$\dot{n}_{C3}$	kmol/s	0.0	2.0	0.000
$\dot{n}_{nC4}$	kmol/s	0.0	4.0	1.008
$\dot{n}_{iC4}$	kmol/s	0.0	2.5	0.000
$\dot{n}_{N2}$	kmol/s	0.0	2.0	0.366

In total, eight degrees of freedom were left to be optimized. The low and high pressure levels of the refrigerant along with the individual component flow rates of the refrigerant components (methane (C1), ethane (C2), propane (C3), i-butane (iC4), n-butane (nC4) and nitrogen (N2)) were chosen as decision variables. Variable values for the best solution obtained are given in the rightmost column of Table 3.2. As can be observed, propane and i-butane were not present in the refrigerant composition for the best solution found.

The best solution was obtained through 20 runs from randomly generated feasible solutions (new candidate initial solutions generated randomly until a design satisfying all inequality constraints is found). For the simple PRICO® process, a feasible solution can be obtained through random generation in relatively few iterations. Of the 20 runs performed, 19 were able to obtain a solution within 0.01 % of the best known solution. The objective function value of the last run was about 156 % higher than the power consumption of the best known solution. None of the constraints were, however, found to be active in this solution. The search did, however, terminate due to an uphill search direction.

From the results, it was observed that the average number of function evaluations (process simulations) carried out in each search was around 857, varying between 54 (for the failed search) and 1788. The number of SQP iterations varied between 5 (again the failed search) and 168, with an average of about 75. In each SQP iteration, nine function evaluations (the number of decision variables plus one) are performed. The remaining function evaluations are connected to the line searches performed in the different SQP iterations. The average time consumption of each function evaluation was observed to be around 0.13 s (with the majority of the time spent in the process simulation). Hence, the average time consumption of each search was just below two minutes.

The best known solution is illustrated in a temperature-entropy diagram in Fig. 3.2 and a pressure-enthalpy diagram in Fig. 3.3 (a). In order to fulfil the minimum superheating constraint, the refrigerant stream must be a superheated vapour (right side of the dew point line) when exiting the hot end of the heat exchanger. In addition, the minimum temperature difference must also be fulfilled in the hot end of the heat exchanger. Hence, based on the values for the minimum temperature difference and the minimum superheating, the maximum feasible dew point temperature for the refrigerant can be calculated.

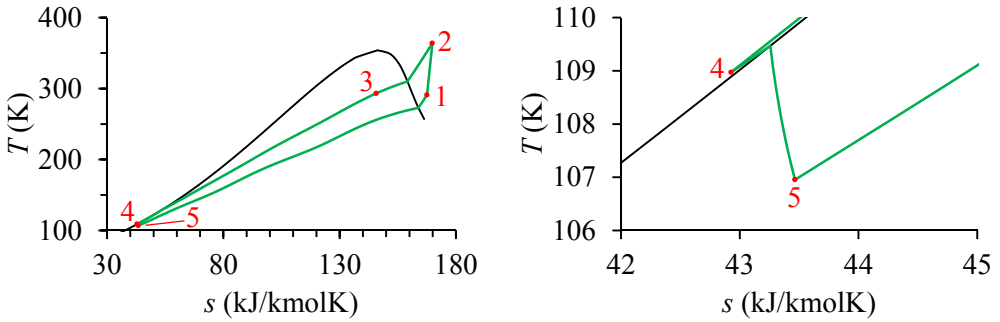

(a) (b)

Figure 3.2. Single mixed-refrigerant process illustrated in temperature-entropy diagram.

In order to fulfil the minimum temperature difference constraint, the temperature drop in the refrigerant throttle valve must be equal to or larger than the minimum temperature difference required. Hence, the Joule-Thomson coefficient must be positive (at least in part of the expansion process). As can be observed from Fig. 3.2 (b), the refrigerant temperature actually increases in the first part of the throttling process, before dropping when reaching the two-phase region.

From the perspective of thermodynamics, a temperature difference in the cold end larger than the minimum required will result in excess irreversibilities. It is therefore likely that the temperature drop in the throttle valve will be equal to the minimum temperature difference, or slightly higher, in the optimal solution.

Due to the nonlinearities of the temperature-enthalpy relations of the natural gas and the refrigerant, a uniform temperature difference equal to the minimum required is not obtained. In the best solution found, however, the smallest temperature difference between the composite curves is equal to the minimum required at five points in the heat exchanger. This can be observed in Fig. 3.3 (b), where the temperature difference is plotted as function of the temperature of the hot composite curve. The minimum temperature difference constraint is close to active also in the cold end of the heat

exchanger. Close to the warm end of the heat exchanger the temperature difference is quite large due to the phase change of the cold stream refrigerant.

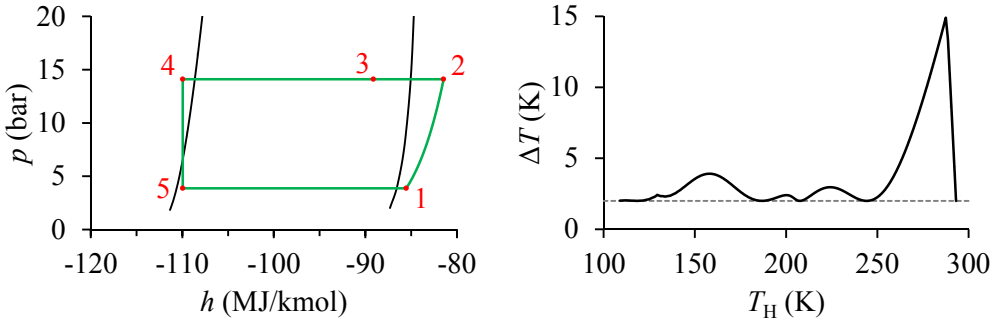

Figure 3.3. (a) Single mixed-refrigerant process illustrated in pressure-enthalpy diagram; (b) Temperature difference between composite curves as function of the hot stream temperature for the best known solution.

As can be observed from Fig. 3.3 (a), the specific cooling load of the hot refrigerant stream in the heat exchanger ($h_2 - h_3$) is almost as large as the specific cooling capacity of the cold refrigerant stream ($h_4 - h_5$). Hence, the majority of the cooling provided in the LNG heat exchanger is used to cool the refrigerant itself. In general, the difference in cooling load and cooling capacity (difference in heat capacity) increases with increasing pressure difference between the hot and cold stream. The reduced refrigerant flow rate does, however, come with increased specific compression power ($h_1 - h_2$).

3.3 Sensitivity analysis

In order to explore the characteristics of the optimization problem, one-dimensional sensitivity studies have been performed around the best known solution. All other variables have been kept at the values found to provide the best solution.

3.3.1 Methane flow rate

Methane is the second most volatile component in the refrigerant mixture. Hence, as can be observed in Fig. 3.4 (a), the dew point temperature of the low pressure refrigerant decreases with increasing methane flow rate (increasing methane fraction in the mixture). Without methane in the refrigerant, the compressor suction temperature is smaller than the dew point temperature, as can be observed from Fig. 3.4 (b). The refrigerant suction temperature is equal to the cold stream outlet temperature of the heat exchanger. Hence the compressor suction temperature is given by the energy balance for the heat exchanger. For small values of the methane flow rate, the specific cooling capacity grows faster than the specific cooling load.

As can be seen in Fig. 3.4 (a), a break point is observed where the temperature of the suction temperature reaches the dew point temperature, beyond which the compressor suction temperature grows with increasing methane flow rate. At higher methane flow rates, vapour, which has a smaller heat capacity than the liquid, will form in the hot end of the heat exchanger. The refrigerant cooling load therefore grows faster than the cooling capacity and the hot stream outlet temperature is increased to fulfil the energy balance for the heat exchanger. As can be observed in Fig. 3.4 (b), the superheating constraint is fulfilled for flow rates higher than about 0.8 kmol/s.

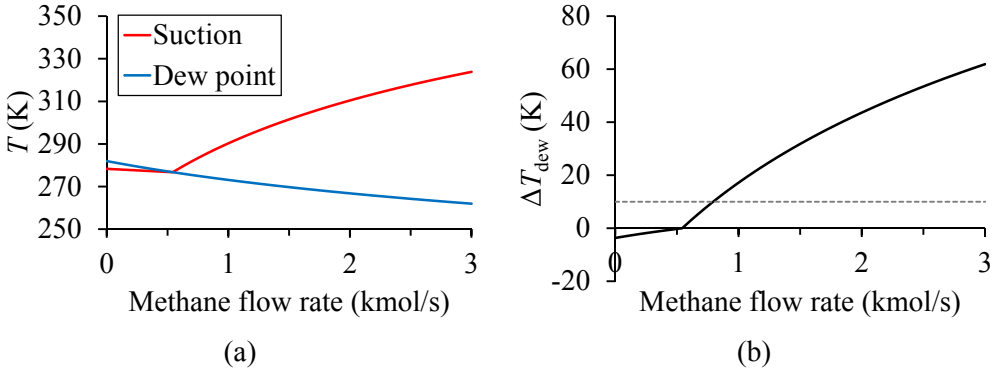

Figure 3.4. (a) Compressor suction temperature and refrigerant low pressure dew point as functions of methane flow rate; (b) Compressor suction superheating as function of methane flow rate.

With increasing methane refrigerant flow rate, the power consumption grows monotonically (close to an affine function) as illustrated in Fig. 3.5 (a). The effect of increased refrigerant flow rate is stronger than the effect of reduced compressor suction temperature for small values of the methane flow rate. For larger values, both effects contribute to increased power consumption (see Eq. (3.3)).

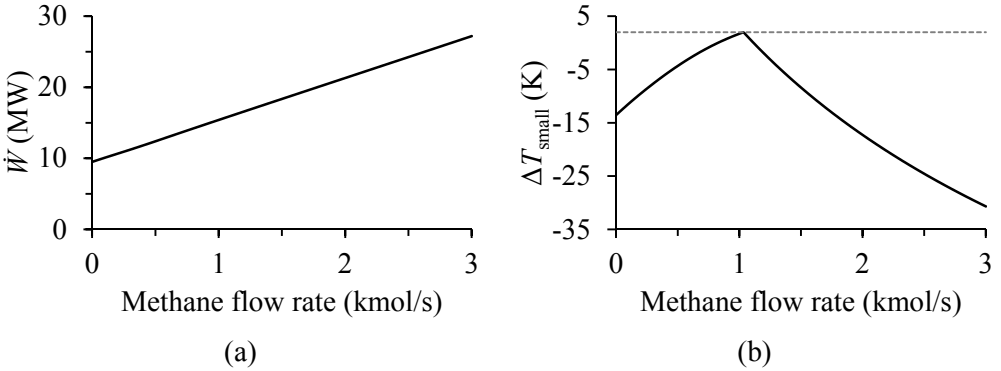

Figure 3.5. (a) Power consumption as function of methane flow rate; (b) Smallest temperature difference in heat exchanger as function of methane flow rate.

The smallest temperature difference in the heat exchanger is given as function of the methane flow rate in Fig. 3.5 (b), illustrating the fact that the minimum temperature difference constraint is fulfilled only at the point where the best solution is found. The smallest temperature difference between the composite curves decreases both when the methane flow rate is reduced and increased from this point. For a majority of the range studied, the design is practically infeasible since the temperature difference is negative.

In Fig. 3.6, the temperature difference throughout the heat exchanger is plotted for the best solution, together with curves for slightly larger and smaller methane flow rate. As can be observed, the temperature difference in the end points of the heat exchanger (and a point in the interior) falls below the minimum required when the methane flow rate is increased from the best solution. When the flow rate is reduced, the minimum temperature difference constraint is violated for points in the interior of the heat exchanger.

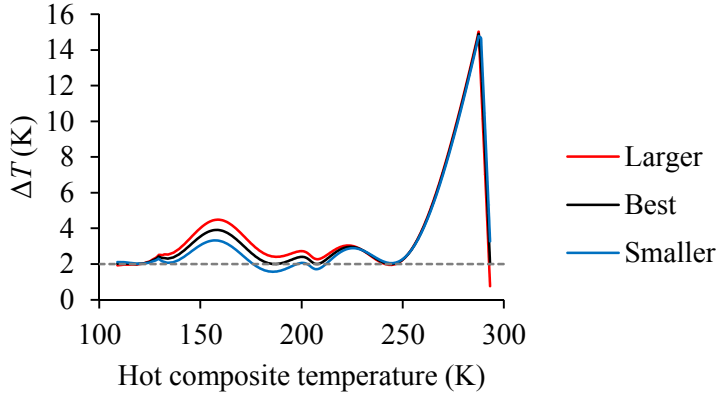

Figure 3.6. Temperature difference in the heat exchanger of a simple PRICO® process for different values of the methane flow rate. Minimum temperature difference requirement indicated by the dotted line.

3.3.2 Ethane flow rate

Just as for the methane component, the process power consumption is found to increase with increasing ethane flow rate, as indicated in Fig. 3.7. Of the refrigerant components used, ethane is in the intermediate range when it comes to volatility. The compressor superheating plotted as a function of the ethane flow rate in Fig. 3.8 (a) does, however, prove that the dew point temperature decreases with increasing ethane flow rate. In conformity with the methane component, the superheating constraint is fulfilled only for high ethene flow rates.

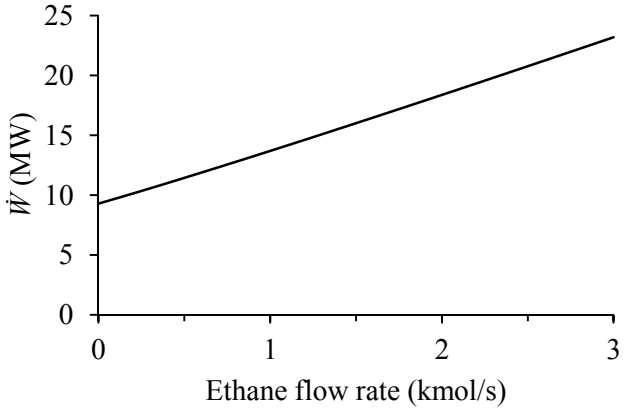

Figure 3.7. Power consumption as function of ethane flow rate around the best solution found for a simple PRICO® process.

The compressor suction superheating increases with increasing ethane flow rate. As for the methane component, the compressor suction temperature decreases with increasing ethane flow rate as long as the cold stream outlet temperature of the heat exchanger is smaller than the dew point temperature of the low pressure refrigerant. As can be observed in Fig. 3.8 (a), a break point is observed for the superheating temperature difference at the point where the compressor suction temperature is equal to the dew point temperature. For large values of the ethane flow rate, the compressor suction temperature grows steeply with increasing flow rate.

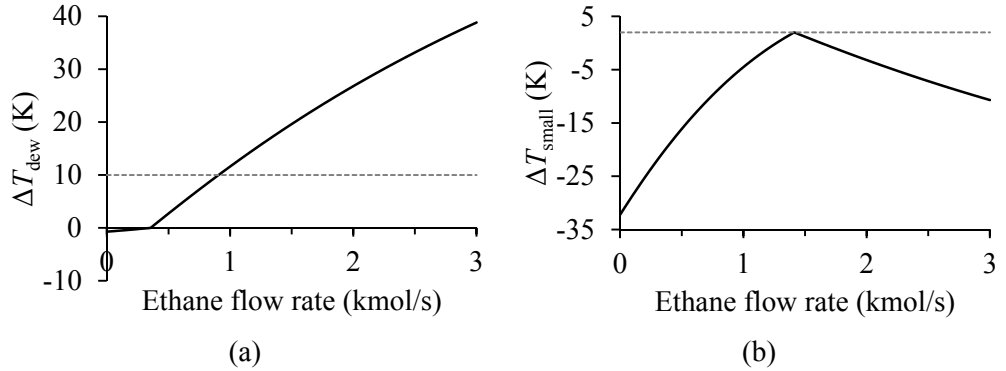

Figure 3.8. (a) Compressor suction superheating as function of ethane flow rate; (b) Smallest temperature difference in heat exchanger as function of ethane flow rate.

The smallest temperature difference in the heat exchanger is plotted as a function of the ethane flow rate in Fig. 3.8 (b). As for methane, the minimum temperature difference constraint is fulfilled only for an ethane flow rate equal to the best solution. For smaller

flow rates, the constraint is violated in the interior of the heat exchanger, while for larger flow rates the constraint is violated in the endpoints.

3.3.3 Propane flow rate

Propane, another component of intermediate volatility, is not present in the refrigerant mixture found to provide the smallest power consumption for the base case (see Table 3.2). As can be observed from Fig. 3.9 (a), the smallest temperature difference in the heat exchanger decreases with increasing propane flow rate and the minimum temperature difference constraint is violated whenever propane is present in the mixture. This does, however, not mean that a feasible design cannot be obtained when using propane in the refrigerant composition.

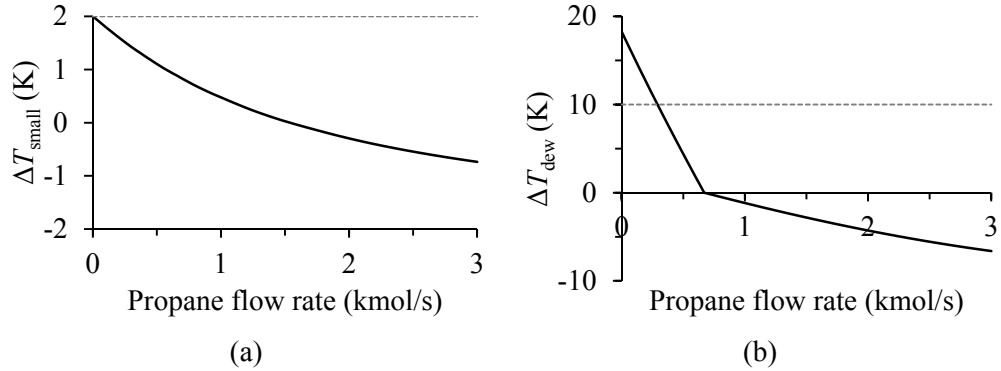

Figure 3.9. (a) Smallest temperature difference in heat exchanger as function of propane flow rate; (b) Compressor suction superheating as function of propane flow rate.

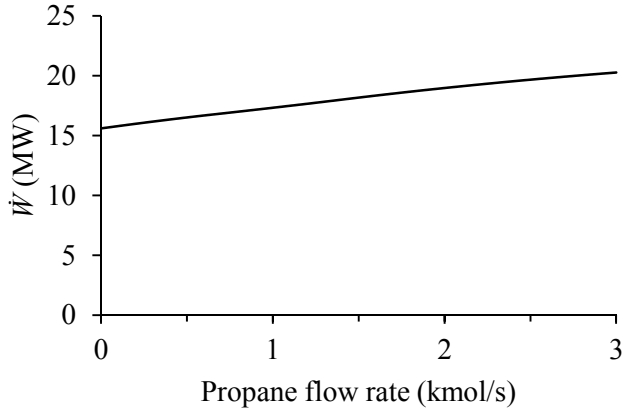

Figure 3.10. Power consumption as function of propane flow rate around the best solution found for a simple PRICO® process.

As for methane and ethane, the dew point temperature of the refrigerant decreases with increasing propane flow rate. A steeper reduction is, however, observed for the

compressor suction temperature. Hence, as illustrated in Fig. 3.9 (b), the compressor superheating decreases with increasing propane flow rate. As illustrated in Fig. 3.10, a growth in power consumption is observed when the propane flow rate is increased.

3.3.4 N-butane flow rate

Since n-butane is less volatile than the mixture, the dew point temperature of the refrigerant increases with increasing n-butane flow rate. For small values of the n-butane flow rate, the compressor suction temperature decreases with increasing flow rate, as can be seen from Fig. 3.11 (a). A minimum temperature is located at the point where the suction temperature reaches the dew point temperature, above which a slight increase is observed with increasing n-butane flow rate. As previously discussed, this is related to the energy balance for the heat exchanger and changes in refrigerant heat capacity. As can be observed from Fig. 3.11 (b), the minimum superheating constraint will be fulfilled only for small values of the n-butane flow rate.

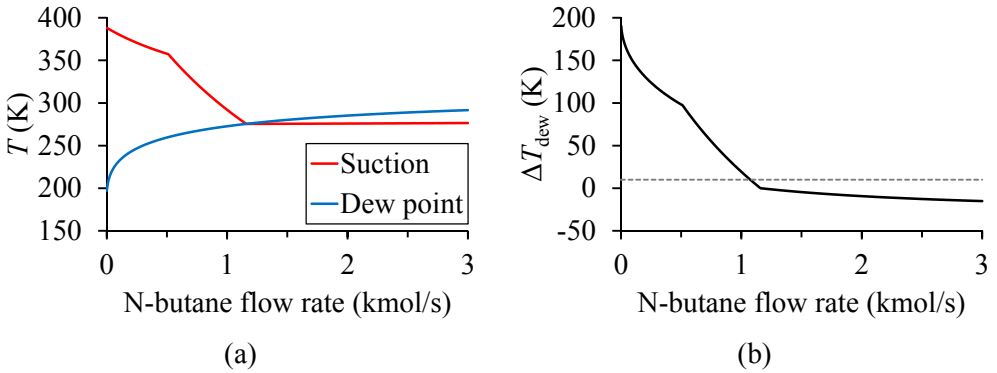

Figure 3.11. (a) Compressor suction temperature and refrigerant low pressure dew point temperature as functions of n-butane flow rate; (b) Compressor suction superheating as function of n-butane flow rate.

The process power consumption is plotted as function of the n-butane flow rate in Fig. 3.12 (a). For small values of the n-butane flow rate, the power consumption increases with increasing flow rate. Hence, the effect of increased refrigerant flow rate is stronger than the effect of reduced suction temperature. As can be observed, the power starts dropping around $\dot{n}_{nC4} = 0.5$ kmol/s, indicating that the effect of reduced suction temperature dominates the increase in flow rate. Another significant change in slope is observed when the n-butane flow rate is about 1.25 kmol/s.

The sudden changes in power consumption coincide with phase transitions for different process streams, as illustrated in Fig. 3.12 (b). For smaller values of the n-butane flow rate, the refrigerant stream entering the hot end of the heat exchanger (stream 3) will be superheated vapour, while for larger values a vapour-liquid mixture will enter the heat

exchanger. In the latter case, part of the refrigerant condensation takes place in the cooler. This leads to a steeper decrease in compressor suction temperature with increasing n-butane flow rate.

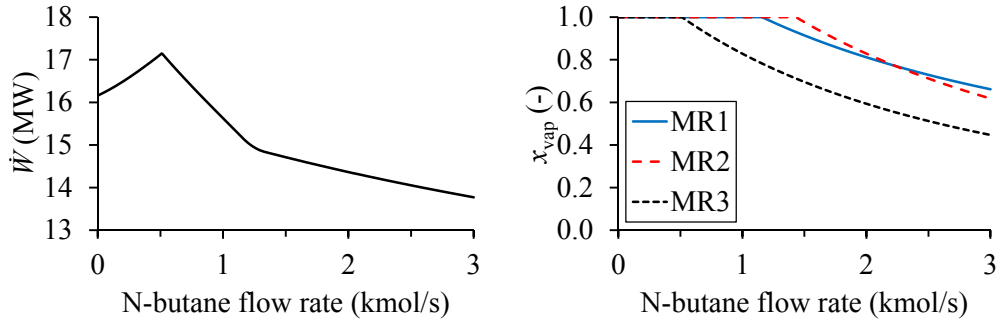

(a) (b)

Figure 3.12. (a) Power consumption as function of n-butane flow rate; (b) Vapour fractions in different refrigerant streams as functions of n-butane flow rate.

Despite the fact that both the refrigerant flow rate and the compressor suction temperature increase with increasing n-butane flow rate higher than about 1.15 kmol/s, the power consumption continues to decrease. The explanation can be found in the characteristics of the compressibility factor of the refrigerant stream and the isentropic volume exponent in the compression process.

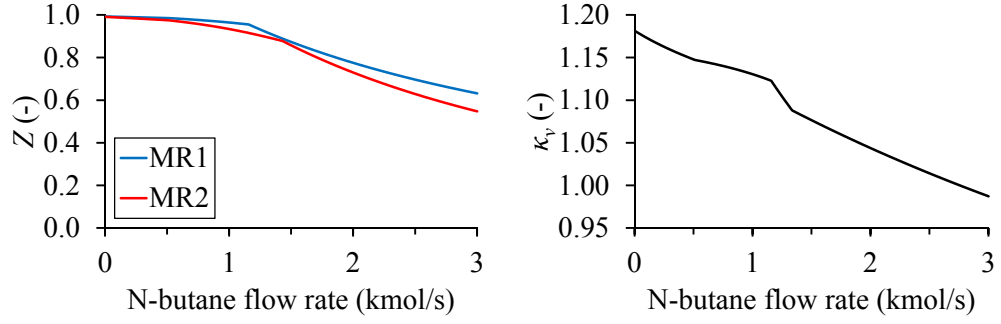

(a) (b)

Figure 3.13. (a) Vapour fraction compressibility factor for different refrigerant streams as functions of n-butane flow rate; (b) Isentropic volume exponent of the compression process as function of n-butane flow rate.

The gradual change in slope for the compression power observed when liquid starts forming in the compressor inlet (and eventually the outlet) is related to changes in the compressibility factor (plotted in Fig. 3.13 (a)) and the isentropic volume exponent of the refrigerant in the compressor (plotted in Fig. 3.13 (b)). Due to the reduction observed in both variables, the power consumption is reduced even though both refrigerant flow rate and suction temperature increase.

Since the flow rate of the refrigerant stream to be cooled increases with increasing n-butane flow rate, so does the cooling load of the main heat exchanger. As can be observed in Fig. 3.14 (a), the slope reduces as the n-butane flow rate reaches the point at which a phase-change is observed for stream MR3 (see Fig. 3.12 (b)). Like for methane and ethane, the minimum temperature difference constraint is fulfilled only for the n-butane flow rate equivalent to the value in the best solution, illustrated in Fig. 3.14 (b). A considerable temperature-cross is observed for smaller values of the n-butane flow rate, given by the significant superheating of the refrigerant in the hot end of the heat exchanger.

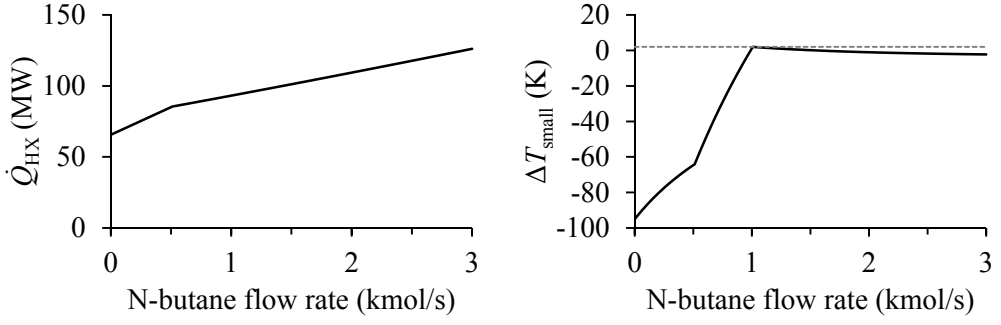

Figure 3.14. (a) Heat exchanger cooling load as function of n-butane flow rate; (b) Smallest temperature difference in heat exchanger as function of n-butane flow rate.

3.3.5 I-butane flow rate

Like for propane, i-butane is not present in the best solution found for the given process specifications. As can be observed from Fig. 3.15 (a), the temperature difference between the composite curves gradually decreases with increasing i-butane flow rate, and the minimum temperature difference constraint is fulfilled only when i-butane is not present in the mixture.

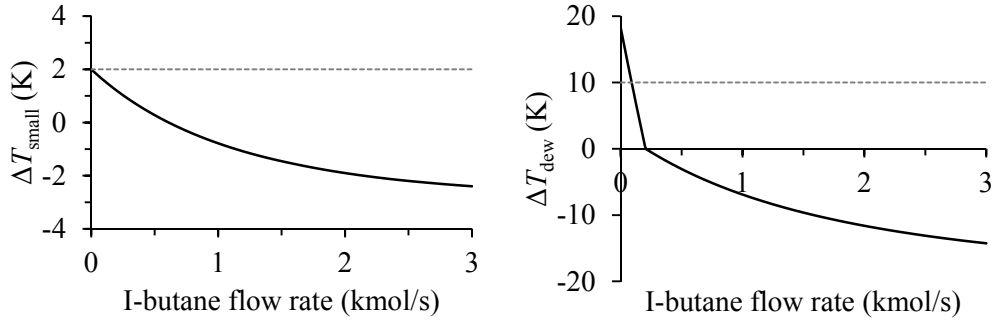

Figure 3.15. (a) Smallest temperature difference in heat exchanger as function of i-butane flow rate; (b) Compressor suction superheating as function of i-butane flow rate.

Similar to n-butane, i-butane is less volatile than the refrigerant mixture. Hence, when i-butane is added to the mixture, the dew point temperature increases. For small values of the i-butane flow rate, the suction temperature decreases with increasing i-butane flow rate. The refrigerant superheating therefore decreases with increasing i-butane flow rate as indicated in Fig. 3.15 (b). Reduced suction temperature is also the reason why the compression power decreases with increasing i-butane flow rate, as illustrated in Fig. 3.16.

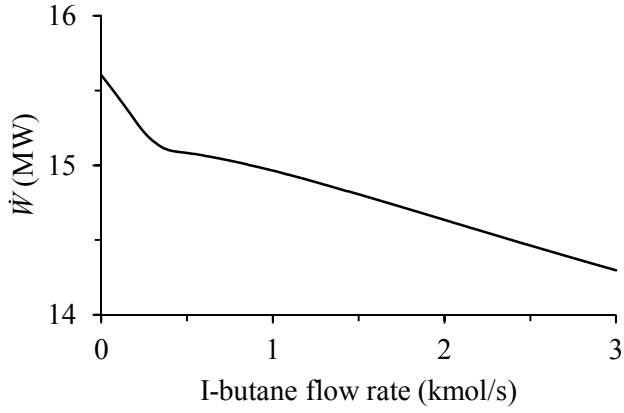

Figure 3.16. Power consumption as function of i-butane flow rate.

3.3.6 Nitrogen flow rate

Nitrogen is the most volatile component in the mixture. Hence, the characteristics of the compression power are expected to be similar to what was observed for methane and ethene. The results in Fig. 3.17 confirm that the power consumption increases with increasing nitrogen flow rate.

Due to decreasing dew point temperature and increasing suction temperature, the compressor superheating increases with increasing nitrogen flow rate, as can be seen in Fig. 3.18 (a). Again, the restrictions on the smallest temperature difference allowed in the heat exchanger are only fulfilled for the nitrogen flow rate in the best known solution. This is illustrated in Fig. 3.18 (b).

The temperature change in the throttling valve is plotted as a function of the nitrogen flow rate in Fig. 3.19 (a). As previously discussed, a temperature drop equal to or larger than the minimum temperature difference in the heat exchanger is required to fulfil the requirements in the cold end of the heat exchanger. This minimum requirement is fulfilled for when the nitrogen flow rate is higher than approximately 0.35 kmol/s.

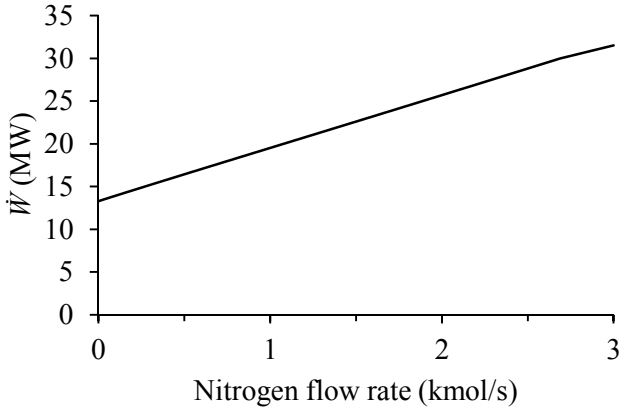

Figure 3.17. Power consumption as function of nitrogen flow rate.

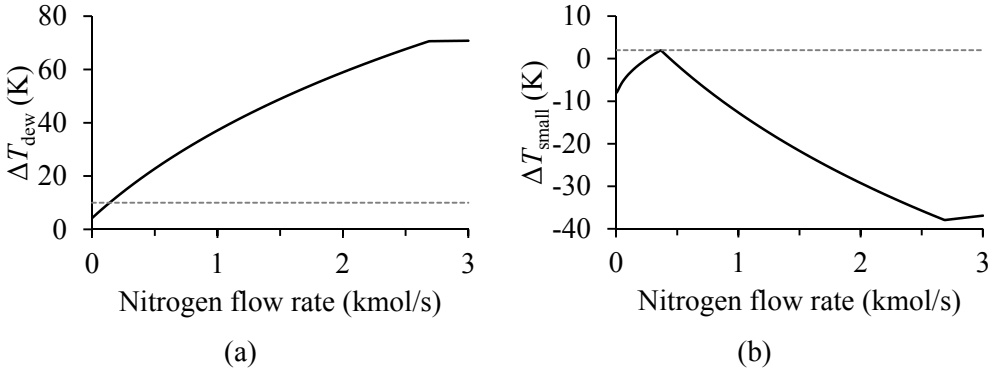

Figure 3.18. (a) Compressor suction superheating as function of nitrogen flow rate; (b) Smallest temperature difference in heat exchanger as function of nitrogen flow rate.

As can be observed in Fig. 3.19 (b), where the vapour fraction of the inlet and outlet streams of the valve is plotted as function of the nitrogen flow rate, the temperature is found to increase in the expansion process when the outlet refrigerant is a sub-cooled liquid ($x_{vap,5} = 0$). When the nitrogen flow rate increases, both the vapour fraction of the outlet stream and the temperature drop increase. The slope is however, reduced when the nitrogen flow rate reaches a level where also the inlet stream of the valve is in the two-phase region (around $\dot{n}_{N2} = 1.2$ kmol/s). For nitrogen flow rates larger than this value, the increase in vapour fraction across the valve decreases with increasing nitrogen flow rate.

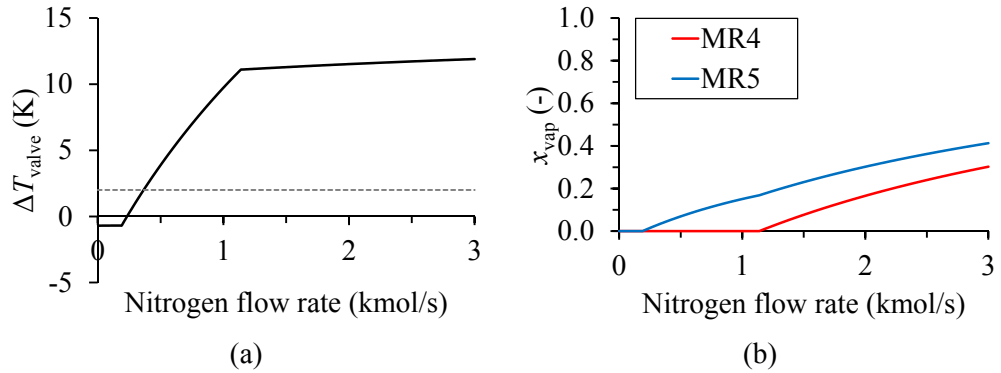

Figure 3.19. (a) Temperature difference across throttle valve as function of nitrogen flow rate; (b) Vapour fractions of refrigerant streams as functions of nitrogen flow rate.

3.3.7 Low pressure level

In the case of variation in the pressure levels, the refrigerant composition remains constant. Hence, with increasing low pressure level, the dew point temperature will increase. The refrigerant hot stream, and thereby the cooling load of the heat exchanger, is independent of the low pressure level. The cooling capacity of the cold stream does, however, decrease with increasing low pressure level. As a consequence, the compressor superheating decreases with increasing low pressure level as given in Fig. 3.20 (a).

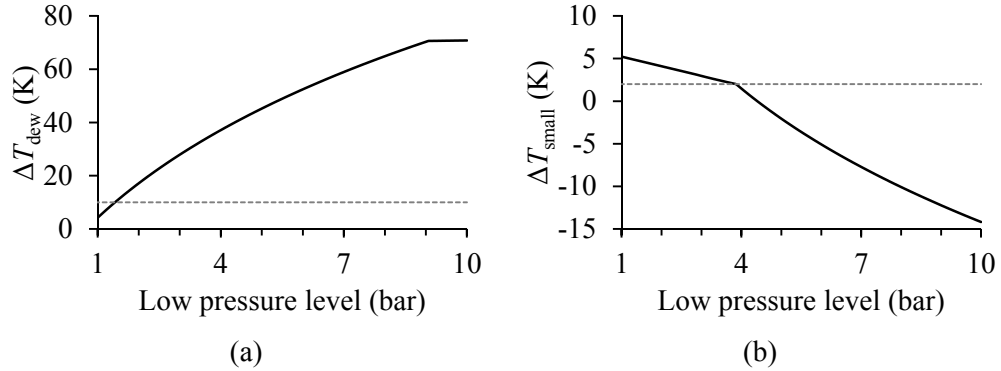

Figure 3.20. (a) Compressor suction superheating as function of low pressure level; (b) Smallest temperature difference in heat exchanger as function of low pressure level.

As can be observed from Fig. 3.20 (b), the smallest temperature difference decreases with increasing low pressure level. The minimum temperature difference constraint is fulfilled for values smaller than the one in the best known solution. A change in slope observed at this point, caused by a change in pinch point in the heat exchanger (similar to the phenomena discussed for the methane flow rate in Section 3.3.1). As expected the power consumption increases with decreasing low pressure level (higher pressure ratio), as illustrated in Fig. 3.21. This also explains why the best known solution is

given for the highest pressure level that fulfils the minimum temperature difference constraint.

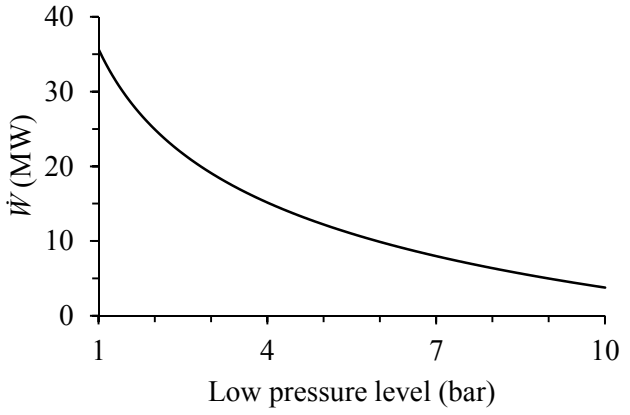

Figure 3.21. Power consumption as function of low pressure level.

In Fig. 3.22, the logarithmic mean temperature difference (or rather a weighted sum of the logarithmic mean temperature difference in the difference sections of the heat exchanger) is plotted as function of the low pressure level. For low pressure levels resulting in a positive temperature difference at all points in the heat exchanger, a smooth curve is observed. As can be observed from Fig. 3.22 (a), ΔT_{LM} monotonically decreases with increasing low pressure level in this region. When the smallest temperature difference is negative (composite curves crossing) considerable noise is observed for the logarithmic mean temperature difference, as illustrated in Fig. 3.22 (b).

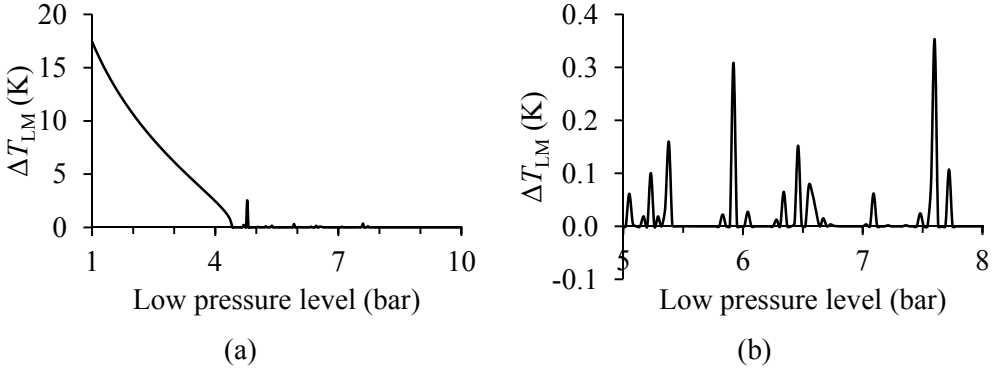

Figure 3.22. Logarithmic mean temperature difference in heat exchanger as function of low pressure level. (a) For the complete range; (b) for a range where the smallest temperature difference is smaller than zero.

The noise observed for the logarithmic mean temperature difference propagates to the heat exchanger conductance (*UA* value), as can be observed in Fig. 3.23 (a). When the

temperature driving force approaches zero, the heat exchanger area grows to infinity. Reasonable values for the *UA* value is observed only for low pressure levels providing a thermodynamically feasible solution (positive temperature driving force throughout the heat exchanger), as can be seen in Fig. 3.23 (b). As expected, the *UA* value increases with increasing low pressure level in this region, since the cooling load increases and the mean driving force decreases.

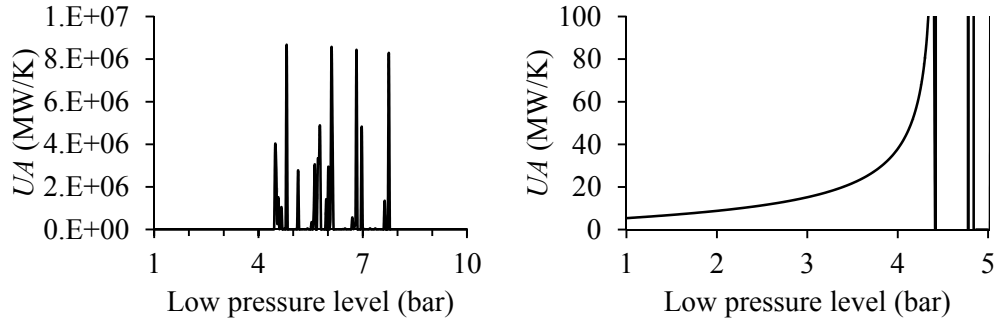

(a) (b)

Figure 3.23. Heat exchanger conductance (*UA* value) as function of low pressure level. (a) For the complete range; (b) for a range where the smallest temperature difference is larger than zero.

3.3.8 High pressure level

When varying the high pressure level, the dew point temperature of the low pressure refrigerant does, of course, remain constant. As illustrated in Fig. 3.24 (a), the compression suction temperature does, however, vary with the high pressure level. When the high pressure level is increased, the cooling load associated with the hot stream refrigerant decreases. Hence, generally, the suction temperature will decrease with increasing high pressure. As can be observed in Fig. 3.24 (a), the slope changes significantly when the suction temperature reaches the dew point temperature. For values higher than this, the compressor suction stream will be a superheated vapour, altering the cooling capacity of the refrigerant in the hot end of the heat exchanger.

The reduction in suction temperature is, however, not large enough to compensate the increase in pressure ratio. As expected, the results given in Fig. 3.25 (a) confirms that the compression power increases with increasing high pressure level. As can be observed from Fig. 3.25 (b), the minimum temperature difference constraint is fulfilled only for the high pressure level of the best known solution.

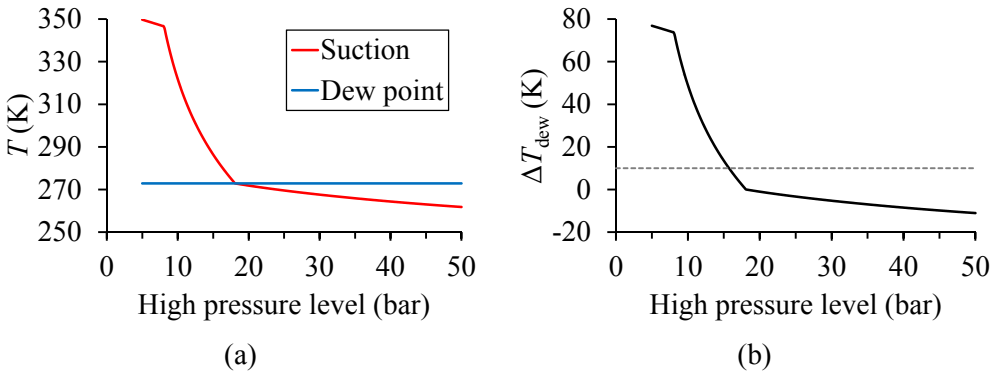

Figure 3.24. (a) Compressor suction temperature and refrigerant low pressure dew temperature point as functions of high pressure level; (b) Compressor suction superheating as function of high pressure level.

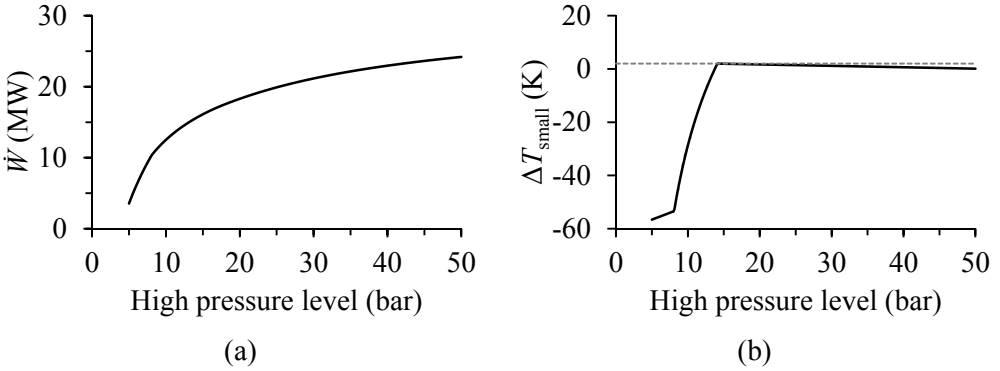

Figure 3.25. (a) Power consumption as function of high pressure level; (b) Smallest temperature difference in heat exchanger as function of high pressure level.

3.3.9 Summary

The sensitivity analysis performed around the best known solution indicates that this solution at least is a local optimal solution of the optimization problem (this could be confirmed by investigation of the Karush-Kuhn-Tucker conditions). A small reduction or increase in the value of any of the decision variables will either lead to increased power consumption or violation of constraints. For all variables except the low pressure level, the minimum temperature difference constraint is fulfilled only for the values of the best known solution.

Non-differentiable points associated with phase change for the different refrigerant streams were observed both for the objective and the constraints. These could potentially cause problems for the optimization search, especially for deterministic search methods relying on derivatives. Since the sensitivity analysis was performed around the best known solution, these issues are likely to be present even if an initial solution close to the global optimum was to be provided for the optimization search.

Considerable noise was observed in the behaviour of composite variables such as the logarithmic mean temperature difference and the heat exchanger conductance in the infeasible region (negative temperature difference in the heat exchanger). Hence, using these variables in the problem formulation is likely to increase the complexity of the optimization problem.

The smallest temperature difference is also a composite function, given as the minimum of the temperature differences at all the points in the heat exchanger. Non-differentiable points are observed when the location of the pinch point in the heat exchanger changes. For this reason, better performance of the optimization search may be observed if the temperature differences in all evaluation points in the heat exchanger are used as constraints rather than only the smallest temperature difference. The optimization problem would then have one constraint for each evaluation point in the heat exchanger, instead of one constraint for smallest temperature difference. Such a formulation was found by Wahl et al. (2013) to give better performance, and is the approach that has been used in this work.

A sensitivity analysis has been performed also for a randomly chosen feasible solution. The results obtained were similar with respect to the behaviour of the objective and the constraints.

3.4 Heat exchanger modelling

When simulating LNG processes in Aspen HYSYS®, the multi-stream heat exchanger models used for natural gas liquefaction are based on energy balances. These models can assure fulfilment of the first law of thermodynamics, yet feasibility with respect to the second law of thermodynamics cannot be guaranteed since the temperature driving forces within the heat exchanger are not considered. In order to account for the feasibility of the heat transfer process, the composite curves must be examined.

Since, in most cases, the temperature-enthalpy relations of the streams are nonlinear, the temperature driving forces must be considered not only in the endpoints of the heat exchanger but also in the interior. This can be done by dividing the heat exchanger in intervals and evaluating the temperature difference between the hot and cold composite curve at every intersection. An estimate for the smallest temperature difference in the heat exchanger is then given by the smallest value observed for these evaluation points. The accuracy of the estimate increases with increasing number of evaluation points.

In Aspen HYSYS®, each stream in the heat exchanger can be divided into segments of uniform enthalpy or temperature change. The overall composite curves for the heat exchanger are then calculated by combining data from the different streams. Each

evaluation for each stream contributes to one point on the heat exchanger composite curve.

Since the evaluation points in general do not coincide for the different streams (neither when discretized with respect to enthalpy nor when discretized with respect temperature), temperature and enthalpy are estimated by linear interpolation in between the evaluation points. This procedure is illustrated for a simplified example assuming three intervals of uniform temperature difference for each stream in Figs. 3.26-3.28. The same procedure applies if the heat exchanger is discretized with uniform enthalpy steps.

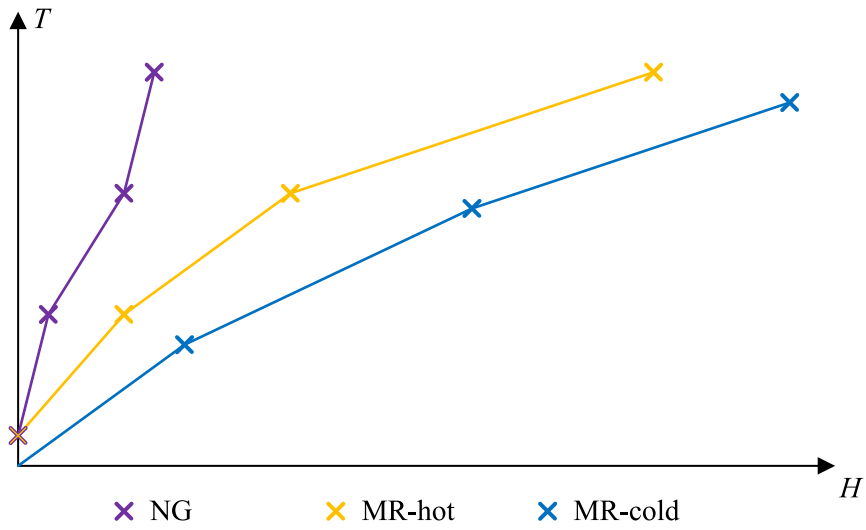

Figure 3.26. Temperature-heat relation for three streams divided into three segments each.

In Fig. 3.26, temperature-enthalpy curves are given for each of the three streams in the heat exchanger. The hot composite curve is obtained by combining the two hot streams, the natural gas stream and the hot mixed-refrigerant stream. Since there is only one cold stream, the cold composite stream is equal to the temperature-enthalpy curve of the cold mixed-refrigerant stream. The composite curves are then found as indicated in Fig. 3.27.

Based on the results given in Fig. 3.27, the temperature difference between the composite curves can be calculated for each of the evaluations points in the heat exchanger as illustrated in Fig. 3.28. For every evaluation point on the hot composite curve, the temperature of the cold composite curve at the same enthalpy level is found by linear interpolation as indicated in Fig. 3.27. The same approach is used when

calculating the temperature difference for the evaluation points originating from the cold composite curve. As can be observed from Fig. 3.28, the evaluation points are not uniformly distributed with respect to enthalpy. Due to the fact that the evaluation points originating from the different streams do not coincide, the evaluation points in Fig. 3.28 would not be uniformly distributed with respect to enthalpy even if the different streams were to be divided segments of uniform enthalpy change.

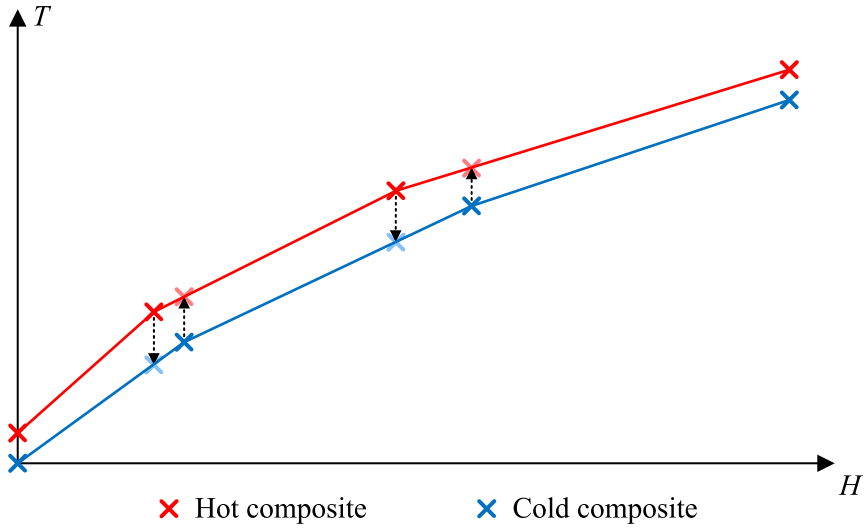

Figure 3.27. Composite curves for a heat exchanger.

The smallest temperature difference in the heat exchanger is given as the smallest temperature difference for all the evaluation points in the heat exchanger. The accuracy of the heat exchanger modelling will increase with increasing number of segments for the streams, especially if the nonlinearities of the temperature-enthalpy relation are pronounced. However, so will also the computational requirements of the simulation.

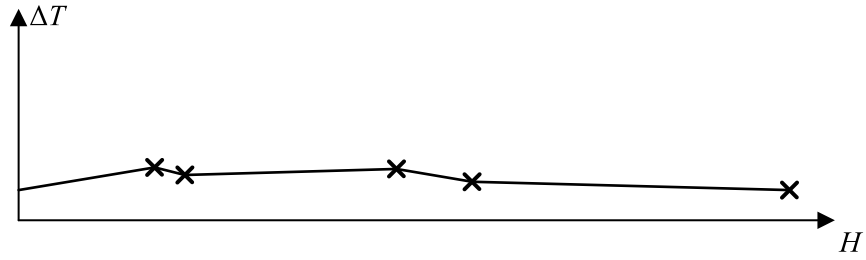

Figure 3.28. Temperature difference between composite curves.

Due to the way the composite curves are calculated in Aspen HYSYS®, numerical noise can result. The relative position of a calculation point can change when any of

the process variables change. This is caused by large variations in the temperature of the cold refrigerant stream at the inlet and especially outlet of the heat exchanger. For the hot streams, the inlet and outlet temperatures are constant. For a case study, the temperature difference at two different points in the heat exchanger is plotted as function of the methane flow rate in Fig. 3.29.

As can be seen, noise is observed for both the cases. For the evaluation point depicted in Fig. 3.29 (a), the noise is mainly related to the fact that the location of this point changes with the methane flow rate. The evaluation points are sorted with respect to temperature level. Hence, when the temperature range for the cold stream refrigerant changes, the number of evaluation points in different regions of the heat exchanger may increase or decrease. In other words, the temperature of the hot stream changes when the methane flow rate changes. In Fig. 3.29 (b), another important source to noise is phase change for the refrigerant stream from vapour-liquid two-phase to vapour.

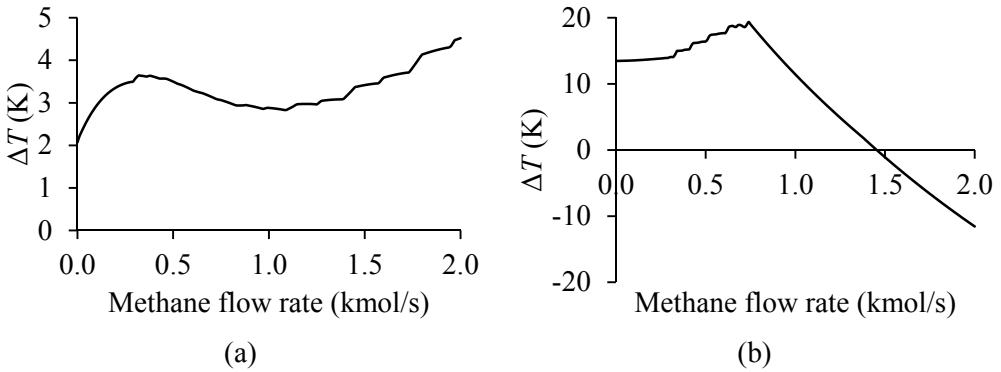

Figure 3.29. Temperature difference at two different points in the heat exchanger as function of the methane flow rate.

The presence of noise is found to be reduced if the heat exchanger is modelled as a set of small heat exchangers such that each heat exchanger model represents one section in the heat exchanger. This set of heat exchangers can be modelled with a uniform temperature interval for all the heat exchangers. In this case, a given evaluation point will have the same hot stream temperature for all values of the methane flow rate. This way, the problem associated with changing position of the evaluation points can be circumvented.

Based on the composite curves returned from Aspen HYSYS® (see Fig. 3.27), the same effect could be obtained by linearizing the composite curves. By linear interpolation between the evaluation points originally passed from the process simulation, a new set of evaluation points with uniform distribution according to either temperature or heat

could be calculated. For the case of uniform temperature intervals, this is illustrated in Fig. 3.30.

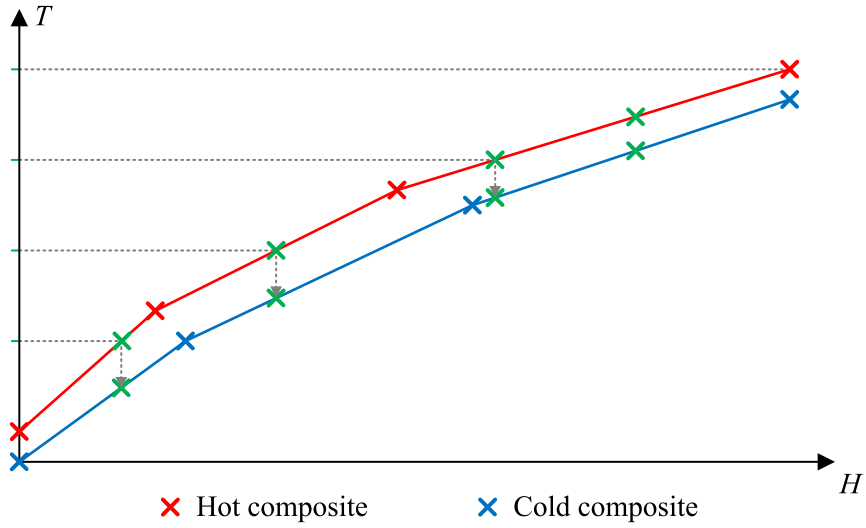

Figure 3.30. Heat exchanger composite curves linearized with respect temperature.

The influence of linearization of the composite curves is illustrated in Fig. 3.31, where the two evaluation points close to the ones given in Fig. 3.29 (the shape of the curves will be different since the location of the points is changing for the results plotted in Fig. 3.29). Here, the evaluation points in the heat exchanger have been linearized with respect to temperature.

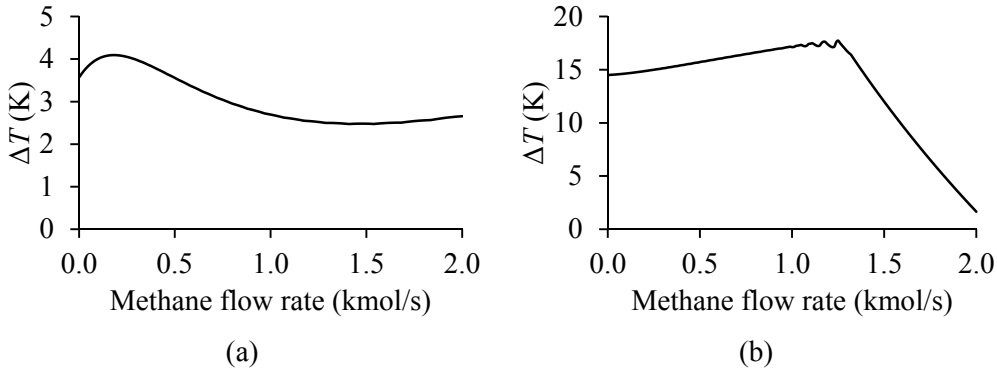

Figure 3.31. Temperature difference at two different points in the heat exchanger as function of the methane flow rate, linearized with respect to temperature.

As can be observed in Fig. 3.31 (a), the noise related to changes in evaluation point location is eliminated. The noise related to the phase change of the cold stream refrigerant is, however, still present for the point illustrated in Fig. 3.31 (b). Phase change is associated with a sudden change in heat capacity. In regions with phase

change, the temperature estimate for the refrigerant will therefore depend on how well the discretization fits with the location of the phase change.

In the Aspen HYSYS® model, additional evaluation points can be added where the stream changes phase. The presence of phase change within the heat exchanger depends on the operating conditions. Hence, the number of evaluation points in the heat exchanger would depend on the operating conditions. For the optimization approach it is beneficial (or required) to keep the number of evaluation points (and thereby the number of constraints) constant. However, by using the approach of calculating the composite curves based on a piecewise linearization of the temperature-enthalpy relations of the different streams in the heat exchanger, a consistent number of evaluations points (and constraints) can be maintained irrespective of the presence of phase change.

By including extra evaluation points for phase change, the accuracy of the linearized temperature profiles could be improved. In Fig. 3.32, the temperature difference between the composite curves is plotted as function of the methane flow rate for the same points in the heat exchanger as in Fig. 3.31. Also here, the distribution of evaluation points has been linearized with respect to temperature. The difference is that extra evaluation points have been added for phase change in the data used for linearization. As can be observed from Fig. 3.32 (b), the noise associated with phase change is eliminated.

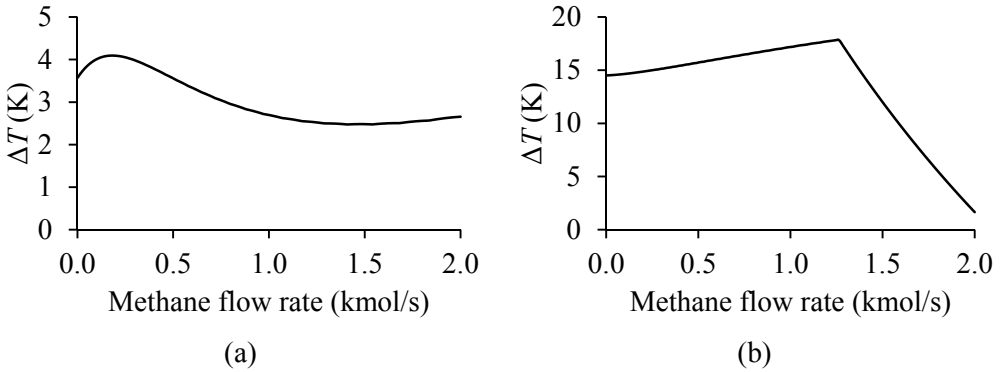

Figure 3.32. Temperature difference at two different points in the heat exchanger as function of the methane flow rate, linearized with respect to temperature and extra evaluation points for phase change.

Issues related to noise in the heat exchanger are present irrespective of the choice of heat exchanger discretization (uniform temperature intervals or uniform enthalpy intervals for each stream). The linearization approach can, however, be used to remove the noise in both cases. Linearization could also be performed with respect to enthalpy, as illustrated in Fig. 3.33, in order to have a heat exchanger model where the evaluations points are distributed uniformly with respect to enthalpy.

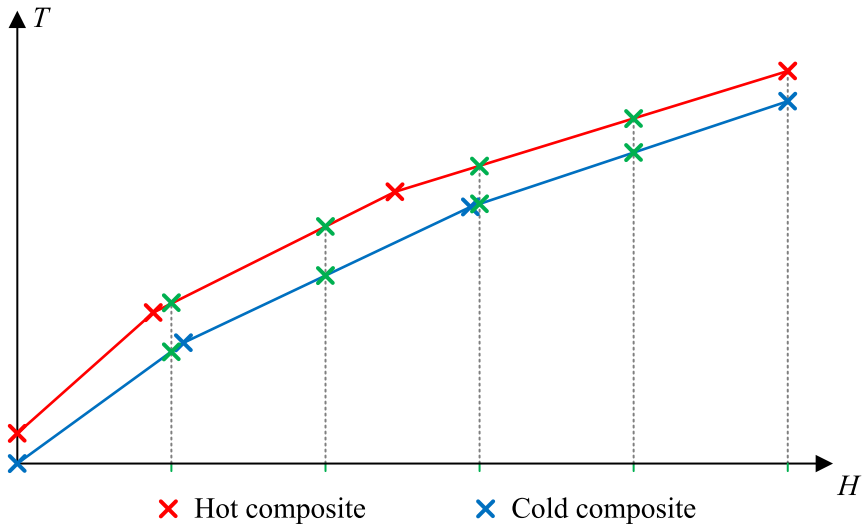

Figure 3.33. Heat exchanger composite curves linearized with respect to enthalpy.

In this work, the evaluation points returned from Aspen HYSYS® have been used in their original form, without any linearization or addition of evaluation points related to phase change. Kamath et al. (2012) argued that discretization with respect to enthalpy would be suitable since the temperature could be constant in large region of the heat exchanger in case of pure-refrigerant phase change. Discretization with respect to enthalpy has been used in this work.

3.5 Problem characteristics

3.5.1 Minimum superheating

In the base case, the minimum superheating constraint was found not to be active in the best known solution. Even though the compressor suction superheating is not directly linked to the process power consumption, it may affect the performance of the heat exchanger. In Fig. 3.34, results are given for optimization of the simple PRICO® process subject to different values of the minimum compressor superheating. The constraint has little or no influence on the solution for values smaller than 20 K. For larger values, however, a significant increase in power consumption is observed.

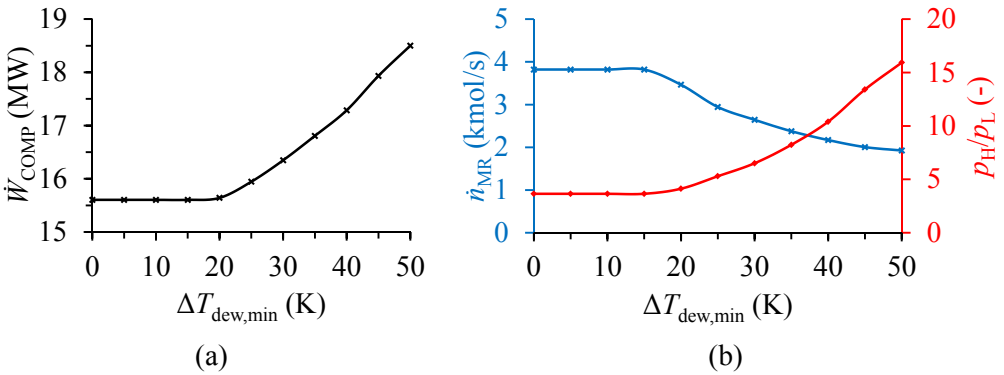

Figure 3.34. (a) Power consumption of best known solution as function of minimum superheating requirement; (b) Refrigerant flow rate (blue) and pressure ratio (red) in best known solution as functions of minimum superheating requirement.

In order to achieve refrigerant superheating of the compressor suction stream, the refrigerant cold stream must exit the hot end of the heat exchanger as superheated vapour. Since the maximum temperature of the compressor suction stream is limited by the constraint on the hot end temperature difference between the composite curves, increased superheating is obtained by decreasing the dew point temperature, as can be observed in Fig. 3.35 (a). The dew point temperature is reduced by reducing the low pressure level and altering the refrigerant composition. In Fig. 3.36, the molar fractions of the different refrigerant components are given as functions of the minimum superheating. For large values of the minimum superheating constraint, n-butane is replaced by i-butane, which has a lower saturation temperature.

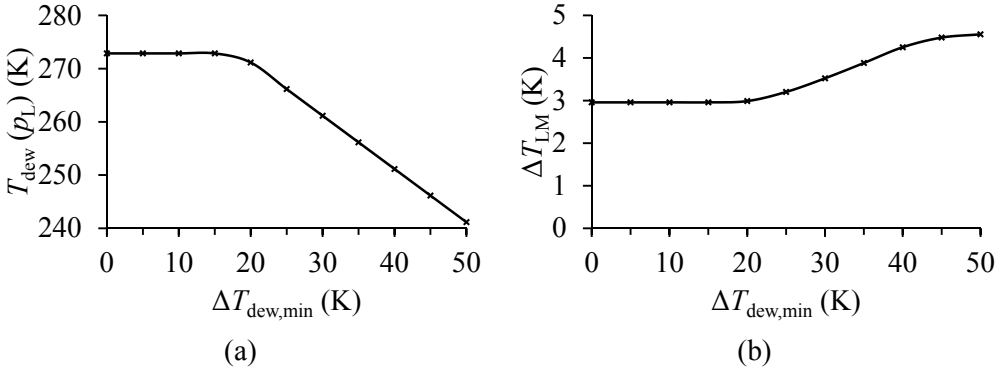

Figure 3.35. (a) Dew point temperature of compressor suction stream in best known solution as function of minimum superheating requirement; (b) Logarithmic mean temperature difference in the heat exchanger for the best known solution as function of minimum superheating requirement.

The phase change from two-phase vapour-liquid to vapour involves a considerable change in specific heat capacity. Refrigerant superheating will therefore lead to a large temperature difference between the composite curves close to the hot end of the heat exchanger. This is reflected by an increase in the logarithmic temperature difference between the composite curves with increasing superheating, as illustrated in

Fig. 3.35 (b). As can be observed in Fig. 3.34 (b), the increased temperature driving forces are partly compensated by shifting the trade-off between refrigerant flow rate and pressure ratio towards smaller flow rate and higher pressure ratio.

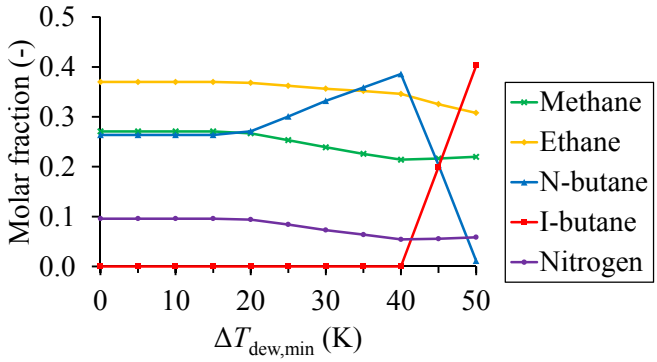

Figure 3.36. Molar composition of mixed refrigerant in best known solution as function of minimum superheating requirement.

3.5.2 Minimum temperature difference

With increasing minimum temperature difference between the composite curves, the feasible region of the optimization problem is reduced. As one would expect, since the temperature driving forces are closely linked to the irreversibilities of the heat exchanger and thereby the power consumption, the compression power increases with increasing $\Delta T_{HX,min}$. This is illustrated in Fig. 3.37 (a), where the power consumption of the best known solution is plotted as function of the minimum temperature difference required between the composite curves.

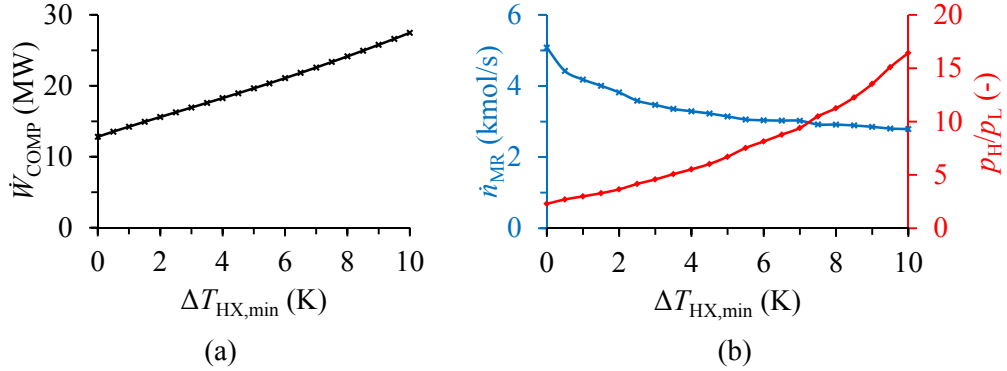

Figure 3.37. (a) Power consumption of best known solution as function of minimum temperature difference requirement; (b) Refrigerant flow rate (blue) and pressure ratio (red) in best known solution as functions of minimum temperature difference requirement.

With increasing minimum temperature difference, a higher temperature drop over the throttling valve is obviously required. This is accommodated by increasing the pressure

ratio and the nitrogen content in the refrigerant. The latter is illustrated in Fig. 3.38, where the molar fractions of the different refrigerant components are plotted as functions of the minimum temperature difference. As can be observed in Fig. 3.37 (b), the optimal trade-off between refrigerant flow rate and pressure ratio is shifted towards smaller refrigerant flow rates and higher pressure ratios when the minimum temperature difference in the heat exchanger increases. This way, the increase in heat exchanger irreversibilities due to larger temperature driving forces is compensated.

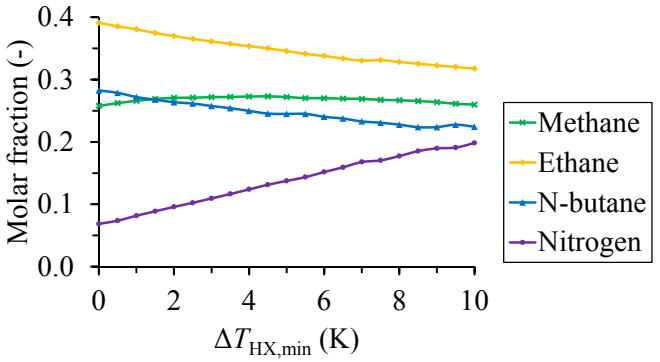

Figure 3.38. Molar composition of mixed refrigerant in best known solution as function of minimum temperature difference requirement.

3.5.3 Compressor efficiency

Conceptual LNG process design is often carried out assuming a constant isentropic efficiency for compressors and expanders. An isentropic compression or expansion process is fully reversible. In a real process, however, irreversibilities are present. The isentropic efficiency of a compression process can be defined as

$$\eta_{s,\mathrm{COMP}} = \frac{\dot{W}_s}{\dot{W}} = \frac{\Delta h_s}{\Delta h}, \tag{3.4}$$

where $\dot{W}_s$ is the power consumption of an isentropic process, $\dot{W}$ the actual power consumption, Δh_s the specific enthalpy change in an isentropic process and Δh is the specific enthalpy change of the actual process (Moran and Shappiro, 2006) . In any real process, the isentropic efficiency is smaller than unity.

Correspondingly, the isentropic efficiency of an expander process can be expressed as

$$\eta_{s,\mathrm{EXP}} = \frac{\dot{W}}{\dot{W}_s} = \frac{\Delta h}{\Delta h_s}. \tag{3.5}$$

In an irreversible expansion process, the isentropic efficiency is smaller than unity and less power can be extracted than what would be the case for isentropic expansion between the two pressure levels.

The effect of the compressor isentropic efficiency on the optimization results has been studied by performing optimization for different values of the isentropic efficiency but otherwise the same conditions as the base case. As can be observed in Fig. 3.39, the power consumption obviously decreases with increasing isentropic efficiency. Also, larger absolute savings in power consumption are obtained when the efficiency is low.

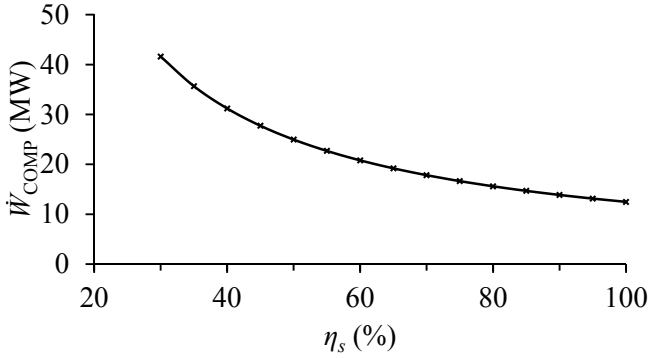

Figure 3.39. Power consumption of best known solution as function of compressor isentropic efficiency.

The isentropic efficiency is decisive for the irreversibilities in the compressor and the cooler. In addition to increased exergy destruction in the compressor itself, reduced isentropic efficiency leads to higher compressor discharge temperature and thereby increased exergy loss in the cooler. One may expect that the optimal trade-off between refrigerant flow rate and pressure ratio would shift to a design with a smaller pressure ratio in order to compensate this effect, in the same way as the optimal refrigerant flow rate is reduced when the minimum temperature difference is increased. The optimization results do, however, indicate that the optimal solution is the same, irrespective of the value of the isentropic efficiency.

Since the isentropic efficiency only affects the compression process and the cooler, the feasible set of the optimization problem will remain the same regardless the value of the isentropic efficiency. From the definition, the isentropic efficiency can therefore be interpreted as a scaling factor for the power consumption ($\dot{W} = \dot{W}_s/\eta_s$). Hence, the solution that provides the smallest power consumption for a given value of the isentropic efficiency should provide the best solution for all values of the isentropic efficiency. As long as the isentropic efficiency is constant, independent of the other process parameters, the optimal design of the PRICO® process does not change with changes in the value of the isentropic efficiency. When the pressure ratio of the

compression process varies, it is, however, not reasonable to assume a constant isentropic efficiency (Saravanamuttoo et al., 2009)

Polytropic efficiency

According to Saravanamuttoo et al. (2009), it is reasonable to assume that the isentropic efficiency of each stage in a multi-stage axial compressor will be the same if the blade design is the same. The friction in a compression stage leads to heat generation (and entropy production) and thereby a higher discharge temperature than the case would be for isentropic compression between the same pressure levels.

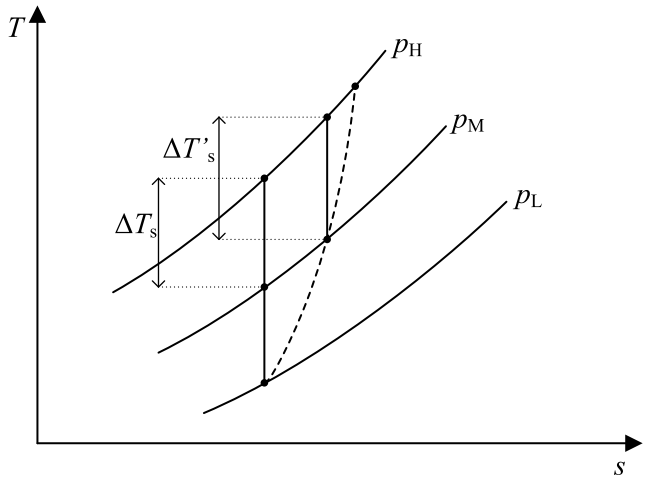

Figure 3.40. Compression process illustrated in simplified temperature-entropy diagram (Saravanamuttoo et al., 2009).

From the temperature-entropy diagram of a real gas, it is evident that the constant pressure lines diverge such that the vertical distance between to isobars increase with increasing entropy. Hence, the entropy production in a compression stage leads to increased isentropic compression work in the subsequent stages. The isentropic efficiency of the overall compression process will therefore be smaller than the isentropic efficiency of the individual stages (Saravanamuttoo et al., 2009). This effect may be referred to as preheating (Saravanamuttoo et al., 2009) and is illustrated in a simplified temperature-entropy diagram in Fig. 3.40, where $\Delta T'_s > \Delta T_s$.

In an expansion process, the effect of flow friction is opposite. The entropy production in an expansion stage leads to a higher input temperature for the subsequent stage than what is observed in the case of fully isentropic expansion. Hence, due to this reheating effect, more work can be extracted in the subsequent stage. As opposed to the compression process, the overall isentropic efficiency of the expansion process will be

higher than the isentropic efficiency of the individual stages (Saravanamuttoo et al, 2009).

A polytropic compression (or expansion) process is defined as an infinite series of elemental compression (or expansion) stages with uniform isentropic efficiency. When the pressure ratio of a compression or expansion process is varied, it is more reasonable to assume that this value will be constant rather than the isentropic efficiency. Assuming constant polytropic efficiency, the isentropic efficiency of a compression process would decrease with increasing pressure ratio, while for an expansion process the isentropic efficiency would increase (Saravanamuttoo et al., 2009).

In Fig. 3.41, results are given for optimization of the simple PRICO® process with different values of the polytropic efficiency, using the approach proposed by Schultz (1962) in Aspen HYSYS®. Like for the case of constant isentropic efficiency, the power consumption does, of course, increase with decreasing polytropic efficiency. As opposed to the case of constant isentropic efficiency, the solution does, however, change with changing polytropic efficiency.

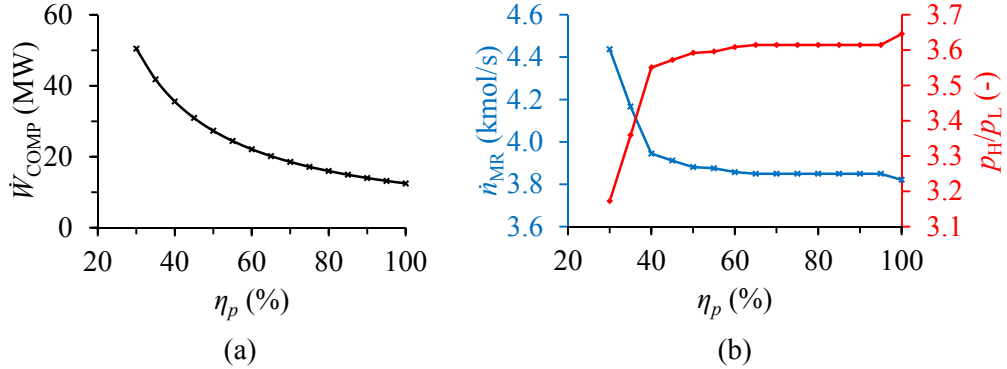

Figure 3.41. (a) Power consumption of best known solution as function of the polytropic efficiency; (b) Refrigerant flow rate (blue) and pressure ratio (red) in best known solution as functions of the polytropic efficiency.

In the case of polytropic efficiency $\eta_p = 1.0$, the compression process will be isentropic and the solution will be equal to the one obtained for a constant isentropic efficiency. Since higher pressure ratio gives smaller isentropic efficiency for the same polytropic efficiency, the optimal solution is shifted towards a smaller pressure ratio when the polytropic efficiency is smaller than unity. For relatively high values of the polytropic efficiency, the change is, however, quite small. The isentropic efficiency of the best known solution is given as function of the polytropic efficiency in Fig. 3.42.

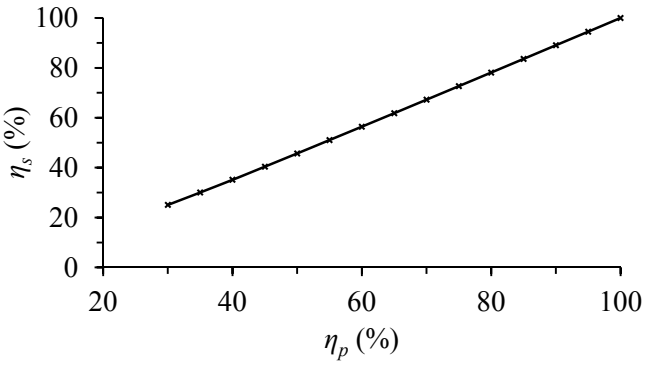

Figure 3.42. Isentropic efficiency of the best known solution as function of the polytropic efficiency.

3.5.4 Natural gas supply pressure

The pressure of the natural gas feed stream is usually given by upstream operations. Since the exergy load associated with cooling reduces with increasing pressure, throttling to the target pressure takes place after cooling. The effect of natural gas inlet pressure on power consumption is indicated in Fig. 3.43 (a). As expected, the power consumption is reduced with increasing inlet pressure. In the base case, the feed stream pressure is actually higher than the critical pressure ($p_{crit} \approx 53.6$ bar) and cricondenbar ($p_{cb} \approx 54.5$ bar) of the natural gas. Hence, the natural gas is cooled at supercritical pressure, before being expanded to the bubble point.

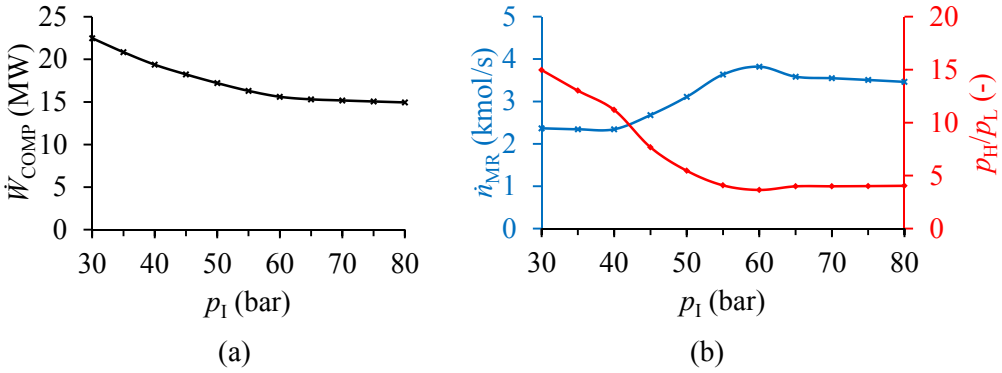

Figure 3.43. (a) Power consumption of best known solution as function of inlet pressure; (b) Refrigerant flow rate (blue) and pressure ratio (red) in best known solution as functions of natural gas inlet pressure.

As can be observed from Fig. 3.43, the refrigerant flow rate generally increases while the pressure ratio decreases with increasing supply pressure. With increasing natural gas pressure, the exergy load of the natural gas cooling is reduced as illustrated in Fig. 3.44 (a). The rational exergy efficiency of the process grows with increasing inlet pressure to reach a maximum value around $p_{in} = 60$ bar. For higher pressure levels,

there is a slight drop in exergy efficiency even though the power consumption is reduced.

The exergy efficiency of the liquefaction process is at least partly connected with the matching of the composite curves. As can be observed in Fig. 3.44 (b), the behaviour of the logarithmic mean temperature difference is similar to the behaviour of the rational exergy efficiency and the smallest value is observed for the same inlet pressure as the highest efficiency.

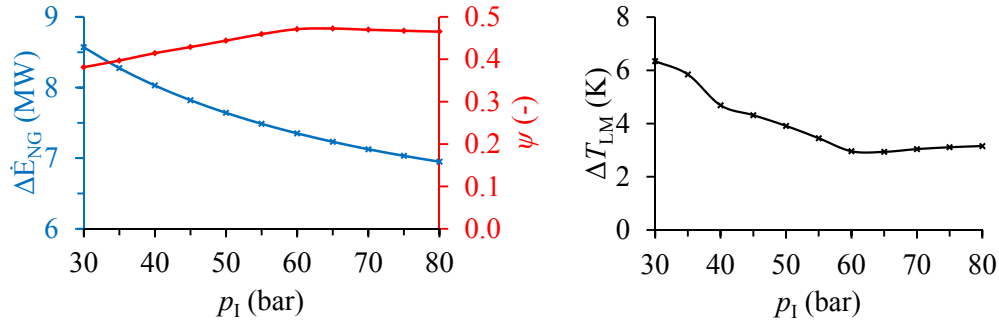

Figure 3.44. (a) Natural gas exergy load (blue) and rational exergy efficiency (red) of best known solution as functions of natural gas inlet pressure; (b) Logarithmic mean temperature difference of best known solution as function of natural gas inlet pressure.

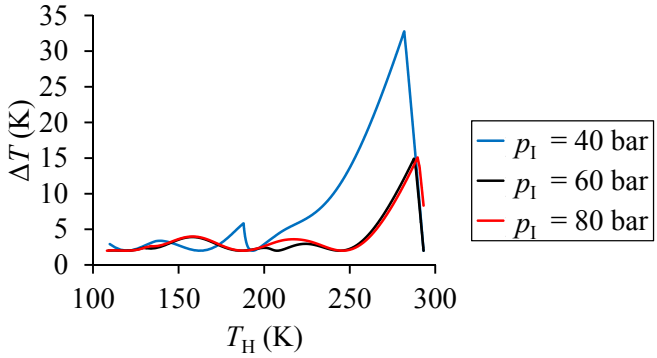

Figure 3.45. Temperature difference between composite curves as function of the hot composite temperature for different values of the natural gas inlet pressure.

In Fig. 3.45, the temperature difference between the composite curves is given as function of the hot stream temperature for different values of the natural gas inlet pressure. At sub-critical pressure, the nonlinearities of the temperature-enthalpy relation for the natural gas stream are more pronounced, making the matching of the composite curves more challenging. In the curve given for $p_{in} = 40$ bar, a sudden change in slope is observed around 190 K caused by the phase change of the natural gas from two-phase vapour-liquid to saturated liquid.

Natural gas compression

Depending on the supply pressure of the natural gas, compressing the natural gas to a higher pressure prior to liquefaction could improve the overall energy efficiency of the LNG process. A prerequisite for this is that the reduction in power consumption for the refrigeration cycle is smaller than the power consumption of the natural gas compressor. Hence, the optimal pressure level depends on the feed pressure of the natural gas. A modified process flowsheet is given in Fig. 3.46, with compression and ambient cooling of the natural gas stream prior to liquefaction.

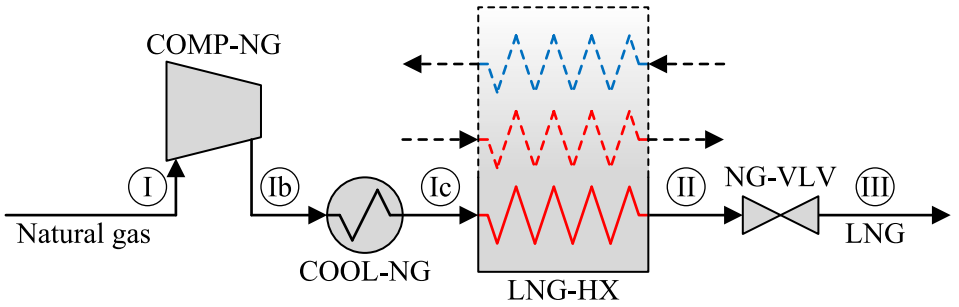

Figure 3.46. Single mixed-refrigerant process with feed gas compression.

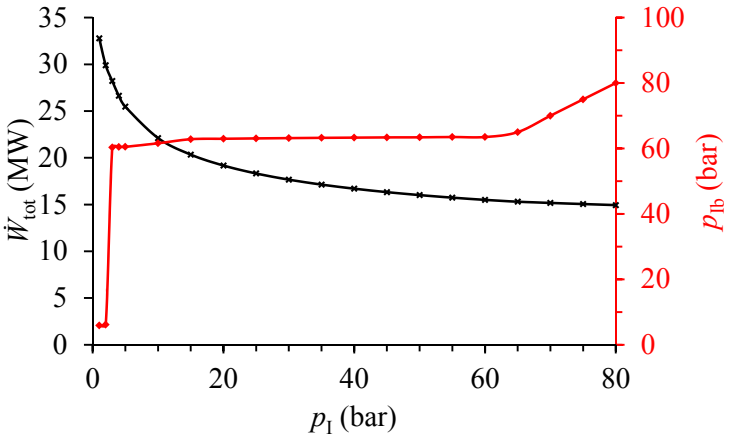

Figure 3.47. Total power consumption (black) and natural gas inlet pressure (red) of best known solution as functions of natural gas feed pressure.

In Fig. 3.47, the total power consumption (refrigeration process and natural gas compressor) and the natural gas inlet pressure (after natural gas compressor) of the best known solution are given as functions of the natural gas feed pressure. The natural gas is assumed compressed with a constant isentropic efficiency $\eta_{s,NG} = 0.80$, and cooled to the same inlet temperature ($T_{Ic} = T_I$).

For very low feed pressure levels, 1-2 bar, compression to around 6 bar is found to give the smallest total energy use. For higher feed pressure levels, the natural gas inlet pressure of the best known solution is in the range 60-64 bar. As discussed in Section 3.5.4, there is only a slight reduction in power consumption in the refrigeration process and decreasing exergy efficiency with increasing natural gas inlet pressure above 60 bar. For feed gas pressure $p_I = 65$ bar or higher, the total power consumption is found to increase if the natural gas is compressed to a higher pressure level prior to liquefaction.

3.5.5 Natural gas supply temperature

The feed temperature of the natural gas is usually given by the ambient temperature. Here, the feed temperature of the natural gas and the precooling temperature for the refrigerant are assumed to be 5 K higher than the ambient temperature. With increasing feed temperature, both the cooling load and exergy load of the natural gas increase. This results in higher power consumption, as illustrated in Fig. 3.48 (a), where optimization results are given for different values of the natural gas inlet temperature. As can be observed from Fig. 3.48 (b), the best known solution is shifted to higher pressure ratios with increasing inlet temperature.

With increased inlet temperature, the refrigeration cycle must cover a wider temperature range. In addition, since the ambient temperature is higher, the exergy required to remove heat below ambient increases. Hence, the exergy load of the natural gas stream to be cooled increases as indicated in Fig. 3.49 (a). The power consumption does, however, grow faster than the exergy load. Hence, as can be observed in Fig. 3.49 (b), the rational exergy efficiency is reduced when the natural gas inlet temperature increases.

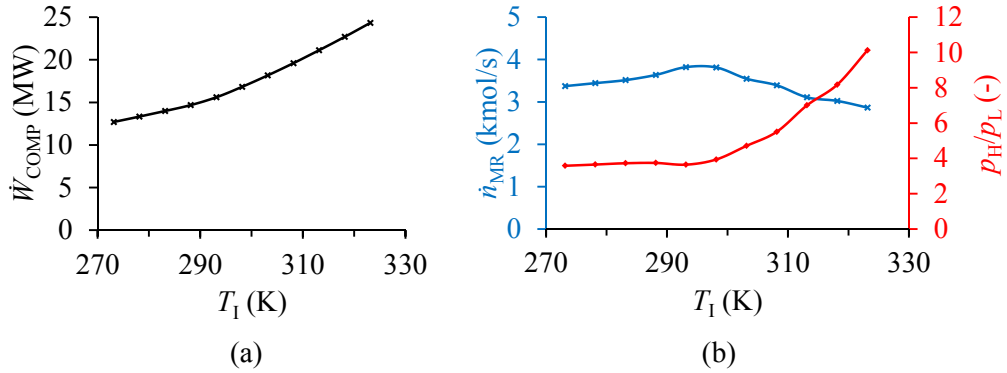

Figure 3.48. (a) Power consumption of best known solution as function of the natural gas inlet temperature; (b) Refrigerant flow rate (blue) and pressure ratio (red) in best known solution as functions of the natural gas inlet temperature.

The reduced exergy efficiency could be explained by the fact that the temperature range to be covered increases, which should indicate that matching the composite curves should be more challenging. Another possible explanation could be that the given refrigerant components do not provide a good matching of the composite curves when the temperature level is increased. Rian and Ertesvåg (2012) found the exergy efficiency of an LNG plant (not only the liquefaction process) to increase with increasing ambient temperature.

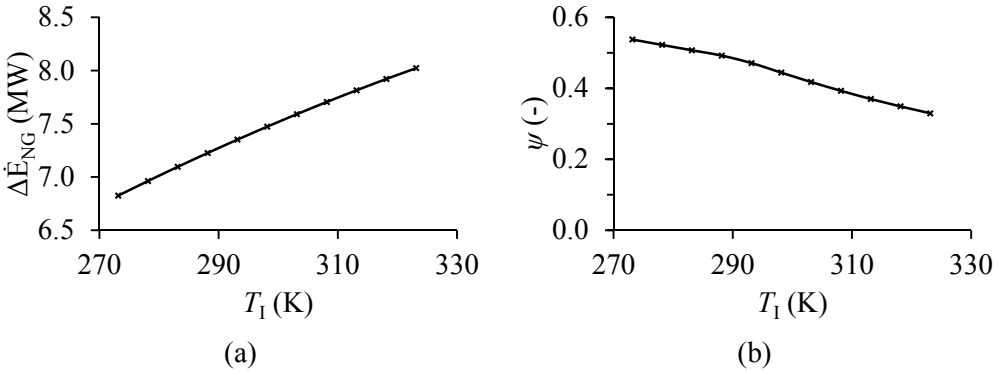

Figure 3.49. (a) Natural gas exergy load as function of natural gas inlet temperature; (b) Rational exergy efficiency as function of natural gas inlet temperature.

In order to fulfil the minimum superheating constraint (the dew point temperature must be smaller since the natural gas inlet temperature is smaller), part of the n-butane is replaced with i-butane. For the same pressure level, i-butane has a smaller saturation temperature than n-butane, which indicates that similar performance could be achieved with smaller dew point temperature if n-butane is replaced with i-butane. This is confirmed by the results in Fig. 3.50, where the refrigeration composition of the best known solution is plotted as function of the natural gas inlet temperature.

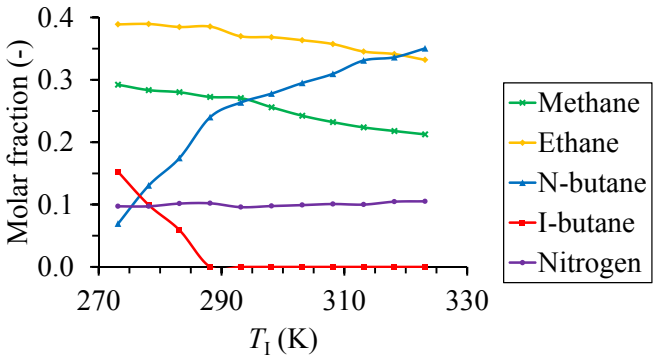

Figure 3.50. Molar composition of mixed refrigerant in best known solution as function of natural gas inlet temperature.

3.5.6 Natural gas target temperature

Like the less volatile components are decisive for the mixed refrigerant behaviour at high temperature levels, the high volatility components nitrogen and methane are important at low temperature levels. The effect of the natural gas target temperature was studied by varying the vapour fraction of the product natural gas stream after expansion (flash gas produced in the throttling valve). As can be observed in Fig. 3.51 (a), increasing the vapour fraction of the product stream is equivalent to increasing the outlet temperature of the natural gas. A molar fraction of vapour equal to 10 % is equivalent to an outlet temperature around 125 K, as opposed to around 109 K for saturated liquid (base case).

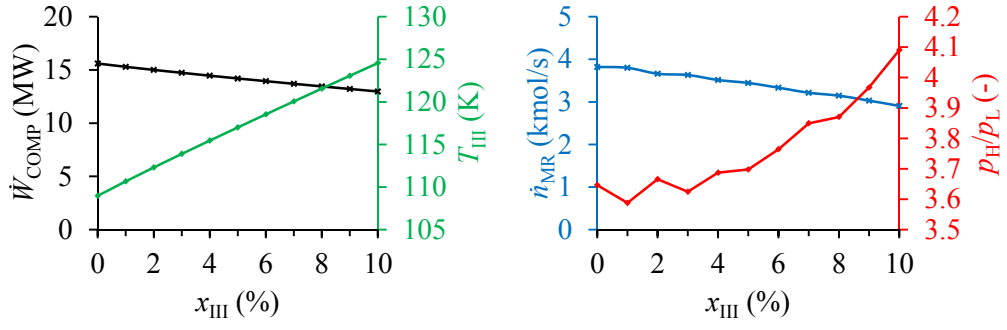

Figure 3.51. (a) Power consumption (black) and natural gas outlet temperature (green) of best known solution as function of the product vapour fraction; (b) Refrigerant flow rate (blue) and pressure ratio (red) in best known solution as functions of the product vapour fraction.

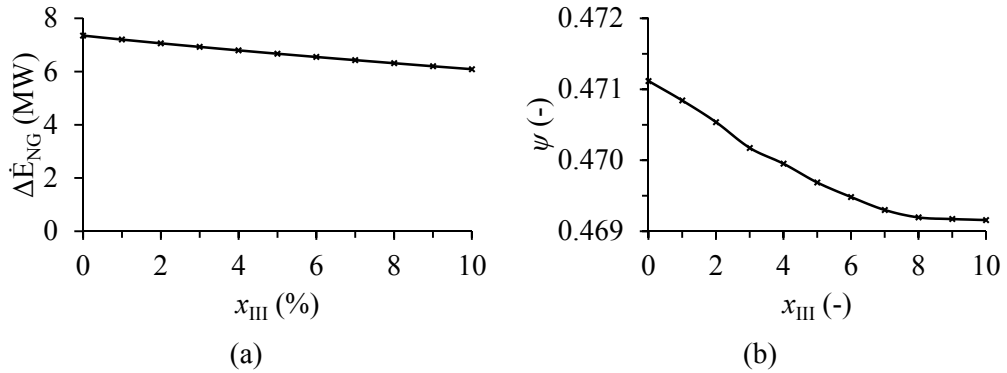

Figure 3.52. (a) Natural gas exergy load as function of product vapour fraction; (b) Rational exergy efficiency as function of product vapour fraction.

As expected, the power consumption is reduced when the target temperature of natural gas is increased. From Fig. 3.51 (b), one may observed that with higher outlet temperature, the trade-off between refrigerant flow rate and pressure ratio is shifted towards smaller flow rates and higher pressure ratios. Since the natural gas is cooled to

a higher temperature, the exergy load of the process decreases with increasing target vapour fraction as indicated in Fig. 3.52 (a).

Since the cooling range is reduced, one may expect the rational exergy efficiency to increase with increasing product vapour fraction. The change in exergy load is, however, quite small and the exergy efficiency practically constant irrespective of the product vapour fraction. This is illustrated in Fig. 3.52 (b), where the rational exergy efficiency is plotted as function of the product vapour fraction.

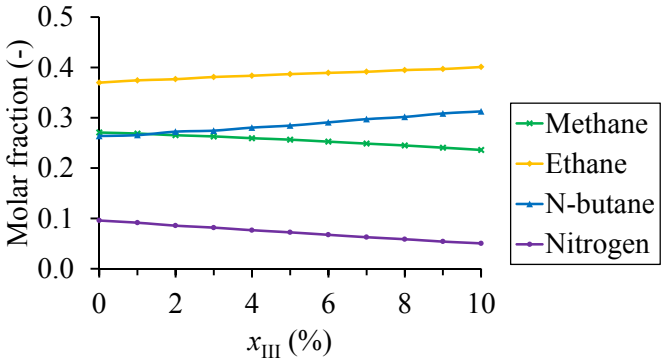

Figure 3.53. Molar composition of mixed refrigerant in best known solution as function of the vapour fraction of the natural gas product stream.

Molar fractions for the different refrigerant components are given in Fig. 3.53 as functions of the product vapour fraction. When the natural gas target temperature increases, the methane and nitrogen contents are reduced while the ethane and n-butane fractions are increased. As expected, the optimal refrigerant composition is less volatile for optimal operation at higher temperature level. For all the cases studied, propane and i-butane are not present in the optimized refrigerant.

3.5.7 Refrigerant composition

In Table 3.3, results are given from optimization with one of the refrigerant components excluded from the mixture. Since there is no propane or i-butane present in the refrigerant composition found to be best for the base case, excluding these components has no effect on the solution. No feasible solution is found without nitrogen in the mixture. An alternative refrigerant mixture including pentane (nC5 and iC5) was also optimized.

Without methane in the mixture, a considerable increase in nitrogen content is observed. The best known solution is characterized by a relatively high pressure ratio and a large refrigerant flow rate. As a result, the power consumption is more than doubled compared to the base case.

Table 3.3. Optimization results for the simple PRICO® process with different components present in the refrigerant mixture.

Property		Base case	No C1	No C2	No nC4	With C5
$\dot{W}_{COMP}$	(kW)	15 604	32 036	23 034	17 324	15 208
p_L	(bar)	3.9	12.5	1.0	3.6	3.4
p_H	(bar)	14.1	73.4	30.7	18.1	13.3
$\dot{n}_{MR}$	(kmol/s)	3.821	5.282	2.220	3.369	3.481
Molar composition:						
y_{C1}	(%)	27.1	-	31.5	24.4	27.5
y_{C2}	(%)	37.0	31.9	-	35.8	35.2
y_{C3}	(%)	0.0	0.0	57.1	0.0	4.1
y_{nC4}	(%)	26.4	9.2	6.6	-	0.0
y_{iC4}	(%)	0.0	0.0	0.0	29.2	13.4
y_{nC5}	(%)	-	-	-	-	2.0
y_{iC5}	(%)	-	-	-	-	8.5
y_{N2}	(%)	9.6	58.9	9.6	10.5	9.2

A very high pressure ratio is observed for the best known solution when ethane is not used in the refrigerant. The absence of ethane is compensated by increasing the content of methane and propane. These are the components closest to ethane with respect to volatility. The refrigerant flow rate is smaller than in the base, but a significant increase in power consumption is still observed.

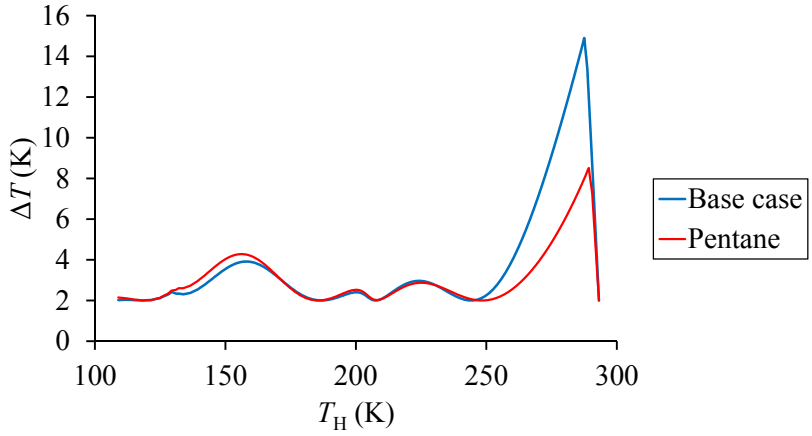

Figure 3.54. Heat exchanger temperature profile without pentane (blue line) and with pentane (red line) in the refrigerant mixture.

The consequence of omitting n-butane is smaller, both with respect to the decision variables and the power consumption. In this case, the n-butane present in the base case solution is replaced with i-butane which has similar properties. Only small changes are observed in the molar fractions of the remaining components. Compared to the base

case, the refrigerant flow rate is slightly smaller and the pressure ratio slightly higher. The net effect is a power increase of about 11 % compared to the base case with n-butane in the mixture.

When n-pentane and i-pentane are included as refrigerant components, the power consumption is reduced by around 2.5 % compared to the base case. Compared to the base case, the trade-off between pressure ratio and refrigerant flow rate is shifted towards a smaller pressure ratio and a higher flow rate, and the molar fractions of less volatile components are significantly changed. The n-butane present in the base case is replaced with propane, i-butane, n-pentane and i-pentane. As can be observed from Fig. 3.54, closer matching of the composite curves is observed in the hot end of the heat exchanger with pentane included in the refrigerant composition.

As was also discussed by Morin et al. (2011), large fractions of pentane are likely to cause problems with freeze-out in the cold end of the heat exchanger. The freezing point of the refrigerant mixture has not been studied here, but pentane could serve as an alternative refrigerant component in mixed-refrigerant precooling cycles.

3.5.8 Natural gas composition

The characteristics of the natural gas cooling curve depend on its composition, which for this reason could be of importance in the design of the refrigeration process. In order to study this, the simple PRICO® process has been optimized with seven different natural gas compositions. Comparisons have been made assuming the operating conditions are the same as in the base case studied for natural gas composition "NG-I". That is, the same supply temperature and pressure, target pressure and vapour fraction, isentropic efficiency, minimum temperature difference and minimum superheating.

Table 3.4. List of natural gas compositions with references.

Natural gas composition	References
NG-I	Aspelund et al. (2010)
NG-II	Aspelund et al. (2010)
NG-III	Venkatarathnam (2008), Hwang et al. (2013a, 2013b)
NG-IV	Khan et al. (2012, 2013), Khan and Lee (2013)
NG-V	Lee et al. (2014)
NG-VI	Shirazi and Mowla (2010)
NG-VII	Wang et al. (2013)

References to the different feed stream compositions are given in Table 3.4, with the molar fraction of the different components listed in Table 3.5. Methane, ethane, propane and n-butane are included in all the compositions considered, while the

presence of i-butane, pentane and nitrogen varies. Irrespective of the compositions, extraction of heavy hydrocarbons was not considered.

Table 3.5. Natural gas compositions (molar basis).

Composition	NG-I	NG-II	NG-III	NG-IV	NG-V	NG-VI	NG-VII
Methane	95.89	88.80	87.50	91.35	86.89	82.00	96.92
Ethane	2.96	5.60	5.50	5.36	5.10	11.20	2.94
Propane	0.72	2.10	2.10	2.14	2.13	4.00	0.06
I-butane				0.46	0.44	1.20	
N-butane	0.06	1.90	0.50	0.47	0.45	0.90	0.01
I-pentane				0.01	0.01		
N-pentane				0.01	0.01	0.70	
Nitrogen	0.37		4.00	0.20	4.97		

Results from the optimization are given in Table 3.6. Even though there is a relatively wide variation in composition for the different natural gas feed streams considered, the best known refrigerant composition is found to be quite similar for all the cases. Propane is found to be present in the refrigerant for three cases (NG-II, NG-IV and NG-VI), which have in common that the natural gas composition is relatively rich. The molar fractions of propane in the refrigerant mixture are, however, relatively small. Iso-butane is not found to be present in the best refrigerant for any of the natural gas compositions.

Table 3.6. Optimization results for different natural gas compositions.

Property	NG-I	NG-II	NG-III	NG-IV	NG-V	NG-VI	NG-VII
$\dot{W}$ (kW)	15 604	15 123	18 066	15 299	18 659	15 723	15 566
$\dot{n}_{MR}$ (kmol/s)	3.821	3.765	3.469	3.724	3.409	3.802	3.635
p_H/p_L (-)	3.65	3.69	5.35	3.79	5.82	3.83	3.86
p_L (bar)	3.87	4.63	2.89	4.50	2.64	4.24	3.53
p_H (bar)	14.10	17.10	15.48	17.09	15.33	16.23	13.60
Molar composition:							
y_{C1} (-)	0.271	0.267	0.256	0.264	0.254	0.263	0.265
y_{C2} (-)	0.370	0.358	0.330	0.371	0.322	0.352	0.373
y_{C3} (-)	0.000	0.021	0.000	0.005	0.000	0.016	0.000
y_{nC4} (-)	0.264	0.249	0.300	0.253	0.308	0.264	0.273
y_{iC4} (-)	0.000	0.000	0.000	0.000	0.000	0.000	0.000
y_{N2} (-)	0.096	0.105	0.114	0.106	0.115	0.106	0.090

A considerable variation in energy use is observed for the different feed stream compositions, and the power consumption is significantly higher for NG-III and NG-V. This is due to the high concentration of nitrogen in these natural gas mixtures, which

gives high exergy load and low target temperature. In order to reach the desired temperature levels, the best solution obtained for these cases has a high fraction of nitrogen and a high pressure ratio. The refrigerant flow rates are, however, slightly smaller than for the other natural gas compositions.

3.6 Conclusions

Sensitivity analysis around the best known design point for a single mixed-refrigerant process illustrated that challenges related to phase change for the different refrigerant streams and alternating locations for the pinch point in the heat exchangers are present even close to the (assumed) optimal solution. The optimization algorithm used must therefore be able to handle the non-differentiable points in both objective and constraint functions resulting from this.

The minimum temperature difference constraint must be fulfilled throughout the heat exchanger. Hence, the temperature drop in the refrigerant throttling valve in the cold end of the heat exchanger must provide a temperature drop equal to or larger than this minimum temperature difference. Thermodynamic considerations suggest that this temperature drop should be close to the minimum required in order to limit the irreversibilities associated with heat transfer.

For the case studied, the temperature of the refrigerant was found to increase while expanding (isenthalpic) in the region of sub-cooled liquid. A drop in temperature was first observed when the refrigerant stream reached the bubble point. Even though no further tests have been performed, this would suggest that isenthalpic expansion into the two-phase region is required in order to achieve the desired temperature drop.

In order to fulfil the minimum superheating constraint, the cold refrigerant stream exiting the hot end of the main heat exchanger must be superheated. Since the inlet temperature of the hot streams to the hot end of the same heat exchanger is fixed, a maximum (feasible) suction temperature for the compressor is given by the minimum temperature difference constraint. From this, the highest feasible dew point temperature for the low pressure refrigerant can be derived.

Since the dew and bubble point temperatures of the mentioned refrigerant streams do depend on both the refrigerant composition and the pressure levels, it would still be challenging to use this information to find appropriate narrow variables bounds for optimization. As was illustrated through the parameter studies, the trade-off between refrigerant flow rate and pressure ratio depends on the operating conditions of the process. Hence, also the process conditions would need to be taken into account for proper confinement of the search space.

The sensitivity analysis also indicate, what others have concluded, that the number of non-differentiable points could be reduced if the temperature difference at all evaluation points are used as constraints, instead of one constraint represented by the smallest of these temperature differences. The noise is even more pronounced for other compound functions such as the logarithmic mean temperature difference and heat exchanger conductance of the heat exchanger.

Discussions around the calculation procedure in Aspen HYSYS® indicated that the noise associated with these constraints could be further reduced by linearization of the composite curves. Since the use of unprocessed composite curves has proven to provide reasonable performance, this has, however, not been tested in this work.

3.7 References

Aspelund A, Gundersen T, Myklebust J, Nowak MP, Tomasgard A. An optimization-simulation model for a simple LNG process. *Computers and Chemical Engineering* 2010;34(10):1606-1617.

Hwang J-H, Ku N-K, Roh M-I, Lee K-Y. Optimal design of liquefaction cycles of liquefied natural gas floating, production, storage, and offloading unit considering optimal synthesis. *Industrial and Engineering Chemistry Research* 2013a;52(15):5341-5356.

Hwang J-H, Roh M-I, Lee K-Y. Determination of the optimal operating conditions of the dual mixed refrigerant cycle for the LNG FPSO topside liquefaction process. *Computer and Chemical Engineering* 2013b;49:25-36.

Kamath RS, Biegler LT, Grossmann IE. Modeling multistream heat exchangers with and without phase changes for simultaneous optimization and heat integration. *AIChE Journal* 2012;58(1):190-204.

Khan MS, Lee M. Design optimization of single mixed refrigerant natural gas liquefaction process using the particle swarm paradigm with nonlinear constraints. *Energy* 2013;49(1):146-155.

Khan MS, Lee S, Lee M. Optimization of single mixed refrigerant natural gas liquefaction plant with nonlinear programming. *Asia-Pacific Journal of Chemical Engineering* 2012;7(Suppl. 1):S62-S70.

Khan MS, Lee S, Rangaiah GP, Lee M. Knowledge based decision making method for the selection of mixed refrigerant systems for energy efficient LNG processes. *Applied Energy* 2013;111:1018-1031.

Lee I, Tak K, Kwon H, Kim J, Ko D, Moon I. Design and optimization of a pure refrigerant cycle for natural gas liquefaction with subcooling. *Industrial and Engineering Chemistry Research* 2014;53(25):10397-10403.

Moran MJ, Shapiro HN. *Fundamentals of Engineering Thermodynamics*. 2nd ed. Chichester: Wiley & Sons Ltd; 2006.

Morin A, Wahl PE, Mølnvik M. Using evolutionary search to optimise the energy consumption for natural gas liquefaction. *Chemical Engineering Research and Design* 2011;89(11):2428-2441.

Rian AB, Ertesvåg IS. Exergy evaluation of the arctic Snøhvit liquefied natural gas processing plant in northern Norway – Significance of ambient temperature. *Energy and Fuels* 2012;26(2):1259-1267.

Saravanamuttoo HIH, Cohen H, Rogers GFC, Straznicky PV. *Gas Turbine Theory*. 6th ed. Harlow: Prentice Hall: 2009.

Schittkowski K. 2006. NLPQLP (Version 2.2) [Computer program], <www.ai7.uni-bayreuth.de/nlpqlp.htm> [accessed 2014 Dec 12].

Schultz JM. The polytropic analysis of centrifugal compressors. *Journal of Engineering for Power* 1962;84(1):69-82.

Shirazi MMH, Mowla D. Energy optimization for liquefaction process of natural gas in peak shaving plant. *Energy* 2010;35(7):2878-2885.

Venkatarathnam G. *Cryogenic Mixed Refrigerant Processes*. New York: Springer Science; 2008.

Wahl PE, Løvseth SW, Mølnvik MJ. Optimization of a simple LNG process using sequential quadratic programming. *Computers and Chemical Engineering* 2013;56:27-36.

Wang M, Khalilpour R, Abbas A. Operation optimization of propane precooled mixed refrigerant processes. *Journal of Natural Gas Science and Engineering* 2013;15:93-105.

4 Stochastic Search

Due to the complex behaviour of the objective and constraints, stochastic search methods may serve as an interesting alternative for optimization of LNG processes. As discussed in Chapter 2, stochastic search methods have seen many applications in the literature on LNG process optimization. While genetic algorithms by far have received the most attention in literature, a simulated annealing algorithm has been used in this work.

Since most stochastic search methods are designed for unconstrained optimization problems, appropriate constraint handling is an important issue in use of such methods. Hence, in addition to studying the performance of simulated annealing, different constraint handling techniques have been compared.

This chapter is based on the following publication:

- Austbø B, Wahl PE, Gundersen T. Constraint handling in stochastic optimization algorithms for natural gas liquefaction processes. *Computer Aided Chemical Engineering* 2013;32:445-450.

4.1 Simulated annealing

Simulated annealing is a stochastic point-to-point search algorithm developed independently by Kirkpatrick et al. (1983) and Černý (1985) for large scale combinatorial problems. The search method is founded on the Metropolis algorithm (Metropolis et al., 1953). An early variant for optimization problems with continuous variables was proposed by Vanderbilt and Louie (1984). Simulated annealing provides measures to avoid getting trapped in local optima but gives no guarantee of finding the global optimum (Rutenbar, 1989).

In simulated annealing, a new candidate solution is randomly generated in each iteration. If the objective function is improved, the candidate solution is always accepted as the new solution. In order to avoid entrapment in local optima, candidate solutions that do not represent an improvement are also occasionally accepted as new

solutions. This is done randomly with a probability based on the level of deterioration and the iteration number.

In general, the probability of accepting a non-improving solution is reduced with the generation number, in accordance with annealing schedules. In an early phase of the search, most deteriorating solutions are accepted and the search closely resembles a random exploration of the search space. In the other end of the scale, towards the end of the search, practically only improving solutions are accepted and the search imitates downhill iterative improvement (Rutenbar, 1989).

The efficiency of a simulated annealing algorithm is dependent upon the annealing schedule. Too fast cooling increases the rate of entrapment in local optima, while too slow cooling leads to an excessively large number of iterations (Vanderbilt and Louie, 1984; Jones and Forbes, 1995). In standard simulated annealing, the acceptance probability is given by the Metropolis algorithm (Metropolis et al., 1953). A review and comparison of different annealing schemes was presented by Nourani and Andresen (1998).

In addition to the annealing schedule, the efficiency of simulated annealing algorithms depends on the search direction and step size (Wang and Chen, 1996). According to Vanderbilt and Louie (1984), the acceptance criteria and step lengths should be such that approximately half of the steps will be accepted as new solutions. A review of different simulated annealing algorithms was given by Schoen (1991).

4.1.1 Adaptive simulated annealing (ASA)

In this work, the adaptive simulated annealing algorithm ASA (Ingber, 1993a) (initially known as very fast re-annealing (Ingber, 1989)) has been used. In order to overcome the deficiencies of standard simulated annealing, ASA incorporates individual annealing schedules for the different optimization variables and information obtained during the search is used to adjust the annealing schedules (Ingber, 1993b). In ASA, an exponential annealing schedule is used.

4.2 Constraint handling

Generally, stochastic search methods lack the ability to handle constrained optimization problems. The idea of constraint handling is to transform a constrained optimization problem into an unconstrained one. According to Hedar and Fukushima (2006), an efficient search requires exploration of both feasible and infeasible regions, especially in the case that the global optimum is located on the boundary of the feasible region or the feasible region is divided into sub-regions. As illustrated in Chapter 3, at least the former is the case of LNG process optimization. In the best solution obtained for the single mixed-refrigerant process, the minimum temperature difference

constraint was found to be active, while the minimum superheating constraint was inactive.

4.2.1 Penalty functions

By use of penalty functions, a constrained optimization problem is transformed into an unconstrained one, thereby enabling use of stochastic search methods (Coello, 2002). Even though a majority of the penalty functions present in literature have been proposed for population-based search methods, most are applicable also for point-to-point methods such as simulated annealing.

Penalty functions may be classified as either exterior or interior. While exterior penalty functions are used to propagate infeasible solutions towards the feasible region, the purpose of interior penalty functions is to lead the search towards the centre of the feasible region by adding an increasing penalty when the feasible boundary is approached (Coello, 2002). In the case of optimization problems where the optimal solution is expected to be located near the feasible boundary (which is the case for LNG process optimization), only the former is of interest.

Further, penalty functions can be classified as static or dynamic. Static penalty functions are kept the same throughout the search, while the opposite is true for dynamic penalty functions. Dynamic penalty functions include subcategories such as annealing penalties that change periodically with the iteration number and adaptive penalties that utilizes feedback from the search process (Coello, 2002).

Static penalties

In the most extreme case, all infeasible solutions are discarded, which is equivalent to an infinite penalty. Since the global optimal solution is expected to be located on the boundary of the feasible region, however, valuable information from near-feasible solution may be important for the convergence of the optimization search. According to Coello (2002), the use of infinite penalties is limited to optimization problems with a convex feasible region covering the majority of the search space.

More commonly, the penalty is given as a function of the magnitude of the constraint violation. Hence, the penalty, and thereby also the modified objective function value, increases with increasing constraint violation. The penalty should be large enough to avoid the search to run wild into the infeasible region, yet small enough to enable exploration of near-feasible solutions.

Assuming only continuous variables, a modified objective function can be derived from the optimization problem defined as in Eq. (2.4) as

$$\varphi(\mathbf{x}) = f(\mathbf{x}) + \sum_{i=1}^{n}\left(r_i \cdot \max\left[0, g_i(\mathbf{x})\right]^{\beta}\right) + \sum_{j=1}^{p} c_j \cdot \left|h_j(\mathbf{x})\right|^{\gamma}, \tag{4.1}$$

where $f(\mathbf{x})$ is the constrained objective function, n is the number of inequality constraints $g_i(\mathbf{x})$, p is the number of equality constraints $h_j(\mathbf{x})$, r_i and c_j are penalty factors and β and γ are exponents usually set to 1 or 2.

A review of different penalty functions and other constraint handling techniques in general proposed in literature was given by Michalewicz et al. (1996). Many of the ideas would, of course, also be valid for point-to-point methods. Common to most penalty function approaches is the dependency on the penalty factors which are problem dependent and therefore must be adjusted for each individual optimization problem. When a specific approach is not available, the appropriate values must be found by trial and error.

In this work, the performance of static penalty functions proportional to constraint violations have been compared with constraint handling measures based on insight in the process characteristics. This has been done for optimization of a single mixed-refrigerant process for liquefaction of natural gas.

4.3 Case study – single mixed-refrigerant process

The simulated annealing algorithm (ASA) and the different constraint handling techniques have been tested for optimization of a single mixed-refrigerant process (PRICO®), as presented by Aspelund et al. (2010). A process flowsheet is given in Fig. 4.1.

This is the same case as considered in Chapter 3, except for the fact that pressure drop in heat transfer equipment is considered. This is done by assigning constant pressure drop values to each stream as indicated in Table 4.1. The Soave-Redlich-Kwong equation of state was used for process simulation in Aspen HYSYS®. Each stream in the main heat exchanger was divided into 100 segments of uniform temperature span and the pressure drop was implemented as a linear function of the enthalpy change.

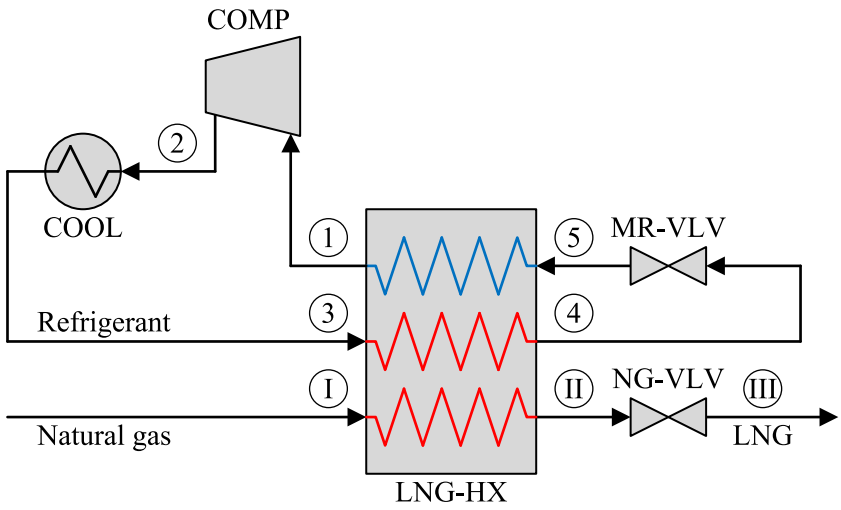

Figure 4.1. Process flowsheet for single mixed-refrigerant process (PRICO®).

Table 4.1. Heat exchanger pressure drop.

Stream	Pressure drop
Condenser	1.0 bar
LNG-HX – NG	5.0 bar
LNG-HX – MR hot side	4.0 bar
LNG-HX – MR cold side	1.0 bar

Power consumption was minimized subject to a minimum superheating of 10 K and a minimum temperature difference equal to 0.1 K, for a natural gas flow rate of 100 kg/s. For constraint handling, static penalty functions were compared with specialized approaches based on thermodynamics and process characteristics. With this problem formulation, all equality constraints are handled by the process simulator and only the inequality constraints are left to be handled in the optimization approach.

4.3.1 Minimum superheating

In the case that the minimum superheating constraint is violated, feasibility can be obtained by increasing the compressor suction temperature and/or reducing the dew point temperature of the refrigerant. As can be observed from Fig. 4.1, the inlet temperature of the compressor is given by the temperature of the cold refrigerant stream leaving the hot end of the heat exchanger. Further, the dew point temperature of the same stream is given by the low pressure level and the refrigerant composition.

The dew point temperature can be lowered by decreasing the low pressure level or reducing the content of low-volatile components in the refrigerant. Both measures would influence also other unit operations in the process, such as the driving forces in

the heat exchanger. Since these effects are difficult to estimate, manipulating the refrigerant composition is not an attractive option. Alternatively, one degree of freedom could be removed from the optimization problem by adjusting the low pressure level.

Increasing the temperature of the refrigerant cold stream exiting the hot end of the heat exchanger is not an option. A maximum value is given by the hot composite temperature in the hot end of the heat exchanger since the minimum temperature difference constraint must be fulfilled also in the end points. The compressor suction stream can, however, be heated after exiting the heat exchanger.

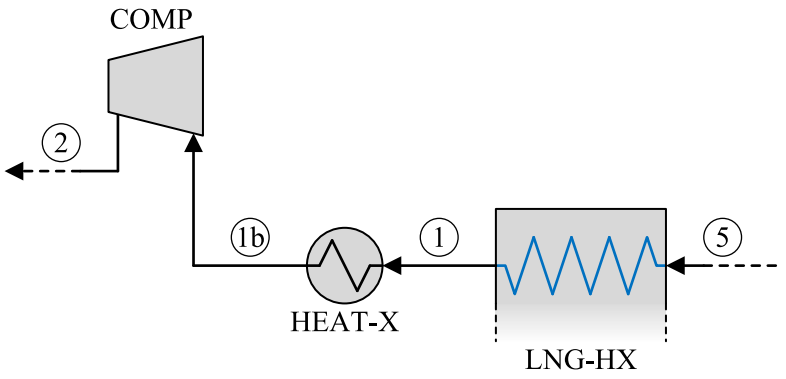

Figure 4.2. Modified flowsheet of PRICO® process with heater installed between the refrigerant cold stream exiting the heat exchanger and the compressor suction stream.

The superheating constraint could be fulfilled by installing a heater prior to the compressor as illustrated in Fig. 4.2. Since heat is available in the compressor discharge stream, this could easily be accomplished in a practical solution. The installed heater is only active when the superheating constraint is violated. That is, the exit temperature of the heater is given as the maximum of the heat exchanger exit temperature and the minimum temperature required in order to fulfil the constraint:

$$T_{1b} = \max\left\{T_1, T_{dew} + \Delta T_{dew,min}\right\}. \tag{4.2}$$

Here, T_1 is the cold refrigerant stream temperature in the hot end of the main heat exchanger, T_{dew} is the dew point of the low pressure refrigerant and $\Delta T_{dew,min}$ is the minimum superheating required. As can be observed from Eq. (3.3), increasing the compressor suction temperature would lead to increased compression power. Hence, applying the heater results in increased power consumption and thereby deterioration of the objective function. In order to avoid this, the search should naturally be lead towards a solution where the compressor suction heater is not active.

It is not necessary to modify the flowsheet to estimate the effect of increasing the compressor suction temperature. Assuming negligible changes in f_s, κ_v and Z_{in} (see Eq. (3.3)), a penalized objective (power consumption) can alternatively be expressed as

$$\dot{W}_{\text{pen}} = \frac{\max\left\{T_{\text{in}}, T_{\text{dew}} + \Delta T_{\text{dew,min}}\right\}}{T_{\text{in}}} \cdot \dot{W}_{\text{COMP}} \,. \tag{4.3}$$

In principle, this will give the same effect as modifying the process flowsheet.

4.3.2 Minimum temperature difference

From the discussion on heat transfer irreversibilities presented in Chapter 2, it is given that the irreversibilities associated with heat transfer increase with increasing temperature difference between the source and the sink. Hence, when the minimum temperature difference constraint is violated, the irreversibilities and thereby the compression power are reduced. If these solutions are not penalized in any way, the search will be lead into the infeasible region.

As discussed in Chapter 3, the minimum temperature difference is a complex function of the decision variables, and there is no obvious strategy to restore the required driving forces in the case of constraint violation. Hence, handling the minimum superheating constraint by altering the decision variables is challenging. An alternative is to add a penalty to the objective function, measuring the thermodynamic cost of increasing the temperature driving forces.

Similar to the approach used for the superheating constraint, a cooler could be installed in the cold end of the heat exchanger, as illustrated in Fig. 4.3, in order to reduce the temperature of the refrigerant cold stream before entering the cold end of the heat exchanger. This would lead to increased driving forces in the heat transfer process.

Due to the nonlinearities of the composite curves, reducing the cold stream inlet temperature equivalent to the constraint violation does not guarantee that the minimum temperature difference constraint is fulfilled throughout the heat exchanger. As opposed to the case of the heater installed upstream the compressor, there is no cold streams available in the process to provide the load required. Hence, a repairing approach is not available. The cooling load required can, however, be used as a basis for calculating a suitable penalty.

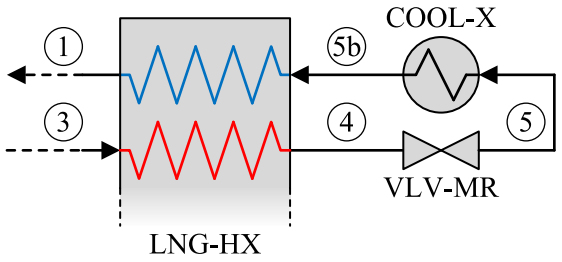

Figure 4.3. Modified flowsheet of PRICO® process with cooler installed between the valve exit stream and the refrigerant cold stream entering the heat exchanger.

The cooling load of the external cooler is given as

$$\dot{Q}_{\text{pen}} = \dot{m}_{\text{MR}} \cdot \left(h_5 - h_{5\text{b}}\right) = \dot{m}_{\text{MR}} \cdot \left(h\left(T_5\right) - h\left(T_{5\text{b}}\right)\right), \tag{4.4}$$

with

$$T_{5\text{b}} = \min\left\{T_5, T_5 - \Delta T_{\text{HX,min}} + \Delta T_{\text{small}}\right\}. \tag{4.5}$$

Here, ΔT_{small} is the smallest temperature difference observed in the heat exchanger, $\Delta T_{\text{HX,min}}$ the minimum temperature difference required in the heat exchanger, $\dot{m}_{\text{MR}}$ the refrigerant flow rate and h the specific enthalpy.

A penalty can then be formulated based on the exergy associated with this heat flow and a given exergy efficiency of the cooler:

$$\dot{W}_{\text{pen}} = \frac{\dot{Q}_{\text{pen}}}{\eta_{\text{pen}}} \cdot \left(1 - \frac{T_0}{T_5 - \Delta T_{\text{min}} - \Delta T_{\text{small}}}\right). \tag{4.6}$$

As a conservative estimate, the temperature at which the heat is to be removed is given by the temperature $T_{5\text{b}}$. In the case that the constraint is fulfilled, $T_{5\text{b}}$ will be equal to T_5 and the cooling load will be zero. Hence, the penalty will be active only when the minimum temperature difference constraint is violated.

The use of this penalty function would still require determination of a parameter value, the efficiency parameter η_{pen} in Eq. (4.6). In order to make sure the penalty is large enough, the value should be smaller than the exergy efficiency of the process. Hence, from experience with the process, finding appropriate parameter values should be easier than for the penalty function defined by Eq. (4.1).

A drawback of the suggested approach is that the penalty is given only by the magnitude of the constraint violation. In order to get a better measure of the effort

required to restore the driving forces should also take into account where the constraint is violated. As discussed in Chapter 2, the exergy of heat grows asymptotically to infinity as the absolute temperature approaches zero, and the irreversibilities associated with heat transfer across the same temperature difference increase with decreasing temperature level. Hence, the effort required to restore the driving forces when the minimum temperature difference constraint is violated increases with decreasing temperature level.

If the minimum temperature difference constraint is fulfilled in the cold end of the heat exchanger, there is no need to reduce the temperature of the refrigerant cold stream before entering the cold end of the heat exchanger in order to restore the driving forces in the hot end of the heat exchanger. An improved constraint handling method would therefore also take the temperature level at which the minimum temperature difference constraint is violated into account when determining the magnitude of the penalty. This has, however, not been considered in this work.

4.4 Results

In this work, the total number of iterations in the ASA search was set to 100 000, and each search was repeated 20 times. Initially, the annealing rate was found to be too fast as the search narrowed in on a small region already in an early phase of the search, allowing only limited exploration of the search space. ASA has more than 100 options for tuning of the search procedure. In this work, four of these were subject to variation.

Table 4.2. Decision variable bounds and values for the best solution found.

Variable	Unit	Lower bound	Upper bound	Best solution
Low pressure, p_L	bar	2.0	5.0	4.09
High pressure, p_H	bar	20.0	60.0	22.8
Methane flow rate, $\dot{m}_{C1}$	kg/s	0.0	200	82.0
Ethane flow rate, $\dot{m}_{C2}$	kg/s	0.0	250	237.9
Propane flow rate, $\dot{m}_{C3}$	kg/s	0.0	200	0.0
N-butane flow rate, $\dot{m}_{nC4}$	kg/s	0.0	300	270.5
Nitrogen flow rate, $\dot{m}_{N2}$	kg/s	0.0	200	53.8

The variable bounds used for the different variables are given in Table 4.2, minimizing the power consumption of the compressor with a natural gas flow rate of 100 kg/s. The best solution obtained is given by the rightmost column in Table 4.2. For this solution the specific power consumption was found to be 1063 kJ/kg LNG. Due to the inclusion of a constant pressure drop in the heat exchanger, the best solution is different from what was obtained in Chapter 3. Obviously, the power consumption is higher when pressure drop is considered.

The best solution obtained in this work is smaller than what was reported by Aspelund et al. (2010) (1105 kJ/kg LNG). This is caused by the fact that the best known solution is located outside the variable bounds used by Aspelund et al. (2010) ($p_H^* < 30.0$ bar, $\dot{m}_{C2}^* > 180.6$ kg/s, $\dot{m}_{C3}^* < 13.9$ kg/s, $\dot{m}_{nC4}^* > 236.1$ kg/s). When using the same variable bounds as used by Aspelund et al. (2010), the specific power consumption of the best solution obtained using ASA was 1100 kJ/kg LNG.

The same problem was studied by Wahl et al. (2013), who used a sequential quadratic programming approach (NLPQLP) for the optimization. They reported a solution with power consumption equal to 1061 kJ/kg LNG, which is slightly better than the solution reported here. The difference could, however, also be related to differences in the problem formulation, especially with respect to the heat exchanger modelling (discretization). When the NLPQLP approach was used for the same problem formulation as used for the ASA search, the best solution was found to be 1063 kJ/kg LNG as well.

Optimization results for different constraint handling methods are given in Table 4.3. Here, the best solution obtained in 20 runs is given together with the average solution and the number of runs returning a feasible solution. The solutions are considered to be feasible only in the case that what is found to be the best solution for the modified optimization problem is a feasible solution of the original formulation. A feasible (possible also good) solution still might have been encountered during the search.

Table 4.3. Optimization results from 20 runs with different constraint handling methods.

Superheating		Heat transfer		Solution (kJ/kg LNG)		
r	β	r	β	Best	Average	% feasible
∞	1	∞	1	1064.3	1068.1	100
10 000	1	10 000	1	1063.9	1069.4	100
1 000	1	1 000	1	1063.7	1072.9	100
100	1	100	1	1063.1	Infeasible	50
1 000 000	2	1 000 000	2	1063.0	1067.4	100
100 000	2	100 000	2	1063.2	Infeasible	90
10 000	2	10 000	2	Infeasible	Infeasible	0
Repair		$\dot{W}_{pen}$ ($\eta_{pen} = 0.1$)		1063.2	1067.3	100
Repair		$\dot{W}_{pen}$ ($\eta_{pen} = 0.2$)		1062.9	Infeasible	55
Repair		$\dot{W}_{pen}$ ($\eta_{pen} = 0.3$)		1064.4	Infeasible	5

Only in one case ($r = 10\,000$ and $\beta = 2$), the penalty is generally too small and all returned solutions are found to be infeasible. For the remaining cases, at least one feasible solution is returned. There is little variation in the solution obtained for the different formulations, both with respect to the best solution and the average solution.

The power consumption of the best solution obtained with an infinite penalty (discarding all infeasible solutions) is less than 0.2 % higher than the overall best solution obtained. The run time of search was in the range 3-5 hours, varying due to differences in computer load and convergence of the simulation model.

4.5 Conclusions

The performance of a simulated annealing algorithm (ASA) has been tested for optimization of a single mixed-refrigerant process for liquefaction of natural gas. Constraint handling based on process characteristics was compared with different static penalty functions. The results indicated that, irrespective of the size of the penalty, the majority of the searches led to solutions close to the best known solution to the optimization problem. Thus, for the given formulation, the constraint handling technique was fond to be of little importance for the search performance. It may, however, be that this would be of more importance if the complexity of the process is increased and/or the number of iterations is reduced.

For the case studied, the results obtained in this study were better than reported in the original paper (Aspelund et al., 2010). This was found to be due to wider variable bounds, as what was found to be the best solution is located outside the bounds used by Aspelund et al. (2010). The results are close to what was obtained using NLPQLP, with only slightly higher power consumption. This can be caused by the inadequacy of stochastic search methods with respect to refining a local optimal solution.

A drawback of simulated annealing, and other stochastic search methods in general, is the slow search compared to deterministic (gradient-based) approaches. Even though a local deterministic search method may occasionally get trapped in local optima, many local searches from different starting points can be performed within the time used by simulated annealing search. Even though the stochastic search methods are simple in nature, different search parameters have to be adjusted for each application.

It may be unfair to evaluate the stochastic search methods based on the results obtained for optimization of a simple PRICO® process, since the results obtained using local deterministic search methods have already proven to give good performance for such processes. Stochastic methods may prove useful when more complex processes are considered. Due to the inefficient local search characteristics, however, stochastic search methods should only be used to locate potentially interesting regions of the search space, leaving local search to be performed by a deterministic search method.

For the remaining part of this work, deterministic search methods (NLPQLP) have been used. Stochastic elements are here present only in the generation of random starting points. Instead of studying the performance of the search algorithm, the work

has been focused on utilizing knowledge about the characteristics of the process behaviour and thermodynamics in order to formulate the optimization problem in a way that increases the likelihood of finding the optimal solution.

4.6 References

Aspelund A, Gundersen T, Myklebust J, Nowak MP, Tomasgard A. An optimization-simulation model for a simple LNG process. *Computers and Chemical Engineering* 2010;34(10):1606-1617.

Černý V. Thermodynamical Approach to the traveling salesman problem: An efficient simulation algorithm. *Journal of Optimization Theory and Applications* 1985;45(1):41-51.

Coello CAC. Theoretical and numerical constraint-handling techniques used with evolutionary algorithms: A survey of the state of the art. *Computer Methods in Applied Mechanics and Engineering* 2002;191(11-12):1245-1287.

Hedar AR, Fukushima M. Derivative-free filter simulated annealing method for constrained continuous global optimization. *Journal of Global Optimization* 2006;35(4):521-549.

Ingber L. Very Fast Simulated Re-Annealing. *Mathematical and Computer Modelling* 1989;12(8):967-973.

Ingber L. 1993a. Adaptive Simulated Annealing (ASA) (Version 28.9) [Computer Program]. Available from: http://www.ingber.com/#ASA-CODE. [accessed 2014 Dec 15].

Ingber L. Simulated Annealing: Practice versus theory. *Mathematical and Computer Modelling* 1993b:18(11):29-57.

Jones AEW, Forbes GW. An adaptive simulated annealing algorithm for global optimization over continuous variables. *Journal of Global Optimization* 1995;6(1):1-37.

Kirkpatrick S, Gelatt CD Jr, Vecchi MP. Optimization by simulated annealing. *Science* 1983;220(4598):671-680.

Metropolis N, Rosenbluth AW, Rosenbluth MN, Teller AH. Equation of state calculations by fast computing machines. *The Journal of Chemical Physics* 1953;21(6):1087-1092.

Michalewicz Z, Dasgupta D, Le Riche RG, Schoenauer M. Evolutionary algorithms for constrained engineering problems. *Computers and Industrial Engineering* 1996;30(4):851-870.

Nourani Y, Andresen B. A comparison of simulated annealing cooling strategies. *Journal of Physics A: Mathematical and General* 1998;31(41):8378-8385.

Rutenbar RA. Simulated annealing algorithms: An overview. *IEEE Circuits and Devices Magazine* 1989;5(1):19-26.

Schoen F. Stochastic Techniques for global optimization: A survey of recent advances. *Journal of Global Optimization* 1991;1(3):207-228.

Vanderbilt D, Louie SG. A Monte Carlo simulated annealing approach to optimization over continuous variables. *Journal of Computational Physics* 1984;56(2):259-271.

Wahl PE, Løvseth SW, Mølnvik MJ. Optimization of a simple LNG process using sequential quadratic programming. *Computers and Chemical Engineering* 2013;56:27-36.

Wang PP, Chen D-S. Continuous Optimization by a variant of simulated annealing. *Computational Optimization and Applications* 1996;6(1):59-71.

5 Process Modelling

Due to the small temperature driving forces in heat transfer, rigorous thermodynamic models are required in LNG process modelling to ensure practical feasibility of the results. While optimization of a simplified model may more easily lead to the global optimum, correspondence between the optimal solution of the process model and the optimal practical solution is just as important. A simplified model may, anyway, serve as a tool in conceptual process design, restricting and/or locate interesting regions of the search space used with a more rigorous process model.

The characteristics of nitrogen indicate behaviour close to that of an ideal gas under the given conditions. For this reason, simplified process models assuming ideal behaviour of the refrigerant may be applicable for optimization of nitrogen expander processes for natural gas liquefaction.

In this chapter, two nitrogen expander processes (single and dual) used for liquefaction of natural gas have been optimized. Comparisons have been made between a simplified process model assuming perfect gas behaviour for the refrigerant and a rigorous model using a cubic equation of state. For the single expander process, optimization of the simplified model was solved analytically, while NLPQLP was used for rigorous model. Optimal intermediate pressure levels in multi-stage compression have also been studied.

This chapter is partly based on the following publication:

- Austbø B, Gundersen T. Optimization of a single expander LNG process. Accepted for publication in *Energy Procedia*.

5.1 Introduction

In expander processes, the refrigerant is kept in gas phase throughout the cycle, indicating potential use of ideal gas models. Nevertheless, the ideal gas law does not apply to real gases. The behaviour of real gases do, however, approach ideal gas behaviour when the pressure is low compared to the critical pressure and/or the

temperature is high compared to the critical temperature. The critical pressure of nitrogen is around 33.9 bar, while the critical temperature is around 126 K (Moran and Shapiro, 2006). Hence, depending on the operating conditions, an ideal gas model may provide decent accuracy for modelling of nitrogen as refrigerant in LNG expander processes.

Studies performed on simulation and optimization of expander based refrigeration processes have used different approaches to thermodynamic modelling. Streit and Razani (2012, 2013) optimized different expander processes for cryogenic single temperature loads, studying the effect of auxiliary cooling. Analytical solutions were derived for the coefficient of performance (COP). The processes were modelled in Engineering Equation Solver (EES) (F-Chart Software) for an ideal monoatomic gas with constant specific heat capacity.

Marmolejo-Correa and Gundersen (2010) designed a single nitrogen expander process for natural gas liquefaction using a method combining pinch analysis and exergy analysis. The refrigerant was assumed to behave as an ideal gas with constant specific heat capacity. An ideal gas model was also used by Wechsung et al. (2011) for optimization of an expander-based LNG process, under the assumption of constant specific heat capacity for the different streams.

Chang et al. (2009) performed sensitivity analysis of a single nitrogen expander process for methane liquefaction using accurate thermodynamic data from the National Institute of Standards and Technology (NIST) for process modelling. Thermodynamic data from NIST were used also by Li et al. (2012) for modelling of helium expander processes used for liquefaction of different pure substances. The exergy efficiency of the process was maximized using a genetic algorithm.

Yoon et al. (2012) and He and Ju (2014) used genetic algorithms to optimize dual nitrogen expander LNG processes modelled with the Peng-Robinson equation of state. Yuan et al. (2014) used a combination of Peng-Robinson and Lee-Kesler-Plöcker equations of state for optimization of a single nitrogen expander LNG process with carbon dioxide precooling and performed optimization using the built-in optimizer in Aspen HYSYS®.

A simplified process model is likely to be easier to optimize. This makes simplified modelling assuming perfect gas (ideal gas with constant specific heat) behaviour an interesting alternative for design of nitrogen expander processes for natural gas. In this work, the performance of a simplified thermodynamic model assuming perfect gas behaviour is compared with cubic equations of state for optimization of nitrogen expander processes. The simplified model is solved analytically (for a single expander

process), while the rigorous model is optimized using sequential quadratic programming.

5.2 Single nitrogen expander process

5.2.1 Problem formulation

Data for the natural gas stream to be liquefied are given in Table 5.1, with a composition similar to the case studies presented by Jensen and Skogestad (2006) and Jacobsen and Skogestad (2013). The process was modelled under the assumption of constant isentropic efficiencies $\eta_{s,\mathrm{COMP}}$ and $\eta_{s,\mathrm{EXP}}$ for the compressor and expander, and negligible pressure drop in heat exchangers.

Table 5.1. Natural gas properties.

Variable	Unit	Value
Flow rate $\dot{m}_{\mathrm{NG}}$	kg/s	1
Feed pressure p_{I}	bar	55
Feed temperature T_{I}	K	293.15
Product temperature T_{III}	K	115.00
Molar composition:		
Methane	-	0.897
Ethane	-	0.055
Propane	-	0.018
N-butane	-	0.002
Nitrogen	-	0.028

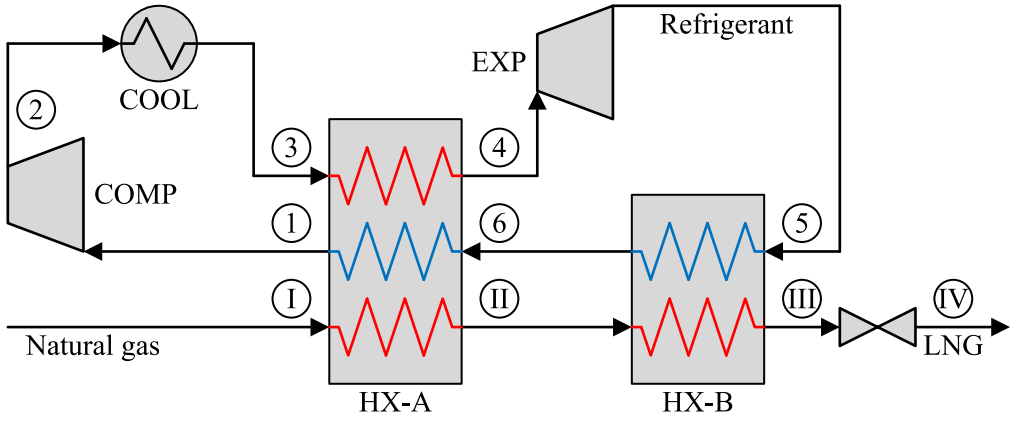

Figure 5.1. Single expander process flowsheet.

A process flowsheet with stream numbers is given in Fig. 5.1. The process was optimized with the objective of minimizing the power consumption subject to a minimum temperature difference ΔT_{min} in the heat exchangers HX-A and HX-B. The

two hot streams in HX-A are assumed to be precooled to the same temperature prior to entering the hot end ($T_3 = T_I$), and to have the same exit temperature ($T_4 = T_{II}$). From this, four degrees of freedom are available for the design optimization. Different decision variables were chosen for the two modelling alternatives.

Simplified model

In the simplified model, the refrigerant was assumed to behave as a perfect gas, i.e. an ideal gas with constant specific heat $c_{p,R}$ (in this work denoted as a perfect gas model). The cooling curve of the natural gas stream is modelled with a constant heat capacity $(\dot{m} \cdot c_p)_{NG}$ equal to the mean value of the heat capacity observed for the natural gas in the rigorous model. Due to the simplicity of the formulation, the optimization problem was solved analytically.

Rigorous model

Aspen HYSYS® was used for modelling of the rigorous process model, using the Soave-Redlich-Kwong cubic equation of state. The optimization problem was solved in a multi-start approach from random starting points using NLPQLP.

5.2.2 Simplified model

From the characteristics of the simplified process, it is given that the smallest temperature differences in the process will be observed in the hot end of HX-A and the cold end of HX-B. This can be observed in Fig. 5.2, where composite curves are given for the cooling of the natural gas. Under the assumption of a perfect gas model, the pressure levels to not influence the model. Hence, one of the four degrees of freedom was not available. The three decision variables used were the stage temperature T_{II}, the hot end temperature difference $\Delta T_{hot} = T_I - T_1$ and the cold end temperature difference $\Delta T_{cold} = T_{III} - T_5$.

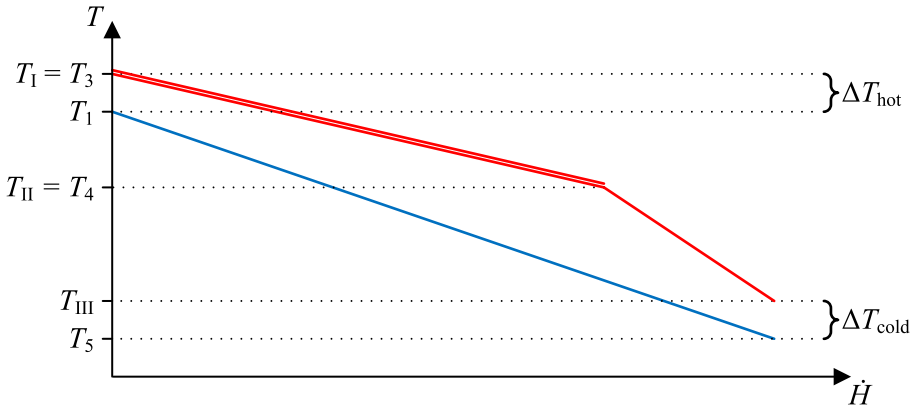

Figure 5.2. Composite curves for simplified model of single expander LNG process.

Based on the choice of decision variables, the refrigerant flow rate can be derived from an overall energy balance for the two heat exchangers:

$$\dot{m}_{\mathrm{R}} = \frac{\left(\dot{m} \cdot c_p\right)_{\mathrm{NG}} \cdot \left(T_{\mathrm{I}} - T_{\mathrm{III}}\right)}{c_{p,\mathrm{R}} \cdot \left(T_{\mathrm{II}} - T_{\mathrm{III}} + \Delta T_{\mathrm{cold}} - \Delta T_{\mathrm{hot}}\right)}. \tag{5.1}$$

For a perfect gas, the enthalpy change is given as $\Delta h = c_p \cdot \Delta T$. Since both the inlet and outlet temperature of the expander are given by the decision variables, the expansion power can therefore be expressed as

$$\dot{W}_{\mathrm{EXP}} = \left(\dot{m} \cdot c_p\right)_{\mathrm{NG}} \cdot \left(T_{\mathrm{I}} - T_{\mathrm{III}}\right) \cdot \frac{T_{\mathrm{II}} - T_{\mathrm{III}} + \Delta T_{\mathrm{cold}}}{T_{\mathrm{II}} - T_{\mathrm{III}} + \Delta T_{\mathrm{cold}} - \Delta T_{\mathrm{hot}}}. \tag{5.2}$$

The isentropic expansion temperature (expander discharge temperature in the case of isentropic expansion) can be calculated from the definition of isentropic efficiency for an expansion process:

$$T_{5\mathrm{s}} = \frac{T_{\mathrm{II}} \cdot \left(\eta_{s,\mathrm{EXP}} - 1\right) + T_{\mathrm{III}} - \Delta T_{\mathrm{cold}}}{\eta_{s,\mathrm{EXP}}}. \tag{5.3}$$

Further, for a perfect gas, the entropy change between two states is given by

$$\Delta s_{1\to 2} = c_p \cdot \ln\frac{T_2}{T_1} - R \cdot \ln\frac{p_2}{p_1}. \tag{5.4}$$

Hence, the pressure ratio of the refrigerant can be expressed as

$$\frac{p_{\mathrm{H}}}{p_{\mathrm{L}}} = \left(\frac{T_{\mathrm{II}} \cdot \eta_{s,\mathrm{EXP}}}{T_{\mathrm{II}} \cdot \left(\eta_{s,\mathrm{EXP}} - 1\right) + T_{\mathrm{III}} - \Delta T_{\mathrm{cold}}}\right)^{\frac{c_{p,\mathrm{R}}}{R}}, \tag{5.5}$$

where p_{H} and p_{L} are the high and low pressure levels of the refrigerant.

The isentropic discharge temperature of the compressor can be calculated by use of Eqs. (5.4) and (5.5):

$$T_{2\mathrm{s}} = \frac{\left(T_{\mathrm{I}} - \Delta T_{\mathrm{hot}}\right) \cdot T_{\mathrm{II}} \cdot \eta_{s,\mathrm{EXP}}}{T_{\mathrm{II}} \cdot \left(\eta_{s,\mathrm{EXP}} - 1\right) + T_{\mathrm{III}} - \Delta T_{\mathrm{cold}}}. \tag{5.6}$$

Further, taking into account the definition of isentropic efficiency for a compression process, the power consumption of the compressor is given by the energy balance:

$$\dot{W}_{\mathrm{COMP}} = \frac{\left(\dot{m}\cdot c_p\right)_{\mathrm{NG}}\cdot\left(T_{\mathrm{I}}-T_{\mathrm{III}}\right)\cdot\left(T_{\mathrm{I}}-\Delta T_{\mathrm{hot}}\right)}{\eta_{s,\mathrm{COMP}}\cdot\left(T_{\mathrm{II}}-T_{\mathrm{III}}+\Delta T_{\mathrm{cold}}-\Delta T_{\mathrm{hot}}\right)}\cdot\left(\frac{T_{\mathrm{II}}\cdot\eta_{s,\mathrm{EXP}}}{T_{\mathrm{II}}\cdot\left(\eta_{s,\mathrm{EXP}}-1\right)+T_{\mathrm{III}}-\Delta T_{\mathrm{cold}}}-1\right) \quad (5.7)$$

The net power consumption is then given as the difference between the compression and expansion power:

$$\dot{W}_{\mathrm{NET}} = \frac{\left(\dot{m}\cdot c_p\right)_{\mathrm{NG}}\cdot\left(T_{\mathrm{I}}-T_{\mathrm{III}}\right)\cdot\left(T_{\mathrm{II}}-T_{\mathrm{III}}+\Delta T_{\mathrm{cold}}\right)}{T_{\mathrm{II}}-T_{\mathrm{III}}+\Delta T_{\mathrm{cold}}-\Delta T_{\mathrm{hot}}} \cdot\left(\frac{T_{\mathrm{I}}-\Delta T_{\mathrm{hot}}}{\eta_{s,\mathrm{COMP}}\cdot\left(T_{\mathrm{II}}\cdot\left(\eta_{s,\mathrm{EXP}}-1\right)+T_{\mathrm{III}}-\Delta T_{\mathrm{cold}}\right)}-1\right). \quad (5.8)$$

As can be observed from Eq. (5.1), the refrigerant flow rate increases with decreasing stage temperature T_{II}. When the stage temperature is reduced, the specific cooling load caused by refrigerant cooling in HX-A increases. Hence, the refrigerant flow rate must be increased to fulfil the energy balance for the two heat exchangers. This is also illustrated in Fig. 5.3 (a), where the refrigerant flow rate and pressure ratio are plotted as functions of the stage temperature T_{II} for $\Delta T_{\mathrm{hot}} = \Delta T_{\mathrm{cold}} = \Delta T_{\mathrm{min}} = 2$ K and $\eta_{s,\mathrm{COMP}} = \eta_{s,\mathrm{EXP}} = 0.80$.

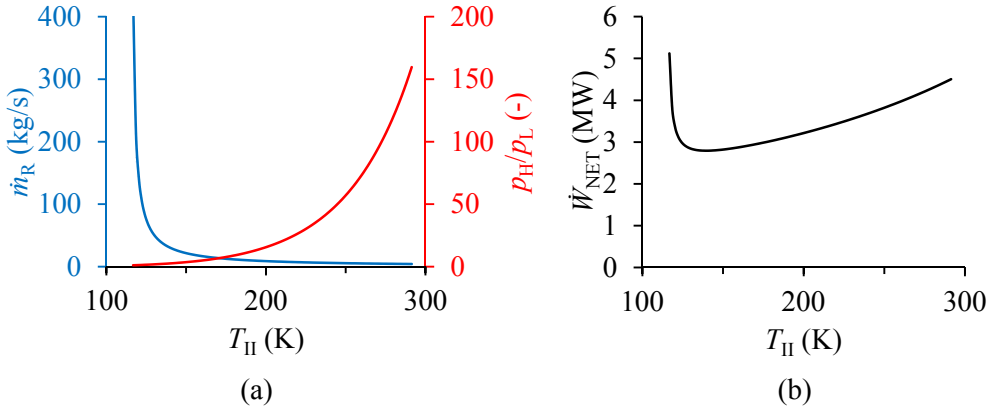

Figure 5.3. (a) Refrigerant flow rate (blue) and pressure ratio (red) for the simplified process model as functions of stage temperature; (b) Net power consumption in the simplified process model as function of stage temperature.

Due to the fact that the temperature drop in the expander is reduced, the pressure ratio of the refrigerant decreases with decreasing stage temperature. When the stage temperature approaches the target temperature of the natural gas stream, the pressure

ratio approaches unity, while the refrigerant flow rate goes to infinity since cooling load from the hot stream refrigerant is equal to the cooling capacity of the cold stream refrigerant. This can be observed from Eq. (5.1) for the case of $\Delta T_{\text{hot}} = \Delta T_{\text{cold}}$.

Increasing flow rate and decreasing pressure ratio have opposite effects on the total power consumption. As can be observed in Fig. 5.3 (b), the smallest power consumption is found at an intermediate stage temperature where the trade-off between the two effects is balanced. The optimal trade-off between the refrigerant flow rate and pressure ratio would depend on the operating conditions.

Optimization

From the choice of decision variables it is given that the design will fulfil the constraints as long as $\Delta T_{\text{cold}} \geq \Delta T_{\text{min}}$ and $\Delta T_{\text{hot}} \geq \Delta T_{\text{min}}$. Larger temperature driving forces in heat transfer leads to increased irreversibilities and thereby increased power consumption. Hence, in order to minimize power consumption, the temperature difference in the heat exchanger should in general be as small as possible. For reasonable values of the remaining process parameters, it can be deduced from Eq. (5.8) that the net power consumption is minimized when $\Delta T_{\text{cold}} = \Delta T_{\text{hot}} = \Delta T_{\text{min}}$.

The optimal stage temperature can be derived as a function of the isentropic efficiencies and end point temperature differences, by allocating points where the derivative of Eq. (5.8) with respect to T_{II} is zero. The optimal stage temperature can then be expressed as

$$T_{\text{II}}^{*} = \frac{A \pm \sqrt{B_1 \cdot B_2}}{C} \tag{5.9}$$

with

$$\begin{aligned}
A &= \left(T_{\text{III}} - \Delta T_{\text{cold}}\right) \cdot \left(\frac{T_{\text{I}} - \Delta T_{\text{hot}}}{\eta_{s,\text{COMP}}} + \Delta T_{\text{hot}} \right), \\
B_1 &= \frac{\eta_{s,\text{EXP}} \cdot \Delta T_{\text{hot}} \cdot \left(T_{\text{III}} - \Delta T_{\text{cold}}\right) \cdot \left(T_{\text{I}} - \Delta T_{\text{hot}}\right)}{\left(\eta_{s,\text{EXP}} - 1\right) \cdot \eta_{s,\text{COMP}}^2}, \\
B_2 &= \left(\Delta T_{\text{hot}} \cdot \left(1 - \eta_{s,\text{EXP}} + \eta_{s,\text{COMP}} \cdot \eta_{s,\text{EXP}}\right) - T_{\text{I}} + \left(T_{\text{III}} - \Delta T_{\text{cold}}\right) \cdot \eta_{s,\text{COMP}} \cdot \eta_{s,\text{EXP}}\right), \\
C &= \frac{T_{\text{I}} - \Delta T_{\text{cold}}}{\eta_{s,\text{COMP}}} - \Delta T_{\text{hot}} \cdot \left(\eta_{s,\text{EXP}} - 1\right).
\end{aligned} \tag{5.10}$$

In the case of $\Delta T_{\text{hot}} = \Delta T_{\text{cold}} = \Delta T_{\text{min}}$ and $\eta_{s,\text{COMP}} = \eta_{s,\text{EXP}} = \eta_s$, Eq. (5.10) can be simplified as follows:

$$
\begin{aligned}
A &= \left(T_{\text{III}} - \Delta T_{\text{min}}\right) \cdot \left(\frac{T_{\text{I}} - \Delta T_{\text{min}}}{\eta_s} + \Delta T_{\text{min}} \right), \\
B_1 &= \frac{\Delta T_{\text{min}} \cdot \left(T_{\text{III}} - \Delta T_{\text{min}}\right) \cdot \left(T_{\text{I}} - \Delta T_{\text{min}}\right)}{\left(\eta_s - 1\right) \cdot \eta_s}, \\
B_2 &= \left(\Delta T_{\text{min}} \cdot \left(1 - \eta_s + \eta_s^2\right) - T_{\text{I}} + \left(T_{\text{III}} - \Delta T_{\text{min}}\right) \cdot \eta_s^2 \right), \\
C &= \frac{T_{\text{I}} - \Delta T_{\text{min}}}{\eta_s} - \Delta T_{\text{min}} \cdot \left(\eta_s - 1\right).
\end{aligned}
\tag{5.11}
$$

The proper solution of Eq. (5.9) was found to be for the solution with a positive sign in front of the square root. As can be observed from Eq. (5.8), the net power consumption is proportional to the heat capacity flow rate of the natural gas and independent of the specific heat capacity of the refrigerant. The optimal stage temperature is therefore only a function of the minimum temperature difference, the isentropic efficiency and the supply and target temperatures of the natural gas stream.

In Fig. 5.4 (a), the optimal stage temperature T_{II} is given as function of the minimum temperature difference for different values of the isentropic efficiency. The corresponding minimum net power consumption is plotted in Fig. 5.4 (b). As one would expect, the power consumption increases with increasing minimum temperature difference and decreasing isentropic efficiency.

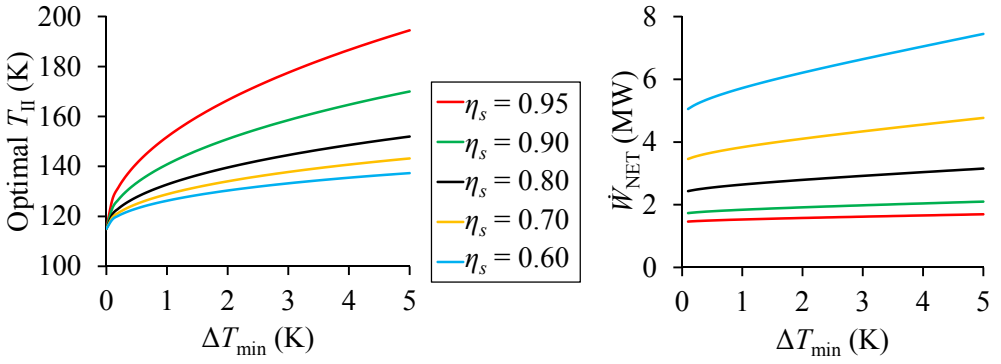

(a) (b)

Figure 5.4. (a) Optimal stage temperature as function of minimum temperature difference and isentropic efficiency; (b) Minimum net power consumption as function of minimum temperature difference and isentropic efficiency.

With increasing isentropic efficiency, the compression and expansion processes become more efficient. Hence, the optimal trade-off between refrigerant flow rate and

pressure ratio will be shifted towards smaller refrigerant flow rate and higher pressure ratio. The same trend is observed for increasing values of the minimum temperature difference, since a larger temperature driving force makes the heat transfer process less efficient.

This is confirmed by the results in Fig. 5.5, where the refrigerant flow rate and pressure ratio of the optimal solution are plotted as functions of the minimum temperature difference for different values of the isentropic efficiency. As can be observed in Fig. 5.4 (a), the trade-off is shifted towards smaller flow rates and larger pressure ratios by increasing the stage temperature when the minimum temperature difference or isentropic efficiency is increased.

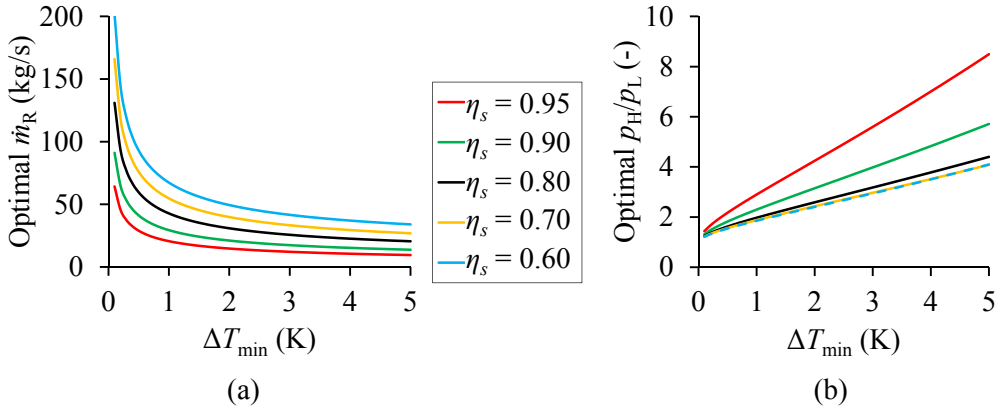

(a) (b)

Figure 5.5. (a) Optimal refrigerant flow rate as function of minimum temperature difference and isentropic efficiency; (b) Optimal pressure ratio as function of minimum temperature difference and isentropic efficiency.

As can be observed from Fig. 5.4 (b), the isentropic efficiency of the rotating equipment has a considerable effect on the net power consumption. For a given stage temperature, the effect of reduced isentropic efficiency of the expander is increased pressure ratio in order to reach the desired target temperature. The power produced remains constant, since refrigerant flow rate (see Eq. (5.1)), inlet and outlet temperatures are the same. The increased pressure ratio does however lead to an increased discharge temperature for the compressor which results in increased irreversibilities in the cooler. This effect is enhanced by the fact that reduced isentropic efficiency of the compressor also leads to increased compressor discharge temperature, resulting in a significant increase in the compressor power.

5.2.3 Rigorous model

In the case of rigorous thermodynamic modelling, the heat capacity is not necessarily constant, neither for the natural gas nor for the refrigerant. Hence, the smallest temperature difference between the composite curves may not necessarily be located in

the end points of the composite curves. One must therefore allow the temperature difference in the hot end of HX-A and the cold end of HX-B to be larger than the minimum temperature difference.

For the modelling with cubic equations of state, the refrigerant flow rate $\dot{m}_R$, stage temperature T_{II}, pressure ratio p_H/p_L and one of the pressure levels (p_L or p_H) were used as decision variables. The pressure ratio was used as a design variable rather than both pressure levels in order to allow quite wide bounds for both pressure levels without risking crossover ($p_H < p_L$). In order to keep the pressure levels within a reasonable range the pressure levels were bounded to be within the range 1-120 bar. Similar to the simplified process model, the process was optimized for different values of ΔT_{min} and η_s.

From the multi-start optimization approach, two different local solutions where found to be present for the different cases; one with the low pressure level at the lower bound ($p_L = 1$ bar) and one with the high pressure level at the higher bound ($p_H = 120$ bar). The net power consumption of the two local solutions is plotted in Fig. 5.6 as functions of the minimum temperature difference and the isentropic efficiency. For small values of both ΔT_{min} and η_s, the solution with $p_L = 1$ bar was found to be the best, while for the remaining cases the solution with $p_H = 120$ bar gave a smaller net power consumption.

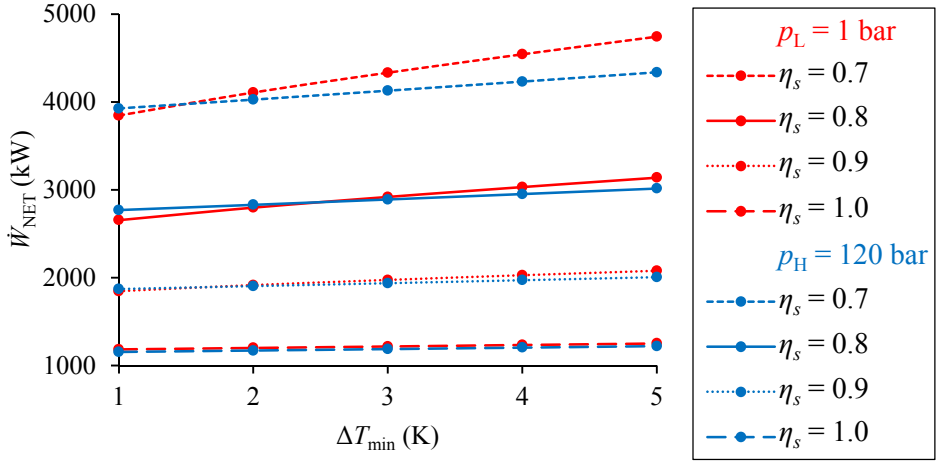

Figure 5.6. Net power consumption of the best solution found for the single nitrogen expander process modelled with SRK for different values of ΔT_{min} and η_s, for solutions with $p_L = 1$ bar (red) and $p_H = 120$ bar (blue).

5.2.4 Comparison

The best results obtained for the rigorous process model are compared with the results for the simplified model for different values of ΔT_{min} and η_s in Table 5.2. For all except

four cases, the solution with $p_H = 120$ bar is found to be best for the rigorous model. As compared with the solution with $p_L = 1$ bar, the refrigerant flow rate is smaller and the pressure ratio higher, which agree with a significantly higher stage temperature. Not taking into account the difference between the two local solutions, the refrigerant flow rate decreases and the pressure ratio increases with increasing values of the minimum temperature difference and/or the isentropic efficiency.

Table 5.2. Comparison of optimization results for the single nitrogen expander process for natural gas liquefaction modelled with simplified and rigorous thermodynamics.

		Simplified		Rigorous						
ΔT_{min}	η_s	$\dot{W}_{net}$	T_{II}	$\dot{W}_{net}$	T_{II}	$\dot{m}_R$	p_L	p_H	ΔT_{cold}	ΔT_{hot}
(K)	(-)	(kW)	(K)	(kW)	(K)	(kg/s)	(bar)	(bar)	(K)	(K)
1.0	0.7	3 836	129	3 846	130	53	1.0	2	1.0	1.0
1.0	0.8	2 644	133	2 655	135	41	1.0	2	1.0	1.0
1.0	0.9	1 841	141	1 848	145	26	1.0	3	1.0	1.0
1.0	1.0	1 239	293	1 156	293	5	5.3	120	1.0	31.5
2.0	0.7	4 106	134	4 026	197	12	13.6	120	2.0	2.0
2.0	0.8	2 793	140	2 797	143	29	1.0	3	2.0	2.0
2.0	0.9	1 917	151	1 904	249	6	6.8	120	2.0	2.0
2.0	1.0	1 257	293	1 172	293	5	5.2	120	2.0	32.5
3.0	0.7	4 340	138	4 128	197	12	13.0	120	3.0	3.0
3.0	0.8	2 921	145	2 890	214	9	10.3	120	3.0	3.0
3.0	0.9	1 982	159	1 938	250	6	6.4	120	3.0	3.0
3.0	1.0	1 275	293	1 188	293	5	5.0	120	3.0	33.5
4.0	0.7	4 558	141	4 232	198	12	12.3	120	4.0	4.0
4.0	0.8	3 040	149	2 952	215	9	9.8	120	4.0	4.0
4.0	0.9	2 043	165	1 972	251	6	6.1	120	4.0	4.0
4.0	1.0	1 293	293	1 205	293	5	4.9	120	4.0	34.5
5.0	0.7	4 770	143	4 337	199	12	11.7	120	5.0	5.0
5.0	0.8	3 154	152	3 015	215	9	9.3	120	5.0	5.0
5.0	0.9	2 100	170	2 006	252	6	5.8	120	5.0	5.0
5.0	1.0	1 312	293	1 222	293	5	4.7	120	5.0	35.5

As can be observed in Table 5.2, the temperature difference in the hot end of HX-A and the cold end of HX-B is equal to the minimum required for the majority of the cases, which indicates that the assumption of a constant heat capacity flow rate for the natural gas in the simplified model does not affect the results. Composite curves are given for the case of $\eta_s = 0.8$ and $\Delta T_{min} = 2$ K in Fig. 5.7, illustrating the fact that the nonlinearities of temperature-enthalpy relations do not cause the temperature difference to approach the minimum required in the interior of the heat exchangers.

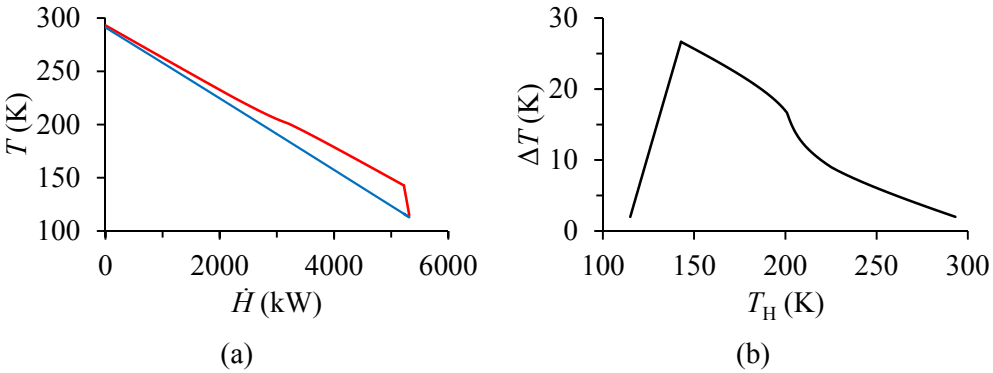

Figure 5.7. (a) Composite curves for the best known solution of the rigorous model for single nitrogen expander process with $\eta_s = 0.80$ and $\Delta T_{min} = 2$ K; (b) Temperature difference as function of hot stream temperature.

The exception is the theoretical case of $\eta_s = 1$, for which the stage temperature of the best solution is equal to supply temperature of the natural gas. In this case, there is no precooling of the refrigerant in HX-A and the entire cooling load in HX-A and HX-B is due to the natural gas. As can be observed from the composite curves given in Fig. 5.8, for the case of $\eta_s = 1.00$ and $\Delta T_{min} = 5$ K, the temperature difference must be increased in one or both of the end points in order to keep the temperature difference larger than the minimum required also in the interior of the heat exchangers. Since increasing the temperature difference in the cold end of the composite curves would lead to a considerable increase in heat transfer irreversibilities, as well as the pressure ratio of the refrigerant, increasing the driving forces in the hot end is more beneficial. This is realised by increasing the refrigerant flow rate compared to the case of $\Delta T_{hot} = \Delta T_{min}$.

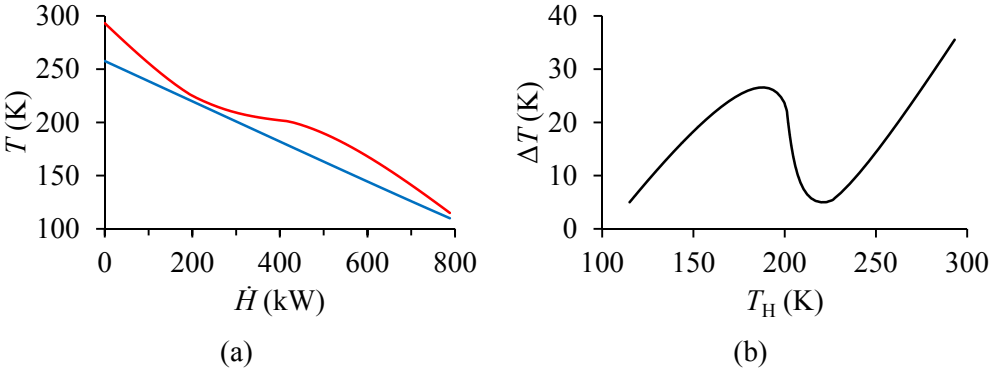

Figure 5.8. (a) Composite curves for best known solution of the rigorous model for single nitrogen expander process with $\eta_s = 1.00$ and $\Delta T_{min} = 5$ K; (b) Temperature difference as function of hot stream temperature.

As can be observed from Table 5.2, the stage temperature of the best solution is relatively close to the optimal stage temperature for the simplified model in the cases where the solutions with $p_L = 1$ bar provides the smallest net power consumption. From

thermodynamics, it is given that the characteristics of nitrogen should be closer to ideal gas behaviour when the pressure level is reduced. In the same cases, the power consumption is slightly higher in the results obtained for the rigorous model. Even closer resemblance with the simplified model, both in terms of stage temperature and net power consumption, was found when the low pressure level was allowed to be smaller than 1 bar.

The compressibility factor Z and the specific heat capacity of the refrigerant $c_{p,R}$ are plotted as functions of the pressure (on a dimensionless scale from p_L to p_H) in Fig. 5.9 for the best solutions obtained for $\eta_s = 0.8$ and $\Delta T_{min} = 2$ K with $p_L = 1$ bar and $p_H = 120$ bar, respectively. On the one hand, the compressibility factor is close to unity and heat capacity is close to constant for the case of $p_L = 1$ bar. In the solution with $p_H = 120$ bar, one the other hand, the compressibility factor is significantly smaller in the expansion process than in the compression process and the specific heat capacity considerably larger.

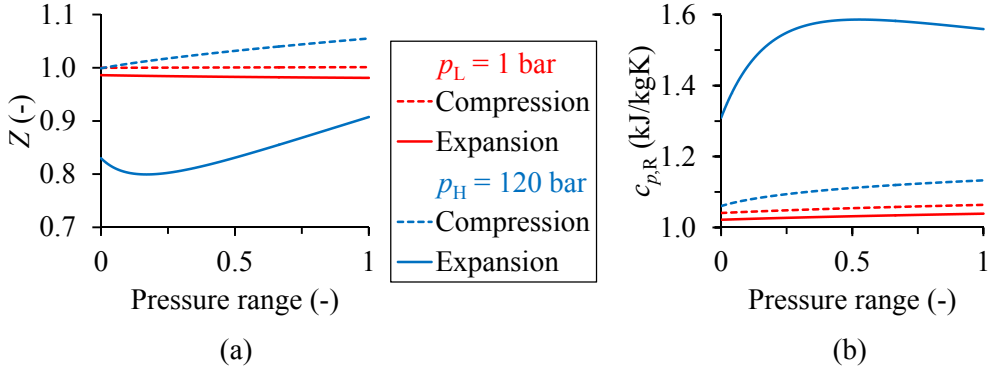

Figure 5.9. Variation in thermodynamic properties through compression and expansion processes for the best known solution for $\eta_s = 0.80$ and $\Delta T_{min} = 2$ K. (a) Compressibility factor; (b) Specific heat capacity.

In the cases where $p_H = 120$ bar is found to give the best solution for the rigorous model, there is a considerable difference in the best stage temperature of the two models. As can be observed in Table 5.2, the stage temperature is significantly higher for the solution of the rigorous model, while the power consumption is smaller. In these solutions the pressure level is quite high, which would indicate that the nitrogen refrigerant does not behave like an ideal gas. This is confirmed by the results plotted in Fig. 5.10, illustrating the variation in compressibility factor and specific heat throughout the compression and expansion processes in the best solution found for $\eta_s = 0.9$ and $\Delta T_{min} = 4$ K.

For high pressure levels, the assumption of ideal gas behaviour is not valid, and for this reason a large deviation is observed between the results of the two models (simplified and rigorous) in the cases where solutions based on high operating pressures are found

to provide the smallest net power consumption in the rigorous model. Since the rigorous model is able to account for the non-ideality of the refrigerant, the power consumption is significantly smaller in the best solution obtained for the rigorous process model.

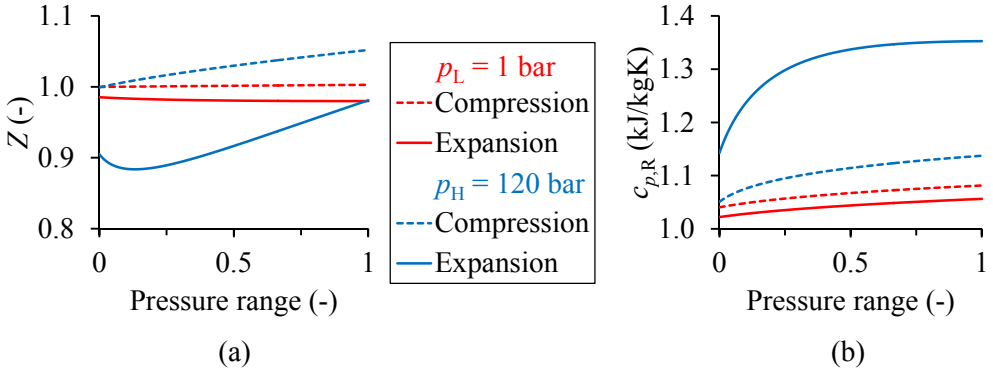

Figure 5.10. Variation in thermodynamic properties through compression and expansion processes for the best known solution for $\eta_s = 0.90$ and $\Delta T_{min} = 4$ K. (a) Compressibility factor; (b) Specific heat capacity.

For $\eta_s = 0.80$ and $\Delta T_{min} = 2.5$ K, the two local solutions ($p_L = 1$ bar and $p_H = 120$ bar) give approximately the same net power consumption. As can be observed in Table 5.3, however, considerable differences are observed for other properties. These data are given for a natural gas flow rate of 1 kg/s. Due to the fact that the stage temperature is higher for the solution with $p_H = 120$ bar, this solution has a higher pressure ratio but smaller refrigerant flow rate. Both the compression power and the expansion power are larger for the solution with $p_L = 1$ bar, yet the net power consumption is approximately the same for the two solutions.

Due to a lower stage temperature, and thereby also higher refrigerant flow rate, the total cooling load of the two heat exchangers is significantly larger for the solution with $p_L = 1$ bar. Enhanced by the fact that the logarithmic mean temperature difference is smaller, the total heat exchanger size (UA) is therefore more than five times larger for the design with $p_L = 1$ bar than for the design with $p_H = 120$ bar. Because of the high refrigerant flow rate and the relatively low pressure, the volumetric flow rates of the refrigerant at the inlet of the compressor and the expander is considerably higher for the solution with $p_L = 1$ bar.

Even though the total irreversibilities are the same, the two different local solutions have a different distribution of the process irreversibilities. This can be observed in Fig. 5.11 (a) for the solution with $p_L = 1$ bar and Fig. 5.11 (b) for the solution with $p_H = 120$ bar. Due to the high cooling, the irreversibilities in the heat exchangers (HX-A and HX-B) are larger for the design with $p_L = 1$ bar even though the

logarithmic mean temperature difference is smaller than for the design with $p_H = 120$ bar.

Table 5.3. Local solutions from optimization of single nitrogen expander process with $\eta_s = 0.80$ and $\Delta T_{min} = 2.5$ K.

Property	Unit	$p_L = 1$ bar	$p_H = 120$ bar
p_H/p_L	bar	3.1	11.4
$\dot{m}_R$	kg/s	26.1	9.0
T_{II}	K	145.9	213.6
T_2	K	425.4	643.6
$\dot{W}_{COMP}$	kW	3 703	3 488
$\dot{W}_{EXP}$	kW	844	628
$\dot{W}_{NET}$	kW	2 860	2 860
$\dot{Q}_A$	kW	4 678	1 243
$\dot{Q}_B$	kW	105	524
$\Delta T_{LM,A}$	K	8.9	14.7
$\Delta T_{LM,B}$	K	11.1	26.0
UA_A	kW/K	525.1	84.6
UA_B	kW/K	9.4	20.1
UA_{total}	kW/K	534.5	104.7
$\dot{V}_{COMP}$	m^3/s	22.53	0.74
$\dot{V}_{EXP}$	m^3/s	3.63	0.04

Higher flow rate also has a stronger influence than smaller pressure ratio on the irreversibilities in the compression and expansion processes. Hence, the exergy destruction is larger in the compressor and expander for the design with $p_L = 1$ bar. The high pressure ratio of the solution with $p_H = 120$ bar gives a very high compressor discharge temperature. Since the heat is dumped to the environment, high quality heat exergy is lost in the cooler. Even though the refrigerant flow rate is smaller, the irreversibilities associated with the cooler are therefore much larger in the solution with $p_H = 120$ bar.

The high pressure ratio and high compressor discharge temperature of the compressor (especially for the solution with $p_H = 120$ bar) suggest that multi-stage compression and expansion is required. Multi-stage compression enables the use of intercooling, which could give a significant reduction in the irreversibilities of the compressor-cooler section.

The high pressure ratio of the refrigerant in the solution with $p_H = 120$ bar, and thereby large irreversibilities in the cooler, suggest that this solution will benefit more from introduction of multi-stage compression, and that these solutions to an even greater extent would dominate the solutions with $p_L = 1$ bar if multi-stage compression is

introduced. With multi-stage compression, the optimal solution is assumed to be shifted towards a higher stage temperature, which would give a smaller refrigerant flow rate and a higher pressure ratio.

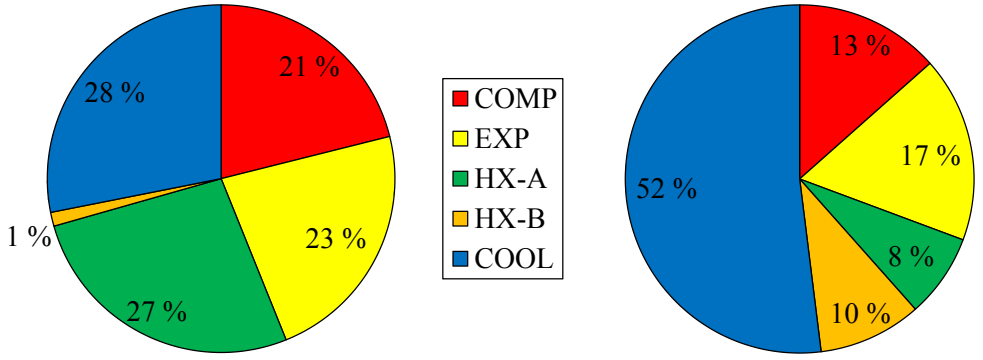

Figure 5.11. Irreversibility distribution for local solutions from optimization of single nitrogen expander process with $\eta_s = 0.80$ and $\Delta T_{min} = 2.5$ K. (a) With $p_L = 1$ bar; (b) With $p_H = 120$ bar.

Table 5.4. Optimization results obtained for single expander LNG process with SRK and PR equations of state.

		Soave-Redlich-Kwong					Peng-Robinson				
ΔT_{min} (K)	η_s (-)	T_{II} (K)	$\dot{m}_R$ (kg/s)	p_L (bar)	p_H (bar)	$\dot{W}_{net}$ (kW)	T_{II} (K)	$\dot{m}_R$ (kg/s)	p_L (bar)	p_H (bar)	$\dot{W}_{net}$ (kW)
1.0	0.7	130.3	53.0	1.0	2	3 846	195.6	11.8	14.9	120	3 717
1.0	0.8	134.9	40.5	1.0	2	2 655	135.0	39.6	1.0	2	2 604
1.0	0.9	145.4	26.2	1.0	3	1 848	145.6	25.6	1.0	3	1 813
2.0	0.7	196.9	12.1	13.7	120	4 026	196.2	11.8	14.2	120	3 810
2.0	0.8	142.8	29.0	1.0	3	2 797	212.6	8.9	11.2	120	2 714
2.0	0.9	248.7	6.0	6.8	120	1 904	248.2	5.7	7.0	120	1 849
3.0	0.7	197.5	12.0	13.0	120	4 128	196.8	11.7	13.5	120	3 906
3.0	0.8	213.9	9.0	10.3	120	2 890	213.3	8.8	10.7	120	2 772
3.0	0.9	249.7	5.9	6.4	120	1 938	249.2	5.8	6.6	120	1 882
4.0	0.7	198.1	12.0	12.3	120	4 232	197.3	11.7	12.8	120	4 003
4.0	0.8	214.6	9.0	9.8	120	2 952	213.9	8.8	10.2	120	2 831
4.0	0.9	250.7	5.9	6.1	120	1 972	250.3	5.8	6.3	120	1 915
5.0	0.7	198.6	12.0	11.7	120	4 337	197.9	11.7	12.2	120	4 102
5.0	0.8	215.1	8.9	9.3	120	3 015	214.5	8.8	9.7	120	2 891
5.0	0.9	251.7	5.8	5.8	120	2 006	251.2	5.7	6.0	120	1 948

Equation of state

The single expander process was also optimized using the Peng-Robinson equation of state. In Table 5.4, the best results obtained are compared with the results obtained

using the Soave-Redlich-Kwong equation of state. For two cases ($\Delta T_{min} = 1.0$, $\eta_s = 0.70$ and $\Delta T_{min} = 2.0$, $\eta_s = 0.80$), the best solution is found at $p_L = 1$ bar for SRK but at $p_H = 120$ bar for PR. Except for these cases, where the optimized variables considerably different, similar solutions were obtained for the two equations of state.

In general, the stage temperature of the best solution is slightly higher with PR for solutions with $p_H = 120$ bar and slightly lower where $p_L = 1$ bar is found to be best. Both the pressure ratio and the refrigerant flow rate are smaller for the solutions obtained using the Peng-Robinson equation of state.

Even though the solutions found for the two equations of state are similar, the net power consumption is smaller for the case of Peng-Robinson. In the solutions where $p_H = 120$ bar is best for both equations of state, the reduction in power consumption is around 5.4 % for $\eta_s = 0.70$, 4.1 % for $\eta_s = 0.80$ and 2.9 % for $\eta_s = 0.90$. The differences are smaller for the other cases.

5.3 Multi-stage compression

For many of the cases studied, the pressure ratio of the nitrogen refrigerant is higher than what can be obtained in a single compression stage. Hence, two or more compression stages must be used in practical applications. Multi-stage compression with intercooling is also an efficient measure for reduced power consumption. With compressor intercooling, the discharge temperature from the compressors is reduced and thereby also the irreversibilities associated with the coolers. Heat rejection to the environment is a major source to irreversibilities in the single expander process with single-stage compression (see Fig. 5.11). As can be observed from Eq. (3.3), the compression power is proportional to the suction temperature (assuming the other parameters to be constant).

5.3.1 Optimal intermediate pressure level

In the case of two-stage compression of a perfect gas assuming constant isentropic efficiencies for the compressors, it is well known that the intermediate pressure level should be given as the geometric mean of the low and high pressure levels:

$$p_M = \sqrt{p_L \cdot p_H} \tag{5.12}$$

This is equivalent to having the same pressure ratio for both compression stages, which has proven to be a decent estimate also for compression of real gases. For multi-stage compression in n stages, the discharge pressure of stage i would be given as

$$p_i = p_L^{(n-i)/n} \cdot p_H^{i/n} \qquad i = 1,....,n\,. \tag{5.13}$$

In the literature, an estimate for the optimal intermediate pressure level based on geometric has often been applied for design of refrigeration processes. According to Jekel and Reindl (2008), the energy savings obtained by dividing the compression process in stages increase with increasing pressure ratio, and that the optimum is quite flat with respect to the intermediate pressure.

Streit and Razani (2013) used intermediate pressure levels given such that the pressure ratio was uniform in their studies of expander processes operating at low temperature levels. Cavallini et al. (2005) specified the intermediate pressure level by the geometric mean when designing a trans-critical carbon dioxide refrigeration process with two-stage compression with intercooling. For a similar process, Agrawal et al. (2007) found that the optimal intermediate pressure was larger than the geometric mean.

Srinivasan (2011) studied transcritical carbon dioxide refrigeration cycles with two-stage intercooled compression. The results indicated that the optimal intermediate pressure was significantly higher than the geometric mean. Since the energy savings compared to single-stage compression was found to be relatively small (less than 10 %), Srinivasan suggested using the same compressor discharge temperature of each compressor as design criterion (in order to reduce the maximum cycle temperature) rather than maximum energy efficiency. Equality of the discharge temperature was found to give marginally higher power consumption than the minimum. The process was modelled using thermodynamic data from NIST, assuming both compression stages to be fully isentropic.

Among others, Zubair et al., (1996), Khan and Zubair (1998), Agnew and Ameli (2004), Torrella et al. (2009) and Arora and Kaushik (2010) have also studied the influence of intermediate pressure levels in refrigeration systems. In these studies, however, the compression stages are connected to horizontal stages in the refrigeration cycle. In this case, factors other than irreversibilities in compression, intercooling and after-cooling are also influential for the optimal intermediate pressure levels.

The estimates in Eqs. (5.12) and (5.13) are based on the assumption that the suction temperature is the same for the two compressors. In many refrigeration processes this may, however, not be the case. Torrella et al. (2011) pointed out that the geometric mean is optimal only in the case of perfect gas behaviour and the same inlet temperature for both compressor stages.

Optimal intermediate pressure level with different suction temperature

In the single expander process it is reasonable to assume that the refrigerant can be cooled to the same temperature as the natural gas inlet temperature before entering the second compression stage, as illustrated in Fig. 5.12. The inlet temperature of the first

compression stage will, however, be smaller, given by the temperature difference in the hot end of the heat exchanger. With a smaller suction temperature in the first stage, it is reasonable to assume that the first compression stage should have a slightly larger pressure ratio than the second stage.

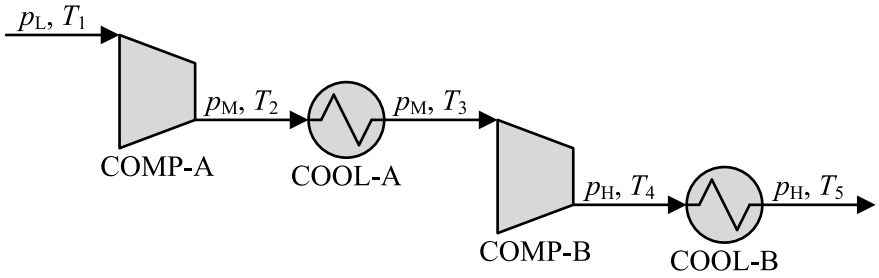

Figure 5.12. Two-stage compression with intercooling.

The total power input of the two-stage compression process with intercooling can be expressed as

$$\frac{\dot{W}_{2\text{stage}}}{\dot{m}} = \frac{\dot{W}_A}{\dot{m}} + \frac{\dot{W}_B}{\dot{m}} = \frac{c_p}{\eta_s} \cdot \left(T_1 \cdot \left(1 - \left(\frac{p_M}{p_L} \right)^{R/c_p} \right) + T_3 \cdot \left(1 - \left(\frac{p_H}{p_M} \right)^{R/c_p} \right) \right). \qquad (5.14)$$

Derivation with respect to p_M gives

$$\frac{\mathrm{d}\left(\dot{W}_{2\text{stage}} / \dot{m} \right)}{\mathrm{d}p_M} = \frac{R}{c_p} \cdot \left(T_3 \cdot p_H^{R/c_p} \cdot p_M^{-R/c_p - 1} - T_1 \cdot p_L^{-R/c_p} \cdot p_M^{R/c_p - 1} \right). \qquad (5.15)$$

Extrema can be found by equating the derivative to zero, which leads to the optimal value for the intermediate pressure level:

$$p_M^* = \sqrt{p_L \cdot p_H} \cdot \left(\frac{T_3}{T_1} \right)^{c_p/(2 \cdot R)}. \qquad (5.16)$$

As long as suction temperature of the first compressor is smaller than for the second compressor, the optimal intermediate pressure level is larger than the geometric mean. The opposite is the case is the suction temperature is larger in the second stage of compression. The deviation from geometric mean increases with increasing difference in suction temperatures for the two compressors and increasing specific heat. Eq. (5.16) holds as long as the intermediate pressure does not exceed the high pressure level. In this case, the power consumption is minimized with single-stage compression.

The isentropic discharge temperature of the compressors can be calculated from Eq. (5.3). For the first compression stage the discharge temperature can be expressed as

$$T_2 = T_1 \cdot \left(1 + \frac{1}{\eta_s} \cdot \left(\sqrt{\left(\frac{T_3}{T_1} \right) \cdot \left(\frac{p_\mathrm{H}}{p_\mathrm{L}} \right)^{R/c_p}} - 1 \right) \right), \tag{5.17}$$

while the discharge temperature of the second compressor is given as

$$T_4 = T_3 \cdot \left(1 + \frac{1}{\eta_s} \cdot \left(\sqrt{\left(\frac{T_1}{T_3} \right) \cdot \left(\frac{p_\mathrm{H}}{p_\mathrm{L}} \right)^{R/c_p}} - 1 \right) \right). \tag{5.18}$$

Further, the isentropic discharge temperature of the first compressor can be expressed as

$$T_{2\mathrm{s}} = T_1 \cdot \left(\left(\frac{p_\mathrm{H}}{p_\mathrm{L}} \right)^{1/2} \cdot \left(\frac{T_3}{T_1} \right)^{c_p/(2 \cdot R)} \right)^{R/c_p} = \sqrt{T_1 \cdot T_3} \cdot \left(\frac{p_\mathrm{H}}{p_\mathrm{L}} \right)^{R/(2 \cdot c_p)}. \tag{5.19}$$

For the second compressor, the isentropic discharge temperature is given as

$$T_{4\mathrm{s}} = T_3 \cdot \left(\left(\frac{p_\mathrm{H}}{p_\mathrm{L}} \right)^{1/2} \cdot \left(\frac{T_1}{T_3} \right)^{c_p/(2 \cdot R)} \right)^{R/c_p} = \sqrt{T_1 \cdot T_3} \cdot \left(\frac{p_\mathrm{H}}{p_\mathrm{L}} \right)^{R/(2 \cdot c_p)}. \tag{5.20}$$

As can be observed from Eqs. (5.19) and (5.20), the isentropic discharge temperatures of the two compressors are the same when the intermediate pressure level is optimal. For the case of identical suction temperatures ($T_1 = T_3$), the results in Eq. (5.16) indicate that the total power consumption of the compression process is minimized when the pressure ratios of the two compressors are the same. In general, however, the optimal intermediate pressure level is given such that the isentropic discharge temperatures are equal rather than the pressure ratios.

Minimization of compression power is equivalent to minimization of irreversibilities in the two compressors and the two coolers. For the special case of isentropic compression, the compression processes are reversible. Hence, the only irreversibilities present are related to dumping heat from the compressors discharge streams to the environment and thereby associated loss of heat exergy. Since the exergy of heat increases with increasing temperature above ambient, these irreversibilities increase with increasing discharge temperature.

By introducing two-stage compression with intercooling, the discharge temperatures of the compressors and thereby the irreversibilities of the coolers can be reduced. As long as the discharge temperatures exceed the intercooling temperature, increasing the intermediate pressure level p_M will lead to increased discharge temperature for the first compression stage (T_2) and reduced discharge temperature for the second compression stage (T_4). From the characteristics of exergy of heat above ambient temperature (see Fig. 2.2), it is evident that the slope with which the exergy grows with increasing temperature decreases with increasing temperature. One may therefore conclude that in the special case of isentropic compression, the power consumption of multi-stage compression with intercooling is minimized when the discharge temperature of all compressors are equal.

As was discussed in Chapter 3, the isentropic efficiency is a scaling factor for the compression power. As long as unit operations other than the compressors and coolers are not affected, the optimal operating conditions are therefore independent of the isentropic efficiency of the compressors (as long as it is constant, equal for both compressors). Reduced isentropic efficiency will lead to increased irreversibilities in both compressors and coolers, but the optimal intermediate pressure level will remain the same.

Influence of different parameters

The geometric mean provides a decent estimate for the optimal intermediate pressure level when the suction temperatures of the different stages are similar. In Fig. 5.13, the savings in total compression power with an optimal intermediate pressure level (given by Eq. (5.16)) compared with the geometric mean are given as function of the difference in suction temperature for the two compression stages. This is done for different intercooling temperatures (the temperature level T_3). The results presented in Fig. 5.13 are based on c_p = 1.039 kJ/kgK, η_s = 0.80, p_L = 1 bar and p_H/p_L = 4.

As expected, the savings in total compression power increase with increasing difference in suction temperature ($T_3 - T_1$). The savings do, however, reach a maximum level at a given temperature difference, which represents a threshold value for the suction temperature of the first compressor. For suction temperatures smaller than this value (larger temperature difference), the discharge temperature of the first compressor will not reach the cooling temperature when the intermediate pressure is given by the geometric mean, and there is no intercooling. When the intercooling temperature is 250 K, this threshold is observed for $T_3 - T_1 \approx 54$ K, as can be observed in Fig. 5.13.

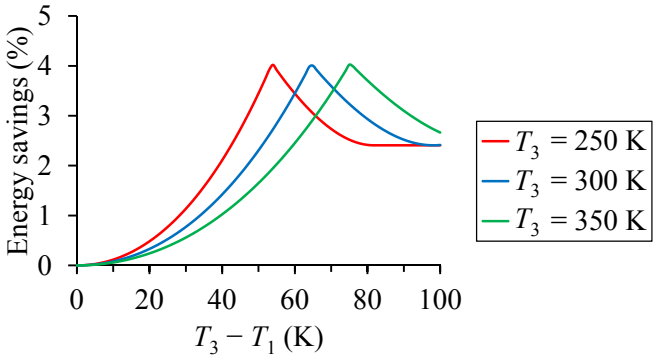

Figure 5.13. Energy savings in two-stage compression with intercooling with optimal intermediate pressure level compared with intermediate pressure given by the geometric mean, plotted as function of difference in suction temperature for different temperature levels.

Another sudden change in slope is observed for the same curve for $T_3 - T_1 \approx 82$ K. For smaller suction temperatures in the first compression stage, the optimal intermediate pressure level will be equal to the high pressure level. Hence, there is only one stage of compression and no intercooling. As discussed in Chapter 3, the preheating effect causes worse conditions in the second compression-stage. This is also the reason why the solution with intermediate pressure level given by the geometric mean results in higher power consumption even though there is no intercooling in either design. If the polytropic efficiency was the same for both compressors (rather than the isentropic efficiency), the power consumption would have been the same in the case of no intercooling.

As can be observed in Fig. 5.13, the energy savings increase with decreasing temperature level for the same difference in suction temperature ($T_3 - T_1$), given that the discharge temperature of the first stage is higher than the intercooling temperature when the intermediate pressure is given by the geometric mean. This is due to the fact that the slope of exergy of heat increases with decreasing temperature.

Fig. 5.14 illustrates the reduction in total compression power in the two-stage compression process with intercooling when the intermediate pressure level is given by Eq. (5.16) rather than the geometric mean for different values of the overall pressure ratio. The energy savings are plotted as function of the difference in suction temperature for the two compressors ($T_3 - T_1$) with the cooling temperature $T_3 = 300$ K. Given that the compressor discharge temperatures exceed the intercooling temperature, the savings are observed to increase with decreasing pressure ratio (for the same difference in suction temperature).

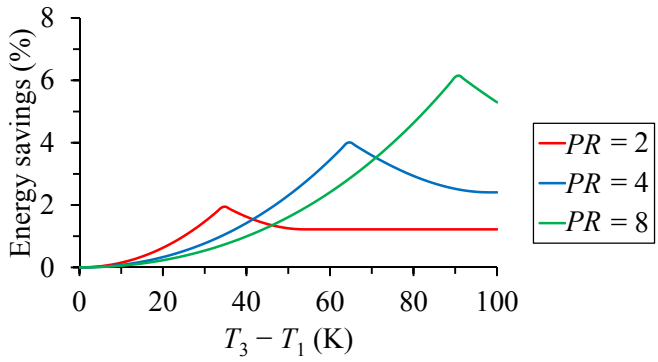

Figure 5.14. Energy savings in two-stage compression with intercooling with optimal intermediate pressure level compared with intermediate pressure given by the geometric mean, plotted as function of difference in suction temperature for different pressure ratios.

With increasing pressure ratio, the peak in energy savings is moved to a smaller value for the suction temperature of the first compressor (larger ($T_3 - T_1$)). Since the overall pressure ratio is larger, so is the discharge temperatures of the compressors. The isentropic efficiency of the compressors and the pressure level do not affect the difference in total compression power related to the intermediate pressure level. The isentropic efficiency would, however, influence the magnitude of suction temperature leading to a discharge temperature equal to the intercooling temperature.

In Table 5.5, the intermediate pressure level and compressor discharge temperatures have been compared for the cases of the intermediate pressure level given by the geometric mean and the optimal value given by Eq. (5.16), respectively. This is done for different values of the overall pressure ratio, the intercooling temperature and the difference in compressor suction temperature, with $c_p = 1.039$ kJ/kgK, $\eta_s = 0.80$ and $p_L = 1$ bar . As expected, there is no difference in the intermediate pressure level (and thereby also the compressor discharge temperatures) when the suction temperatures of the two compression stages are equal.

As can be observed from Table 5.5, the geometric mean provides a smaller intermediate pressure level than the optimal when the suction temperature of the first compression stage is smaller than the suction temperature of the second compression stage. Compared with the optimal solution, the discharge temperature of the first compressor will therefore be lower, while the discharge temperature of the second stage is higher. The difference in discharge temperature for the two compression stages is larger for the case where the intermediate pressure level given by the geometric mean than for the optimal intermediate pressure level.

Table 5.5. Two-stage compression with intermediate pressure level given by the geometric mean and the optimal intermediate pressure level.

			Geometric			Optimal		
PR	T_3	$T_3 - T_1$	p_M	T_2	T_4	p_M	T_2	T_4
(-)	(K)	(K)	(bar)	(K)	(K)	(bar)	(K)	(K)
2	250	0	1.414	282.5	282.5	1.414	282.5	282.5
2	250	25	1.414	254.3	282.5	1.701	271.1	264.8
2	300	0	1.414	339.0	339.0	1.414	339.0	339.0
2	300	25	1.414	310.8	339.0	1.647	327.6	321.4
4	250	0	2.000	318.4	318.4	2.000	318.4	318.4
4	250	25	2.000	286.6	318.4	2.405	305.1	298.9
4	300	0	2.000	382.1	382.1	2.000	382.1	382.1
4	300	25	2.000	350.3	382.1	2.329	368.9	362.6

5.4 Single nitrogen expander process with two-stage compression

5.4.1 Simplified model

The influence of two-stage compression on the single expander process has been studied in the following. Since the suction temperature of the first compressor and the inlet temperature of the refrigerant to the first heat exchanger are independent of the compression process, only the performance of the compressors and coolers will be affected. Hence, the refrigerant flow rate (Eq. (5.1)), the pressure ratio (Eq. (5.5)) and the expander power (Eq. (5.2)) will be the same.

The inlet temperature of the first compression stage will be equal to $T_I - \Delta T_{hot}$, while for the second compressor it is equal to the ambient cooling temperature T_I. The optimal intermediate pressure level is then given as

$$p_M = \sqrt{p_L \cdot p_H} \cdot \left(\frac{T_I}{T_I - \Delta T_{hot}} \right)^{c_{p,R}/(2 \cdot R)} . \tag{5.21}$$

Further, from Eq. (5.4), the isentropic discharge temperatures can be expressed as

$$T_{2as} = T_{2bs} = \sqrt{T_I \cdot (T_I - \Delta T_{hot}) \cdot \left(\frac{T_{II} \cdot \eta_{s,EXP}}{T_{II} \cdot (\eta_{s,EXP} - 1) + T_{III} - \Delta T_{cold}} \right)} . \tag{5.22}$$

From this, the power consumption of the first compression stage can be calculated from

$$\dot{W}_{\mathrm{A}} = \frac{\dot{m}_R \cdot c_{p,\mathrm{R}}}{\eta_{s,\mathrm{COMP}}} \cdot \left(T_{2\mathrm{as}} - \left(T_{\mathrm{I}} - \Delta T_{\mathrm{hot}} \right) \right), \tag{5.23}$$

while the power consumption of the second compression stage is given as

$$\dot{W}_{\mathrm{B}} = \frac{\dot{m}_R \cdot c_{p,\mathrm{R}}}{\eta_{s,\mathrm{COMP}}} \cdot \left(T_{2\mathrm{bs}} - T_{\mathrm{I}} \right). \tag{5.24}$$

The total power consumption is then equal to

$$\begin{aligned} \dot{W}_{\mathrm{COMP}} &= \dot{W}_{\mathrm{A}} + \dot{W}_{\mathrm{B}} \\ &= \frac{2 \cdot \dot{m}_{\mathrm{R}} \cdot c_{p,\mathrm{R}}}{\eta_{s,\mathrm{COMP}}} \cdot \left(\sqrt{\frac{T_{\mathrm{I}} \cdot \left(T_{\mathrm{I}} - \Delta T_{\mathrm{warm}} \right) \cdot T_{\mathrm{II}} \cdot \eta_{s,\mathrm{EXP}}}{T_{\mathrm{II}} \cdot \left(\eta_{s,\mathrm{EXP}} - 1 \right) + T_{\mathrm{III}} - \Delta T_{\mathrm{cold}}}} - T_{\mathrm{I}} + \frac{\Delta T_{\mathrm{hot}}}{2} \right). \end{aligned} \tag{5.25}$$

Since there is little difference in the inlet temperatures of the two compressors (ΔT_{hot}), the geometric mean is expected to provide a good estimate for the intermediate pressure level.

5.4.2 Results

In Fig. 5.15, the power consumption of the single expander process is plotted as function of the stage temperature for the cases of one- and two-stage compression. This is done for the case of isentropic efficiency $\eta_s = 0.80$ and $\Delta T_{\mathrm{min}} = 2$ K. A significant power reduction is observed for the case of two stages of compression with intercooling. As expected, the optimal stage temperature is shifted to a higher value compared to the case of one stage of compression. Since the compression process is more efficient, the trade-off between refrigerant flow rate and pressure ratio is shifted to a higher pressure ratio and smaller flow rate. One may notice from Fig. 5.15 that the optimum is quite flat and relatively small changes are observed in the power consumption when varying the stage temperature around the optimum.

Since the difference in suction temperature is small ($\Delta T_{\mathrm{hot}} = 2$ K), the optimal intermediate pressure level is close to the geometric mean, and a design with the intermediate pressure level given by the geometric mean practically leads to the same power consumption. Compared to the case of single-stage compression, the power consumption is reduced by around 16 %.

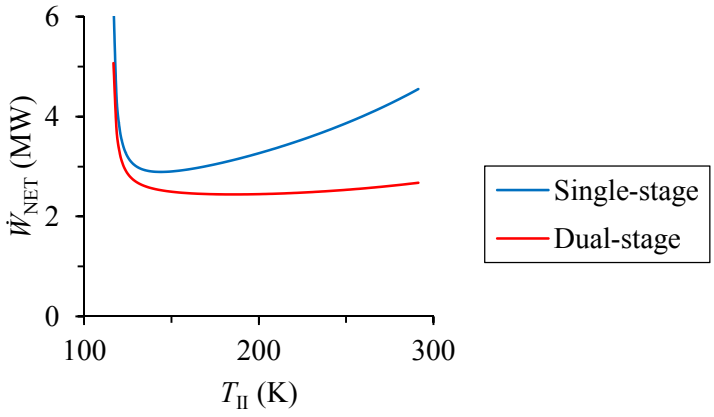

Figure 5.15. Net power consumption in single expander process for natural gas liquefaction with one (blue) and two (red) stages of compression.

The net power consumption is a unimodal function of the stage temperature. In this work, the net power consumption of the process was minimized in Microsoft Excel (Microsoft Corporation) using the built-in generalized reduced gradient algorithm. In Table 5.6, the net power consumption is compared for the cases of single- and two-stage compression for different values of ΔT_{min} and η_s. In the case of two-stage compression, using an intermediate pressure level equal to the geometric mean would for all the cases lead to an energy penalty of less than 0.02 %.

As can be observed from Table 5.6, the energy savings resulting from introducing two-stage compression with intercooling increase with both increasing isentropic efficiency and increasing minimum temperature difference. Like discussed for the single expander in Section 5.2.2, the trade-off between refrigerant flow rate and pressure ratio is shifted towards increased pressure ratio with increasing isentropic efficiency and temperature difference. Since two-stage compression improves the compression process, one would expect the potential for improvement to be better when the pressure ratio is higher.

As expected, the optimal trade-off between refrigerant flow rate and pressure ratio is shifted to higher stage temperatures and thereby higher pressure ratios when two-stage compression is introduced. For the case of $\eta_s = 0.90$, the stage temperature is equal to the inlet temperature of the natural gas and there is no precooling of the refrigerant in HX-A. Further increasing the inlet temperature of the expander (beyond T_I) would lead to increased power consumption. In this case, the refrigerant flow rate would be constant, while the pressure ratio would continue increasing since the temperature drop in the expander increases. The compression power will therefore increase with a steeper rate than the expander power, leading to a net increase in power consumption.

Table 5.6. Comparison of power consumption for single nitrogen expander process with one and two stages of compression, modelled with simplified thermodynamics.

		Single-stage		Two-stage		
ΔT_{min}	η_s	T_{II}	$\dot{W}_{net}$	T_{II}	$\dot{W}_{net}$	Savings
(K)	(-)	(K)	(kW)	(K)	(kW)	(%)
1.0	0.7	129	3 836	141	3 573	6.8
1.0	0.8	133	2 644	177	2 382	9.9
1.0	0.9	141	1 841	293	1 409	23.5
2.0	0.7	134	4 106	149	3 727	9.2
2.0	0.8	140	2 793	185	2 441	12.6
2.0	0.9	151	1 917	293	1 431	25.4
3.0	0.7	138	4 340	154	3 865	10.9
3.0	0.8	145	2 921	192	2 499	14.4
3.0	0.9	159	1 982	293	1 453	26.7
4.0	0.7	141	4 558	159	3 997	12.3
4.0	0.8	149	3 040	196	2 557	15.9
4.0	0.9	165	2 043	293	1 476	27.7
5.0	0.7	143	4 770	162	4 127	13.5
5.0	0.8	152	3 154	200	2 614	17.1
5.0	0.9	170	2 100	293	1 499	28.6

5.4.3 Rigorous model

For the rigorous model, a second compression stage was added to the model used in Section 5.2.3. The process was optimized using the intermediate pressure level as an extra decision variable, or alternatively given by the geometric mean or as suggested by Eq. (5.16). Since the specific heat capacity is not constant in the case of cubic equations of state, the intermediate pressure ratio was calculated using the mean of the specific heat capacity for the streams entering the first stage of compression and leaving the second cooler. The optimization results are given in Table 5.7 together with the results obtained with single-stage compression.

In this case, solutions with $p_H = 120$ bar are found to be the best for all the cases studied. Since these solutions proved to be better than solutions with $p_L = 1$ bar for single-stage compression in cases where the optimal trade-off between refrigerant flow rate and pressure ratio is shifted towards smaller flow rates and higher pressure ratios, it is expected that these solutions would dominate even more when the compression process is improved with the inclusion of a second compression stage.

The net power consumption of the best solutions found with $p_L = 1$ bar is 5-15 % larger than for the best known solutions, with increasing deviation with increasing isentropic efficiency. Still, the power consumption is up to 6 % smaller than for the simplified model. In both cases (both with $p_L = 1$ bar and with $p_H = 120$ bar), the stage

temperature of the best known solution deviates considerably from the optimal solution of the simplified model. Hence, for the case of a single expander process with two-stage compression, the simplified thermodynamic does not provide a close starting point for the rigorous model.

Table 5.7. Comparison of power consumption for single nitrogen expander with one and two stages of compression, modelled with rigorous thermodynamics.

		Single-stage		Two-stage					
ΔT_{min}	η_s	T_{II}	$\dot{W}_{net}$	T_{II}	$\dot{m}_R$	p_L	p_H	$\dot{W}_{net}$	Savings
(K)	(-)	(K)	(kW)	(K)	(kg/s)	(bar)	(bar)	(kW)	(%)
1.0	0.7	129	3 836	209	10.0	9.8	120	3 191	17.0
1.0	0.8	133	2 644	241	6.6	5.5	120	2 137	19.5
1.0	0.9	141	1 841	268	5.1	4.9	120	1 323	28.4
2.0	0.7	134	4 106	210	9.9	9.2	120	3 263	19.0
2.0	0.8	140	2 793	242	6.5	5.2	120	2 177	22.2
2.0	0.9	151	1 917	268	5.1	4.8	120	1 344	29.4
3.0	0.7	138	4 340	211	9.9	8.7	120	3 335	19.2
3.0	0.8	145	2 921	243	6.5	4.9	120	2 217	23.3
3.0	0.9	159	1 982	268	5.1	4.6	120	1 365	29.5
4.0	0.7	141	4 558	211	9.8	8.1	120	3 409	19.4
4.0	0.8	149	3 040	243	6.4	4.6	120	2 258	23.5
4.0	0.9	165	2 043	268	5.1	4.4	120	1 387	29.6
5.0	0.7	143	4 770	212	9.7	7.6	120	3 484	19.7
5.0	0.8	152	3 154	244	6.4	4.3	120	2 299	23.7
5.0	0.9	170	2 100	268	5.1	4.3	120	1 410	29.7

The solutions obtained by estimating the optimal intermediate pressure level using Eq. (5.16) leads to net power consumption less than 0.01 % larger than the case of using the intermediate pressure level as a decision variable. The best solutions found with the intermediate pressure level given by the geometric mean deviate less than 0.04 % from the best solutions found. Since the difference in suction temperature for the two compression stages is small, the geometric mean provides a decent estimate for the optimal intermediate pressure level.

5.5 Dual nitrogen expander process

The power extraction from expansion processes can be increased be dividing the expansion process in stages with reheating. This does, however, not make sense for a refrigeration process where the main objective of the expansion process is to reach a temperature level suitable for cooling. The process energy efficiency can, however, be improved by introducing a second stage of expansion in parallel. In the single expander process, expansion of all refrigerant to the lowest temperature leads to unnecessary

large irreversibilities. These can be reduced by starting expansion of part of the refrigerant at a higher temperature.

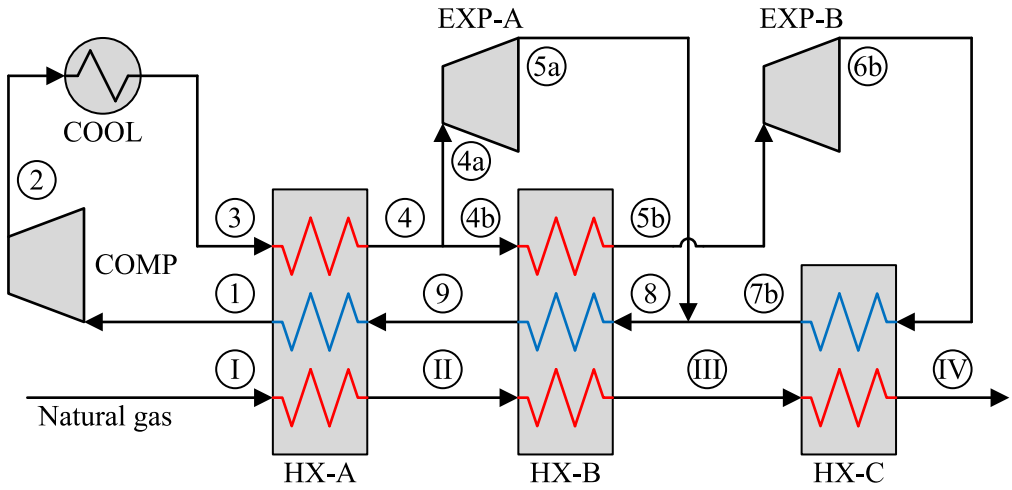

Figure 5.16. Dual expander process flowsheet.

One alternative layout for a dual expander process is given in Fig. 5.16. Since only one compressor is used, the same two pressure levels are used in both expansion cycles. In total six degrees are freedom are available for design of the dual expander process presented used in this work.

5.5.1 Simplified model

As for the single expander process, one degree of freedom is unavailable (pressure levels) when assuming a perfect gas model. Further, two degrees of freedom are locked by assuming the temperature difference between the two composite curves to be equal to the minimum required in both ends. In addition, the temperature difference in the hot end of HX-C is set to the minimum temperature difference. In order to avoid losses caused by mixing of streams at different temperature, the process is designed such that the temperature of the streams 5a and 7b is the same.

Finally, only one degree of freedom is left for the design optimization. The decision variable chosen for the simplified model is the intermediate temperature T_{III} between the heat exchangers HX-B and HX-C. Composite curves for the dual expander process are illustrated in Fig. 5.17.

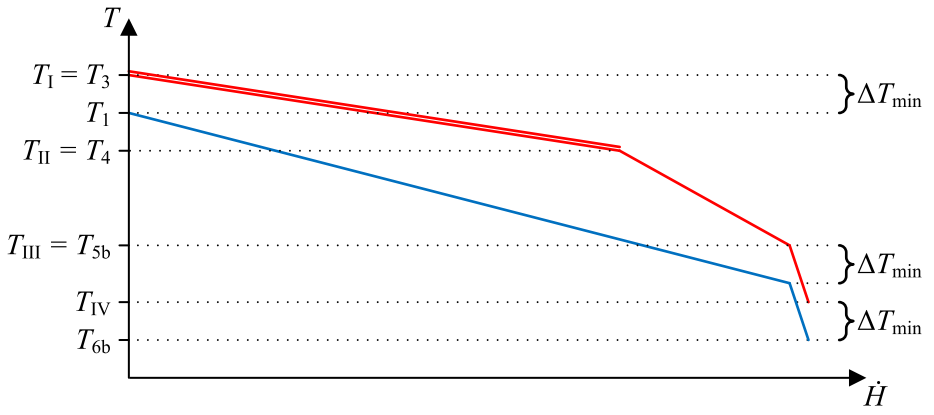

Figure 5.17. Composite curves for simplified model of dual nitrogen expander process.

The flow rate of refrigerant stream b can be calculated from an energy balance for HX-C. Due to the fact that the temperature difference in both ends is equal to the minimum temperature difference, this gives

$$\dot{m}_{\mathrm{R,b}} = \frac{\left(\dot{m} \cdot c_p\right)_{\mathrm{NG}}}{c_{p,\mathrm{R}}}, \tag{5.26}$$

which means that the refrigerant flow rate in sub-cycle b is constant, independent of the temperature range covered by heat exchanger HX-C. With the inlet and outlet temperatures given, the isentropic discharge temperature of expander EXP-B can be calculated from the definition of isentropic efficiency:

$$T_{\mathrm{6bs}} = \frac{T_{\mathrm{III}}\left(\eta_{s,\mathrm{EXP}} - 1\right) + T_{\mathrm{IV}} - \Delta T_{\min}}{\eta_{s,\mathrm{EXP}}} \tag{5.27}$$

Further, from Eq. (5.4), the pressure ratio of the refrigerant can be expressed as

$$\frac{p_{\mathrm{H}}}{p_{\mathrm{L}}} = \left(\frac{T_{\mathrm{III}} \cdot \eta_{s,\mathrm{EXP}}}{T_{\mathrm{III}} \cdot \left(\eta_{s,\mathrm{EXP}} - 1\right) + T_{\mathrm{IV}} - \Delta T_{\min}} \right)^{\frac{c_{p,\mathrm{R}}}{R}}, \tag{5.28}$$

similar to the single expander process. The power production of expander EXP-B is then given as

$$\dot{W}_{\text{EXP-B}} = \left(\dot{m} \cdot c_p\right)_{\mathrm{NG}} \cdot \left(T_{\mathrm{III}} - T_{\mathrm{IV}} + \Delta T_{\min}\right). \tag{5.29}$$

The pressure ratio is the same for the two expanders. An expression for the intermediate temperature of the natural gas stream between the heat exchangers HX-A and HX-B can therefore be derived as

$$T_{\mathrm{II}} = \frac{T_{\mathrm{III}} \cdot \left(T_{\mathrm{III}} - \Delta T_{\min}\right)}{T_{\mathrm{IV}} - \Delta T_{\min}}, \tag{5.30}$$

which is equivalent to having the same temperature ratio for the two expanders.

Similar to the single expander process, the refrigerant flow rate in sub-cycle a is given by the energy balance for the heat exchangers HX-A and HX-B:

$$\dot{m}_{\mathrm{R,a}} = \frac{\left(\dot{m} \cdot c_p\right)_{\mathrm{NG}}}{c_{p,\mathrm{R}}} \cdot \frac{\left(T_{\mathrm{I}} - T_{\mathrm{III}}\right) \cdot \left(T_{\mathrm{III}} - \Delta T_{\min}\right)}{T_{\mathrm{III}} \cdot \left(T_{\mathrm{III}} - T_{\mathrm{IV}}\right)}. \tag{5.31}$$

The power production of expander EXP-A can then be expressed as

$$\dot{W}_{\text{EXP-A}} = \left(\dot{m} \cdot c_p\right)_{\mathrm{NG}} \cdot \frac{\left(T_{\mathrm{I}} - T_{\mathrm{III}}\right) \cdot \left(T_{\mathrm{III}} - \Delta T_{\min}\right) \cdot \left(T_{\mathrm{III}} - T_{\mathrm{IV}} + \Delta T_{\min}\right)}{T_{\mathrm{III}} \cdot \left(T_{\mathrm{III}} - T_{\mathrm{IV}}\right)}. \tag{5.32}$$

From the definition of isentropic efficiency and the energy balance, the power consumption of the compressor is given as

$$\begin{aligned} \dot{W}_{\mathrm{COMP}} = {} & \frac{\left(\dot{m} \cdot c_p\right)_{\mathrm{NG}}}{\eta_{s,\mathrm{COMP}}} \cdot \left(1 + \frac{\left(T_{\mathrm{I}} - T_{\mathrm{III}}\right) \cdot \left(T_{\mathrm{IV}} - \Delta T_{\min}\right)}{T_{\mathrm{III}} \cdot \left(T_{\mathrm{III}} - T_{\mathrm{IV}}\right)}\right) \\ & \cdot \frac{\left(T_{\mathrm{I}} - \Delta T_{\min}\right)\left(T_{\mathrm{III}} - T_{\mathrm{IV}} + \Delta T_{\min}\right)}{T_{\mathrm{III}} \cdot \left(\eta_{s,\mathrm{EXP}} - 1\right) + T_{\mathrm{IV}} - \Delta T_{\min}}. \end{aligned} \tag{5.33}$$

Finally, the net power consumption can be found by summarizing the contributions from the compressor and the expanders:

$$\dot{W}_{\mathrm{net}} = \dot{W}_{\mathrm{COMP}} - \dot{W}_{\text{EXP-A}} - \dot{W}_{\text{EXP-B}}. \tag{5.34}$$

A premise for the energy balance for the heat exchangers HX-A and HX-B used to derive Eq. (5.31) is that $T_{\mathrm{II}} \leq T_{\mathrm{I}}$. Since temperature T_{II} is linked to T_{III}, T_{II} will increase with increasing T_{III}. Since the isentropic efficiency and pressure ratio is the same, the temperature ratio ($T_{\mathrm{in}}/T_{\mathrm{out}}$) will be equal for the two expanders. From Eq. (5.30), the

limiting value for the stage temperature T_{III} can be expressed as

$$T_{III,max} = \frac{\Delta T_{min} + \sqrt{\Delta T_{min}^2 + 4 \cdot T_I \cdot (T_{IV} - \Delta T_{min})}}{2}. \tag{5.35}$$

Assuming $\Delta T_{min} \ll T_{IV}$, an estimated is given as

$$T_{III,max} \approx \sqrt{T_I \cdot T_{IV}}\ . \tag{5.36}$$

For values of T_{III} higher than $T_{III,max}$, the expansion of refrigerant stream a will start at a temperature higher than the ambient cooling temperature. Hence, there will be no precooling of refrigerant stream a in HX-A. The refrigerant flow rate of sub-stream b can then by derived from an energy balance for HX-A and HX-B as

$$\dot{m}_{R,a} = \frac{\left(\dot{m} \cdot c_p\right)_{NG}}{c_{p,R}}. \tag{5.37}$$

One may notice that in this case, the flow rate of both sub-streams is constant. Further, the power consumption of EXP-A can be expressed as

$$\dot{W}_{EXP\text{-}A} = \left(\dot{m} \cdot c_p\right)_{NG} \cdot (T_{III} - \Delta T_{min}) \cdot \left(\frac{T_{III}}{T_{IV} - \Delta T_{min}} - 1\right). \tag{5.38}$$

The remaining Eqs. (5.26)-(5.34) still hold.

The net power consumption of the simplified model of the dual expander process is plotted as function of the stage temperature T_{III} in Fig. 5.18 for the case of $\Delta T_{min} = 2$ K and $\eta_s = 0.80$. A steep increase in power consumption is observed at the point at which the limiting value of T_{III} is reached. Even though the refrigerant flow rates are constant for values of $T_{III} > T_{III,max}$, the pressure ratio increases with increasing T_{III}. The optimal stage temperature T_{III} is, however, found to be quite close to the limiting value.

From a thermodynamic point of view, it does not make sense to start expansion of the refrigerant at temperatures higher than the ambient cooling temperature. If a solution where T_{III} is above the limiting value is sought, the compression process should be divided into stages, allowing the refrigerant used in sub-stream a to operate with a smaller pressure ratio than the refrigerant in sub-stream b.

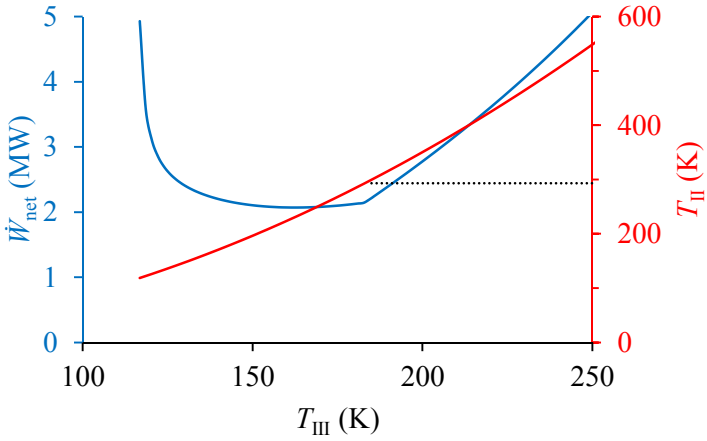

Figure 5.18. Net power consumption in simplified model of dual expander process as function of the stage temperature.

Table 5.8. Comparison of power consumption for single and dual nitrogen expander processes modelled with simplified thermodynamics.

		Single expander				Dual expander					
ΔT_{min}	η_s	T_{II}	$\dot{m}_R$	p_H/p_L	$\dot{W}_{net}$	T_{II}	T_{III}	$\dot{m}_R$	p_H/p_L	$\dot{W}_{net}$	Savings
(K)	(-)	(K)	(kg/s)	(-)	(kW)	(K)	(K)	(kg/s)	(-)	(kW)	(%)
1.0	0.7	129	54.8	1.9	3 836	191	148	18.5	4.1	3 150	17.9
1.0	0.8	133	42.8	2.0	2 644	225	161	13.0	4.9	2 015	23.8
1.0	0.9	141	29.4	2.3	1 841	262	173	10.0	5.3	1 274	30.8
2.0	0.7	134	39.9	2.4	4 106	198	151	17.0	4.7	3 262	20.6
2.0	0.8	140	30.9	2.6	2 793	231	163	12.4	5.4	2 070	25.9
2.0	0.9	151	21.1	3.1	1 917	266	174	9.8	5.7	1 302	32.1
3.0	0.7	138	33.3	3.0	4 340	204	153	15.9	5.3	3 371	22.3
3.0	0.8	145	25.7	3.2	2 921	235	164	12.0	5.8	2 124	27.3
3.0	0.9	159	17.4	4.0	1 982	270	175	9.6	6.0	1 331	32.9
4.0	0.7	141	29.5	3.5	4 558	208	154	15.2	6.0	3 480	23.7
4.0	0.8	149	22.6	3.8	3 040	239	165	11.6	6.3	2 179	28.3
4.0	0.9	165	15.3	4.8	2 043	273	176	9.4	6.4	1 360	33.4
5.0	0.7	143	26.9	4.1	4 770	212	155	14.6	6.6	3 589	24.7
5.0	0.8	152	20.5	4.4	3 154	243	166	11.3	6.8	2 235	29.1
5.0	0.9	170	13.8	5.7	2 100	276	177	9.2	6.7	1 389	33.9

Like for the case of two-stage compression, the simplified model of the dual expander process was optimized using the generalized reduced gradient search method in Microsoft Excel. The results are given in Table 5.8, compared with the simplified model of the single expander process. As can be observed, the net power consumption

of the dual expander process is around 18-34 % smaller than for the single expander, with savings growing for increasing isentropic efficiency and minimum temperature difference.

5.5.2 Rigorous model

In the rigorous process model, the low pressure level p_L, the pressure ratio p_H/p_L, the refrigerant flow rate in each sub-stream $\dot{m}_A$ and $\dot{m}_B$, and the two intermediate natural gas temperatures T_{II} and T_{III} were used as decision variables. In order to avoid cross-over, the first stage temperature T_{II} was bounded to be within T_I and T_{III} for all values of T_{III}. The optimization results are given in Table 5.9.

Table 5.9. Optimization results for dual nitrogen expander process modelled with rigorous thermodynamics.

		Single	Dual expander									
ΔT_{min}	η_s	$\dot{W}_{net}$	T_{II}	T_{III}	$\dot{m}_{Ra}$	$\dot{m}_{Rb}$	$\dot{m}_R$	p_L	p_H	p_H/p_L	$\dot{W}_{net}$	Savings
(K)	(-)	(kW)	(K)	(K)	(kg/s)	(kg/s)	(kg/s)	(bar)	(bar)	(-)	(kW)	(%)
1.0	0.7	3 836	253	177	8.6	2.7	11.3	18.6	97.0	5.22	2387	37.8
1.0	0.8	2 644	253	175	8.2	2.7	10.9	18.6	85.4	4.60	1643	37.8
1.0	0.9	1 841	252	173	8.0	2.7	10.7	17.5	71.4	4.08	1123	39.0
2.0	0.7	4 106	253	177	8.7	2.7	11.4	17.6	94.4	5.37	2448	40.4
2.0	0.8	2 793	253	175	8.3	2.7	11.0	17.6	82.9	4.71	1682	39.8
2.0	0.9	1 917	253	173	8.0	2.7	10.7	17.3	72.4	4.19	1148	40.1
3.0	0.7	4 340	254	177	8.7	2.8	11.5	16.6	92.0	5.53	2512	42.1
3.0	0.8	2 921	253	175	8.3	2.8	11.1	16.6	80.4	4.83	1723	41.0
3.0	0.9	1 982	253	173	8.0	2.7	10.7	16.6	71.5	4.30	1173	40.8
4.0	0.7	4 558	251	177	8.7	2.8	11.6	15.7	89.5	5.69	2577	43.5
4.0	0.8	3 040	252	175	8.3	2.8	11.1	15.7	78.1	4.97	1764	42.0
4.0	0.9	2 043	253	173	8.0	2.8	10.8	15.7	69.2	4.40	1199	41.3
5.0	0.7	4 770	253	177	8.8	2.9	11.6	14.8	87.0	5.88	2646	44.5
5.0	0.8	3 154	252	175	8.3	2.8	11.2	14.8	75.9	5.11	1807	42.7
5.0	0.9	2 100	252	173	8.0	2.8	10.8	14.8	67.0	4.51	1226	41.6

The net power consumption of the optimized dual expander process is 38-44 % smaller than that of the single expander process operating under the same conditions. One may notice that, opposed to the single expander process and the simplified model of the dual expander, there is little variation in the decision variables for the different cases. The main difference observed between the different solutions is the high pressure level which decreases with increasing isentropic efficiency and temperature difference. Since the inlet temperatures of the expanders and the low pressure level take similar values for the different cases, the pressure ratio must be increased in order to reach the required expander outlet temperatures when the isentropic efficiency is reduced or the minimum temperature difference increased. Apparently, the refrigerant flow rates,

stage temperatures and low pressure level give a cold composite curve that fits well with the cooling curve of the natural gas.

One may notice that the refrigerant flow rate in sub-cycle b is smaller in the rigorous model (see Table 5.8) than the simplified model (see Table 5.9). In addition, as opposed to the simplified model (see Eq. (5.26)), the refrigerant flow rate in sub-cycle b varies between the different cases in the best solutions known for the rigorous model. This is because the heat capacity of the natural gas stream passing through HX-C is smaller than the average heat capacity throughout the cooling process. Due to this, the refrigerant flow rate found to be optimal in the simplified model is higher than what is required to keep the temperature difference equal to the minimum required in both ends of HX-C.

Table 5.10. Process properties for best known design of dual nitrogen expander process modelled with rigorous thermodynamics.

ΔT_{min} (K)	η_s (-)	T_{5a} (K)	T_{7b} (K)	$\Delta T_{small,A}$ (K)	$\Delta T_{small,B}$ (K)	$\Delta T_{small,C}$ (K)
1.0	0.70	175.9	175.8	1.00	1.00	1.00
1.0	0.80	173.7	173.7	1.00	1.00	1.00
1.0	0.90	172.0	172.0	1.00	1.00	1.00
2.0	0.70	175.0	175.0	2.00	2.00	2.00
2.0	0.80	172.8	172.8	2.00	2.00	2.00
2.0	0.90	170.9	170.9	2.00	2.00	2.00
3.0	0.70	174.0	174.0	3.00	3.00	3.00
3.0	0.80	171.8	171.8	3.00	3.00	3.00
3.0	0.90	169.8	169.8	3.00	3.00	3.00
4.0	0.70	173.1	172.8	4.00	4.00	4.00
4.0	0.80	170.7	170.7	4.00	4.00	4.00
4.0	0.90	168.7	168.7	4.00	4.00	4.00
5.0	0.70	172.0	172.0	5.00	5.00	5.00
5.0	0.80	169.7	169.7	5.00	5.00	5.00
5.0	0.90	167.6	167.6	5.00	5.00	5.00

In Table 5.9, the assumptions made for the simple dual expander process have been tested for the best known solutions obtained with the rigorous thermodynamic model. In the simplified model, the temperatures of the two refrigerant cold streams mixed in the cold end of HX-B (T_{5a} and T_{7b}) were assumed to be equal for optimal design. As can be observed, these stream temperatures are equal or close to equal for all the case studies performed with the rigorous model. Only for the case with $\Delta T_{min} = 4$ K and $\eta_s = 0.70$ a small deviation is observed. A possible reason for this deviation could be that the global optimal solution was not found for this case.

In the simplified model the temperature difference in the hot end of HX-C was assumed to be equal to the minimum required. As can be observed from Table 5.10, the smallest temperature difference in each of the three heat exchangers is equal to the minimum required for all the cases studied with the rigorous model. By comparing T_{III} in Table 5.9 and T_{7b} in Table 5.10, the temperature difference in the hot end of HX-C is found to be close to minimum required for all cases except with $\Delta T_{min} = 4$ K and $\eta_s = 0.70$, since the temperatures of the streams to be mixed in the cold end of HX-B are slightly different. Overall, the assumptions made for the simplified model (mixing at equal temperature and minimum temperature difference in hot end of HX-C) seem to hold.

Composite curves for the best solution obtained with the rigorous model for $\Delta T_{min} = 2$ K and $\eta_s = 0.80$ are given in Fig. 5.19. As can be observed, the minimum temperature difference constraint is observed in the hot end of HX-A, the interior and cold end of HX-B and both ends of HX-C. Compared to the single expander process, both the total cooling load and the driving forces are considerably smaller. The former is, however, also related to the fact that the solution with small pressure ratio and high refrigerant flow rate was found to be best for the rigorous model in this case. As was discussed in Section 5.2.4, the total cooling load is significantly smaller for the design with a high pressure ratio and a small refrigerant flow rate.

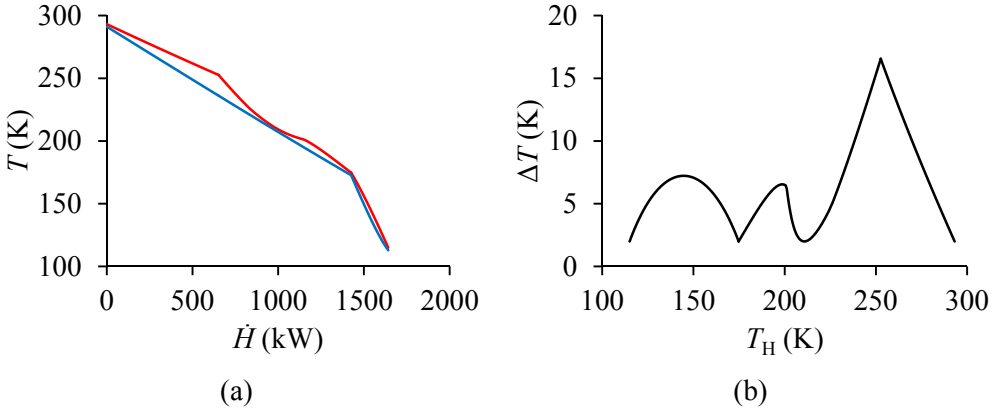

Figure 5.19. (a) Composite curves for best known solution of rigorous model for dual nitrogen expander process with $\eta_s = 0.80$ and $\Delta T_{min} = 2$ K; (b) Temperature difference as function of hot stream temperature.

5.6 Discussion

5.6.1 Practical implications

In order to find the optimal design solution, practical implications should also be considered. As was illustrated in Section 5.2.4, properties such as cooling load, heat

exchanger size and volumetric flow rate may be significantly different for two different design solutions, even though the estimated power consumption and smallest temperature difference are similar. Hence, the cost associated with different design solutions may differ considerably.

For the single expander process, two local solutions were observed with the rigorous process model. In general, the solutions with $p_L = 1$ bar have a considerably larger cooling load and thereby larger heat exchanger area (assuming the heat transfer coefficients to be comparable for the two cases) than the solutions with $p_H = 120$ bar. Due to a significantly higher volumetric flow rate, the compressor investment cost is also likely to be higher for the design with $p_L = 1$ bar. A design operating at low pressure is also more prone to be affected by pressure drop in the heat exchangers.

These results also indicate that the minimum temperature difference constraint may not perform well as a trade-off parameter for optimal balance between investment and operating costs. This will be further discussed in Chapter 7.

5.6.2 Alternative refrigerants

Alternative refrigerants in expander processes for liquefaction of natural gas include methane and nitrogen-methane mixtures. The simplified process model is used in this work does not make any assumptions with respect to the refrigerant used, other than perfect gas behaviour under the given operating conditions. Hence, the applicability of the simplified model depends on the accuracy of the perfect gas model.

With a different refrigerant, the specific heat capacity is likely to be different. Hence, as can be observed from Eqs. (5.1) and (5.5), the optimal solution of the simplified process model for the single expander process will be shifted towards a different refrigerant flow rate and pressure ratio. The suggested optimal stage temperature (see Eq. (5.9)) is, however, independent of the properties of the refrigerant and will remain the same irrespective of the refrigerant.

Methane has a higher critical temperature ($T_c \approx 191$ K (Moran and Shappiro, 2006)) than nitrogen, which suggests that the prerequisites of the simplified process model are less likely to be fulfilled with methane or a nitrogen-methane mixture as refrigerant. The critical pressure of methane ($p_c \approx 46$ bar (Moran and Shappiro, 2006)) is, however, also higher than for nitrogen.

5.6.3 Alternative process flowsheets

In this work, the dual expander process was modelled with the same pressure level for both expansion stages. Freedom to operate the two expansion stages with dissimilar pressure ratio could be achieved by dividing the compression process in stages. This

way, the dependence between the two stages in the dual expander process could be reduced and the process energy efficiency potentially improved.

5.7 Conclusions

In this chapter, nitrogen expander processes have been simulated and optimized both using a simplified process model assuming perfect gas behaviour for the refrigerant and constant specific heat for the natural gas, and a rigorous process model based the Soave-Redlich-Kwong equation of state. Both a single and a dual expander process were studied. For the former, the influence of two-stage compression was also tested.

Based on thermodynamic considerations, and the given process conditions, the simplified process model was formulated with one degree of freedom left for optimization. For the single expander process with single-stage compression this enabled the optimization problem to be solved analytically. Slightly more complex models were required to describe the process with dual-stage compression and the dual expander process, making the problem harder to solve analytically. Since the problems were still found to be unimodal, and therefore simple to optimize, a generalized reduced gradient method was used for the optimization search. The rigorous process model was simulated using Aspen HYSYS® and the optimization problem solved using a sequential quadratic programming algorithm.

The results obtained for the single expander process indicated close agreement between the best solutions found with the rigorous process model and the optimal solution of the simplified model for small values of the minimum temperature difference and low to moderate values for the isentropic efficiency. This would suggest that the simplified model could be used as a tool for early-stage screening of the nitrogen expander process, identifying interesting regions of the search space and a starting point for optimization of the rigorous model.

For the majority of the cases studied, however, the best results obtained with the rigorous process model were found to be significantly different from the optimal solution of the simplified model. Design solutions close to the ones suggested by the simplified model could still be implemented, but by accounting for the non-linearity of the refrigerant, design solutions with considerable savings in net power consumption were observed.

The simplified model was found to provide a good estimate for the best solution of the rigorous model when the optimal trade-off between refrigerant flow rate and pressure ratio is shifted towards high flow rates and small pressure ratios. This was found to be true only for small values of the minimum temperature difference. Due to the large temperature difference between the composite curves, the assumption of a constant

specific heat capacity for the natural gas stream was found not to influence the performance of the simplified process model when optimizing the single expander process.

With dual-stage compression, reductions in net power consumption ranging 7-29 % were observed for the simplified process model. The savings increased with increasing minimum temperature difference and isentropic efficiency, which is related to the fact that the optimal design of the single expander process is shifted towards smaller refrigerant flow rates and higher pressure ratios for these operating conditions. With dual-stage compression, the compression and expansion processes become more efficient. Compared to single-stage compression, a flatter optimum was observed (as function of the stage temperature).

Also for the rigorous process model, increased savings were observed for increasing values of the minimum temperature difference and the isentropic efficiency. Compared to the simplified model, the relative savings in net power consumption (percent) were even higher. Since the design was shifted towards smaller flow rates and larger pressure ratios, the local solutions with $p_H = 120$ bar were found to give the smallest power consumption for all the cases studied. Hence, for all cases, significant differences were observed for the optimized design of the two process models.

The net power consumption of the optimized dual expander process was found to be even smaller than for the single expander process with dual-stage compression. For the simplified process model, the savings ranged 18-34 % compared to the single expander process (with single-stage compression), while for the rigorous model the net power consumption was reduced by 38-45 % compared to the single expander process. For the simplified model, the relative savings were found to increase with increasing minimum temperature difference and isentropic efficiency.

In general, little agreement was observed between the simplified and rigorous process models for the dual expander process. While the optimal values for the different decision variables were found to change considerably between the different cases for the simplified model, only small variations were observed for the best solutions obtained with the rigorous model.

For the dual expander process, the assumption of a constant heat capacity for the natural gas stream in the simplified model was found to have a considerable effect on the results. Since pinch points are observed not only in the end points of the composite curves, more accurate models are required for the cooling curve of the natural gas stream. In this case, the assumption of a constant heat capacity for the natural gas could lead to solutions that are not feasible for the rigorous process model.

Better performance is expected if the natural gas cooling curve is divided into segments with constant heat capacity, as was done by Marmolejo-Correa and Gundersen (2010). This would, however, also lead to increased complexity for the optimization problem.

For optimization of the single expander process with dual-stage compression, expressions for the optimal intermediate pressure level were derived. While the geometric mean suggests that the different compression stages should have the same pressure ratio, the results indicate that the pressure ratio should be larger for the compression stage with the lowest suction temperature. An optimality criterion for multi-stage compression of a perfect gas with constant isentropic efficiency was deduced.

Rather than uniform pressure ratios, the optimal intermediate pressure levels are characterized by uniform isentropic discharge temperatures (discharge temperature in the case of fully isentropic compression) for the different compression stages. For the special case of equal suction temperatures, this criterion is equivalent with uniform pressure ratios. For the case of the single expander process, the intermediate pressure level was found to be of relatively little importance for the net power consumption, and the geometric mean provided results within 0.04 % of the best known for rigorous process model. In situations where the difference in suction temperature is larger, however, the geometric mean is expected to provide poorer performance. This is further studied in Chapter 8.

5.8 References

Agnew B, Ameli SM. A finite time analysis of a cascade refrigeration system using alternative refrigerant. *Applied Thermal Engineering* 2004;24(17-18):2557-2565.

Agrawal N, Bhattacharyya S, Sarkar J. Optimization of two-stage transcritical carbon dioxide heat pumps. *International Journal of Thermal Sciences* 2007;46(2):180-187.

Arora A, Kaushik SC. Energy and exergy analyses of a two-stage vapour compression refrigeration system. *International Journal of Energy Research* 2010;34(10):907-923.

Cavallini A, Cecchinato L, Corradi M, Fornasieri E, Zilio C. Two-stage transcritical carbon dioxide cycle optimisation: A theoretical and experimental analysis. *International Journal of Refrigeration* 2005;28(8):1274-1283.

Chang H-M, Chung MJ, Kim MJ, Park SB. Thermodynamic design of methane liquefaction system based on reverse-Brayton cycle. *Cryogenics* 2009;49(6):226-234.

He T, Ju Y. A novel conceptual design of parallel nitrogen expansion liquefaction process for small-scale LNG (liquefied natural gas) plant in skid-mount packages. *Energy* 2014;75:349-359.

Jacobsen MG, Skogestad S. Active constraint regions for a natural gas liquefaction process. *Journal of Natural Gas Science and Engineering* 2013;10:8-13.

Jekel TB, Reindl DT. Single- or two-stage compression. *ASHRAE Journal* 2008;50(8):46-48+50-51.

Jensen JB, Skogestad S. Optimal operation of a simple LNG process. In: Doyle FJ III, Trierweiler JO, Secchi AR, editors. Proceedings of the International Symposium on Advanced Control of Chemical Processes. 2006 Apr 2-5; Gramado, Brazil. Oxford: Elsevier; 2006. p. 241-246.

Khan J-U-R, Zubair SM. Design and rating of a two-stage vapor-compression refrigeration system. *Energy* 1998;23(10):867-878.

Li Y, Wang X, Ding Y. An optimal design methodology for large-scale gas liquefaction. *Applied Energy* 2012;99:484-490.

Marmolejo-Correa D, Gundersen T. New graphical representation of exergy applied to low temperature process design. *Industrial and Engineering Chemistry Research* 2010;52(22):7145-7156.

Moran MJ, Shapiro HN. *Fundamentals of Engineering Thermodynamics*. 2nd ed. Chichester: Wiley & Sons Ltd; 2006.

Srinivasan K. Identification of optimum inter-stage pressure for two-stage transcritical carbon dioxide refrigeration cycles. *The Journal of Supercritical Fluids* 2011;58(1):26-30.

Streit J, Razani A. Thermodynamic optimization of reverse Brayton cycles of different configurations for cryogenic applications. *International Journal of Refrigeration* 2013;36(5):1529-1544.

Streit JR, Razani A. Second-law analysis and optimization of reverse brayton cycles of different configurations for cryogenic applications. *AIP Conference Proceedings* 2012;1434(57):1140-1148.

Torrella E, Larumbe JA, Cabello R, Llopis R, Sanchez D. A general methodology for energy comparison of intermediate configurations in two-stage vapour compression refrigeration systems. *Energy* 2011;36(7):4119-4124.

Torrella E, Llopis R, Cabello R. Experimental evaluation of the inter-stage conditions of a two-stage refrigeration cycle using a compound compressor. *International Journal of Refrigeration* 2009;32(2):307-315.

Wechsung A, Aspelund A, Gundersen T, Barton PI. Synthesis of heat exchanger networks at subambient conditions with compression and expansion of process streams. *AIChE Journal* 2011;57(8):2090-2108.

Yoon S, Cho H, Lim D-H, Kim J-K. Process design and optimization of natural gas liquefaction processes. *Chemical Engineering Transactions* 2012;29:1585-1590.

Yuan Z, Mengmeng C, Xie Y, Li C. Design and analysis of a small-scale natural gas liquefaction process adopting single nitrogen expansion with carbon dioxide pre-cooling. *Applied Thermal Engineering* 2014;64(1-2):139-146.

Zubair SM, Yaqub M, Khan SH. Second-law-based thermodynamic analysis of two-stage and mechanical-subcooling refrigeration cycles. *International Journal of Refrigeration* 1996;19(8):506-516.

6 Decision Variables

The choice of decision variables and variable bounds are important factors for the optimization performance. In this chapter, this is studied for a pure-refrigerant cascade LNG process with three vertical stages. Based on thermodynamic insight, a set of decision variables have been proposed that can easily be bounded. Compared with a set of fairly intuitive decision variables, the optimization search is significantly improved.

Thermodynamic analysis was used to study the influence of different parameters illustrate the importance of considering interactions between the different refrigeration cycles in a cascade process. The results indicate that the operating conditions that give minimum compression power in individual cycles may not coincide with the solution that gives the smallest overall power consumption.

This chapter is partly based on the following publications:

- Austbø B, Gundersen T. Using thermodynamic insight in the optimization of LNG processes. *Computer Aided Chemical Engineering* 2014;33:1273-1278.
- Austbø B, Gundersen T. Thermodynamic analysis in LNG process optimization. In: Zevenhoven R, editor. Proceedings of the 27th International Conference on Efficiency, Cost, Optimization, Simulation and Environmental Impact of Energy Systems (ECOS 2014), Turku, Finland, 2014.

6.1 Introduction

Pure-refrigerant cascade processes for liquefaction of natural gas have, compared to other process concepts, received relatively little attention in the literature. This may be related to the fact that these processes are relatively easy to design (Castillo and Dorao, 2013), or that more promising process concepts have been developed. A cascade refrigeration process was used in the first base-load LNG plant in Arzew, Algeria, in 1964, and also the Kenai LNG plant started up 1969 in Alaska, USA (Bosma and Nagelvoort, 2009). Over the years, however, propane-precooled mixed-refrigerant processes have become the dominant technology in the LNG industry.

According to Ransbarger (2007), pure-refrigerant cascade processes are seldom included in studies comparing the performance of different LNG process concepts. The studies that are present often deal with the classical cascade. ConocoPhillips' Optimized Cascade®, which represents an improvement of the classical cascade, is seldom considered. This process includes an optimized heat recovery system and the closed loop methane cycle is replaced with an open loop system. The availability of technical details on the Optimized Cascade® is, however, fairly limited (Ransbarger, 2007). In this work, classical cascade processes with closed loop refrigeration cycles have been studied.

According to Finn et al. (1999), the pure-refrigerant cascade process is the most energy efficient process concept for natural gas liquefaction, mainly due to the small refrigerant flow rates required. Pure-refrigerant cascade processes also benefit from relatively small heat exchanger areas compared to mixed-refrigerant process, due to larger temperature driving forces. The different refrigeration cycles can be controlled separately, which makes the process more flexible in operation (Finn et al., 1999).

The high number of refrigeration stages does, however, result in high capital and maintenance costs. Another drawback of the high number of stages is increased complexity of the machinery configuration. Due to the economy of scale, pure-refrigerant cascade processes are best suited for large LNG train sizes (Finn et al., 1999).

Compared to mixed-refrigerant processes, the thermodynamics are simpler since isobaric evaporation and condensation takes place at constant temperature. Hence, detection of pinch candidates in the heat exchangers is easier. The challenges represented by phase change and interaction between the different refrigeration cycles in the cascade are, however, still present.

By studying the simpler pure-refrigerant cascade processes, the idea is therefore to generate ideas and insight that can be transferred to more complex mixed-refrigerant cascade processes. The objective is also to illustrate the influence of choice of decision variables on optimization search performance. Both a simple cascade process with one horizontal stage in each vertical stages and a complex cascade process with three horizontal stages in each vertical stage have been studied.

6.1.1 Optimization

Barnés and King (1974) proposed a synthesis method for minimization of total annual cost in pure-refrigerant cascade processes. Dynamic programming was used to construct the process in descending order of refrigeration temperature, while the optimal number of horizontal stages in each vertical stage was determined through an

evolutionary approach. Barnés and King (1974) applied heuristic rules for appropriate use of economizers, pre-saturators, after-coolers, inter-coolers, side loads and internal heat transfer in order to reduce the number of design variables prior to optimization.

Cheng and Mah (1980) found that potentially favourable design solutions may be omitted in the approach proposed by Barnés and King (1974). They therefore proposed alternative heuristics for synthesis of cascade refrigeration systems with multiple cooling loads at different temperatures. As opposed to the methodology of Barnés and King (1974), the temperature approach was not generalized but evaluated individually for each heat exchanger. In the work by Cheng and Mah (1980), heat capacities and heat transfer properties were assumed constant. In another study, Shelton and Grossmann (1986) presented a superstructure for optimization of cascade refrigeration systems integrated with heat recovery networks.

Later, Colmenares and Seider (1989) proposed and NLP model for design of cascade refrigeration systems covering a continuous range of operating temperatures. In their approach, appropriate refrigerants and number of intermediate temperature levels were determined at an early stage of the optimization, before introducing complex cycles. An extension of the superstructure presented by Shelton and Grossmann (1986) was proposed by Vaidyaraman and Maranas (1999) for optimization of pure-refrigerant processes with multiple constant-temperature cooling loads. Structural decisions and choice of refrigerants were addressed simultaneously in an MINLP approach.

Another approach to synthesis of integrated refrigeration systems was proposed by Wu and Zhu (2002). The approach did not provide details on the heat exchanger network design but provides area targets and matches in the refrigeration system. More recently, Zhang and Xu (2011) proposed an MINLP model for maximization of exergy efficiency of a cascade refrigeration system. The model was developed for retrofit design of the refrigeration system in an olefin plant.

While few studies are available on optimization of pure-refrigerant LNG processes, more optimization studies are present for propane-precooled mixed-refrigerant processes (Taleshbahrami and Saffari, 2010; Alabdulkarem et al., 2011; Wang et al., 2011, 2013; Lee et al., 2014). The precooling stage of such processes is similar to the first vertical stage of the pure-refrigerant cascade process.

In the process studied by Wang et al. (2011), the propane refrigerant is sub-cooled by recuperative cooling. Alabdulkarem et al. (2011) also found refrigerant sub-cooling to give smaller power consumption. Lee et al. (2014) proposed using refrigerant cold streams to sub-cool the hot refrigerant prior to expansion, instead of increasing the condensation pressure above the saturation pressure at the ambient cooling

temperature. The proposed design is, however, not compared with a design without refrigerant sub-cooling. Common to the three different studies, the propane refrigerant exits the hot end of the heat exchangers as saturated vapour.

From the flowsheets presented, it seems that the vapour formed in each expansion stage is not separated from the liquid phase before expanding further to the next pressure level in the studies presented by Taleshbahrami and Saffari (2010) and Wang et al. (2013). This is, however, done in the flowsheets given by Alabdulkarem et al. (2011), Mortazavi et al. (2010, 2012) and Lee et al. (2014). Castillo and Dorao (2013) and Castillo et al. (2013) compared different refrigerant alternatives, among them propane, for a precooling process in a mixed-refrigerant LNG process. Details on process flowsheet and optimization variables were, however, not given.

Optimal load distribution

Barnés and King (1974) found the intermediate pressure levels for horizontal stages to be optimal when the stages with large refrigerant flow rate had a pressure ratio with a pressure ratio smaller than the geometric mean, while pressure ratio for stages with small refrigerant flow rate were larger than the geometric mean. They did, however, also find that the location of the intermediate pressure levels had little influence on the total cost of the refrigeration process.

Based entropy generation minimization, Ratts and Brown (2000) proposed a design criterion for optimal intermediate temperature levels for the horizontal stages in a general refrigeration cycle. The compression processes were assumed to be fully isentropic and the exergy losses associated with heat transfer in condensation and evaporation were neglected. Hence, only irreversibilities related to isenthalpic expansion and cooling of superheated vapour subsequent to compression were considered. For a two-stage process, the proposed approach predicted the optimal intermediate temperature within 2 % of the optimum value, whereas the solution suggested by the geometric mean deviated 5 % from the optimum.

Agnew and Ameli (2004), Bhattacharyya et al. (2007), Sarkar et al. (2013) and Park et al. (2013) have also studied optimal load distribution in cascade refrigeration systems. According to Agnew and Ameli (2004), the compressor efficiency has a significant influence on the optimal intermediate pressure levels in two-stage refrigeration cycles. Sarkar et al. (2013) developed correlations for optimal intermediate temperature levels in a two-stage refrigeration process for different refrigeration pairs.

6.1.2 Exergy analysis

Exergy analyses of pure-refrigerant cascade processes for natural gas liquefaction have been presented by Kanoğlu (2002), Cipolato et al. (2012) and Tsatsaronis and Morosuk

(2010) with different process layouts. Neither of these studies considers the possibility of utilizing refrigerant superheating for cooling. Kanoğlu (2002) and Cipolato et al. (2012) studied a process with ethane used as refrigerant in the intermediate stage. In the process studied by Tsatsaronis and Morosuk (2010), all heat was absorbed from the natural gas stream in the methane cycle and rejected to the ambient through a cascade with propane and ethene used in the other refrigeration cycles.

Cascade refrigeration also has applications other than LNG. Mafi et al. (2009) presented an exergy analysis of the cascade refrigeration process in an olefin plant and used shaftwork targeting (Linnhoff and Dhole, 1992) to identify opportunities for improvements in exergy efficiency. The refrigeration system consisted. They concluded that increased efficiency resulting from adding a new horizontal stage in one of the vertical stages had to be weighed against increased investment cost. Göktun (1996) and Kilicarslan and Hosoz (2010) have presented exergy analyses of cascade refrigeration processes used for other cooling applications.

6.2 Problem formulation

In this work, the power consumption of two pure-refrigerant cascade processes has been minimized subject to a minimum temperature difference of 2 K and a minimum superheating of 10 K for compressor suction streams. As illustrated in the flowsheet in Fig. 6.1, three vertical stages with different pure refrigerants were used. The process was studied both with one horizontal stage in each vertical stage and with three horizontal stages in each vertical stage. The processes were modelled as partial cascades, but the use of coolers depends on the inlet temperature of the refrigerant stream (no cooling if the refrigerant temperature is smaller than the ambient cooling temperature).

The pure-refrigerant cascade process has been studied assuming the same operating conditions as for the case study of the nitrogen expander processes. Properties for the natural gas stream are given in Table 6.1. All compressor have been assumed to operate with a constant isentropic efficiency $\eta_s = 0.80$ and the outlet temperature of the coolers was set to $T_{\text{cool}} = 293.15$ K (if the compressor discharge temperature was higher than this value). The lower bound on the pressure level of the refrigerant was given as 1 bar. In practice, a higher limit may be applied in order to make sure there is no leak into the system with a safety margin. The process was been modelled in Aspen HYSYS® using the Soave-Redlich-Kwong equation of state.

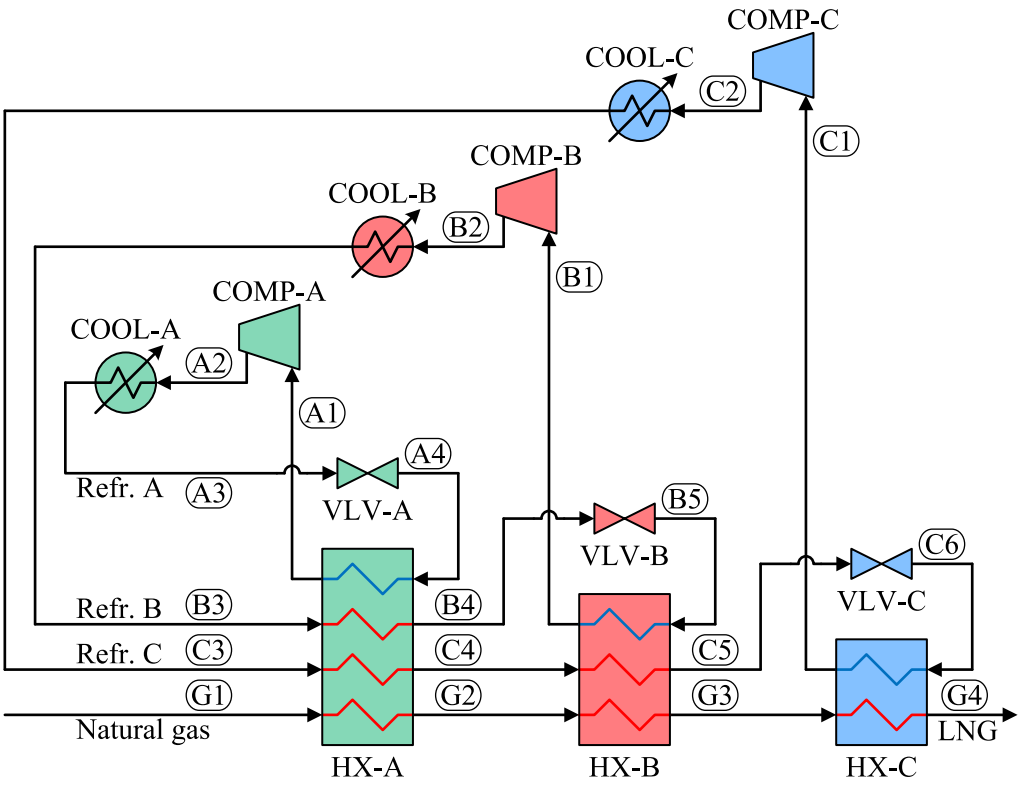

Figure 6.1. Flowsheet for simple pure-refrigerant cascade process.

Table 6.1. Natural gas properties.

Variable	Unit	Value
Flow rate $\dot{m}_{NG}$	kg/s	1.0
Feed pressure p_{in}	bar	55.0
Feed temperature T_{in}	K	293.15
Product temperature T_{out}	K	115.00
Molar composition		
Methane	-	0.897
Ethane	-	0.055
Propane	-	0.018
N-butane	-	0.002
Nitrogen	-	0.028

In pure-refrigerant cascade processes, cooling is provided by evaporation of single-component refrigerants. The refrigerants must therefore operate below critical pressure and temperature. Vapour pressure curves are given in Fig. 6.2 for a set of relevant refrigerant candidates. For each refrigerant the saturation temperature is plotted for pressure levels ranging from 1 bar to the critical pressure.

In order to cool the natural gas to the required outlet temperature, the saturation temperature of the refrigerant in refrigeration cycle C must be at least ΔT_{min} smaller for the smallest pressure level allowed. With a target temperature of 115 K and $\Delta T_{min} = 2$ K, the saturation temperature of the refrigerant operating in the last vertical stage must therefore be 113 K or smaller at 1 bar. From Fig. 6.2, it is therefore obvious that methane is a suitable refrigerant candidate for cycle C. At 1 bar pressure, the saturation temperature of methane is around 111.6 K (Soave-Redlich-Kwong). Hence, for the given minimum temperature difference, methane could potentially be used to cool the natural gas to around 113.6 K given the limit on the low pressure level.

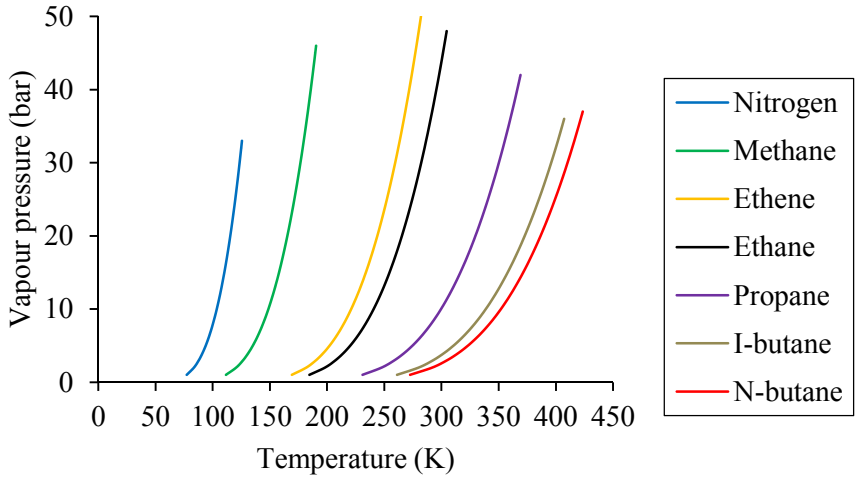

Figure 6.2. Saturation pressure as function of temperature for different refrigerant alternatives.

Given that each refrigerant should be condensed prior to expansion, the refrigerant used in refrigeration cycle B must have a saturation temperature at 1 bar low enough to be able to liquefy methane. From Fig. 6.2, one may observe that both ethane and ethene (ethylene) fulfil this requirement. In this work, both alternatives have been tested in order to study the influence of choice of refrigerant.

Nitrogen is an alternative refrigerant in cycle C, but condensation of nitrogen cannot be obtained using neither ethane nor ethene. Using nitrogen as refrigerant would therefore require one additional refrigeration stage, since (of the refrigerant alternatives presented here) methane would be required to liquefy nitrogen. For this reason, nitrogen was not considered as refrigerant in this work.

In cycle A, propane is an obvious candidate refrigerant which is able to liquefy both ethene and ethane and cover the remaining cooling range of the natural gas stream. I-butane and n-butane are other refrigerant alternatives for cycle A, but these

refrigerants can only cover a small part of the natural gas temperature range. In this work, propane has been used as refrigerant in cycle A.

In the literature, the refrigerants used are typically propane in cycle A, ethane or ethene in cycle B and methane in cycle C. In the ConocoPhillips Optimized Cascade®, an open refrigeration cycle is used for the lowest temperature level. This enables better matching of the composite curves in the cold end of the temperature range, but has not been considered in this work.

The heat of vaporization is plotted as function of the saturation temperature for the different refrigerant alternatives in Fig. 6.3. Comparing with Fig. 6.2, one may observe that the refrigerants with lower vapour pressure have a higher heat of evaporation for the same temperature. Of the two alternatives considered for refrigerant cycle B, ethane has a higher heat of vaporization at the same temperature level. This may indicate that ethane is a better refrigerant candidate if the two refrigerants are used to cover the same temperature range. However, load distribution (temperature range covered) and interaction between the different refrigeration cycles are also important factors for the overall efficiency.

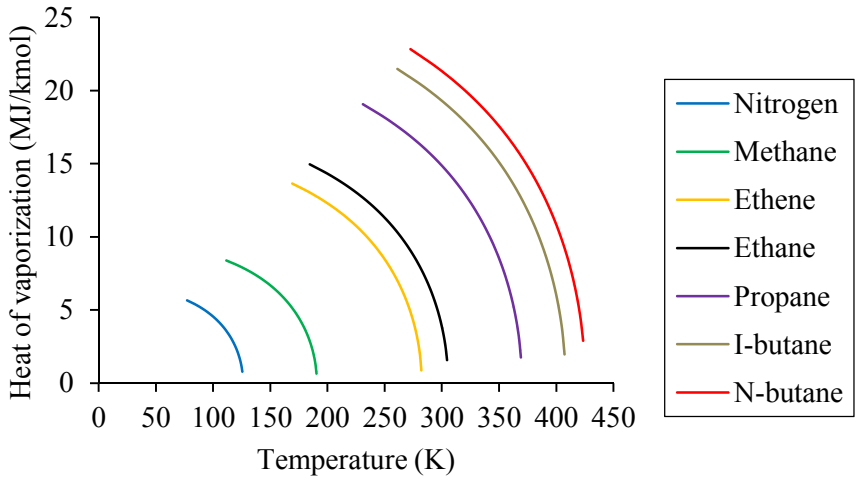

Figure 6.3. Heat of vaporization as function of temperature for different refrigerant alternatives.

6.3 Simple cascade

The propane refrigeration cycle is illustrated in pressure-enthalpy and temperature-entropy diagrams in Fig. 6.4. In the pressure-enthalpy diagram, the specific cooling capacity (q_{cool}), specific compression power (w_{comp}) and specific de-superheating and condensation heat (q_{cond}). The refrigerant superheating (ΔT_{dew}) entering the compressor is indicated in the temperature-entropy diagram.

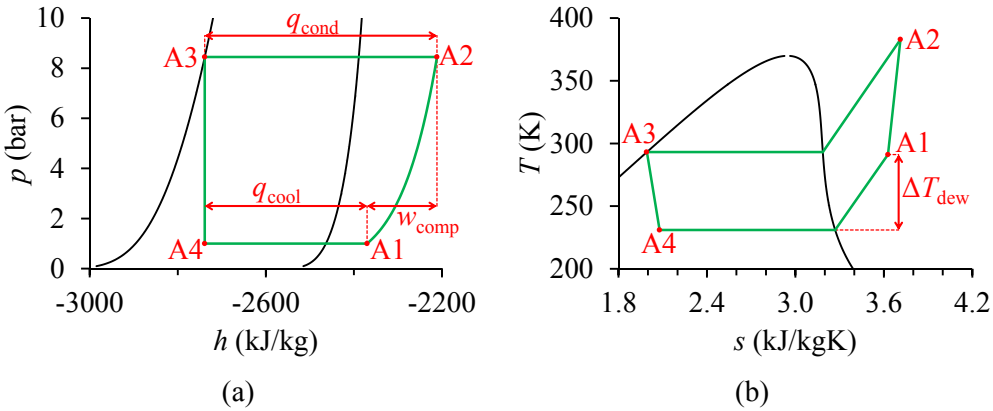

(a) (b)

Figure 6.4. (a) Propane refrigeration cycle illustrated in pressure-enthalpy diagram; (b) Propane refrigeration cycle illustrated in temperature-entropy diagram.

6.3.1 Decision variables

Based on the given assumptions, 11 degrees of freedom are available when optimizing the simple cascade process illustrated in Fig. 6.1. A fairly obvious choice of decision variables is given in the leftmost column in Table 6.2 (alternative 1). In this formulation, the load distribution between the three refrigeration cycles is given by the two intermediate temperature levels of the natural gas stream. The operating conditions of the refrigeration cycles are given by the refrigerant flow rates and the low and high pressure levels.

Table 6.2. Decision variables used for design optimization of simple cascade process.

Alternative 1	Alternative 2
p_{A1}	p_{A1}
p_{B1}	p_{B1}
p_{C1}	$\Delta T_{cold,C}$
T_{G2}	$\Delta T_{cold,A}$
T_{G3}	$\Delta T_{cold,B}$
p_{A2}	$\Delta p_{sub,A}$
p_{B2}	$\Delta p_{sub,B}$
p_{C2}	$\Delta p_{sub,C}$
$\dot{m}_A$	$z_{sup,A}$
$\dot{m}_B$	$z_{sup,B}$
$\dot{m}_C$	$z_{sup,C}$

Based on thermodynamic insight, an alternative set of decision variables have been proposed. These are given in the rightmost column in Table 6.2. In this formulation, intermediate temperature levels, refrigerant flow rates and high pressure levels are given indirectly through variables describing other properties of the process. The

background and characteristics of these variables are given in the following thermodynamic analysis.

6.4 Thermodynamic analysis

The pure-refrigerant cascade process is characterized by the fact that isobaric condensation and evaporation of the refrigerant take place at constant temperature. By taking advantage of this, the optimization problem could potentially be formulated in a way that improves the optimization search performance. In the following, studies of the characteristics of the proposed set of decision variables (alternative 2 in Table 6.2) are presented.

6.4.1 Intermediate temperatures – cold end temperature difference

The temperature differences in the cold end of the heat exchangers are given by the difference between the intermediate natural gas temperatures and the evaporation temperatures of the refrigerants. In order to fulfil the minimum temperature difference constraint, the two temperature levels must be at least $\Delta T_{\min}$ apart:

$$\begin{aligned} T_{\mathrm{G2}} &\geq T_{\mathrm{A4}} + \Delta T_{\min}, \\ T_{\mathrm{G3}} &\geq T_{\mathrm{B5}} + \Delta T_{\min}, \\ T_{\mathrm{G4}} &\geq T_{\mathrm{C1}} + \Delta T_{\min}. \end{aligned} \tag{6.1}$$

From thermodynamic considerations, it is given that the temperature difference between the composite curves should be as small as possible in order to minimize irreversibilities. The characteristics of single-component refrigerants (evaporation at constant temperature) indicate that the smallest temperature difference will be observed in the end points of the heat exchanger. The temperature difference in the cold end of the heat exchangers should therefore be equal to the minimum required.

For refrigeration cycles A and B, this means that the outlet temperature of the natural gas stream should be $\Delta T_{\min}$ larger than the evaporation temperature of the refrigerant, or vice versa. For refrigeration cycle C, the outlet temperature of the natural gas stream is given. Hence, from this temperature, the optimal evaporation temperature of refrigerant C, and thereby also its low pressure level, is given. The intermediate natural gas temperatures T_{G2} and T_{G3}, and the evaporation temperature of refrigerant C can be expressed as functions of the cold end temperature difference in the respective heat exchangers:

$$\begin{aligned} T_{\mathrm{G2}} &= T_{\mathrm{A4}} + \Delta T_{\mathrm{cold,A}}, \\ T_{\mathrm{G3}} &= T_{\mathrm{B5}} + \Delta T_{\mathrm{cold,B}}, \\ T_{\mathrm{C1}} &= T_{\mathrm{G4}} - \Delta T_{\mathrm{cold,C}}. \end{aligned} \tag{6.2}$$

The cold end temperature differences ΔT_{cold} must be equal to ΔT_{min} or larger. Increasing the temperature difference in the cold end of the heat exchanger will require a lower evaporation pressure. With increasing pressure ratio, the compressor power will increase. This is related to increased irreversibilities in the heat exchanger, caused by larger temperature driving forces. Hence, thermodynamic insight suggests that the optimal solution is obtained for $\Delta T_{\text{cold}} = \Delta T_{\text{min}}$.

6.4.2 High pressure level – refrigerant sub-cooling

In order to achieve condensation prior to expansion, the high pressure levels of the refrigerants must be equal to the saturation pressure equivalent to the precooling temperature or higher:

$$\begin{aligned} p_{\text{A2}} &\geq p_{\text{sat}}\left(T_{\text{A3}}\right), \\ p_{\text{B2}} &\geq p_{\text{sat}}\left(T_{\text{B4}}\right), \\ p_{\text{C2}} &\geq p_{\text{sat}}\left(T_{\text{C5}}\right). \end{aligned} \tag{6.3}$$

While the precooling temperature in refrigeration cycle A (T_{A3}) is constant, the precooling temperatures in cycles B and C (T_{B4} and T_{C5}) depend on other decision variables. If the low pressure level in refrigeration cycle A (p_{A1}) is increased, the evaporation temperature in cycle A (T_{A4}) increases. As a consequence, the intermediate temperature of the natural gas stream and the refrigerant hot streams ($T_{\text{G2}} = T_{\text{B4}} = T_{\text{C4}}$) will increase. Hence, the high pressure level in refrigeration cycle B (p_{B2}) required to obtain condensation will also increase. The same applies to the high pressure level in refrigeration cycle C (p_{C2}) when the low pressure level in refrigeration cycle B (p_{B1}) is subject to change.

Bounding variables directly describing the high pressure level in each cycle may therefore be challenging, at least keeping narrow bounds guaranteeing inclusion of the global optimum. It may therefore be useful to define the three high pressure levels based on the required saturation pressure. In alternative 2 (see Table 6.2), the high pressure levels are defined as

$$\begin{aligned} p_{\text{A2}} &= p_{\text{sat}}\left(T_{\text{A3}}\right) + \Delta p_{\text{sub,A}}, \\ p_{\text{B2}} &= p_{\text{sat}}\left(T_{\text{B4}}\right) + \Delta p_{\text{sub,B}}, \\ p_{\text{C2}} &= p_{\text{sat}}\left(T_{\text{C5}}\right) + \Delta p_{\text{sub,C}}. \end{aligned} \tag{6.4}$$

Here, the variables $\Delta p_{\text{sub,A}}$, $\Delta p_{\text{sub,B}}$ and $\Delta p_{\text{sub,C}}$ represent an elevation of the high pressure level above the saturation pressure.

When the high pressure level is equal to the saturation pressure of the precooled refrigerant, the refrigerant will enter the expansion valve as saturated liquid. If the pressure is raised above the saturation pressure, the refrigerant will be a sub-cooled liquid. Sub-cooling the liquid gives a smaller enthalpy level at the inlet of the expansion valve, which means that the specific cooling load of the refrigerant increases (more heat can be transferred to the refrigerant with the same refrigerant flow rate).

However, since a higher pressure ratio is required, the specific compression power will also increase (more power is required to compress the same refrigerant flow rate). These two effects have opposite influence on the power consumption since the same cooling duty can be delivered with a smaller refrigerant flow rate but with higher compression power per unit of mass. The optimal high pressure level therefore depends on the relative strengths of these two effects.

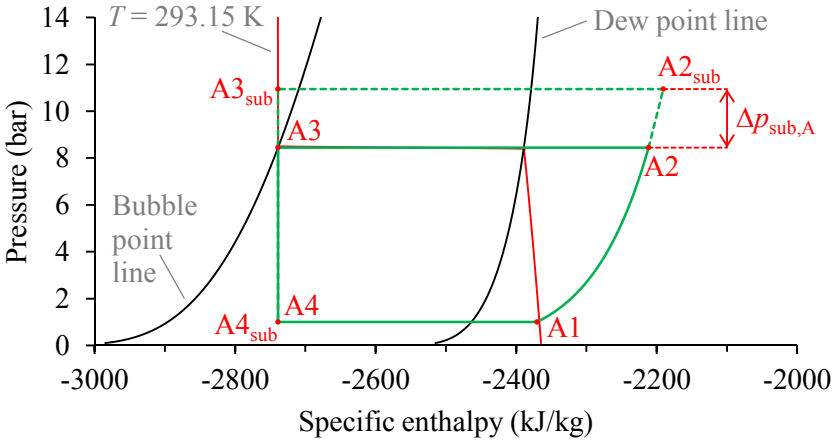

Figure 6.5. Pressure-enthalpy for propane refrigeration cycle with (solid line) and without (dotted lined) sub-cooling.

In Fig. 6.5, the effect of refrigerant sub-cooling is illustrated in a pressure-enthalpy diagram for propane. Here, the refrigeration cycle is plotted with a solid line for the case of no sub-cooling ($p_{A2} = p_{sat}(T_{A3})$) and with a dotted line for a case of sub-cooling ($p_{A2} = p_{sat}(T_{A3}) + 2.5$ bar). As can be observed, the isotherm indicated by the red line is close to vertical in the region of saturated liquid. Hence, even though the pressure is raised by 2.5 bar, only a very small change is observed for the specific enthalpy in the valve inlet. Since the increased high pressure level leads to a significant increase in specific compression power, the net effect will be increased power consumption. This indicates that refrigerant sub-cooling is not beneficial. Similar diagrams can be drawn for the ethene and methane cycles, with the same results.

6.4.3 Low pressure level – load distribution

The low pressure levels of the refrigerants A and B determine the evaporation temperatures of the same refrigerants and thereby the load distribution between the three refrigeration cycles. If the evaporation temperature of refrigerant A is increased, the cooling load and temperature difference between the composite curves in heat exchanger A will decrease. As a consequence, increased cooling load is observed in heat exchanger B. For the heat load that is transferred from HX-A to HX-B, the temperature difference will be significantly larger. The optimal evaporation temperatures in the different cycles are given by the optimal load distribution between the different refrigeration cycles.

A pressure-enthalpy diagram for refrigeration cycle A (propane) is given in Fig. 6.6 (a) for two different values of the low pressure level. In the cycle plotted with a solid line, the evaporation pressure is 1 bar. The dotted line represents a cycle where the evaporation pressure is 2 bar. Since the high pressure level is kept at the same level, the state at the inlet of the throttle valve is the same for the two cycles. The specific cooling capacity is slightly larger in the case of $p_{A1} = 1$ bar, since the refrigerant in both cycles is superheated to the same temperature. If only the latent heat was to be used for cooling, the specific cooling capacity would have been larger for the cycle with $p_{A1} = 2$ bar.

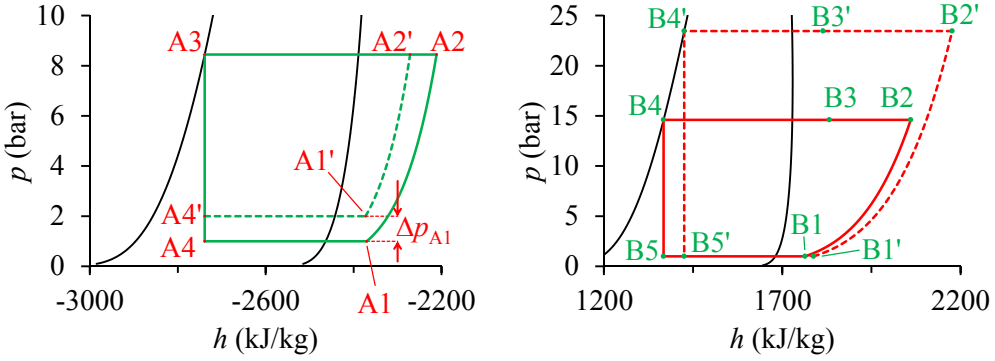

Figure 6.6. Pressure-enthalpy diagrams with different low pressure level in the propane cycle. (a) Propane cycle; (b) Ethene cycle.

As can be observed in Fig. 6.6 (a), a significant reduction in specific compression power is observed in the refrigeration cycle with $p_{A1} = 2$ bar. In total, the power consumption per unit of cooling is reduced when the evaporation pressure of the propane cycle is increased from 1 bar to 2 bar. As a consequence of higher evaporation pressure, and thereby higher evaporation temperature, the temperature range covered by refrigeration cycle A is reduced. Correspondingly, the temperature range covered by refrigeration cycle B will increase.

Refrigeration cycle B (with ethene as refrigerant) is illustrated in a temperature-enthalpy in Fig. 6.6 (b). The solid line represents the case where the evaporation pressure in the propane cycle is 1 bar, while the dotted line represents the case where $p_{A1} = 2$ bar. In both cases, the refrigerant enters the throttle valve as saturated liquid and maximum superheating is applied. Increased evaporation pressure in the propane cycle means that the high pressure level in the ethene cycle must be raised to enable condensation.

With increased high pressure level in the ethene cycle, the specific cooling load is reduced (more vapour is formed in the expansion process), while the specific compression power increases. Both effects contribute to increased compression power in the ethene refrigeration cycle. The optimal low pressure level in cycle A is characterized by optimal load distribution between the cycles A and B. An equivalent trade-off applies for the load distribution between the cycles B and C, which is determined by the evaporation pressure in refrigeration cycle B.

Simplified case study

In the following, optimal load distribution for the simplified model illustrated in Fig. 6.7 have been derived with respect to minimum irreversibilities associated with heat transfer. The objective is to find the values of T_A and T_B that give minimum irreversibilities. In this case, cooling was assumed provided in three stages with constant temperature (T_A, T_B and T_C). The cooling curve of the natural gas was estimated by a stream with constant heat capacity flow rate.

From Chapter 2, the irreversibilities associated with heat transfer can be expressed as

$$\dot{I} = \int_0^{\dot{Q}} \dot{m} \cdot c_p \cdot T_0 \cdot \frac{\Delta T}{T_H \cdot (T_H - \Delta T)} \mathrm{d}T_H , \tag{6.5}$$

where T_H is the temperature of the hot composite curve. Since the cold stream temperature in each heat exchanger is constant, the temperature difference between the composite curves is given as

$$\begin{aligned} \Delta T_A(T_H) &= T_H - T_A , \\ \Delta T_B(T_H) &= T_H - T_B , \\ \Delta T_C(T_H) &= T_H - T_C = T_H - (T_{out} - \Delta T_{min}) . \end{aligned} \tag{6.6}$$

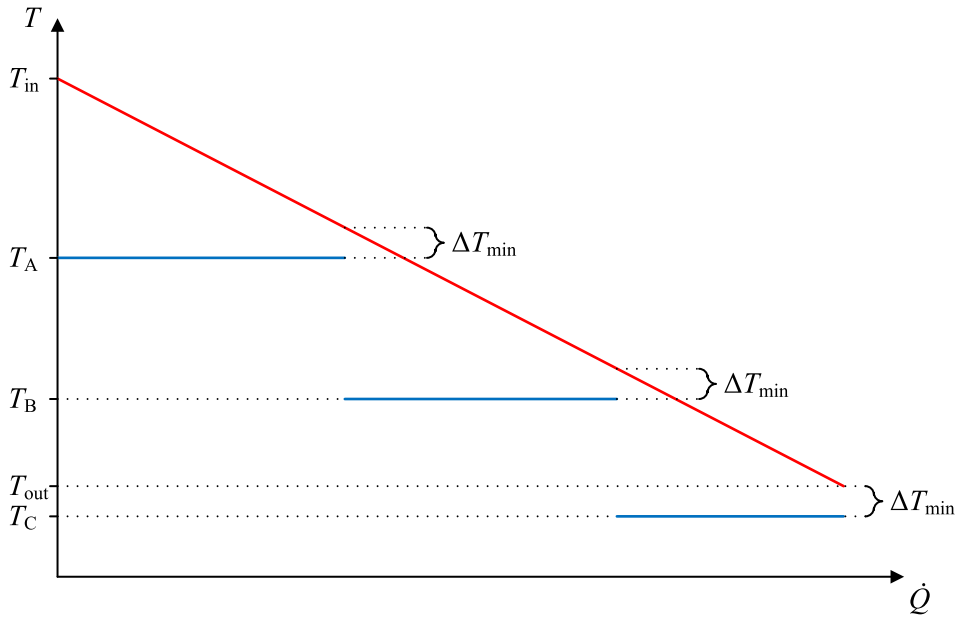

Figure 6.7. Composite curves for simplified cascade process.

From this, the irreversibilities in each of the three heat exchangers can be expressed as

$$\begin{aligned}
\dot{I}_{\mathrm{A}} &= T_0 \cdot \dot{m} \cdot c_p \cdot \int_{T_{\mathrm{out}}}^{T_{\mathrm{B}}+\Delta T_{\min}} \frac{T_{\mathrm{H}} - \left(T_{\mathrm{out}} - \Delta T_{\min}\right)}{\left(T_{\mathrm{out}} - \Delta T_{\min}\right) \cdot T_{\mathrm{H}}} \mathrm{d}T_{\mathrm{H}}, \\
\dot{I}_{\mathrm{B}} &= T_0 \cdot \dot{m} \cdot c_p \cdot \int_{T_{\mathrm{B}}+\Delta T_{\min}}^{T_{\mathrm{A}}+\Delta T_{\min}} \frac{T_{\mathrm{H}} - T_{\mathrm{B}}}{T_{\mathrm{B}} \cdot T_{\mathrm{H}}} \mathrm{d}T_{\mathrm{H}}, \\
\dot{I}_{\mathrm{C}} &= T_0 \cdot \dot{m} \cdot c_p \cdot \int_{T_{\mathrm{A}}+\Delta T_{\min}}^{T_{\mathrm{in}}} \frac{T_{\mathrm{H}} - T_{\mathrm{A}}}{T_{\mathrm{A}} \cdot T_{\mathrm{H}}} \mathrm{d}T_{\mathrm{H}}.
\end{aligned} \tag{6.7}$$

The total heat transfer irreversibilities can be found by summing the contributions from the three heat exchangers:

$$\begin{aligned}
\dot{I} &= \dot{I}_{\mathrm{A}} + \dot{I}_{\mathrm{B}} + \dot{I}_{\mathrm{C}} \\
&= T_0 \cdot \dot{m} \cdot c_p \cdot \left(\frac{T_{\mathrm{B}}}{T_{\mathrm{out}} - \Delta T_{\min}} + \frac{T_{\mathrm{A}}}{T_{\mathrm{B}}} + \frac{T_{\mathrm{in}} - \Delta T_{\min}}{T_{\mathrm{A}}} - \ln\left(\frac{T_{\mathrm{in}}}{T_{\mathrm{out}}}\right) - 3 \right).
\end{aligned} \tag{6.8}$$

The derivatives with respect to the stage temperatures T_A and T_B can further de expressed as

$$\begin{aligned}\frac{\partial \dot{I}}{\partial T_A} &= T_0 \cdot \dot{m} \cdot c_p \cdot \left(\frac{1}{T_B} - \frac{T_{in} - \Delta T_{cold}}{T_A^2} \right), \\ \frac{\partial \dot{I}}{\partial T_B} &= T_0 \cdot \dot{m} \cdot c_p \cdot \left(\frac{1}{T_{out} - \Delta T_{cold}} - \frac{T_A}{T_B^2} \right).\end{aligned} \tag{6.9}$$

From this, the optimal intermediate temperatures can be found by identifying the extrema ($\partial \dot{I}/\partial T_A = 0$ and $\partial \dot{I}/\partial T_B = 0$):

$$\begin{aligned}T_A^* &= \left(T_{in} - \Delta T_{min}\right)^{2/3} \cdot \left(T_{out} - \Delta T_{min}\right)^{1/3}, \\ T_B^* &= \left(T_{in} - \Delta T_{min}\right)^{1/3} \cdot \left(T_{out} - \Delta T_{min}\right)^{2/3}.\end{aligned} \tag{6.10}$$

One may notice that the optimal temperature levels are given by the geometric mean of the inlet and outlet temperatures for the natural gas stream (shifted by the ΔT_{min} value), which is a result similar to optimal intermediate pressure levels in multi-stage compression of a perfect gas with uniform suction temperatures (see Chapter 5). Similar results were obtained by Jeong and Smith (1994), who found that the temperature ratio (condensation temperature divided by evaporation temperature) should be the same for all stages in a complete cascade refrigeration system transferring heat from a constant temperature source to a constant temperature sink, in order to minimize entropy generation.

The suggested optimal intermediate temperature levels do not take into account all relevant aspects of the overall process. First, the derivation only considers minimization of heat transfer irreversibilities, not the overall irreversibilities. Minimum heat transfer irreversibilities do not necessarily coincide with minimum total irreversibilities. Second, the actual cooling curve of the natural gas stream is not represented by a constant heat capacity. In addition, refrigerant precooling and condensation are also important components in the hot composite curve. Optimal load distribution may also be affected by the characteristics of the different refrigerants. Finally, in the case of refrigerant superheating, the temperature of the cold stream will not be equal to the evaporation temperature throughout the heat exchangers.

However, the results may still give valuable insight in the characteristics of optimal load distribution. With $T_{in} = 293.15$ K and $T_{out} = 115$ K, $T_A^* \approx 212.4$ K and $T_B^* \approx 154.9$ K. Considering the actual temperature-enthalpy relation of the natural gas stream (but no other of the aspects mentioned), sensitivity analysis indicate that minimum irreversibilities are obtained for smaller values of the stage temperatures

($T_A^* \approx 196$ K and $T_B^* \approx 153$ K). In order to obtain the suggested evaporation temperatures in the propane and ethene cycles, the low pressure levels would have to be smaller than 1 bar.

Choice of refrigerants

In refrigeration cycle B, two refrigerant options have been considered. Ethene and ethane have similar properties with respect to operating range. As can be observed from Fig. 6.2, ethene has a lower saturation temperature than ethane at the minimum pressure (1 bar). At the same temperature level, the heat of vaporization is higher for ethane than for ethene, as illustrated in Fig. 6.3.

The process performance is compared for the two refrigerant alternatives in Table 6.3. In this case, the remaining decision variables were kept at the same level. That is, no refrigerant sub-cooling, maximum superheating in all refrigeration cycles, cold end temperature difference equal to the minimum required and 1 bar evaporation pressure in the propane cycle. Both refrigerant alternatives were compared with the evaporation pressure equal to 1 bar. The ethene refrigerant alternative was also tested with an evaporation pressure resulting in the same evaporation temperature as the ethane refrigerant.

As can be observed from Table 6.3, the smallest total power consumption is observed with ethene as refrigerant in cycle B. With ethane as refrigerant, the evaporation temperature is more than 15 K higher, resulting in about 13 % increase in power consumption. Since a smaller temperature range is covered by refrigeration cycle B with ethane as refrigerant, both the refrigerant flow rate and the pressure ratio is smaller than in the case of ethene as refrigerant. This also results in smaller compressor power in refrigeration cycle B. The compressor power in refrigeration cycle C, however, is significantly higher since the temperature range covered is considerably wider. The compression power in refrigeration cycle A is slightly higher with ethane as refrigerant in cycle B, indicating that the precooling load is higher.

When the evaporation pressure with ethene as refrigerant is set to a level providing the same evaporation temperature as the ethane refrigerant, the total power consumption is smaller with ethane as refrigerant. Since the temperature range covered by the methane refrigerant is the same, the compression power in cycle C is, of course, the same. Due to the larger specific cooling capacity (related to higher heat of vaporization as illustrated in Fig. 6.3), the refrigerant flow rate is smaller with ethane as refrigerant. The pressure ratio is, however, larger than with ethene as refrigerant.

The results indicate that as long as the two refrigerants cover the same temperature range, ethane provides better performance than ethene. In this case, the characteristics

of ethane enable a higher ratio of specific cooling capacity to specific compression power. Ethene can, however, cover a wider temperature range than ethane under the given conditions. Due to better load distribution, it seems that ethene is a better refrigerant alternative for cycle B under the given operating conditions.

Table 6.3. Simple cascade process with different refrigerants in cycle B.

Property	Unit	Ethene 1	Ethene 2	Ethane
Evaporation pressure, p_{B1}	bar	1.0	2.3	1.0
Evaporation temperature, T_{B5}	K	169.2	184.6	184.6
Pressure ratio, p_{B2}/p_{B1}	-	14.6	6.4	7.8
Refrigerant flow rate, $\dot{m}_R$	kg/s	1.684	1.645	1.487
Power consumption:				
Cycle A	kW	443.2	463.8	469.6
Cycle B	kW	499.2	305.7	285.3
Cycle C	kW	263.5	610.3	610.3
Total	kW	1 205.9	1 379.8	1 365.2

Since the ethane evaporation temperature at 1 bar is significantly higher than for ethene at the same pressure level and higher than the optimal value suggested by Eq. (6.10), it may be that the optimal evaporation pressure in the propane cycle is higher when ethane is used as refrigerant in refrigeration cycle B. This is because the geometric mean of the natural gas inlet temperature and the evaporation temperature in cycle B will be shifted to a higher value.

One may conclude that ethene is a better refrigerant alternative for the simple cascade process given in Fig. 6.1 due to the fact that a smaller evaporation temperature enables better load distribution between the refrigeration cycles. This does, however, only hold for the operating conditions studied in this work. If the natural gas inlet and/or outlet temperature is increased, the optimal intermediate temperature levels will also increase. At some point, the optimal intermediate temperature levels are likely to reach a level at which ethane provides better performance than ethene as refrigerant in cycle B.

6.4.4 Refrigerant flow rate – refrigerant superheating

The refrigerant flow rate decides the state of the refrigerant exiting the hot end of the heat exchanger. A maximum refrigerant flow rate is given by the fact that the refrigerant should be fully evaporated and superheated equivalent to the minimum superheating requirement (as will be discussed later, refrigerant superheating in the form discussed here, may not be directly applicable in industrial applications). With the minimum feasible flow rate, the hot end temperature difference will be equal to the minimum required (ΔT_{min}).

One may notice that both the lower and upper bounds on the refrigerant flow rates can be related to the temperature of the refrigerant temperature in the hot end of the heat exchangers. Hence, in alternative 2 (see Table 6.2), the refrigerant flow rates have been defined indirectly through the hot end temperatures:

$$\begin{aligned} T_{\mathrm{A1}} &= \left(T_{\mathrm{A4}} + \Delta T_{\min}\right) + z_{\mathrm{sup,A}} \cdot \left(\left(T_{\mathrm{G1}} - \Delta T_{\min}\right) - \left(T_{\mathrm{A4}} + \Delta T_{\min}\right)\right), \\ T_{\mathrm{B1}} &= \left(T_{\mathrm{B5}} + \Delta T_{\min}\right) + z_{\mathrm{sup,A}} \cdot \left(\left(T_{\mathrm{G2}} - \Delta T_{\min}\right) - \left(T_{\mathrm{B5}} + \Delta T_{\min}\right)\right), \\ T_{\mathrm{C1}} &= \left(T_{\mathrm{C6}} + \Delta T_{\min}\right) + z_{\mathrm{sup,A}} \cdot \left(\left(T_{\mathrm{G3}} - \Delta T_{\min}\right) - \left(T_{\mathrm{C6}} + \Delta T_{\min}\right)\right). \end{aligned} \tag{6.11}$$

The temperature of the refrigerant streams entering the compressors are given by the variables z_{sup}, which are bounded within zero and unity. A value of zero is equivalent to a compressor suction temperature exactly fulfilling the minimum superheating constraint, while a value of unity means that the temperature difference in the hot end of the heat exchanger is equal to the minimum required.

Combined with the variables specified for the temperature difference in the cold end of the heat exchangers, the variables proposed for indirect determination of the refrigerant flow rates ensure that both the minimum temperature difference constraint and the minimum superheating constraint are fulfilled for all combinations (with the given shape of the natural gas cooling curve). The variables actually cover the complete feasible region. That is, one of the constraints would be violated if the refrigerant flow rate is either smaller or larger than what is given by the bounds for the superheating variables.

The same argument does not hold if refrigerant flow rates are used as variables (alternative 1 in Table 6.2). When the value of other decision variables are changed, the smallest and largest flow rate providing a feasible design will also change. Hence, if refrigerant flow rates are used as variables, the search space would either need to include parts of the infeasible region or exclude parts of the feasible region.

Influence of refrigerant superheating

The effect of refrigerant superheating is illustrated in the process diagrams for the propane cycle in Fig. 6.8. A cycle with maximum superheating (minimum flow rate) is given by the solid line, while minimum superheating (maximum flow rate) is given by a dotted line. Equivalent diagrams can be drawn for the other refrigeration cycles.

As can be observed from the pressure-enthalpy diagram in Fig. 6.8 (a), increased refrigerant superheating leads to both increased specific cooling capacity and increased specific compression power. The latter is related to increased compressor suction temperature, which can be observed in the temperature-entropy diagram in Fig. 6.8 (b).

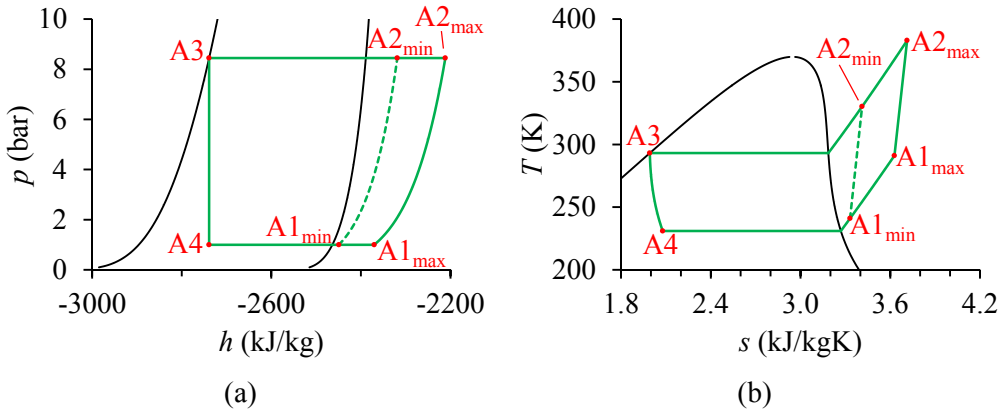

Figure 6.8. Process diagrams for the propane stage in the simple cascade process: a) Pressure-enthalpy diagram; b) Temperature-entropy diagram.

Increased specific cooling capacity and increased specific compression power have opposite effects on the compression power. While the compression power required per unit flow increases, the refrigerant flow needed to provide the same cooling load rate is reduced. The net effect on the power consumption will therefore depend on the refrigerant properties and the process characteristics.

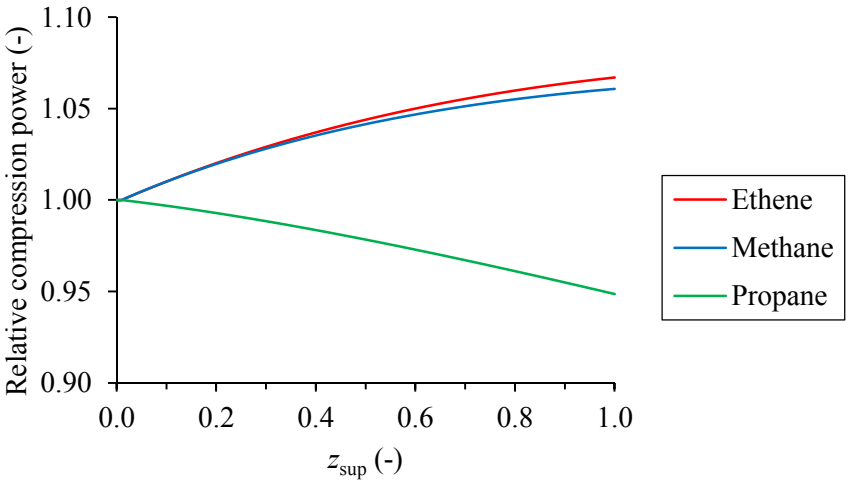

Figure 6.9. Compression power per unit of cooling as function of the degree of superheating for each of the three refrigerant used in the cascade process.

In Fig. 6.9, the power consumption in the individual refrigeration cycles are plotted as function of the degree of superheating in the same cycle. The compression power is plotted relative to the power consumption with minimum superheating. The effect has been studied for one refrigerant at the time. That is, all variables other than the degree of superheating in a given cycle has been kept constant. For methane and ethene, the

compression power is observed to increase with increasing degree of superheating. The compression power in the propane cycle is found to decrease with increasing superheating.

Based on the results presented in Fig. 6.9, one may assume that the process power consumption is minimized when the methane and ethene refrigeration cycles are operated with minimum superheating and the propane cycle is operated with maximum superheating. One must, however, also consider the interaction between the three refrigeration cycles.

6.4.5 Exergy analysis

In order to study the interaction between the refrigeration cycles, exergy analyses have been performed for the simple cascade process with minimum and maximum superheating applied in all refrigeration cycles. Irreversibility rates for the different unit operations and power consumption in the different refrigeration cycles are given in Table 6.4. Notice, however, that all irreversibilities in HX-A and HX-B have been assigned to cycle A and cycle B, respectively. The results in Table 6.4 have been obtained with no refrigerant sub-cooling, cold end temperature differences equal to the minimum required and low pressure levels at the lower bound (1 bar).

Table 6.4. Irreversibility distribution in simple cascade process with minimum and maximum superheating.

	Minimum superheating				Maximum superheating			
Property	A	B	C	Total	A	B	C	Total
Irreversibilities (kW):								
Compressor	108	93	51	251	68	72	40	180
Cooler	52	21	1	74	89	71	22	182
Heat exchanger	81	147	104	332	30	104	76	210
Valve	115	116	103	334	69	85	77	231
Total	356	377	258	991	256	331	215	802
Compression power (kW)	606	536	253	1394	443	499	263	1 206

As can be observed, the total irreversibilities (and therefore also the total power consumption) is smallest for the process with maximum superheating in all cycles. The compression power in cycle C is, however, smaller in the cycle with minimum superheating. This is in accordance with the results presented in Fig. 6.9. When the degree of superheating is increased in cycle C, the compression power grows. Also in conformity with Fig. 6.9, the power consumption in cycle A is reduced when the degree of superheating is increased.

Since the power consumption in cycle B is smallest with maximum superheating, one may conclude that this is in conflict with the results presented in Fig. 6.9, where the compression power in the ethene cycle is found to increase with increasing degree of superheating. However, the fact that the power consumption in cycle B is smaller in the process with maximum superheating in all cycles is related to the superheating of refrigerant C, not the superheating of refrigerant B. With the same configurations for refrigerant cycle C, the compression power in cycle B would have been smaller with minimum superheating.

As can be observed in Table 6.4, the irreversibilities in cycle C is smallest with maximum superheating even though the compression power is higher. This is because the compression power does not represent all the exergy supplied to refrigerant B. In order to precool and condense refrigerant C at sub-ambient temperature, exergy must be supplied in HX-A and HX-B (see Fig. 6.1).

In a cascade process, heat is transferred from vertical stages operating at low temperature levels to the ambient, not only directly but also indirectly via vertical stages operating at higher temperature levels. This heat load varies with the operating conditions. Due to this interaction between the different refrigeration cycles in the cascade, the solution that gives the smallest power consumption in individual cycles may not coincide with the solution providing the smallest total power consumption.

The influence of interaction between the vertical stages in a cascade can be explained using refrigeration cycle C as example. With reference to Fig. 6.4, an energy balance for a single refrigeration cycle can be expressed as

$$\dot{Q}_{\text{cond}} = \dot{Q}_{\text{cool}} + \dot{W}_{\text{comp}}, \tag{6.12}$$

where $\dot{Q}_{\text{cond}}$ is the heat rejected (de-superheating and condensation), $\dot{Q}_{\text{cool}}$ is the heat absorbed (evaporation and superheating) and $\dot{W}_{\text{comp}}$ the supplied compression power. For a given load distribution between the refrigeration cycles, the heat absorbed in refrigeration cycle C is the same irrespective of the degree of superheating. Hence, increased power consumption with increased refrigerant superheating means that the heat to be rejected increases correspondingly. One must, however, also consider the temperature at which this heat is rejected.

With increased superheating in refrigeration cycle C, the compressor suction temperature increases. As a consequence, also the compressor discharge temperature will be higher, which means that more heat can be rejected directly to the ambient in COOL-C. Irrespective of the degree of superheating, the refrigerant is compressed to the same pressure prior to de-superheating and condensation. Hence, due to the

reduced refrigerant flow rate with increased superheating, less heat must be removed from refrigerant C in HX-A and HX-B (as long as the compressor discharge temperature exceeds the ambient cooling temperature in both cases).

With reduced cooling load in HX-A and HX-B, the power consumption in cycle A and cycle B will be reduced when the degree of superheating in refrigeration cycle C is increased. In Fig. 6.10, composite curves are plotted for the simple cascade with minimum (Fig. 6.10 (a)) and maximum (Fig. 6.10 (b)) superheating. As can be observed, the total cooling load is significantly smaller for the case of maximum superheating. Since the temperature driving forces also are smaller, the irreversibilities in the heat exchanger will be smaller. This is confirmed by the results in Table 6.4.

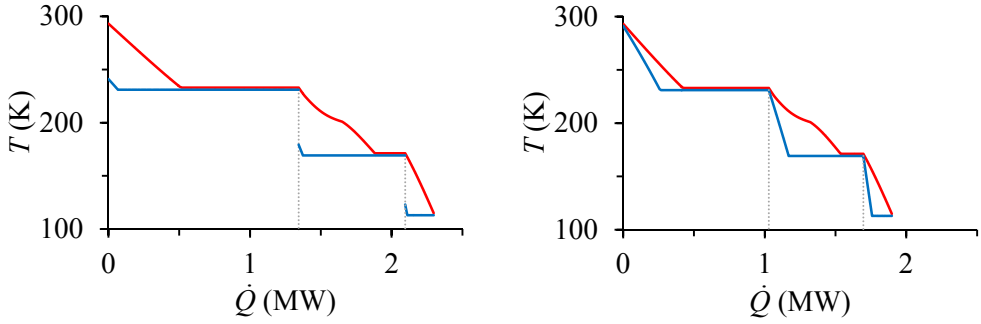

Figure 6.10. Composite curves for simple cascade process. (a) With minimum superheating; (b) With maximum superheating.

The influence of interaction between the different refrigeration cycles can also be explained from the perspective of exergy. Even though the amount of heat to be removed from refrigerant C (de-superheating and condensation) increases when the degree of superheating is increased, the exergy associated with this heat is reduced. Increased refrigerant superheating gives larger irreversibilities in the cooler but reduced exergy load in the precooling heat exchangers.

Similar arguments can be made for effects of superheating in refrigeration cycle B. In refrigeration cycle A, however, all heat is rejected directly to the ambient and refrigerant flow rate in this cycle does not influence any other vertical stages. These results illustrate the importance of also considering the interaction between the different refrigeration cycles in a cascade process.

6.4.6 Optimization

The simple cascade process was optimized with the two different choices of decision variables described in Section 6.3.1. In order to study the performance of the optimization search, this was done for different sets of decision variables, with the

remaining variables set to what was found to provide the best solution. Variables bounds for the different formulations are given in Table 6.5. The narrow variable bounds are set based on the best known solution to the optimization problem.

One may notice that the variables in alternative 2 are defined such that the constraints are fulfilled for any combinations within the variables bounds. They do, however, still cover all interesting parts of the feasible search space. In the leftmost column of Table 6.5, the different decision variables have been assigned to different groups. These groups define different sets of decision variables that have been used for optimization.

Table 6.5. Decision variables with bounds for optimization of simple cascade process.

	Alternative 1					Alternative 2		
		Wide		Narrow				
Groups	Var.	LB	UB	LB	UB	Var.	LB	UB
I, II, III, IV	p_{A1}	1.0	2.0	1.0	1.5	p_{A1}	1.0	2.0
I, II, III, IV	p_{B1}	1.0	2.0	1.0	1.5	p_{B1}	1.0	2.0
I, III	p_{C1}	1.0	1.2	1.0	1.13	$\Delta T_{cold,C}$	2.0	5.0
I, III	T_{G2}	220	260	232	235	$\Delta T_{cold,A}$	2.0	5.0
I, III	T_{G3}	160	190	171	175	$\Delta T_{cold,B}$	2.0	5.0
I, II	p_{A2}	8.4	10.5	8.4	9.4	$\Delta p_{sub,A}$	0.0	2.0
I, II	p_{B2}	14.5	25.5	14.5	15.5	$\Delta p_{sub,B}$	0.0	2.0
I, II	p_{C2}	24.8	39.9	24.8	25.8	$\Delta p_{sub,C}$	0.0	2.0
I, II, III, IV	$\dot{m}_A$	2.0	6.0	2.6	3.0	$z_{sup,A}$	0.0	1.0
I, II, III, IV	$\dot{m}_B$	1.0	4.0	1.6	2.0	$z_{sup,B}$	0.0	1.0
I, II, III, IV	$\dot{m}_C$	0.5	2.0	0.5	0.6	$z_{sup,C}$	0.0	1.0

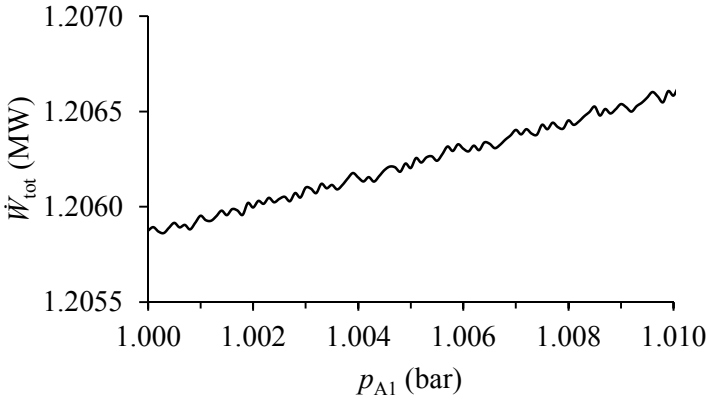

Figure 6.11. Total power consumption as function of propane low pressure level.

With the original step length used for estimation of derivatives in the sequential quadratic programming approach (10^{-4}), noise was observed for the objective and constraint functions as illustrated for the total power consumption as function of the propane low pressure level in Fig. 6.11. The optimization search was therefore carried out with a longer step length (10^{-2}) for the derivative estimates.

The best known solution to the optimization problem is given in Table 6.6, confirming the findings in the thermodynamics analysis. As expected, the best solution is characterized by no refrigerant sub-cooling ($\Delta p_{sub} = 0$ bar), cold end temperature differences equal to the minimum required ($\Delta T_{cold} = 2$ K) and low pressure levels at the lower bound ($p_{A1} = p_{B1} = 1$ bar). The results also indicate that the power consumption is minimized for maximum refrigerant superheating ($z_{sup} = 1.0$), which confirms that the solutions that gives minimum power consumption in a single cycle not necessarily coincides with the overall best solution. The best known solution is equivalent to a total power consumption of 1205.9 kW.

Table 6.6. Best known solution for simple cascade process.

Alternative 1			Alternative 2		
Variable	Unit	Value	Variable	Unit	Value
p_{A1}	bar	1.000	p_{A1}	bar	1.000
p_{B1}	bar	1.000	p_{B1}	bar	1.000
p_{C1}	bar	1.121	$\Delta T_{cold,C}$	K	2.0
T_{G2}	K	233.0	$\Delta T_{cold,A}$	K	2.0
T_{G3}	K	171.2	$\Delta T_{cold,B}$	K	2.0
p_{A2}	bar	8.44	$\Delta p_{sub,A}$	bar	0.0
p_{B2}	bar	14.60	$\Delta p_{sub,B}$	bar	0.0
p_{C2}	bar	24.9	$\Delta p_{sub,C}$	bar	0.0
$\dot{m}_A$	kg/s	2.791	$z_{sup,A}$	-	1.0
$\dot{m}_B$	kg/s	1.684	$z_{sup,B}$	-	1.0
$\dot{m}_C$	kg/s	0.524	$z_{sup,C}$	-	1.0

A measure for performance of the optimization algorithm is given in Fig. 6.12. Here, 50 optimization runs from randomly generated starting points have been performed for different problem formulations and different selections of decision variables (variable groups). As given in Table 6.5, group I includes all 11 degrees of freedom. In group II, the process flowsheet is defined such that the temperature differences in the cold end of the heat exchangers are equal to the minimum required. Further, in group III, the variables describing the high pressure levels are removed from the set of decision variables. Variable group IV includes only the variables describing the refrigerant flow rates and the low pressure levels in cycles A and B.

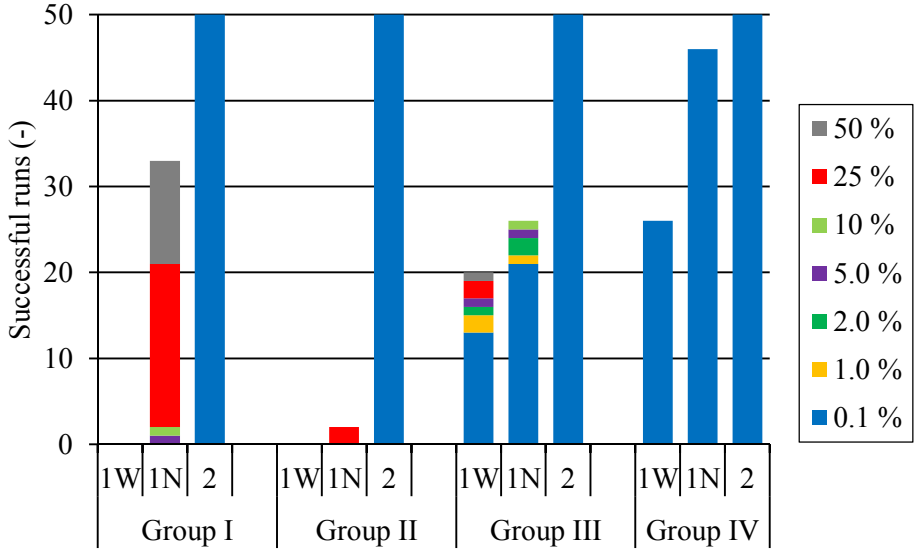

Figure 6.12. Performance of optimization search for different problem formulations measured as the deviation from the best known solution in each run.

With the choice of decision variables used in alternative 2, the best solution obtained in each run was within 0.1 % of the best known solution for all runs, also when all the degrees of freedom are used. With wide variable bounds, none of the 50 runs ended up within 50 % of the best solutions for variable alternative 1. Better performance was achieved with narrow variable bounds, as a solution with power consumption deviating 50 % or less from the best known solution was obtained in 33 runs when all degrees of freedom are used.

With the high pressure level set to the saturation pressure equivalent to the given precooling temperature, 13 and 21 runs ended up within 0.1 % of the best known objective value with wide and narrow variable bounds, respectively. With all variables but refrigerant flow rates and the low pressure levels in cycles A and B set to the best known value ($\Delta p_{sub} = 0$ bar and $\Delta T_{cold} = 2$ K), all runs leading to a feasible solution were able to get within 0.1 % of the best known solution. This applies to 26 of the runs with wide variable bounds and 46 runs with narrow bounds.

Choice of refrigerants

In Table 6.7, optimization results are given with ethene and ethane as refrigerants in cycle B. As can be observed, the power consumption is reduced if pressure levels below 1 bar are accepted. The evaporation temperatures in the two refrigeration cycles do to some extent approach the estimated optimal values discussed in Section 6.4.3.

Table 6.7. Optimization results with different refrigerant in cycle B and different lower bound on pressure level.

		Ethene		Ethane	
Property	Unit	$p_{B1} \geq 1$ bar	$p_{B1} \geq 0.1$ bar	$p_{B1} \geq 1$ bar	$p_{B1} \geq 0.1$ bar
p_{A1}	bar	1.00	0.19	1.25	0.65
p_{B1}	bar	1.00	0.33	1.00	0.29
T_{A4}	K	231.0	199.2	236.2	221.7
T_{B5}	K	169.2	152.7	184.6	164.5
$\dot{W}_A$	kW	443.2	844.0	410.2	559.0
$\dot{W}_B$	kW	499.2	230.5	340.2	405.1
$\dot{W}_C$	kW	263.5	103.4	610.1	205.4
$\dot{W}_{tot}$	kW	1 205.9	1 177.9	1 360.5	1 169.6

When the low pressure limit is reduced, the optimized evaporation temperatures (T_{A4} and T_{B5}) are actually quite close to values estimated to give the smallest heat transfer irreversibilities for the simplified process model (196 K and 153 K) when ethene is used as refrigerant in cycle B. Since many factors of considerable influence are not covered by the simplified model, this is, however, likely to be somewhat incidental. The fact that the optimized evaporation temperatures are significantly different with ethene and ethane as refrigerant in cycle B indicates that the choice of refrigerant has a considerable influence on the optimal load distribution.

As discussed in Section 6.4.3, the optimal evaporation pressure in the propane cycle (p_{A1}) will be larger with ethane as refrigerant in refrigeration cycle B, since the evaporation temperature of ethane at 1 bar is relatively high. This gives a better load distribution between the propane and ethane cycles. The results in Table 6.7 also indicate that the total power consumption is smallest with ethane as refrigerant in cycle B when no restrictions apply to the low pressure levels.

6.5 Complex cascade

The pressure ratios observed for the different refrigeration cycles in the optimized simple cascade indicate that multi-stage compression would be required (especially for refrigeration cycles B and C). Multi-stage compression with intercooling would also render possible savings in energy use by reduction of irreversibilities in the compression and heat transfer processes.

Even larger savings could be obtained by also dividing the vertical stages into horizontal stages. By dividing the refrigeration cycles into stages, irreversibilities related to heat transfer, compression and expansion can be reduced. Here, a complex cascade process with three horizontal stages in each vertical stage has been studied.

With three horizontal stages, three evaporation temperatures are used. The vapour formed in each expansion stage is separated from the liquid before expanding to the next pressure level. This could be returned directly to the compressor. Here, coolers are installed after each compression stage in the flowsheet, but these are only used if the compressor discharge temperatures exceed the ambient cooling temperature. The horizontal stages are constructed as illustrated for one of the vertical stages in Fig. 6.13. Potential precooling of other refrigerants is indicated by the dotted lines through the three heat exchangers.

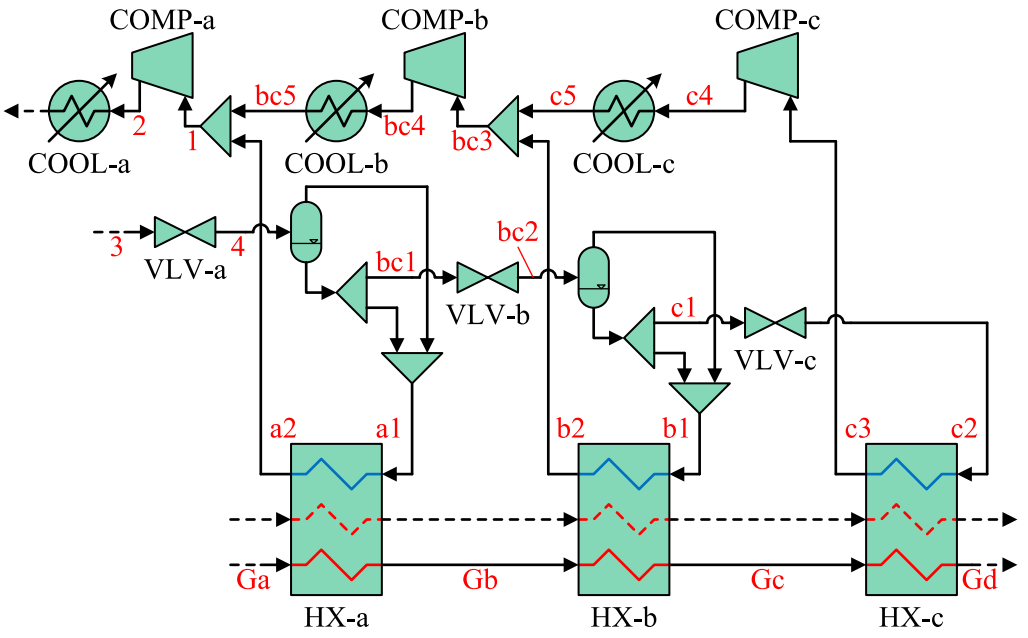

Figure 6.13. Flowsheet of vertical stage with three horizontal stages in pure-refrigerant cascade process.

Due to the introduction of splitters and mixers, the modelling of the complex cascade process is slightly more involved than for the simple cascade. With the proposed problem formulation (hot end refrigerant temperatures specified rather than flow rates), refrigerant flow rates can be calculated from energy balances for the horizontal stages.

In Fig. 6.14, the propane refrigeration cycle of the complex cascade is illustrated in a temperature-entropy diagram for the case with minimum superheating in all heat exchangers. The diagram has been divided into two parts with different scaling along the abscissa axis in order to better visualize the streams close to the dew point line. Streams located close to the bubble point line are given in Fig. 6.14 (a), while streams located close to the dew point line are depicted in Fig. 6.14 (b). Since splitters, mixers and phase separators are not illustrated in this diagram, the process lines are broken.

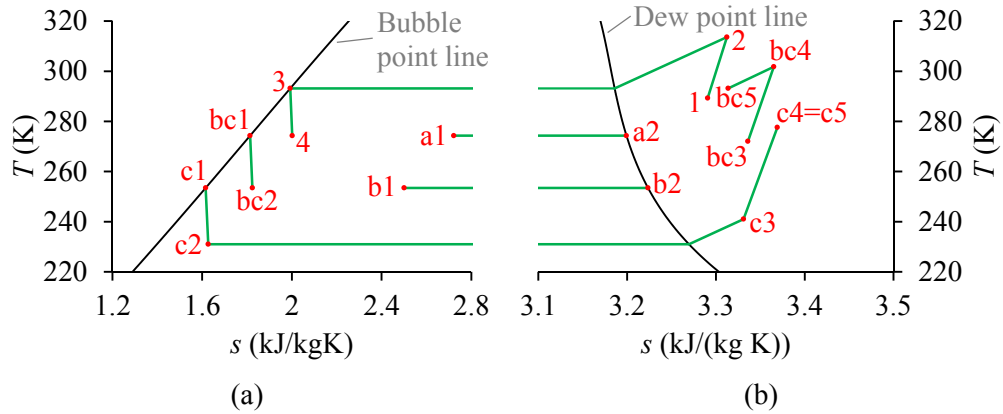

Figure 6.14. Temperature-entropy diagram for propane cycle in complex cascade process with minimum superheating.

As can be observed from Fig. 6.14 (b), the compressor discharge temperature from the first compression stage (COMP-c) does not exceed the ambient cooling temperature. Hence, there is no cooling in COOL-c ($T_{Ac5} = T_{Ac4}$). Before entering the second compression stage (COMP-b) this stream (c4) is mixed with the cold refrigerant stream exiting the hot end of HX-b (b2), which has the same pressure but a different temperature.

Since the cold refrigerant streams exiting the hot end of the heat exchangers in the intermediate stages (b2 from HX-b and a2 from HX-a) are mixed with the compressor discharge streams from preceding cycles (c5 and bc5, respectively) before entering the compressors at the intermediate stages (COMP-b and COMP-a), superheating is not required to fulfil the superheating constraints. Hence, the streams a2 and b2 are located at the dew point line in Fig. 6.14 (b).

Since part of the liquid is separated from the remaining refrigerant stream and sent to the preceding horizontal stage after the valves in the intermediate stages (VLV-a and VLV-b), the refrigerant streams entering the cold end of the heat exchangers in the same stages (HX-a and HX-b) have a higher vapour fraction than the streams exiting the valves. Hence, the specific cooling capacity in these stages is reduced. This is, however, compensated by increased cooling capacity in the last horizontal stage (HX-c). In addition, the specific compression power in the intermediate stages is smaller since the pressure ratio for the compression is reduced.

The methane refrigeration cycle is illustrated in pressure-enthalpy diagrams in Fig. 6.15 and temperature-entropy diagrams in Fig. 6.16 for the cases of minimum and maximum superheating. As for the simple cascade, both the specific cooling capacity and the specific compression power is larger for the case with maximum superheating. The differences are, however, smaller since the superheating potential is reduced

(smaller temperature range for each horizontal stage than for the vertical stages in the simple cascade).

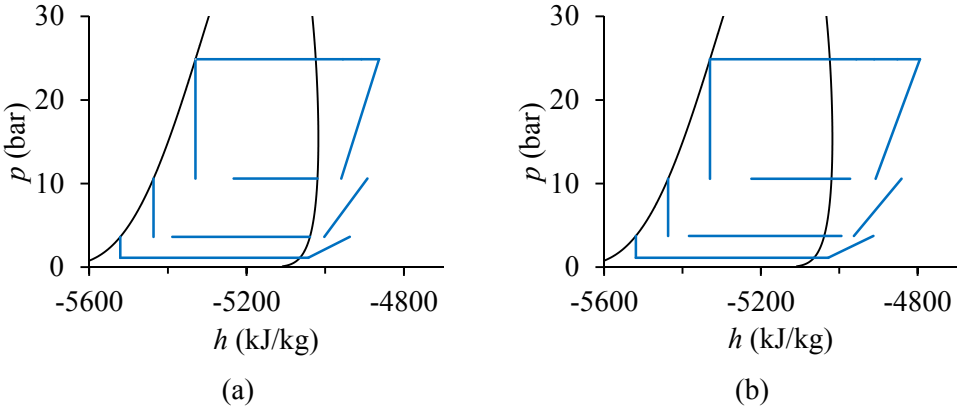

Figure 6.15. Pressure-enthalpy diagram for methane cycle in complex cascade process. (a) With minimum superheating; (b) With maximum superheating.

As can be observed from Fig. 6.16, the discharge temperature is smaller than the ambient cooling temperature for all the compression stages in refrigeration cycle C (methane) both with minimum and maximum superheating. Hence, the coolers are not used and all heat is rejected to ambient through the refrigeration cycles A and B. In conformity with the simple cascade, the compressor suction and discharge temperatures are higher for the alternative with maximum superheating.

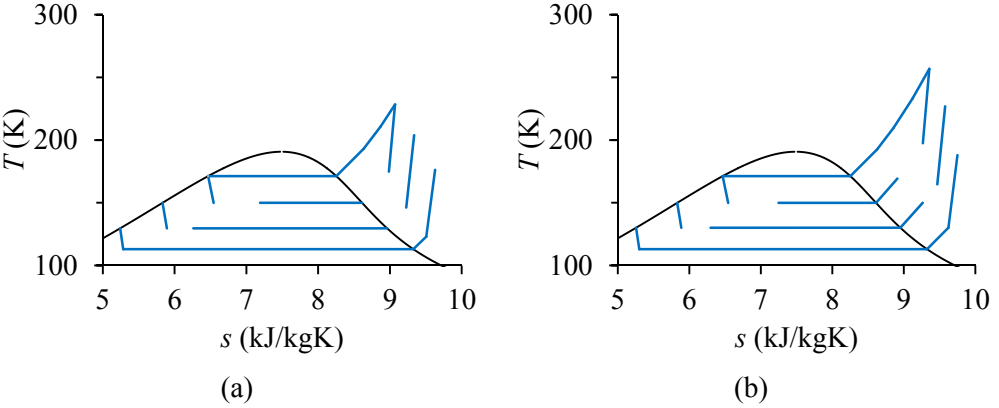

Figure 6.16. Temperature-entropy diagram for methane cycle in complex cascade process. (a) With minimum superheating; (b) With maximum superheating.

6.5.1 Optimization

By introducing horizontal stages in the cascade process, the number of degrees of freedom is increased. For each additional horizontal stage, an intermediate pressure level, an intermediate natural gas temperature and a refrigerant flow rate must be

determined. In the cascade process with three vertical stages with three horizontal stages each, there are in total 29 degrees of freedom.

The decision variables used for optimization are given in Table 6.8, together with the variable bounds used and the best solution found. As for the case of the simple cascade, the temperature levels in between the vertical stages ($T_{Gd,A}$ and $T_{Gd,B}$) were defined as function of refrigerant low pressure levels and cold end temperature differences. Refrigerant flow rates were defined indirectly through the degree of superheating, while the high pressure levels where defined relative to the minimum condensation pressure.

In order to be able to fulfil the superheating constraint, the temperature range covered by each horizontal stage must be larger than the minimum superheating. In order to guarantee that this was fulfilled for all combinations of the decision variables, the intermediate temperature levels for the natural gas stream were defined instead of the intermediate pressure levels. For the simplified case where the temperature difference in the cold end of all heat exchangers is equal to the minimum required, the intermediate temperature levels can be expressed as

$$\begin{aligned} T_{Gc} &= \left(T_{Gd} + \Delta T_{dew,min}\right) + T'_{Gc} \cdot \left(T_{Ga} - T_{Gd} - 3 \cdot \Delta T_{dew,min}\right), \\ T_{Gb} &= \left(T_{Gc} + \Delta T_{dew,min}\right) + T'_{Gb} \cdot \left(T_{Ga} - T_{Gc} - 2 \cdot \Delta T_{dew,min}\right). \end{aligned} \tag{6.13}$$

In Eq. (6.13), $\Delta T_{dew,min}$ is the minimum superheating required and T'_{Gc} and T'_{Gb} are variables bounded between zero and unity. The remaining temperature levels (T_{Ga} and T_{Gd}) are defined by other variables or the natural gas properties.

As for the simple cascade process, the best solution was obtained with the cold end temperature in the nine heat exchangers equal to the minimum required, maximum superheating in all heat exchangers, no sub-cooling in of the refrigerants prior to expansion and low pressure levels at the lower bound.

For 100 runs from randomly generated starting points, all searches ended up within 1 % of the best known solution, even with all 29 degrees of freedom used. When the refrigerant flow rates in the different horizontal stages were used as decision variables instead of the degree of superheating, none of 50 runs were able to identify a feasible solution even though the sub-cooling and cold end temperature difference variables were set to the values found to provide the best design.

In Table 6.9, the temperature and pressure ratios of the different horizontal stages are listed for the best known solution. For temperature, these are given as the ratios of the refrigerant evaporation temperatures in the different horizontal stages. The pressure

relations are given as the ratios of the evaporation pressure of the different cycles (ratio between condensation pressure and evaporation pressure for cycle a).

Table 6.8. Decision variables with bounds and best solution for optimization of complex cascade process.

Variable	LB	UB	Best
p_{A1}	1.0	2.0	1.0
p_{B1}	1.0	2.0	1.0
$T'_{Gb,A}$	0.0	1.0	0.638
$T'_{Gc,A}$	0.0	1.0	0.595
$T'_{Gb,B}$	0.0	1.0	0.167
$T'_{Gc,B}$	0.0	1.0	0.168
$T'_{Gb,C}$	0.0	1.0	0.487
$T'_{Gc,C}$	0.0	1.0	0.232
$\Delta T_{cold,Aa}$	2.0	5.0	2.0
$\Delta T_{cold,Ab}$	2.0	5.0	2.0
$\Delta T_{cold,Ac}$	2.0	5.0	2.0
$\Delta T_{cold,Ba}$	2.0	5.0	2.0
$\Delta T_{cold,Bb}$	2.0	5.0	2.0
$\Delta T_{cold,Bc}$	2.0	5.0	2.0
$\Delta T_{cold,Ca}$	2.0	5.0	2.0
$\Delta T_{cold,Cb}$	2.0	5.0	2.0
$\Delta T_{cold,Cc}$	2.0	5.0	2.0
$\Delta p_{sub,A}$	0.0	2.0	0.0
$\Delta p_{sub,B}$	0.0	2.0	0.0
$\Delta p_{sub,C}$	0.0	2.0	0.0
$z_{sup,Aa}$	0.0	1.0	1.0
$z_{sup,Ab}$	0.0	1.0	1.0
$z_{sup,Ac}$	0.0	1.0	1.0
$z_{sup,Ba}$	0.0	1.0	1.0
$z_{sup,Bb}$	0.0	1.0	1.0
$z_{sup,Bc}$	0.0	1.0	1.0
$z_{sup,Ca}$	0.0	1.0	1.0
$z_{sup,Cb}$	0.0	1.0	1.0
$z_{sup,Cc}$	0.0	1.0	1.0

As can be observed, there is no clear relation between the different properties for the different vertical and horizontal stages. The findings in Section 6.4.3 would indicate that the temperature ratio should be equal for the horizontal stages within each vertical stage. This is close to fulfilled for refrigeration cycle C. For cycle A, the temperature ratio is significantly higher in stage c, while in cycle B as significantly larger temperature ratio is observed for stage a. The optimum was observed to be quite flat with respect to variation in the horizontal stages. Different refrigerant properties, the nonlinear cooling curve for the natural gas, precooling of refrigerants and use of

refrigerant superheating are obvious reasons why the findings in Section 6.4.3 do not apply to the modelled process.

In refrigeration cycle A and refrigeration cycle B the pressure ratio is highest for the first compression stage (COMP-c) and smallest for the last compression stage (COMP-a). For refrigeration cycle B, however, the pressure ratio is highest in the last stage (COMP-a) and smallest in the intermediate stage (COMP-b). Hence, no general trend is observed.

Table 6.9. Process properties for the best solution obtained for the complex cascade process.

	Refrigeration cycle		
Property	Cycle A	Cycle B	Cycle C
Temperature ratio			
TR_a	1.05	1.16	1.14
TR_b	1.07	1.08	1.15
TR_c	1.12	1.09	1.14
Pressure ratio			
PR_a	1.59	3.34	2.46
PR_b	1.77	1.92	2.88
PR_c	2.99	2.28	3.13

The total power consumption of the complex cascade process was 785.4 kW. With ethane used as refrigerant in refrigeration cycle B, the power consumption of the best solution found was 831.8 kW, about 5.9 % higher than the best solution obtained with ethene as refrigerant.

Optimization search performance

For the simple cascade process, the average process flowsheet evaluation time was found to be around 0.3-0.4 s, while for the complex cascade, the time consumed per function evaluation was in the range 0.5-0.6 s. Using the proposed set of decision variables for optimization of the simple cascade (alternative 2), the average number of function evaluations in each search was 41 for the case with all degrees of freedom used and 31 with only the low pressure levels and the degree of superheating used as decision variables. For the conventional choice of decision variables (alternative 1), the number of function evaluations required in each search varied considerably between the different sets of variables and the different runs (partly because many of the runs fail to locate a feasible solution), yet the number of evaluations was typically between 100 and 1000.

Since there are more decision variables in the complex cascade process, more function evaluations were observed for the optimization search (derivatives are estimated for

each variable in each SQP iteration). With the proposed set of decision variables (Table 6.8), the average number of process evaluations was 2885 with all degrees of freedom in use, and 2177 when the cold end temperature differences and high pressure levels were fixed at the values of the best known solution.

6.5.2 Exergy analysis

An overview of the irreversibilities in the complex cascade process is given in Table 6.10, both with minimum and maximum superheating in all horizontal stages. The irreversibilities have been categorized according to the type of unit operation, i.e. the compressor irreversibilities in a vertical stage are equal to the sum of irreversibilities in the three compressors in that stage. In addition to irreversibility sources in the simple cascade, exergy destruction is observed also in the mixers located at the inlet of the compressors COMP-a and COMP-b. These losses are related to mixing of streams at different temperature. The vapour-liquid separators, the splitters and the mixers located in the cold end of the heat exchangers HX-a and HX-b do not contribute to the irreversibilities.

Table 6.10. Irreversibility distribution in complex cascade process with minimum and maximum superheating.

	Minimum superheating				Maximum superheating			
Property	A	B	C	Total	A	B	C	Total
Irreversibilities (kW):								
Compressors	74	65	30	169	67	61	29	157
Coolers	33	3	0	36	34	9	0	42
Heat exchangers	28	51	34	113	24	43	32	99
Valves	26	26	20	73	24	32	20	76
Mixers	0	7	6	14	0	2	5	8
Total	162	153	90	405	149	147	85	382
Compression power (kW)	382	313	113	808	357	312	116	785

Also for the complex cascade, the smallest irreversibilities are observed for the alternative with maximum superheating in all heat exchangers. In both cases, the irreversibilities are reduced by more than 50 % (around 58 % with minimum superheating and around 52 % with maximum superheating) compared to the simple cascade. Correspondingly, the total power consumption is reduced with around 41 % and 35 %, respectively.

Since the vapour is separated from liquid after every expansion stage and only part of the refrigerant is expanded to the lowest pressure levels, a considerable reduction in irreversibilities associated with the throttling valves is observed in Table 6.10. Smaller

refrigerant flow rates in the low pressure compressors also leads to smaller irreversibilities in the compressors. The introduction of horizontal stages also brings lower compressor discharge temperatures, and thereby reduced irreversibilities in the coolers. Due to higher flow rates and larger differences in inlet temperatures, the losses in the mixers are larger for the case with minimum superheating.

Composite curves for the complex cascade are given in Fig. 6.17, clearly indicating better matching of the composite curves than for the simple cascade (see Fig. 6.10). One may notice that, due to changes in refrigerant flow rate, the total heat transfer is reduced for the process with minimum superheating in all heat exchangers but slightly increased for the process with maximum superheating. However, the cooling load is still smallest for the latter. Notice from Tables 6.4 and 6.10, that the increased refrigerant flow rates in the process with maximum superheating has led to increased irreversibilities in the heat exchangers in refrigeration cycle A.

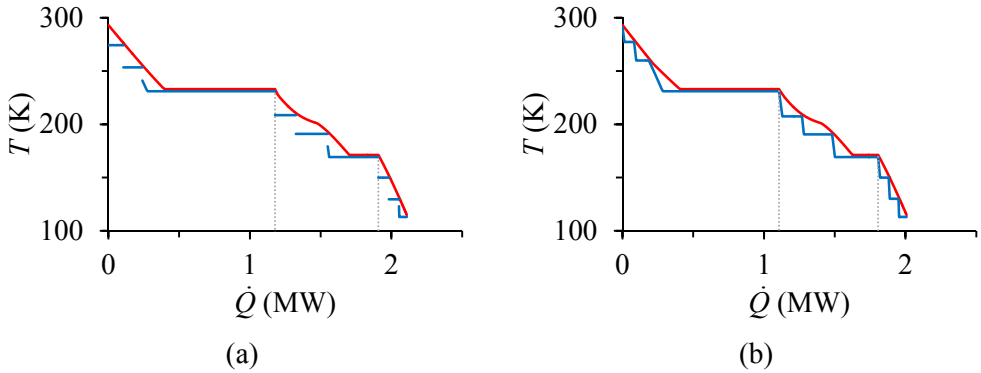

Figure 6.17. Composite curves for complex cascade process. (a) With minimum superheating; (b) With maximum superheating.

6.6 Discussion

6.6.1 Optimal process design

Generally, increasing the number of horizontal stages in the vertical stages of a refrigeration process will give reduced power consumption but increased investment cost. The power consumption in the optimized complex cascade is about 35 % lower than the power consumption of the best solution found for the simple cascade. The unit count is, however, considerable higher.

The optimal number of horizontal stages is given by a trade-off between investment and operating costs. Hence, in order to optimize the number of horizontal stages in each vertical stage, the objective must be based on cost. The temperature driving forces and heat transfer properties are also important for the heat exchanger cost.

In this study, heat transfer properties are not taken into account. The film heat transfer coefficient is likely to be lower for the vapour phase refrigerant than the two-phase refrigerant. Hence, in the section of the heat exchangers where heat is transferred by superheating the refrigerant, more heat transfer area is likely to be required per unit of heat transferred.

6.6.2 Practical implications

In practical pure-refrigerant cascade processes, flooded evaporators are often used. According to Castillo and Dorao (2013), plate exchangers are often used in pure-refrigerant cascade processes for natural gas liquefaction. According to Shukri (2004), plate-fin heat exchangers are used in ConocoPhillips' Optimized Cascade®, with the precooling potentially carried out in core-in-kettle type exchangers. Using such a heat exchanger design, refrigerant superheating cannot be utilized in the sense discussed in this work. The available cooling capacity can, however, be used in other ways with minor modifications of the process flowsheet.

An alternative layout for a horizontal stage in the complex cascade is illustrated in Fig. 6.18. Instead of utilizing refrigerant superheating for cooling in HX-b, the refrigerant stream could be superheated prior to compression by exchanging heat with the refrigerant stream entering the same stage. This recuperative heat transfer must be take place before the refrigerant stream is expanded to the evaporation temperature.

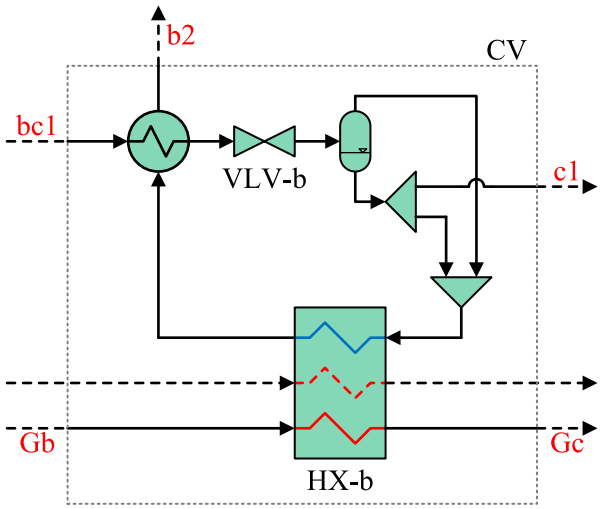

Figure 6.18. Alternative layout of horizontal stage in complex cascade.

With the design given in Fig. 6.18, the refrigerant cold stream is assumed to exit the hot end of HX-b as saturated liquid (only latent heat transferred in HX-b). The sensible heat available by superheating the refrigerant is used to sub-cool the liquid refrigerant stream entering the stage (bc1). As a consequence, less vapour will be formed in

VLV-b. Since the temperature of stream bc1 is lower than the temperature of the natural gas stream (Gb) (at least ΔT_{min} lower), the heat that can be transferred is slightly smaller than when the heat is transferred by superheating in HX-b.

From an energy balance for the control volume indicated in Fig. 6.18, it is obvious that the operating conditions of the remaining process do not change. That is, for the same degree of superheating of stream b2, the properties of the streams Gc and c1 are the same irrespective of the stage layout. The operating conditions within the stage (heat transfer properties and temperature driving forces in heat transfer) will, however, change. This has not been studied here, but will affect the size of heat exchangers and thereby the investment cost.

By recuperative heat transfer, the superheating potential could also be used to precool other streams. After precooling stream bc1, stream b2 could be used to precool stream 3 in Fig. 6.13. The principles here discussed for the complex cascade apply also to the simple cascade. For example, stream B1 in Fig. 6.1 could be used to sub-cool stream B4 prior to expansion. Potentially, it is also possible with recuperative heat transfer in between the refrigeration cycles (i.e. stream B1 could be used to precool stream A3). These options have not been considered here.

6.7 Conclusions

Optimization has been performed for pure-refrigerant cascade processes with three vertical stages, with one and three horizontal stages in each vertical stage, respectively. The results illustrate the impact of choice of decision variables and bounds in optimization and the influence of interaction between refrigeration cycles in cascade refrigeration processes.

Based on process insight, at set of decision variables was suggested for design optimization. Instead of using intermediate natural gas temperatures, high pressure levels and refrigerant flow rates as variables, these parameters were rather specified indirectly by variables for cold end temperature difference, elevation above required saturation pressure and degree of refrigerant superheating. With the suggested decision variables, the design was found to be feasible for all combinations even though no interesting regions were left outside the search space.

Compared to the fairly intuitive choice, the suggested set of decision variables gives considerable improvement in the optimization search performance. For the simple cascade process, the suggested formulation returned a solution within 0.1 % of the best known solution in all the 50 searches performed. With all available degrees of freedom used, no run returned a solution within 2 % of the best known using the intuitive formulation, even with relatively narrow variable bounds. The performance was

improved by utilizing knowledge about the best known solution to reduce the number of degrees of freedom. The specific power consumption of the optimized process was 1206 kJ/kg LNG.

For the complex cascade, none of 50 runs was able to locate a feasible solution when using the intuitive formulation, even though only the variables for flow rates and pressure levels were used. With the suggested formulation based on process insight, all 50 runs returned a solution within 1 % of the best known solution, even when using all 29 degrees of freedom. The specific power consumption of the optimized process was 787 kJ/kg LNG, a reduction of around 34.7 % compared to the simple cascade. This reduction in power consumption does, however, come with a significant increase in equipment count and investment cost.

For both processes, the best known solution was characterized by no refrigerant sub-cooling and cold end temperature differences equal to the minimum required. The smallest power consumption was observed for low pressure levels at the lower bound and maximum superheating (minimum refrigerant flow rates). As opposed to what is often considered in literature, the studies presented here indicate that the process power consumption can be reduced by utilizing the option of refrigerant superheating.

From comparison of ethane and ethene as refrigerant in the intermediate refrigeration cycle, it was found that ethene was a better alternative under the given operating conditions. Due to a lower saturation temperature at the low pressure limit, ethene provides a better load distribution between the different refrigeration cycles than ethane. The results indicate, however, that with the same load distribution, smaller power consumption is observed with ethane as refrigerant. This suggests that the optimal choice of refrigerant would depend on the process operating conditions, especially the inlet and outlet temperatures of the natural gas stream.

The thermodynamic analysis underlined an important feature of cascade refrigeration processes. Since the configuration of a vertical stage may influence the operating conditions of other stages, the solution that provides the smallest compression power in a given cycle may not agree with the solution that gives the smallest power consumption for the overall process. This issue will be studied further for mixed-refrigerant cascade processes in Chapter 8.

6.8 References

Agnew B, Ameli SM. A finite time analysis of a cascade refrigeration system using alternative refrigerant. *Applied Thermal Engineering* 2004;24(17-18):2557-2565.

Alabdulkarem A, Mortazavi A, Hwang Y, Radermacher R, Rogers P. Optimization of propane pre-cooled mixed refrigerant LNG plant. *Applied Thermal Engineering* 2011;31(6-7):1091-1098.

Barnés FJ, King CJ. Synthesis of cascade refrigeration and liquefaction systems. *Industrial and Engineering Chemistry Process Design and Development* 1974;13(4):421-433.

Bhattacharyya S, Bose S, Sarkar J. Exergy maximization of cascade refrigeration cycles and its numerical verification for a transcritical CO_2-H_3H_8 system. *International Journal of Refrigeration* 2007;30(4):624-632.

Bosma P, Nagelvoort RB. Liquefaction technology; developments through history. In: Alfadala H, Reklaitis GVR, El-Halwagi MM, editors. *Proceedings of the 1st Annual Gas Processing Symposium*; 2009 Jan 10-12; Doha, Qatar. Amsterdam: Elsevier; 2009. p. 19-31.

Castillo L, Dahouk MM, Di Scipio S, Dorao CA. Conceptual analysis of the precooling stage for LNG processes. *Energy Conversion and Management* 2013;66:41-47.

Castillo L, Dorao CA. On the conceptual design of pre-cooling stage of LNG plants using propane or an ethane/propane mixture. *Energy Conversion and Management* 2013;65:140-146.

Cheng WB, Mah RSH. Interactive synthesis of cascade refrigeration systems. *Industrial and Engineering Chemistry Process Design and Development* 1980:19(3):410-420.

Cipolato L, Lirani MCA, Costa TV, Fábrega FM, d'Angelo JVH. Exergetic optimization of a refrigeration cycle for natural gas liquefaction. *Computer Aided Chemical Engineering* 2012;31:440-444.

Colmenares TR, Seider WD. Synthesis of cascade refrigeration systems integrated with chemical processes. *Computers and Chemical Engineering* 1989;13(3):247-258.

Finn AJ, Johnson GL, Tomlinson TR. Developments in natural gas liquefaction. *Hydrocarbon Processing* 1999;78(4):47-59.

Göktun S. Coefficient of performance for an irreversible combined refrigeration cycle. *Energy* 1996;21(7-8):721-724.

Jeong S, Smith Jr JL. Optimum temperature staging of cryogenic refrigeration system. *Cryogenics* 1994;34(11):929-933.

Kanoğlu M. Exergy analysis of multistage cascade refrigeration cycle used for natural gas liquefaction. *International Journal of Energy Research* 2002;26(8):763-774.

Kilicarslan A, Hosoz M. Energy and irreversibility analysis of a cascade refrigeration system for various refrigerant couples. *Energy Conversion and Management* 2010;51(12):2947-2954.

Lee I, Tak K, Kwon H, Kim J, Ko D, Moon I. Design and optimization of a pure refrigerant cycle for natural gas liquefaction with subcooling. *Industrial and Engineering Chemistry Research* 2014;53(25):10397-10403.

Linnhoff B, Dhole VR. Shaftwork targets for low-temperature process design. *Chemical Engineering Science* 1992;47(8):2081-2091.

Mafi M, Naeynian SMM, Amidpour M. Exergy analysis of multistage cascade low temperature refrigeration systems used in olefin plants. *International Journal of Refrigeration* 2009;32(2):279-294.

Mortazavi A, Somers C, Alabdulkarem A, Hwang Y, Radermacher R. Enhancement of APCI cycle efficiency with absorption chillers. *Energy* 2010;35(9):3877-3882.

Mortazavi A, Somers C, Hwang Y, Radermacher R, Rodgers P, Al-Hashimi S. Performance enhancement of propane pre-cooled mixed refrigerant LNG plant. *Applied Energy* 2012;93:125-131.

Park H, Kim DH, Kim SO. Thermodynamic analysis of optimal intermediate temperatures in R134a-R410A cascade refrigeration systems and its experimental verification. *Applied Thermal Engineering* 2013;54(1):319-327.

Ransbarger W. A fresh look at LNG process efficiency. *Hydrocarbon Engineering* 2007;12(Suppl.):73-74,76-78,80.

Ratts EB, Brown JS. A generalized analysis for cascading single fluid vapor compression refrigeration cycles using an entropy generation minimization method. *International Journal of Refrigeration* 2000;23(5):353-365.

Sarkar J, Bhattacharyya S, Lal A. Performance comparison of natural refrigerants based cascade systems for ultra-low-temperature applications. *International Journal of Sustainable Energy* 2013;32(5):406-420.

Shelton MR, Grossmann IE. Optimal synthesis of integrated refrigeration systems – I. Mixed-integer programming model. *Computers and Chemical Engineering* 1986;10(5):445-459.

Shukri T. LNG technology selection. *Hydrocarbon Engineering* 2004;9(2):71-76.

Taleshbahrami H, Saffari H. Optimization of the C3MR Cycle with genetic algorithm. *Transactions of the Canadian Society for Mechanical Engineering* 2010;34(3-4):433-448.

Tsatsaronis G, Morosuk T. Advanced exergetic analysis of a refrigeration system for liquefaction of natural gas. *International Journal of Energy and Environment Engineering* 2010;1(1):1-18.

Vaidyaraman S, Maranas CD. Optimal synthesis of refrigeration cycles and selection of refrigerants. *AIChE Journal* 1999;45(5):997-1017.

Wang M, Khalilpour R, Abbas A. Operation optimization of propane precooled mixed refrigerant processes. *Journal of Natural Gas Science and Engineering* 2013;15:93-105.

Wang M, Zhang J, Xu Q, Li K. Thermodynamic-analysis-based energy consumption minimization for natural gas liquefaction. *Industrial and Engineering Chemistry Research* 2011;50(22):12630-12640.

Wu G, Zhu XX. Design of integrated refrigeration systems. *Industrial and Engineering Chemistry Research* 2002;41(3):553-571.

Zhang J, Xu Q. Cascade refrigeration system synthesis based on exergy analysis. *Computers and Chemical Engineering* 2011;35(9):1901-1914.

7 Constraint Formulation

Optimization of chemical processes involves finding the optimal balance between investment and operating costs. For LNG process optimization, the balance between power consumption and heat exchanger cost is of particular importance. In conceptual process design, however, detailed cost models are seldom available. A trade-off parameter is therefore often introduced to limit the size of the heat exchanger(s). The common formulation using a minimum temperature difference constraint does, however, lead to non-optimal distribution of driving forces and thereby non-optimal utilization of heat exchanger area.

In this chapter, a fairly extensive review of research on optimal distribution of driving forces in heat transfer is presented. Different guidelines for specifying the temperature profiles in heat exchangers have been compared, confirming that the irreversibilities associated with heat transfer is minimized when the temperature difference is proportional to the absolute temperature. Compared to a design with a uniform temperature difference between the composite curves, sensitivity analyses indicate that the savings obtained with optimal temperature profiles increase with increasing temperature span for the cooling load and decreasing temperature level. This is the case for natural gas liquefaction processes.

A single mixed-refrigerant process (PRICO®) has been optimized using four different trade-off constraint formulations. The results indicate savings in compression power (for the same heat exchanger size) when the constraint is based on a maximum heat exchanger conductance rather than a minimum temperature difference between the composite curves. The former leads to better distribution of driving forces with respect to temperature level, better adaption to the nonlinear behaviour of the temperature-enthalpy relationships and better trade-of between refrigerant flow rate and pressure ratio. The savings are found to increase with decreasing heat exchanger size.

This chapter is based on following publications:

- Austbø B, Gundersen T. Impact of problem formulation on LNG process optimization. Submitted to *AIChE Journal*, November 2014.
- Austbø B, Gundersen T. The impact of problem formulation on LNG process optimization. 2013 AIChE Annual Meeting, 3-8 November 2013, San Francisco, USA.

7.1 Introduction

Process design and operation is carried out with the prevailing objective of maximizing profit, or alternatively minimizing cost. Since detailed cost data seldom are available in an early design phase, a simplified approach is often taken. Both investment and operating costs are important for the overall economy of a plant. They are, however, often in conflict, since improvements in process unit operations typically come at the expense of increased investment cost. Hence, in order to minimize the total cost of a process, the optimal trade-off between investment and operating costs must be found.

The thermodynamic performance of a heat exchanger and thereby the energy cost related to its operation can be improved by reducing the temperature driving forces. This does, however, require larger heat exchangers and thereby increased investment cost. In heat exchanger network synthesis and design, this conflict is often accommodated by assigning a minimum temperature difference in the heat exchangers. This approach has in many studies been adopted also for design of processes for liquefaction of natural gas. However, as pointed out by Jensen and Skogestad (2008), this leads to non-optimal utilization of the heat exchanger area.

The scope of this study is to investigate why a minimum temperature difference approach is not suitable for design of processes for liquefaction of natural gas and discuss alternative formulations to accommodate the trade-off between investment and operating costs. The focus will be on the temperature driving forces in heat transfer.

First, the use of a minimum temperature difference in heat exchanger network design is discussed. Second, a brief review of studies of liquefied natural gas (LNG) processes is presented. This is followed by a discussion on exergy of heat and optimal distribution of temperature driving forces in heat exchangers. Based on this, different design strategies are compared for design of a simple heat exchanger. Then, the impact of the problem formulation on LNG process design optimization is illustrated by comparing different trade-off parameters for optimization of a single mixed-refrigerant process. Finally, different approaches to early-phase LNG process design are discussed with a view to optimal utilization of temperature driving forces, along with a discussion on limitations of simplified heat exchanger modelling.

7.2 Background

7.2.1 Heat exchanger network design

Pinch analysis

Appropriate balance between energy and capital costs is an important aspect in design of heat exchanger networks (Linnhoff et al., 1979). While the energy cost is closely linked to the utility consumption of the process, the number and size of heat exchangers are decisive for the capital cost. By reducing the driving forces in heat transfer, the energy use can be reduced, while the heat exchanger size increases. The heat exchanger network minimizing total annual cost is given by the optimal trade-off between utility consumption, number of heat transfer units and size of heat exchangers (Colberg and Morari, 1990).

The pinch design method is a sequential and evolutionary design method for heat exchanger networks. For a given minimum temperature difference ΔT_{min}, pinch analysis provides an energy target for which a heat exchanger network can be designed (Linnhoff and Hindmarsh, 1983). The pinch divides the heat exchanger network into two sub-systems (one with surplus of heat and one with deficit), for which the pinch design method can be used to determine the minimum number of heat transfer units required to meet the energy target. Further, an initial heat exchanger network can be designed for which heat exchanger areas and capital cost can be calculated (Linnhoff and Hindmarsh, 1983). From this initial design, the network may be improved by relaxing the ΔT_{min} criterion (Linnhoff and Ahmad, 1990).

In early design methods, the value of the minimum temperature difference was typically based on engineering experience with the energy-capital trade-off (Linnhoff and Ahmad, 1990). Over time, certain ΔT_{min} values have been acknowledged as somewhat optimal within different industrial contexts (Fraser, 1989). According to Kemp (2007), reasonable values for ΔT_{min} are around 20 K for typical bulk duties of reasonably free-flowing liquids, around 10 K for processes with high throughput or continuous operation, while for cryogenic processes 2-3 K is a typical value.

Supertargeting

Since the optimal trade-off between energy and capital costs varies from case to case, different methods have been proposed for determination of optimal value of the minimum temperature difference. The optimal trade-off can be identified by completing the targeting and design procedures for different values of the minimum temperature difference. While obtaining an energy target for different values of ΔT_{min} is relatively simple, finalizing the heat exchanger network and determining the capital cost is more time consuming. Hence, different approaches have been proposed with the

objective of estimating the optimal value of the minimum temperature difference prior to design (Li and Motard, 1986; Linnhoff and Ahmad, 1990).

By using a simplified and common cost model for the heat exchangers and assuming vertical heat transfer between the composite curves, the capital cost can be estimated without designing the heat exchanger network. This way, the value for the minimum temperature difference can be optimized prior to the network design. Linnhoff and Ahmad (1990) found this procedure to give near-optimal designs for which little or no evolution was required to obtain the global optimal design. Vertical matching of the composite curves may, however, not lead to optimal design of the heat exchanger network in all cases (Hall et al., 1990).

Heat transfer characteristics

In addition to temperature driving forces and heat duty, the area requirements of a heat exchanger also depend on the heat transfer characteristics. In general, better heat transfer is observed in a heat exchanger transferring heat between two liquid streams rather than between two gas streams. Hence, a smaller heat exchanger area is required in a liquid-liquid heat exchanger for the same heat load and temperature difference than for a gas-gas heat exchanger, and the optimal trade-off between capital and energy costs is shifted towards smaller values for the minimum temperature difference (Saboo and Morari, 1984).

One way to account for different heat transfer characteristics of different streams is to define individual contributions to the minimum temperature difference for each stream (Linnhoff and Flower, 1978; Saboo and Morari, 1984). Determination of the optimal value for each of the individual ΔT_{min} contributions would, however, lead to a multi-dimensional optimization problem (Fraser, 1989). Hence, in order to maintain the simplicity of the design approach, different techniques have been suggested to link the heat transfer characteristics to the optimal individual ΔT_{min} contributions.

For an idealized problem where the capital cost was assumed to be proportional to the total heat exchanger area and the heating and cooling demands were in balance, Nishimura (1980) found that the optimal individual contribution to the minimum temperature difference of each stream i should be proportional to the inverse of the square root of the film heat transfer coefficient of the same stream ($\Delta T_{min,i} \sim 1/\sqrt{h_i}$). This approach was also used by Ahmad et al. (1990). Fraser (1989) suggested specifying a minimum heat flux instead of a minimum temperature difference in order to account for different heat transfer characteristics. The individual ΔT_{min} contribution for each stream would then be proportional to the inverse of the heat transfer coefficient of the stream ($\Delta T_{min,i} \sim 1/h_i$).

Rev and Fonyo (1991) proposed the diverse pinch concept to accommodate the fact that vertical heat transfer may lead to non-optimal heat exchanger networks when the differences in heat transfer coefficients are significant. In their approach, the individual ΔT_{min} contributions are determined based on empirical formulas. In a method proposed by Trivedi et al. (1989), a pseudo-pinch concept is used where separate minimum temperature differences are defined for the overall network and for individual heat exchangers.

Heat exchanger type

In addition to size, important factors for the cost of heat exchanger equipment include materials of construction, design pressure and design temperature (Smith, 2005). A corrosive stream could, for example, require special materials of construction that are more expensive than the materials applicable for non-corrosive streams (Ahmad et al., 1990). Heat exchangers operating at higher pressure are more costly since thicker walls are required to withstand the forces (Smith, 2005). Further, at high temperature levels, care must be taken in heat exchanger design as the allowable stress decreases (Smith, 2005). Individual contributions to ΔT_{min} could also be used to account for heat exchanger surfaces prone to fouling (Kemp, 2007).

Hall et al. (1990) acknowledged the fact that different cost laws apply to different heat exchanger types. For capital cost targets, different heat exchanger types are therefore accounted for by adding weighting factors in the cost function. Ahmad et al. (1990) and Jegede and Polley (1992) also used weighting factors to account for different heat exchanger types, materials of construction, pressure ratings and heat transfer coefficients when estimating the capital cost using nonlinear cost functions. A review of different heat exchanger cost estimates was provided by Taal et al. (2003), indicating the complexity of heat exchanger cost calculations.

Total site targeting

Total site targeting is a special case of heat exchanger network synthesis considering integration of different processes within the same site. A large plant may be composed of many different processes with different characteristics. Hence, the optimal ΔT_{min} value may vary significantly between the different processes. For this reason, taking into account individual ΔT_{min} contributions may be of extra importance for total site targeting (Fodor et al., 2010, 2012). Varbanov et al. (2012) suggested using different ΔT_{min} values for each process in the plant, allowing for different ΔT_{min} values for heat exchangers operating within a process, between different processes and between process streams and utilities.

Environmental impact

Other factors than economy may also be decisive for the optimal process design. Wen and Shonnard (2003) and Jin et al. (2014) studied the influence of environmental impact on heat exchanger network synthesis. Wen et al. (2003) found the optimal value of the minimum temperature difference to be smaller when environmental impact was considered in the trade-off, as opposed to only energy and capital cost.

7.2.2 LNG process optimization

In conformity with heat exchanger network design, detailed cost data are seldom available in early-stage design of liquefaction processes for natural gas. Both heat exchangers and rotating equipment (compressors and expanders) are decisive for the investment cost of LNG process, while the operating cost to a great extent is depending on the process power consumption. As for the case of heat exchanger networks, minimizing the cost of heat exchangers and minimizing energy use are found to be conflicting objectives. In general, the process power consumption can be reduced if the size of the heat exchangers is increased and vice versa. The cost of rotating equipment, however, is found to be less sensitive to the process parameters. In addition, there is no clear link between the energy use of the process and the cost of compressors and expanders, beyond the fact that smaller duties indicate smaller units.

Due to the arguments given above, LNG process design optimization has traditionally been focused on finding the optimal trade-off between power consumption and heat exchanger size. In the literature, this is sometimes done by optimizing a simplified total annual cost function where the operating cost is represented by the energy cost and the capital cost is given as a function of the heat exchanger area.

More often, however, the minimum temperature difference approach used in heat exchanger network design has been adopted. In this case, the power consumption is minimized subject to a minimum temperature difference in the process heat exchangers. A summary of $\Delta T_{\min}$ values used in LNG process optimization are given in Table 7.1, ranging from 0.1 K to 5.0 K. Alabdulkarem et al. (2011) studied the influence of the minimum temperature difference on the power consumption in a propane-precooled mixed-refrigerant process by performing optimization with different values (0.01 K, 1 K, 3 K and 5 K). Hasan et al. (2010) optimized the heat exchanger network in an LNG plant (including mixed-refrigerant liquefaction process, fractionation and fuel supply) subject to a minimum temperature difference of 3 K.

For simplicity, Aspelund et al. (2010) proposed using a minimum temperature difference approach in early-stage process design. In more detailed design, a simplified cost function taking into account energy use and heat exchanger investment cost was suggested. For optimization of a single mixed-refrigerant process, Del Nogal et al.

(2008) found that while the power consumption increased monotonically with increasing minimum temperature difference, the minimum capital cost was realized for a minimum temperature difference in the range of 1-5 K. This was caused by the fact that the cost of the compressor decreased with decreasing power consumption. When using minimum capital cost as objective, the compression power of the resulting design was slightly higher than when using minimum power consumption as objective, yet a significant reduction was observed for the capital cost (Del Nogal et al., 2008).

Table 7.1. Overview of optimization studies using ΔT_{min} as trade-off parameter.

Process	ΔT_{min} (K)	References
Single mixed-refrigerant	0.1	Aspelund et al. (2010)
		Wahl et al. (2013)
	1.2	Del Nogal et al. (2008)
		Skaugen et al. (2010)
		Kamath et al. (2012)
	1.5	Shirazi and Mowla (2010)
	2.0	Morin et al. (2011)
		He and Ju (2014)
	3.0	Lee et al. (2012)
		Khan et al. (2012)
		Khan and Lee (2013)
		Xu et al. (2013, 2014)
	5.0	Del Nogal et al. (2008)
		Kamath et al. (2012)
		Yoon et al. (2012)
Propane-precooled mixed refrigerant	2.0	Wang et al. (2011, 2012)
	3.0	Taleshbahrami and Saffari (2010)
		Lee et al. (2014)
Dual mixed-refrigerant	2.0	Morin et al. (2011)
	3.0	Del Nogal et al. (2010)
Dual nitrogen expander	5.0	Yoon et al. (2012)

Hatcher et al. (2012) compared different objective function formulations for optimization of a mixed-refrigerant cycle, both for design and operation. For design, maximizing the net present value was found to give the best solution with respect to operating cost, while minimizing the sum of compression power and total *UA* requirement was found to give the solution with the smallest capital cost. In operation, when equipment sizes are given, directly minimizing the compression power was found to provide the best results.

Castillo and Dorao (2012) performed a multi-objective optimization of a single mixed-refrigerant process with the objectives of minimizing heat exchanger area, minimizing

power consumption and minimizing market cost. A multi-objective optimization approach was also taken by Shah et al. (2009) with different pair-wise combinations of four objectives; maximization of energy efficiency, minimization of capital cost, minimization of annualized cost and minimization of hydrocarbon inventory. In these studies, the minimum temperature difference was kept within 2-6 K.

For the case of optimal operation of an existing plant, the investments are already made and the equipment sizes given. Hence, the objective is usually either to maximize the plant production rate or to minimize the operating cost associated with a given production rate. Aspelund et al. (2010), Wahl et al. (2013) and Jacobsen and Skogestad (2013) minimized the power consumption of a single mixed-refrigerant process subject to a given heat exchanger conductance *UA*. Wang et al. (2013) did the same for a propane-precooled mixed-refrigerant process.

Jensen and Skogestad (2008) studied both optimal design and optimal operation of a single mixed-refrigerant process. First, the power consumption was minimized subject to a minimum temperature difference in the heat exchanger. From the resulting design, a *UA* value was calculated for the heat exchanger. Second, the process was re-optimized without restrictions on the temperature driving force but subject to a maximum heat exchanger *UA* value equal to the *UA* value found for the first design. Despite the same heat exchanger size, the results indicated significant savings in the power consumption for the second design. Jensen and Skogestad (2008) concluded that the $\Delta T_{\min}$ approach leads to non-optimal solutions.

In order to avoid this, Jensen and Skogestad (2008) suggested using a simplified cost function for optimization of refrigeration processes. The total annual cost was modelled with operating cost represented by energy cost and capital cost modelled as a constant multiplied by the sum of areas raised to a power less than unity. As an alternative, Jensen and Skogestad (2008) proposed using a constraint based on the mean temperature difference rather than the smallest temperature difference, as the mean temperature difference links the heat exchanger cooling load and overall heat transfer coefficient to the heat exchanger area.

The results of the studies performed by Jensen and Skogestad (2008) indicate that a minimum temperature difference approach leads to non-optimal utilization of the heat exchanger conductance. The inadequacy of the $\Delta T_{\min}$ approach may be partially explained from the perspective of exergy of heat.

7.2.3 Exergy of heat

As discussed in Chapter 2, the thermodynamic performance of a process can be measured through its exergy efficiency. The rational efficiency of a system can be defined as the ratio of exergy output to exergy input

$$\psi = \frac{\sum \Delta \dot{\mathrm{E}}_{\mathrm{out}}}{\sum \Delta \dot{\mathrm{E}}_{\mathrm{in}}} = \frac{\sum \Delta \dot{\mathrm{E}}_{\mathrm{out}}}{\sum \Delta \dot{\mathrm{E}}_{\mathrm{out}} + \dot{I}}, \tag{7.1}$$

where $\dot{I}$ is the sum of process irreversibilities (Kotas, 1995). When the operating conditions are given, maximizing the exergy efficiency is equivalent to minimizing the irreversibilities.

A prerequisite for reversible processes is infinitesimal driving forces. For a heat transfer process, this is equivalent to an infinitesimal temperature difference between the heat source and the heat sink. Since this would give an infinite heat transfer area, a finite temperature difference is required in practical applications. This temperature driving force is a source to entropy production (irreversibilities).

For a given overall heat transfer coefficient U, the heat exchanger area required to transfer a heat flow $\dot{Q}$ across a temperature difference ΔT is given as

$$A = \frac{\dot{Q}}{U \cdot \Delta T}. \tag{7.2}$$

As discussed in Chapter 2, the exergy of a heat flow $\dot{Q}_{\mathrm{i}}$ available at an absolute temperature T_{i} is given as

$$\dot{\mathrm{E}}\left(\dot{Q}_{\mathrm{i}}\right) = \dot{Q}_{\mathrm{i}} \cdot \left(1 - \frac{T_0}{T_{\mathrm{i}}}\right), \tag{7.3}$$

where T_0 is the ambient temperature (Kotas, 1995). From Eq. (7.3), the irreversibilities associated with heat transfer between two constant temperature systems can be expressed as

$$\dot{I} = \dot{Q} \cdot T_0 \cdot \left(\frac{1}{T_{\mathrm{C}}} - \frac{1}{T_{\mathrm{H}}}\right) = \dot{Q} \cdot T_0 \cdot \frac{\Delta T}{T_{\mathrm{H}} \cdot \left(T_{\mathrm{H}} - \Delta T\right)}, \tag{7.4}$$

where T_{H} is the temperature of the source and T_{C} is the temperature of the sink. The exergy of heat indicates that, in order to minimize irreversibilities associated with heat transfer, more attention should be paid to keeping the driving forces small at low temperature levels.

7.2.4 Optimal heat exchanger design

Many studies have been performed on the subject of optimal design and operation of heat exchangers. In this work, the primary focus is on the influence of the driving forces in heat transfer. Over the years, a variety of theories have been proposed for optimal utilization of heat exchanger area, in order to minimize the entropy production or irreversibilities associated with heat transfer.

Optimal distribution of driving forces

The theory of equipartition of entropy production was introduced by Tondeur and Kvaalen (1987) as a framework for optimal configuration of heat and mass transfer processes. They found that the total entropy production within a unit operation or process was minimized when the entropy production rate was uniformly distributed in space and time. For the case of constant phenomenological transport coefficients (in the validity range of linear equilibrium thermodynamics and Onsager's relations), this was found to be equivalent to equipartition of driving forces (Tondeur and Kvaalen, 1987; Tondeur,1990).

Later, Sauar et al. (1996) proposed the principle of equipartition of forces, as an alternative approach to design optimization. From irreversible thermodynamics, they found exergy loss in coupled transport of heat, mass or charge to be minimized when the driving forces in the process were uniformly distributed. This was derived for heat transfer processes with the driving force expressed as $\Delta(1/T)$. The heat flux is then given as

$$\dot{q} = \frac{\dot{Q}}{A} = L \cdot \Delta\left(1/T\right), \tag{7.5}$$

where L is a phenomenological heat transfer coefficient that depends on the intensive thermodynamic variables of the system but not the driving force (Sauar et al., 1996). Further, the entropy production rate per unit of area can then be expressed as

$$\frac{\dot{S}_{\text{prod}}}{A} = L \cdot \left(\Delta\left(1/T\right)\right)^2 . \tag{7.6}$$

The principle of equipartition of forces was derived under the assumption that the transport process is described by independent forces and that the system is linked by the Gibbs-Duhem equation (Sauar et al., 1996). According to Kjelstrup et al. (1998), the principle of equipartition of forces is a general principle that also holds for cases where the transfer coefficients are not constant. Sauar et al. (1996) stated that when L and $\dot{Q}$ are not constant in space and time, a uniform local entropy production rate will

not give the minimum total entropy production. Other studies have, however, reached a different conclusion.

According to Xu (1997), the phenomenological heat transfer coefficient can be approximated by $L \approx U \cdot T^2$, where U is the heat transfer coefficient in the conventional heat transfer equation. Based on simplified economic considerations, Xu (1997) derived that the temperature driving force at any point i in a heat exchanger should be given as

$$\Delta\left(1/T\right)_{\mathrm{i}} = \sqrt{\frac{a}{e \cdot T_0 \cdot L_{\mathrm{i}}}} \tag{7.7}$$

in order to minimize the sum of capital and operating costs of the heat exchanger. In Eq. (7.7), a is assumed to be the unit cost of heat transfer area and e the unit cost of thermal exergy. In this derivation, exergy losses due to pressure drop were omitted. On conventional form, the driving force was approximated as

$$\Delta T_{\mathrm{i}} \approx T_{\mathrm{i}} \cdot \sqrt{\frac{a}{e \cdot T_0 \cdot U_{\mathrm{i}}}}\,, \tag{7.8}$$

where T_{i} is the temperature at which the heat is transferred.

For a given heat exchanger area A, Xu (1997) found that the optimal heat transfer driving force could be expressed as

$$\Delta\left(1/T\right)_{\mathrm{i}} = \frac{1}{A} \cdot \frac{c}{\sqrt{L_{\mathrm{i}}}}\,, \tag{7.9}$$

or alternatively as

$$\Delta T_{\mathrm{i}} \approx \frac{T_{\mathrm{i}}}{A} \cdot \frac{c}{\sqrt{U_{\mathrm{i}}}}\,. \tag{7.10}$$

Here,

$$c = \int_0^Q \frac{dq}{\sqrt{L_{\mathrm{i}}}} \approx \int_0^Q \frac{dq}{T\sqrt{U_{\mathrm{i}}}}\,. \tag{7.11}$$

Under the assumption that $T \gg \Delta T$, Chang et al. (2011) reached the same conclusion as Xu (1997) (Eqs. (7.10) and (7.11)) when minimizing the entropy generation in a heat exchanger with a given area.

Bejan (1979, 1996, 1997) also arrived at the conclusion that the temperature difference between the hot and cold streams in a heat exchanger should be proportional to the absolute temperature, and also noted that this is a well-known design principle in cryogenic engineering (Bejan, 1997). From variational calculus, Balkan (2003) deduced equivalence between the theory of equipartition of entropy generation and heat exchanger temperature profiles where the ratio T_H/T_C is constant. This is equivalent to the statements of Xu (1997) and Chang et al. (2011) that the temperature difference should be proportional to the absolute temperature.

As can be observed from Eqs. (7.7) and (7.9), the findings of Xu (1997) and Chang et al. (2011) imply that the optimal driving force $\Delta(1/\mathrm{T})$ is inversely proportional to the square root of the phenomenological heat transfer coefficient. This indicates that the driving force $\Delta(1/T)$ would be constant only if L is constant. Xu (1997) found the principle of equipartition of forces (Sauar et al., 1996) to be equivalent to a temperature difference ΔT proportional to the square of the temperature and independent of heat transfer coefficient, which can be deduced assuming $T \gg \Delta T$. Haug-Warberg (2000) also raised questions about the principle of equipartition of forces, and found that it did not provide a solution of minimum total entropy production in the case of heat transfer with a non-constant phenomenological heat transfer coefficient. This was illustrated by an example where the heat transfer was defined in different ways for two sections of a heat exchanger.

In response, Sauar et al. (1997) pointed out that the principle of equipartition of forces is based on local linear relations between fluxes and forces in the system. Kjelstrup et al. (2000) pointed out that in order for the theory to hold, the phenomenological heat transfer coefficient can be an arbitrary function of the temperature and spatial parameters of the heat exchanger, yet it must be independent of the heat flux or the driving force. Further, Kjelstrup et al. (2000) found the example presented by Haug-Warberg (2000) not to fulfil this requirement. Hence, for this case, the principle does not apply (Kjelstrup et al., 2000). The deviations from optimality were for this case, however, found to be so small that the principle of equipartition of forces could be a useful rule of thumb also in cases where it does not apply in a strict sense (Kjelstrup et al., 2000).

With the purpose of verifying that the principle of equipartition of forces does not depend on a constant phenomenological transfer coefficient, Nummedal and Kjelstrup (2001) presented examples were the overall heat transfer coefficient U was assumed constant. However, no comparison was made with other principles for optimal distribution of driving forces. In a later study, Johannessen et al. (2002) found that uniform distribution of entropy production led to smaller total entropy production than uniform distribution of driving forces $\Delta(1/T)$. The results did, however, indicate that

the principle of equipartition of forces would be likely to estimate the real solution within an error less than one percent in practical applications (Johannessen et al., 2002).

Design strategies similar to the principle of equipartition of forces have also been used in LNG process design. Among others, Fredheim (1994) stated that the composition of the mixed refrigerant in an LNG process should be optimized such that the relative exergy loss as a function of temperature is constant, which is equivalent to a uniform driving force $\Delta(1/T)$.

Performance assessment

Balkan (2003) compared the performance of different strategies for distribution of driving forces for design of a heat exchanger with given heat duty and area, assuming a constant overall heat transfer coefficient U. The principle of equipartition of entropy production was found to give slightly smaller total entropy production than the principle of equipartition of forces, and only a small increase in entropy production was observed for a design with a constant temperature difference ΔT (Balkan, 2003). The results presented by Balkan (2003) may, however, be influenced by the fact that the heat transfer took place at relatively high temperature, distributed over a relatively narrow temperature range.

Balkan (2003) found that iterations were required to find the proper operating conditions using the principle of equipartition of forces or the principle of equipartition of entropy production. Hence, since only small performance deterioration was observed, Balkan (2003) suggested applying a uniform temperature difference (which requires no iterations) as a short-cut design method.

In order to assess the thermodynamic performance of a heat exchanger, an equipartition factor was defined by Thiel et al. (2014) as the ratio of entropy production in the actual system to the entropy production in a system where the theory of equipartition of entropy production is fulfilled. Thiel et al. (2014) found the potential for exergy efficiency improvement by moving to a system with equipartition of entropy production to be largest in systems where both the equipartition factor and the rational efficiency are low. If a system already has small irreversibilities, the effect of redistributing the temperature driving forces is, of course, small.

In the following, different strategies for distribution of heat transfer driving forces are compared for design of a simple heat exchanger under different operating conditions, in order to identify the influence of these design guidelines on the performance of the final design.

7.3 Simple counter-current heat exchanger

In order to examine the influence of the distribution of temperature driving forces on heat transfer performance, a case study was performed for a simple counter-current heat exchanger model as illustrated in Fig. 7.1. For a given hot stream with a constant heat capacity flow rate $(\dot{m}\cdot c_p)_H$, supply temperature T_{high} and target temperature T_{low}, the cold stream temperature profile was designed such that the heat exchanger conductance value (UA) was kept constant. The heat exchanger irreversibilities were then compared for different cold composite curve designs. Since the objective was to study the influence of temperature driving forces on heat transfer irreversibilities, this case study was performed under the assumption of a constant overall heat transfer coefficient U.

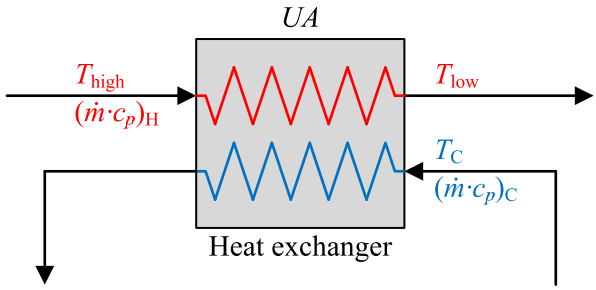

Figure 7.1. Simple heat exchanger model.

Based on the findings in the preceding sections, four different design guidelines were compared for the cold composite curve:

1. Uniform temperature difference throughout the heat exchanger: $\Delta T = C_{uniform}$.
2. Temperature difference proportional to the temperature of the hot stream: $\Delta T = C_{linear}\cdot T_H$.
3. Constant value for the difference in the inverse of the temperature: $\Delta(1/T) = C_{inverse}$.
4. Temperature difference proportional to the square of the temperature of the hot stream: $\Delta T = C_{square}\cdot T_H^2$.

For the design solutions where the temperature difference is defined as a function of the hot stream temperature, the cold stream temperature could also have been used with a slight modification of the value of the constant (exactly the same for design specification 2, but slightly different for design specification 4). One may notice that the design specifications 3 and 4 cannot be obtained for a constant value of the constant heat capacity flow rate for the cold stream $(\dot{m}\cdot c_p)_C$.

7.3.1 Heat exchanger conductance and irreversibilities

The heat exchanger conductance is given as

$$UA = \int_{T_{\text{low}}}^{T_{\text{high}}} \left(\frac{\left(\dot{m} \cdot c_p\right)_{\text{H}}}{\Delta T\left(T_{\text{H}}\right)} \right) \mathrm{d}T_{\text{H}} = \left(\dot{m} \cdot c_p\right)_{\text{H}} \cdot \int_{T_{\text{low}}}^{T_{\text{high}}} \left(\frac{1}{\Delta T\left(T_{\text{H}}\right)} \right) \mathrm{d}T_{\text{H}}, \tag{7.12}$$

where $\Delta T(T_{\text{H}})$ means that ΔT is a function of T_{H}. The irreversibilities associated with the same heat transfer can be found by integrating the difference in exergy of heat between the heat source (hot stream) and the heat sink (cold stream) through the heat exchanger. This can be expressed as

$$\dot{I} = T_0 \cdot \int_0^{\dot{Q}} \left(\frac{1}{T_{\text{C}}} - \frac{1}{T_{\text{H}}} \right) \delta\dot{Q} = \left(\dot{m} \cdot c_p\right)_{\text{H}} \cdot T_0 \cdot \int_{T_{\text{low}}}^{T_{\text{high}}} \left(\frac{1}{T_{\text{H}} - \Delta T\left(T_{\text{H}}\right)} - \frac{1}{T_{\text{H}}} \right) \mathrm{d}T_{\text{H}}, \tag{7.13}$$

where T_0 is the ambient temperature.

Uniform temperature difference

For a heat exchanger with a uniform temperature difference $\Delta T = C_{\text{uniform}}$ between the composite curves, the driving forces required to obtain the given heat transfer conductance UA is

$$\Delta T = C_{\text{uniform}} = \frac{\left(\dot{m} \cdot c_p\right)_{\text{H}} \cdot \left(T_{\text{high}} - T_{\text{low}}\right)}{UA}. \tag{7.14}$$

From Eq. (7.13), the resulting irreversibilities are given as

$$\begin{aligned} \dot{I}_{\text{uniform}} &= \left(\dot{m} \cdot c_p\right)_{\text{H}} \cdot T_0 \cdot \int_{T_{low}}^{T_{high}} \left(\frac{1}{T_H - C_{\text{uniform}}} - \frac{1}{T_H} \right) \mathrm{d}T_H \\ &= \left(\dot{m} \cdot c_p\right)_{\text{H}} \cdot T_0 \cdot \ln\left(\frac{\left(T_{\text{high}} - C_{\text{uniform}}\right) \cdot T_{\text{low}}}{\left(T_{\text{low}} - C_{\text{uniform}}\right) \cdot T_{\text{high}}} \right). \end{aligned} \tag{7.15}$$

Using Eq. (7.14), the irreversibilities can be expressed as a function of UA:

$$\dot{I}_{\text{uniform}} = \left(\dot{m} \cdot c_p\right)_{\text{H}} \cdot T_0 \cdot \ln\left(\frac{\left(T_{\text{high}} - \left(\dot{m} \cdot c_p\right)_{\text{H}} \cdot \left(T_{\text{high}} - T_{\text{low}}\right) / UA\right) \cdot T_{\text{low}}}{\left(T_{\text{low}} - \left(\dot{m} \cdot c_p\right)_{\text{H}} \cdot \left(T_{\text{high}} - T_{\text{low}}\right) / UA\right) \cdot T_{\text{high}}} \right). \tag{7.16}$$

Temperature difference proportional to temperature

For the case where the temperature difference is given as a linear function of the absolute temperature, the temperature difference in the hot and cold endpoints of the heat exchanger are given as $\Delta T_{\text{cold}} = C_{\text{linear}} \cdot T_{\text{low}}$ and $\Delta T_{\text{hot}} = C_{\text{linear}} \cdot T_{\text{high}}$, respectively. The heat exchanger conductance can be formulated as

$$UA = \frac{\left(\dot{m} \cdot c_p\right)_{\text{H}} \cdot \left(T_{\text{high}} - T_{\text{low}}\right)}{\Delta T_{\text{LM}}}, \tag{7.17}$$

with the logarithmic temperature ΔT_{LM} difference given as

$$\Delta T_{\text{LM}} = \frac{C_{\text{linear}} \cdot \left(T_{\text{high}} - T_{\text{low}}\right)}{\ln\left(T_{\text{high}} / T_{\text{low}}\right)}. \tag{7.18}$$

The value of the constant C_{linear} can then be expressed as a function of the heat exchanger conductance:

$$C_{\text{linear}} = \frac{\left(\dot{m} \cdot c_p\right)_{\text{H}} \cdot \ln\left(T_{\text{high}} / T_{\text{low}}\right)}{UA}. \tag{7.19}$$

With the use of Eq. (7.13), the irreversibility associated with the heat transfer can be expressed as

$$\begin{aligned} \dot{I}_{\text{linear}} &= \left(\dot{m} \cdot c_p\right)_{\text{H}} \cdot T_0 \cdot \int_{T_{\text{low}}}^{T_{\text{high}}} \left(\frac{1}{\left(1 - C_{\text{linear}}\right) T_{\text{H}}} - \frac{1}{T_{\text{H}}} \right) \mathrm{d}T_{\text{H}} \\ &= \left(\dot{m} \cdot c_p\right)_{\text{H}} \cdot T_0 \cdot \frac{C_{\text{linear}}}{1 - C_{\text{linear}}} \ln\left(\frac{T_{\text{high}}}{T_{\text{low}}} \right), \end{aligned} \tag{7.20}$$

which by utilizing Eq. (7.19) can be written as

$$\dot{I}_{\text{linear}} = \left(\dot{m} \cdot c_p\right)_{\text{H}} \cdot T_0 \cdot \frac{\left(\ln\left(T_{\text{high}} / T_{\text{low}}\right)\right)^2}{UA / \left(\dot{m} \cdot c_p\right)_{\text{H}} - \ln\left(T_{\text{high}} / T_{\text{low}}\right)}. \tag{7.21}$$

Constant difference in inverse temperature

When the difference in the inverse of the temperature is constant ($\Delta(1/T) = C_{\text{inverse}}$), the heat exchanger temperature difference can be expressed as

$$\Delta T = \frac{C_{\text{inverse}} \cdot T_{\text{H}}^2}{1 + C_{\text{inverse}} \cdot T_{\text{H}}} . \tag{7.22}$$

Using this, the heat exchanger conductance can be expressed as

$$\begin{aligned} UA &= \left(\dot{m} \cdot c_p\right)_{\text{H}} \cdot \int_{T_{\text{low}}}^{T_{\text{high}}} \left(\frac{1 + C_{\text{inverse}} \cdot T_{\text{H}}}{C_{\text{inverse}} \cdot T_{\text{H}}^2} \right) \mathrm{d}T_{\text{H}} \\ &= \frac{\left(\dot{m} \cdot c_p\right)_{\text{H}}}{C_{\text{inverse}}} \cdot \left(\frac{1}{T_{\text{low}}} - \frac{1}{T_{\text{high}}} + C_{\text{inverse}} \cdot \ln\left(\frac{T_{\text{high}}}{T_{\text{low}}} \right) \right), \end{aligned} \tag{7.23}$$

and the constant C_{inverse} as

$$C_{\text{inverse}} = \frac{T_{\text{high}} - T_{\text{low}}}{T_{\text{low}} \cdot T_{\text{high}} \cdot \left(UA / \left(\dot{m} \cdot c_p\right)_{\text{H}} - \ln\left(T_{\text{high}} / T_{\text{low}}\right) \right)} . \tag{7.24}$$

The total irreversibilities can be calculated from Eq. (7.13) as

$$\dot{I}_{\text{inverse}} = \left(\dot{m} \cdot c_p\right)_{\text{H}} \cdot T_0 \cdot \int_{T_{\text{low}}}^{T_{\text{high}}} C_{\text{inverse}} \, \mathrm{d}T_{\text{H}} = \left(\dot{m} \cdot c_p\right)_{\text{H}} \cdot T_0 \cdot C_{\text{inverse}} \cdot \left(T_{\text{high}} - T_{\text{low}}\right), \tag{7.25}$$

which combined with Eq. (7.24) gives the following result:

$$\dot{I}_{\text{inverse}} = \left(\dot{m} \cdot c_p\right)_{\text{H}} \cdot T_0 \cdot \frac{\left(T_{\text{high}} - T_{\text{low}}\right)^2}{T_{\text{low}} \cdot T_{\text{high}} \cdot \left(UA / \left(\dot{m} \cdot c_p\right)_{\text{H}} - \ln\left(T_{\text{high}} / T_{\text{low}}\right) \right)} . \tag{7.26}$$

Temperature difference proportional to the square of the temperature

For a design with the temperature difference given as a the square of the temperature of the hot stream, the heat exchanger conductance can be expressed as

$$UA = \left(\dot{m} \cdot c_p\right)_{\text{H}} \cdot \int_{T_{\text{low}}}^{T_{\text{high}}} \left(\frac{1}{C_{\text{square}} \cdot T_{\text{H}}^2} \right) \mathrm{d}T_{\text{H}} = \frac{\left(\dot{m} \cdot c_p\right)_{\text{H}}}{C_{\text{square}}} \cdot \left(\frac{1}{T_{\text{low}}} - \frac{1}{T_{\text{high}}} \right). \tag{7.27}$$

Hence, the constant C_{square} is given as

$$C_{\text{square}} = \frac{\left(\dot{m} \cdot c_p\right)_{\text{H}}}{UA} \cdot \left(\frac{1}{T_{\text{low}}} - \frac{1}{T_{\text{high}}} \right). \tag{7.28}$$

Again, the irreversibilities associated with the heat transfer can be calculated from Eq. (7.13):

$$\begin{aligned} \dot{I}_{\text{square}} &= \left(\dot{m} \cdot c_p\right)_{\text{H}} \cdot T_0 \cdot \int_{T_{\text{low}}}^{T_{\text{high}}} \left(\frac{1}{T_{\text{H}} - C_{\text{square}} \cdot T_{\text{H}}^2} - \frac{1}{T_{\text{H}}} \right) \mathrm{d}T_{\text{H}} \\ &= \left(\dot{m} \cdot c_p\right)_{\text{H}} \cdot T_0 \cdot \ln\left(\frac{1 - C_{\text{square}} \cdot T_{\text{low}}}{1 - C_{\text{square}} \cdot T_{\text{high}}} \right). \end{aligned} \tag{7.29}$$

With the expression from Eq. (7.28), this can be rewritten as a function of the heat exchanger conductance:

$$\dot{I}_{\text{square}} = \left(\dot{m} \cdot c_p\right)_{\text{H}} \cdot T_0 \cdot \ln\left(\frac{\left(T_{\text{high}} - \left(\dot{m} \cdot c_p\right)_{\text{H}} \cdot \left(T_{\text{high}} - T_{\text{low}}\right) / UA\right) \cdot T_{\text{low}}}{\left(T_{\text{low}} - \left(\dot{m} \cdot c_p\right)_{\text{H}} \cdot \left(T_{\text{high}} - T_{\text{low}}\right) / UA\right) \cdot T_{\text{high}}} \right). \tag{7.30}$$

One may observe that the results in Eqs. (7.16) and (7.30) are exactly the same. Hence, quite surprisingly, a design with a uniform temperature difference and a design with a temperature difference proportional to the square of the absolute temperature would lead to the same total irreversibilities for a given UA value.

7.3.2 Comparison

The difference between the four design guidelines have been illustrated for an example where $T_{\text{low}} = 100$ K and $T_{\text{high}} = 200$ K. Here, the heat transfer conductance $UA = 50$ kW/K and the hot stream heat capacity flow rate $(\dot{m} \cdot c_p)_{\text{H}} = 1$ kW/K are given such that the uniform temperature difference required to transfer the heat is equal to 2 K (see Eq. (7.14)). For these calculations, the ambient temperature T_0 was assumed to be 298.15 K.

As can be observed in Table 7.2, the smallest irreversibilities are obtained for the solution where the temperature difference is given as a linear function of the absolute temperature (design specification 2). As previously discussed, the irreversibilities obtained for a design with a uniform temperature difference and a design where the temperature difference is proportional to the square of the absolute temperature are equal. The irreversibilities in these cases are the largest in the set of four design

guidelines. The design where the difference of the inverse of the temperature is constant throughout the heat exchanger provides slightly smaller irreversibilities.

Actually, it was found that a solution with temperature difference $\Delta T = C_1 \cdot T^{1-b}$ gives the same total irreversibilities attributed to heat transfer as a solution with temperature difference $\Delta T = C_2 \cdot T^{1+b}$, where b is any constant. Best performance was then found for $b = 0$, with monotonically increasing irreversibilities for increasing values of b.

Table 7.2. Heat transfer irreversibilities for different heat exchanger designs.

Design strategy	Irreversibilities (kW)
1. Uniform temperature difference	3.027
2. Linear function of temperature	2.905
3. Uniform difference in inverse temperature	3.023
4. Quadratic function of temperature	3.027

The temperature difference throughout the heat exchanger is given as a function of the hot stream temperature for the four different design solutions in Fig. 7.2. Since the heat transfer conductance is inversely proportional to the temperature difference (see Eq. (7.12)) and the UA value is fixed, a larger average temperature difference must be applied in the cases where the temperature difference is reduced in the cold end of the heat exchanger. The designs with $\Delta(1/T) = C_{\text{inverse}}$ and $\Delta T = C_{\text{square}} \cdot T^2$ (design strategies 3 and 4) are nearly identical. Again, this can be explained by the fact that for $\Delta T \ll T_H$, $\Delta(1/T_H) \approx \Delta T / T_H^2$. This also explains why the irreversibilities in these designs are comparable (3.027 kW vs. 3.023 kW).

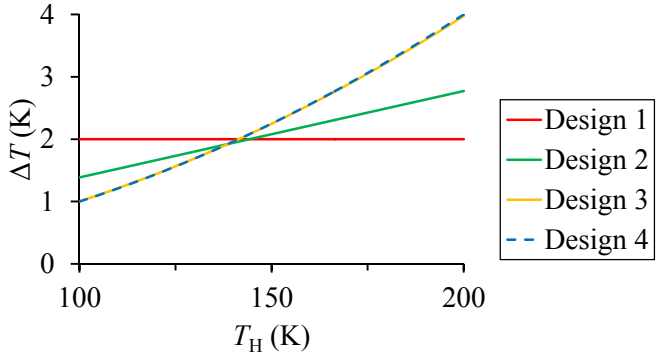

Figure 7.2. Temperature difference in the heat exchanger as a function of the hot stream temperature.

In Fig. 7.3 (a), the ratio of irreversibility rate to heat transfer conductance is plotted as a function of the hot stream temperature for the four different design solutions. As can be observed, $\Delta T = C_{\text{linear}} \cdot T_H$ (design 2) is equivalent to a uniform distribution of

irreversibilities per unit of area. This corresponds to the theory of equipartition of entropy production, where the entropy production rate is uniform in time and space.

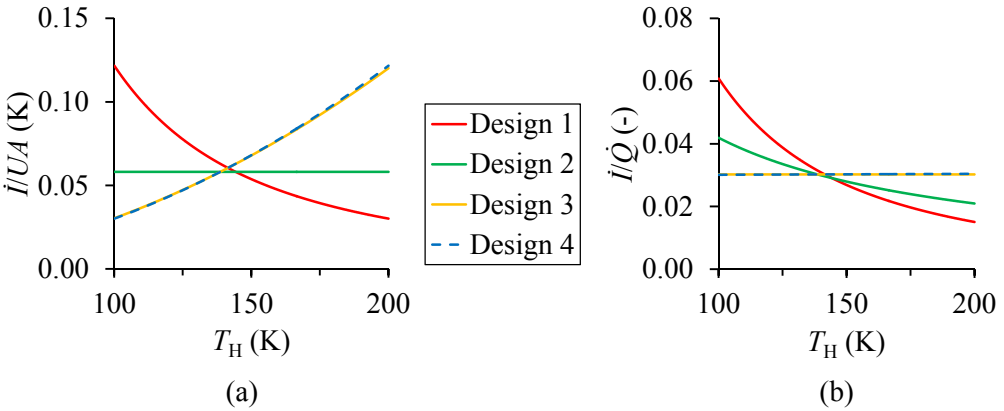

Figure 7.3. (a) Ratio of irreversibility rate to heat transfer conductance as function of the hot stream temperature; (b) Ratio of irreversibility rate to heat flow as function of the hot stream temperature.

The ratio of irreversibilities to heat flow is plotted in Fig. 7.3 (b) for the four design guidelines. A design with $\Delta(1/T) = C_{\text{inverse}}$ (design 3) is equivalent to a uniform distribution of irreversibilities per unit of heat flow. This is illustrated by a horizontal line in Fig. 7.3 (b) and can easily be proven mathematically from Eq. (7.25). For large values of UA (typically the case for LNG processes), this is close to true also for the design with $\Delta T = C_{\text{square}} \cdot T_{\text{H}}^2$, as can be observed in Fig. 7.3 (b) where design 4 has the same horizontal behaviour (constant $\dot{I}/\dot{Q}$) as design 3. When the heat transfer coefficient is assumed constant, a uniform temperature difference (design 1) is equivalent to a uniform distribution of heat flow per unit of area, as can be observed from Eqs. (7.2) and (7.14).

7.3.3 Influence of operating conditions

For a given heat exchanger size, it was illustrated in Sections 7.3.1 and 7.3.2 that a heat exchanger design where the temperature difference between the hot and cold composite curves is given as a linear function of the absolute temperature leads to less exergy destruction than a design with a uniform temperature difference throughout the heat exchanger. In order to quantify the savings obtainable in such a design, the influence of temperature level, temperature span and heat exchanger size has been studied.

The savings available when switching from a heat exchanger design with a uniform temperature profile to a design with an optimal temperature profile can be expressed through the ratio of the irreversibilities observed in the former case to the irreversibilities observed in the latter case (this is equivalent to the equipartition factor defined by Thiel et al. (2014)). The ratio of irreversibilities in the two cases could be

expressed as a function of the low temperature level of the hot stream T_{low}, the temperature span of the hot stream $\Delta T_{span} = T_{high} - T_{low}$, and the minimum temperature difference ΔT_{min}:

$$\frac{\dot{I}_{linear}}{\dot{I}_{uniform}} = \frac{\left(\ln\left(\left(T_{low} + \Delta T_{span}\right) / T_{low}\right)\right)^2}{\left(\frac{\Delta T_{span}}{\Delta T_{min}} - \ln\left(\frac{T_{low} + \Delta T_{span}}{T_{low}}\right)\right) \cdot \ln\left(\frac{\left(T_{low} + \Delta T_{span} - \Delta T_{min}\right) \cdot T_{low}}{\left(T_{low} - \Delta T_{min}\right) \cdot \left(T_{low} + \Delta T_{span}\right)}\right)} \tag{7.31}$$

The minimum temperature difference is used as a parameter defining the heat exchanger size rather than the heat exchanger conductance since this is a property that more easily relates to practical experience. The heat exchanger conductance *UA* is still the same for both designs, yet expressed indirectly through the equivalent uniform temperature difference calculated from Eq. (7.14). Here, the problem is defined such that with variation in the temperature span for the hot stream, the ratio of heat transfer conductance to total heat flow is constant rather than the total heat transfer conductance. The difference between the two formulations (uniform vs. linear) is illustrated in a temperature-enthalpy diagram in Fig. 7.4.

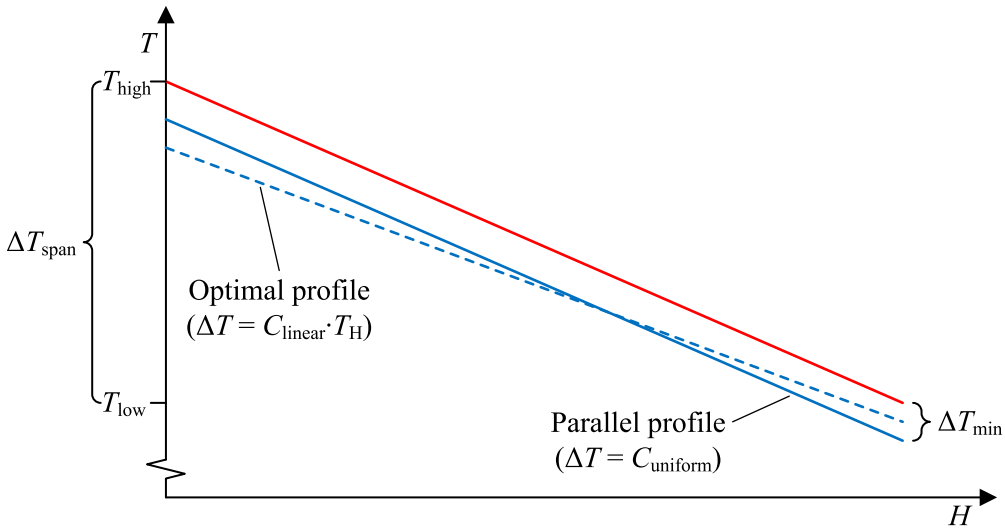

Figure 7.4. Composite curves for a simple heat exchanger.

In Fig. 7.5, the ratio of irreversibilities obtained with $\Delta T = C_{linear} \cdot T_H$ to irreversibilities obtained with $\Delta T = C_{uniform}$ is plotted as a function of the hot stream target temperature T_{low}. This is done for different values of temperature span for the hot stream ΔT_{span}, with a *UA* value equivalent to $\Delta T_{min} = 2$ K. For large values of the target temperature, savings observed for the optimal temperature profile are relatively small as the ratio of

irreversibilities approaches unity with increasing temperatures. For small values of the target temperature, however, significant savings are observed for a design where the temperature difference is proportional to the absolute temperature. This can be explained by the fact that the exergy of heat grows steeply with decreasing temperature below ambient, as discussed in Section 7.2.3.

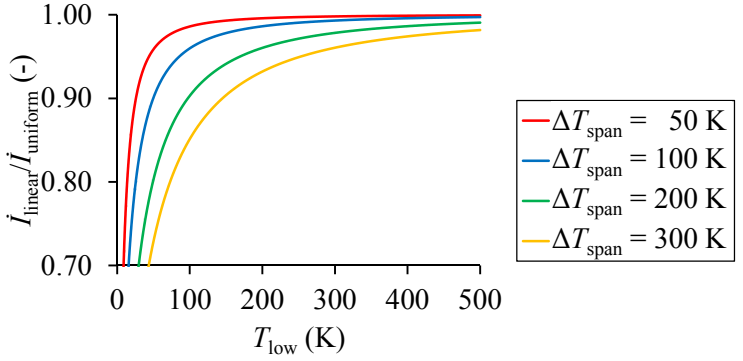

Figure 7.5. Ratio between irreversibilities in a heat exchanger for the optimal temperature profile to irreversibilities with a uniform temperature difference as a function of the hot stream target temperature for different values of temperature span and with a UA value corresponding to $\Delta T_{min} = 2$ K.

As can be observed in Fig. 7.5, the savings obtained for the optimal temperature profile relative to a uniform temperature difference increase with increasing temperature span for the hot stream. With increasing temperature span, the relative difference in exergy of heat increases. Hence, the influence of distribution of the driving forces increases. For the same temperature span, the difference in exergy of heat between the supply and target temperatures increases with decreasing absolute temperature.

The influence of the minimum temperature difference (or indirectly the heat transfer conductance) is illustrated in Fig. 7.6, where the ratio of irreversibilities obtained with $\Delta T = C_{linear} \cdot T_H$ to irreversibilities obtained with $\Delta T = C_{uniform}$ is plotted as a function of the temperature span. This is done for different values of the minimum temperature difference, with a hot stream target temperature $T_{low} = 100$ K. The results indicate that the size of the heat exchanger is of little influence with respect to the potential savings with an optimal temperature profile. Only for large values of the temperature span and/or low target temperatures, increased savings from using the optimal temperature profile are observed for increasing value of the temperature difference (smaller heat exchangers).

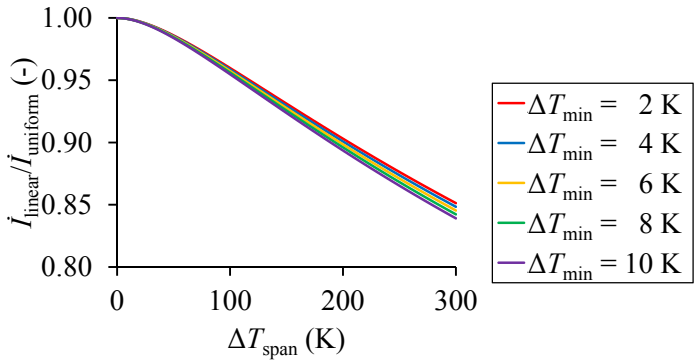

Figure 7.6. Ratio between irreversibilities in a heat exchanger for the optimal temperature profile and a uniform temperature difference as a function of the temperature span for different values of the minimum temperature difference and hot stream target temperature T_{low} = 100 K.

At relatively high temperature levels, for cooling loads distributed over a relatively narrow temperature span, the energy penalty associated with a uniform temperature difference ΔT is quite small. Hence, for many heat exchanger network design problems encountered in industry, optimal distribution of temperature driving forces with respect to exergy of heat is of little importance, confirming the success of the pinch design method. This also explains why little difference in entropy production was observed between designs with equipartition of entropy production, equipartition of forces and uniform temperature difference in the studies presented by Balkan (2003).

For low-temperature refrigeration applications, however, these results indicate large potential savings with an optimal distribution of the temperature driving forces. In LNG applications, the cooling load is distributed over a wide temperature range at relatively low temperature levels. In the following, different constraint formulations are compared for the trade-off between operating and investment costs in the optimization of LNG process design.

7.4 LNG process optimization

7.4.1 Problem formulation

As a case study, four different constraint formulations have been compared for optimization of the single mixed-refrigerant process PRICO®. In this process, the natural gas is precooled, liquefied and sub-cooled in a single stage. Hence, the heat exchanger operates over a wide temperature range, providing cooling down to about 109 K for the given natural gas specifications. A process flowsheet is given in Fig. 7.7.

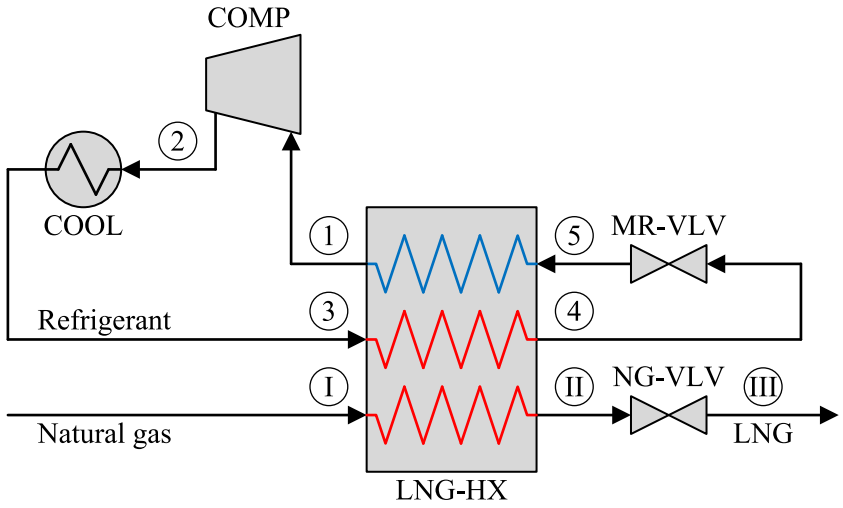

Figure 7.7. PRICO® process flowsheet.

Again, the case study is based on a process model presented by Aspelund et al. (2010), with the process characteristics given in Table 7.3. Pressurized natural gas is cooled a single stage, before being expanded to near-atmospheric pressure. The outlet temperature of the heat exchanger (T_{II}) is given such that the product stream is at the bubble point ($x_{III} = 0$). Both the natural gas and the refrigerant were assumed to be precooled to the same given temperature ($T_3 = T_I$), 5 K above ambient temperature which was assumed to be 288.15 K.

Table 7.3. Natural gas properties.

Property	Unit	Value
Molar flow rate $\dot{n}_{NG}$	kmol/s	1.00
Feed temperature T_I	K	293.15
Feed pressure p_I	bar	60.00
Product pressure p_{III}	bar	1.05
Product vapour fraction x_{III}	-	0.00
Molar composition:		
Methane	-	0.9589
Ethane	-	0.0296
Propane	-	0.0072
N-butane	-	0.0006
Nitrogen	-	0.0037

The isentropic efficiency of the compressor was assumed to be constant $\eta_s = 0.80$, independent of the other process parameters. Since the objective has been to study the influence of irreversibilities caused by heat transfer across finite temperature

differences, pressure drop in heat exchangers was neglected. Since this cooling takes place at higher temperature levels with larger driving forces, the investment cost of the cooler is small compared to the main cryogenic heat exchanger (LNG-HX). The focus is therefore to balance the size of the main heat exchanger and the compressor power consumption.

In the main heat exchanger, the refrigerant is cooled to the same outlet temperature as the natural gas stream in order to provide the temperature level required for the cooling process ($T_4 = T_{II}$). Hence, the total cooling load in the process is composed of both the cooling load of the natural gas and the cooling load of the refrigerant. Since the operating conditions of the refrigerant are part of the design, so is the cooling load. The two hot streams are assumed to have the same temperature profile, and the overall heat transfer coefficient is assumed to be constant.

7.4.2 Simulation-optimization framework

The process was modelled and simulated in Aspen HYSYS® using the Peng-Robinson equation of state. The LNG heat exchanger was modelled with 100 intervals for each of the streams, divided into segments of equal enthalpy change.

For a given natural gas flow rate, the process flowsheet was optimized with the objective of minimizing the power consumption of the compressor. The sequential quadratic programming method NLPQLP was used for optimization, with derivatives estimated by finite forward differences with step length 10^{-4}. The results reported are the best solutions obtained in 25 or 50 searches (depending on the case) from randomly generated starting points within the variable bounds.

In total, eight degrees of freedom were available for the optimization of the process model, with the refrigerant assumed to be composed of potentially six different components; methane (C1), ethane (C2), propane (C3), iso-butane (iC4), normal-butane (nC4) and nitrogen (N2). In addition to individual molar flow rates for each of the refrigerant components, the low and high pressure levels were used as decision variables. Due to the fact that the process was optimized over a wide range of conditions (from very small heat exchanger size to very large heat exchanger size), the variable bounds were altered for the different cases in order to increase the likelihood of finding global optimal solutions. The objective of this study was to investigate the influence of the problem formulation on the thermodynamic performance of the process, not to examine the performance of the optimization algorithm.

A minimum superheating of 10 K was specified for the compressor suction stream as a safety measure to avoid liquid formation in the compressor. Four different

formulations were compared for the trade-off between operating cost and investment cost:

C1: Constant minimum temperature difference: $\Delta T \geq \Delta T_{min}$
C2: Minimum temperature difference linear with temperature: $\Delta T \geq c \cdot T$
C3: Minimum logarithmic mean temperature difference: $\Delta T_{LM} \geq \Delta T_{LM,min}$
C4: Maximum heat exchanger conductance: $UA \leq UA_{max}$

The logarithmic mean temperature difference is calculated as a weighted average of the logarithmic mean temperature difference for each of the segments in the heat exchanger, such that $\dot{Q} = UA \cdot \Delta T_{LM}$. For the constraints C3 and C4, an additional constraint requiring a positive temperature difference between the composite curves at all points in the heat exchanger ($\Delta T > 0$) was applied.

For all except the constraint formulation based on a maximum *UA* value, the heat exchanger *UA* value will be a result of the design optimization. Since the heat exchanger conductance is closely related to the cost of the heat exchanger, the different constraint formulations have been compared for the same value of *UA*. This way, the performance of the different constraint formulations is compared with respect to utilization of a given heat exchanger conductance (or heat exchanger size).

7.4.3 Results

In Table 7.4, results are presented from optimization of the simple PRICO® process using different values for minimum temperature difference (constraint formulation C1) and different values for maximum *UA* (constraint formulation C4). As mentioned in Section 7.4.2, the same value for *UA* has been used in the two cases (C1 and C4). It can be observed that significant savings in energy use can be obtained for the same heat exchanger cost (same *UA*) when constraint formulation C4 is used, and that these savings increase with increasing ΔT_{min} value.

Table 7.4. Comparison of power consumption.

$\Delta T \geq \Delta T_{min}$ (C1)			$UA \leq UA_{max}$ (C4)			
ΔT_{min} (K)	*UA* (MW/K)	$\dot{W}/\dot{n}_{NG}$ (MJ/kmol)	*UA* (MW/K)	ΔT_{small} (K)	$\dot{W}/\dot{n}_{NG}$ (MJ/kmol)	Savings (%)
1	59.2	14.2	59.2	0.51	14.0	1.7
2	31.5	15.6	31.5	0.78	15.0	4.0
3	20.2	16.9	20.2	1.07	15.9	5.9
4	14.8	18.3	14.8	1.26	16.8	8.1
5	11.4	19.6	11.4	1.45	17.6	10.4

In Fig. 7.8, the power consumption and heat exchanger conductance are given as functions of the minimum temperature difference for the best solution obtained using constraint formulation C1. As expected, and discussed in Chapter 3, the power consumption grows close to linearly with increasing minimum temperature difference, while the heat exchanger conductance is approximately inversely proportional to the minimum temperature difference.

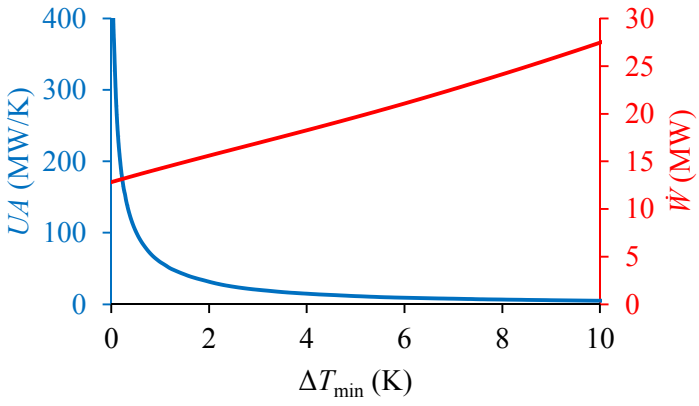

Figure 7.8. Power consumption (red) and resulting heat exchanger conductance (blue) as functions of the minimum temperature difference for the best solution found for constraint formulation C1.

In Fig. 7.9 (a), reductions in compression power when switching from constraint formulation C1 to each of the other three constraint formulations are plotted as functions of the heat exchanger conductance *UA*. As opposed to the case of the simple heat exchanger, the savings depend heavily on the heat exchanger size (or indirectly the value of the minimum temperature difference). For a small heat exchanger, significant savings are obtained, while for large heat exchangers the saving potential is moderate. For constraint formulation C2, a small increase in power consumption is actually observed for large *UA* values.

The largest savings in power consumption are found for constraint formulation C4, while the second best performance is observed for constraint formulation C3. For small values of the heat exchanger conductance, significant savings are evident also for the constraint formulation C2. The same results are plotted in Fig. 7.9 (b) with corresponding values for the minimum temperature difference constraint along the abscissa axis. The results indicate that for the minimum temperature difference values most commonly encountered in literature (1-3 K), the power consumption could be reduced by 2-5 % with optimal utilization of the heat exchanger conductance.

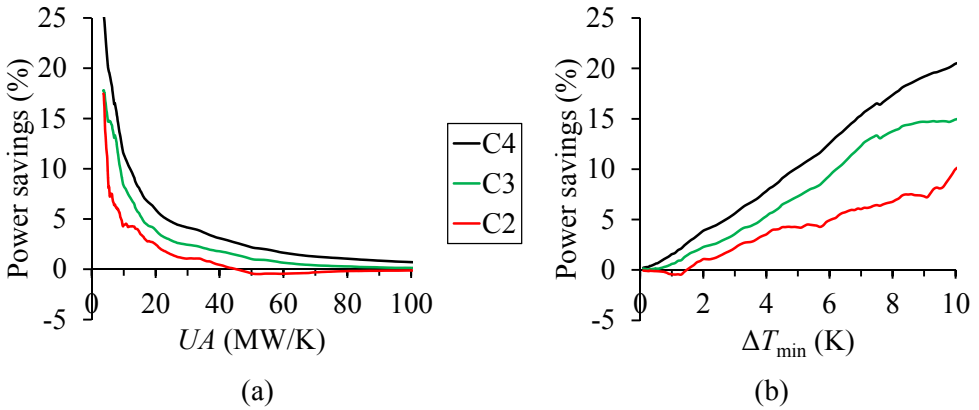

Figure 7.9. Reductions in compression power when switching from constraint formulation C1 to each of the other three formulations. (a) As function of heat exchanger conductance; (b) As function of the minimum temperature difference.

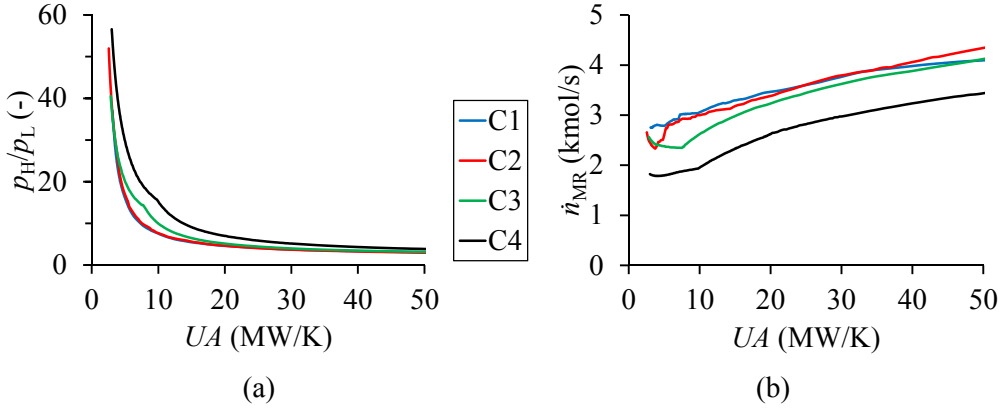

Figure 7.10. (a) Pressure ratio of the best solution found for the four different constraint formulations as function of the heat exchanger conductance; (b) Refrigerant flow rate of the best solution found for the four different constraint formulations as function of the heat exchanger conductance.

As can be observed in Fig. 7.10 (a), where the pressure ratio in the best solution found for the four different constraint formulations is plotted as function of the heat exchanger conductance, a significantly higher pressure ratio is obtained with constraint C4. A sudden change in slope is observed around $UA = 10$ MW/K for the curves representing constraint formulations C3 and C4. For smaller values of UA, the low pressure levels of the two solutions are at the lower bound. One may expect that an increased pressure ratio would lead to increased power consumption. However, as illustrated in Fig. 7.10 (b), this is compensated by a reduced refrigerant flow rate in design solutions resulting from constraint formulation C4. Despite very high pressure ratios, especially for small UA values, multi-stage compression has not been considered in this work.

The process power consumption comes as a result of a trade-off between refrigerant flow rate and pressure ratio. In general, as discussed in Chapter 3, the specific cooling

capacity of the refrigerant increases with increasing pressure ratio since the difference in specific heat capacity of the refrigerant cold stream and the refrigerant hot stream increases, and therefore the same cooling can be provided with a smaller flow rate. This is confirmed by the results given in Fig. 7.11 (a) where the total cooling loads of the best solutions are plotted as functions of heat exchanger conductance for the four different constraint formulations.

The irreversibilities of the heat transfer depend on the heat flow and the temperature driving forces. When the heat exchanger size is increased, the temperature driving forces are smaller, and a larger cooling load can be accepted. Hence, the trade-off is shifted towards higher refrigerant flow rate and smaller pressure ratio when the heat exchanger size increases (increasing *UA* value). This applies to all four constraint formulations.

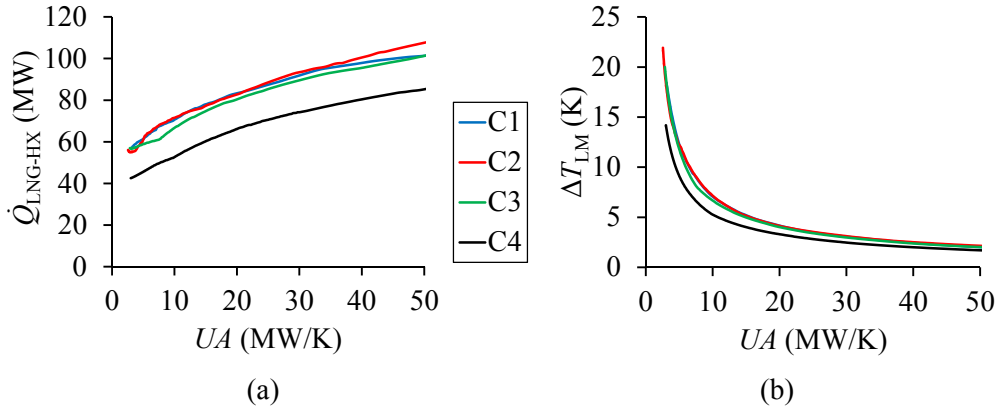

Figure 7.11. (a) Total heat exchanger cooling load of the best solution found for the four different constraint formulations as function of the heat exchanger conductance; (b) Logarithmic mean temperature difference of the best solution found for the four different constraint formulations as function of the heat exchanger conductance.

Due to the smaller flow rate but higher pressure ratio, the total cooling load is significantly smaller in the design solutions obtained for constraint formulation C4. With a smaller refrigerant flow rate, and thereby smaller cooling load, the same heat exchanger can be operated with a smaller temperature difference. This is confirmed by the results in Fig. 7.11 (b), which illustrates the logarithmic temperature difference in the heat exchanger for the four different constraint formulations.

Irreversibilities

As opposed to the simple heat exchanger studied in Section 7.3, the performance of the heat exchanger in an LNG process must be balanced with the performance of the other unit operations. In the following, the irreversibilities of the different pieces of equipment in the simple PRICO® process in Fig. 7.7 will be presented as function of

UA. Here, the irreversibilities in the natural gas throttle valve are not considered since they are given by the operating conditions and otherwise independent of the design.

The compressor irreversibilities are given in Fig. 7.12 (a) for the four different constraint formulations as functions of the heat exchanger conductance. Clearly, the reduced refrigerant flow rate has a greater impact than the increased pressure ratio, and the irreversibilities in the compressor are found to be significantly smaller for the solutions obtained with constraint formulation C4. A higher pressure ratio leads to a higher discharge temperature, which also means that the specific exergy of the compressor discharge stream is higher. For the other three constraint formulations (C1, C2 and C3), the compressor irreversibilities are quite similar, especially for large values of the heat exchanger conductance.

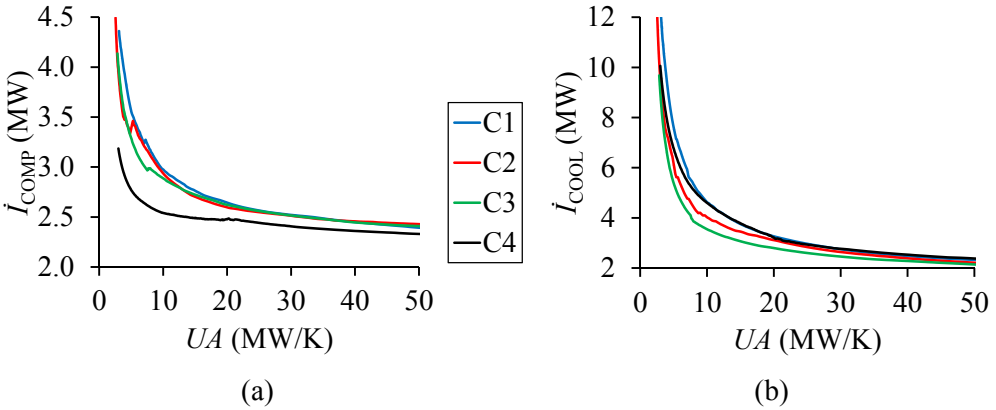

(a) (b)

Figure 7.12. (a) Irreversibilities in the compressor for the best solution found for the four different constraint formulations as function of the heat exchanger conductance; (b) Irreversibilities in the cooler for the best solution found for the four different constraint formulations as function of the heat exchanger conductance.

In the cooler, the heat of the compressor discharge stream is rejected to the ambient. Since the compressor discharge temperature, and thereby the exergy content, is higher for the design obtained for constraint formulation C4, the irreversibilities are relatively high despite a smaller flow rate. The irreversibilities observed in the cooler are given in Fig. 7.12 (b). The smallest irreversibilities are found in the design obtained from constraint formulation C3, while the largest irreversibilities are found for constraint formulation C1.

A distinct effect of reduced cooling load and temperature driving forces in the solutions obtained for constraint formulation C4 is observed for the heat exchanger irreversibilities given in Fig. 7.13 (a). For the other three constraint formulations, the heat exchanger irreversibilities are of comparable magnitude for the same heat exchanger size.

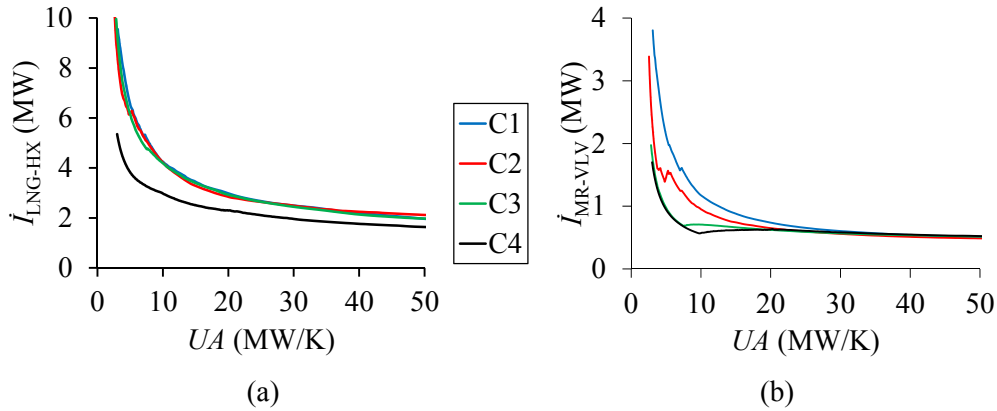

(a) (b)

Figure 7.13. (a) Irreversibilities in the LNG heat exchanger for the best solution found for the four different constraint formulations as function of the heat exchanger conductance; (b) Irreversibilities in the refrigerant throttle valve for the best solution found for the four different constraint formulations as function of the heat exchanger conductance.

The irreversibilities in the refrigerant throttle valve are given in Fig. 7.13 (b) for the different constraint formulations, as functions of the heat exchanger conductance. For small values of the heat exchanger conductance, significant reductions are found for the constraint formulations C3 and C4. For large heat exchangers, however, only small differences are observed between the different formulations.

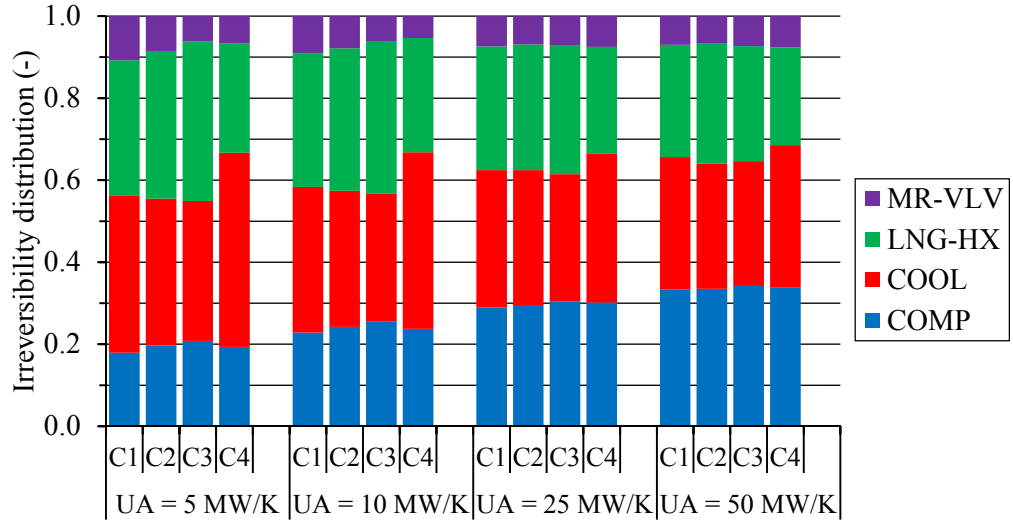

Figure 7.14. Irreversibility distribution between unit operations in the best solution obtained from the different constraint formulations for different *UA* values.

With the exception of a few disturbances, the irreversibilities in the compressor, cooler and heat exchanger decrease monotonically with increasing heat exchanger size for all the constraint formulations. In the throttling valve, however, a small increase in irreversibilities is observed for the constraint formulations C3 and C4 with growing

heat exchanger size from around 10 MW/K. The points at which the irreversibilities start growing coincide with the points at which the lower bound is reached for the low pressure level.

Within the range of heat exchanger sizes considered, the throttling valve contributes the least to the total irreversibilities for all the constraint formulations. The share of irreversibilities attributed the compressor increases with increasing heat exchanger size. Except for some minor disturbances for small *UA* values, the heat exchanger accounts for a smaller amount of the total irreversibilities when the heat exchanger size increases. The distribution of irreversibilities between the unit operations is illustrated in Fig. 7.14 for the best solutions obtained for selected *UA* values. Since the total irreversibilities are normalized for each case, Fig. 7.14 does not provide any information about the magnitude of the irreversibilities.

Composite curves

In addition to potential numerical noise in the thermodynamic model and the accuracy of the optimization approach, the noise observed in the results for variations in heat exchanger size is likely to be caused by switching between different local solutions. Even though the power consumption grows quite steadily with increasing values for the constraints C1, C2 and C3, different local solutions may have a distribution of the driving forces that leads to pronounced changes in heat exchanger conductance. This can be observed by examining the composite curves of the different solutions.

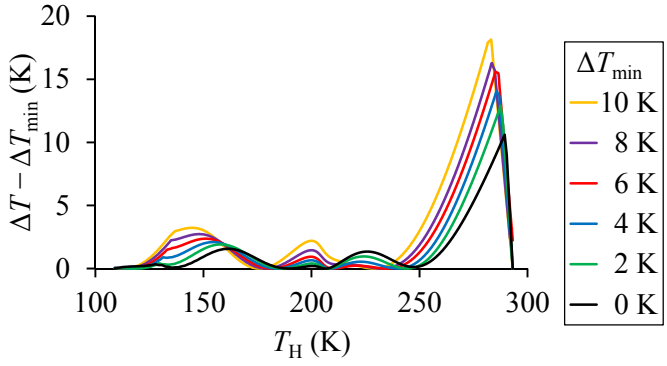

Figure 7.15. Temperature difference in the heat exchanger as function of hot stream temperature for the best solution found for different values of the minimum temperature difference.

In Fig. 7.15, the actual temperature difference between the composite curves minus the minimum temperature difference required is plotted as a function of the hot stream temperature. This is done for the best solution found for different values of ΔT_{min} in constraint formulation C1. Due to the nonlinearities in the temperature-enthalpy relations of the streams, a uniform temperature difference throughout the heat

exchanger cannot be obtained. In all cases, a relatively large temperature difference is observed in the warm end of the heat exchanger, related to the superheating of the refrigerant stream entering the compressor. For the cases of $\Delta T_{min} = 0$ K, $\Delta T_{min} = 2$ K, $\Delta T_{min} = 4$ K and $\Delta T_{min} = 6$ K, the shape of the curves is fairly similar. In the solutions found for $\Delta T_{min} = 8$ K and $\Delta T_{min} = 10$ K, however, the shape of composite curves is significantly different in the range 200-250 K.

The temperature difference between the composite curves is plotted as functions of the hot stream temperature for the four different constraint formulations in Fig. 7.16. In Fig. 7.16 (a) this is done for the solutions obtained for $UA = 5$ MW/K, while the results in Fig. 7.16 (b) represent the case of $UA = 50$ MW/K. As can be observed, the difference in results obtained for the different constraint formulations is more pronounced for the smallest heat exchanger size. It is also evident that the design obtained for constraint formulation C1 has a more uniform distribution of the temperature driving forces ΔT. The shape of the curves is quite similar for the constraint formulations C2 and C3, yet more smooth for C2. Due to the reduced cooling load, constraint formulation C4 provides a design with a smaller mean temperature difference.

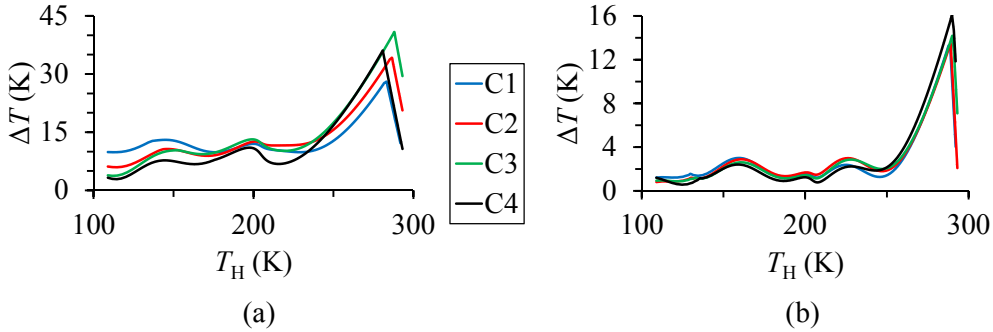

Figure 7.16. Temperature difference between the composite curves plotted as function of the hot stream temperature for the four constraint formulations. (a) With $UA = 5$ MW/K; (b) With $UA = 50$ MW/K.

When the heat exchanger area is small, the temperature driving forces are large. Since the area requirement is inversely proportional to the temperature difference, this means that local changes can be made to the temperature driving forces with relatively small impact on the overall heat exchanger size. For large heat exchangers, however, the temperature driving forces are small and a small adjustment in the temperature difference between the composite curves leads to significant changes in the heat exchanger size. In this case, there is less freedom to manipulate the composite curves in order to improve the process design. This is one of the reasons why the saving potential decreases with increasing heat exchanger size. One may notice that the sudden changes in slope observed around $T_H = 130$ K in Fig. 7.16 (b) are caused by a

phase change of the refrigerant hot stream, from two-phase vapour-liquid to sub-cooled liquid.

7.4.4 Comparisons

The results obtained for the four different constraint formulations illustrate three reasons why a uniform minimum temperature difference does not provide optimal utilization of heat exchanger area in a low-temperature refrigeration process.

First, the distribution of temperature driving forces is not optimal as a smaller temperature difference should be applied in the cold end of the heat exchanger and a larger temperature difference in the hot end. This is, however, accounted for in the three other constraint formulations.

Second, the nonlinearities of the composite curves in the heat exchanger are not accounted for. For a reasonable design, it is not possible to find a solution where the temperature driving force constraint is active at all points in the heat exchanger. With a constraint based on the logarithmic mean temperature difference, the restrictions on local temperature driving forces are relaxed. As long as the mean temperature difference is kept above a lower limit, the temperature difference at individual points in the heat exchanger is less important.

A smaller temperature difference in parts of the heat exchanger leads to disproportionate use of heat exchanger area in that region. Since this is not beneficial for the process design, a minimum logarithmic mean temperature difference constraint will indirectly lead to a distribution of the temperature driving forces where the temperature difference is close to a linear function of the absolute temperature. However, to better fit the composite curves, smaller temperature differences are accepted in parts of the heat exchanger, for instance where pinch points are observed for the composite curves. This effect is not accounted for in constraint formulations C1 and C2.

Finally, for a process such as the PRICO® process, the cooling load in the heat exchanger is a result of the design. Hence, if a solution with a smaller refrigerant flow rate and thereby smaller refrigerant cooling load is used, the heat exchanger conductance can be kept at the same level with smaller temperature driving forces. A constraint based on a maximum heat exchanger conductance takes into account the ratio of cooling load to mean driving forces, whereas a constraint based on a minimum logarithmic mean temperature difference only considers the aspect of the driving forces. The trade-off between cooling load and driving forces is only accounted for by constraint formulation C4.

The feasible set of an optimization problem is defined by its constraints. When compared for the same maximum *UA* value, the feasible sets for constraint formulations C1, C2 and C3 will be subsets of the feasible set for C4 since these constraints put additional restrictions on the design (in terms of the magnitude of the driving forces). Hence, the optimal solution of constraint formulation C4 will always be equal to or better than the optimal solution of the other three formulations. The constraint formulations C1 and C2 represent different subsets of the feasible set for C4, and for *UA* values close to the maximum defined they are disjoint sets since they require different distributions of the driving forces. Since constraint formulation C3 does not consider the distribution of driving forces but only the mean driving force, this constraint represents a larger feasible set than constraint formulations C1 and C2.

The constraint formulations are also important for the performance of the optimization search. As discussed in Chapter 3, the logarithmic mean temperature difference and the heat exchanger conductance are calculated as functions of the temperature difference at all the evaluation points in the heat exchanger. Instead of having one constraint for each evaluation point in the heat exchanger, information from all these points is gathered in one single constraint. This may lead to increased complexity of the optimization problem for constraint formulations C3 and C4. In addition, local temperature differences must be considered to ensure a positive driving force throughout the heat exchanger.

Since random initial solutions are used, the performance with respect to calculation time and success rate would vary from case to case. In order to get a general impression of the performance, however, the optimization search was repeated for six selected values of *UA*. This was done for all the four constraint formulations, using the same 100 randomly generated starting points and the same variable bounds. In the case of constraint formulations C1, C2 and C3, the constraint values where chosen such that the *UA* value of the best solution obtained would be close to the selected *UA* values. For constraint formulations C1 and C2, the final solution was found to be within 1 % of the best known for 50-80 of the runs, with the success rate increasing with increasing *UA* value. For constraint formulation C3, 30-60 % of the runs lead to a solution within 1 % of the best known, while for constraint formulation C4 the success rate was 10-20 %.

Among the successful runs, the average number of evaluations per search varies in the range 600-1300 between the different cases for constraint formulations C1 and C2. For constraint formulation C3, the average number of evaluations varies between 1100 and 1800 for the successful runs, while on average 1200-1900 evaluations are used for constraint formulation C4. The average number of function evaluations is smaller for the runs that do not succeed to get within 1 % of the best known solution. With most of

the time used for the Aspen HYSYS® simulation, one function evaluation takes from 0.1 to 0.3 seconds, varying in different regions of the search space.

7.5 Discussion

7.5.1 Conceptual LNG process design

The results presented in this study illustrate why a minimum temperature difference approach does not provide an optimal trade-off between operating and investment costs, irrespective of the value of the temperature difference. The penalty of using this approach depends on the operating conditions, but will always lead to non-optimal utilization of heat exchanger conductance. Of the four constraint formulations compared, only a constraint based on a maximum UA value leads to optimal utilization of the heat exchanger conductance. However, since the heat exchanger conductance is a property that is difficult to relate to, and the optimal value would depend considerably on the operating conditions, it is hard to set a value for optimal trade-off between operating and capital costs using UA.

Like the minimum temperature difference, the logarithmic mean temperature difference is a measure that is much easier to relate to than the heat exchanger conductance. Hence, for optimization of refrigeration processes where the cooling load is given, ΔT_{LM} would be a promising trade-off parameter candidate. The value should, however, be adjusted according to the operating temperature region of the process, since operating at lower temperature requires more energy input for the same heat transfer. Given necessary cost data, a simplified annual cost function as suggested by Jensen and Skogestad (2008) could be used for conceptual process design.

An alternative constraint formulation could be to introduce a value for the maximum heat exchanger conductance per unit of exergy load ($UA/\Delta\dot{E}_{NG}$). Such a constraint would enable optimal utilization of the heat exchanger conductance, yet still account for the fact that the trade-off between investment and capital costs will be shifted towards larger heat exchangers in processes operating at low temperature levels. The value of this constraint could then be based on previous experience with the optimal trade-off between capital and energy costs, which will vary for different industrial applications. For example, one would expect the unit cost of heat exchanger area to be higher for remote and offshore LNG production than for onshore base-load plants.

Alternatively, the maximum heat exchanger conductance could be given by a target exergy efficiency for the final design ψ_{target}. Since the rational exergy efficiency is given by the ratio between the exergy load of the natural gas and the power consumption (i.e. derived from Eq. (7.1)), the optimal trade-off between heat

exchanger area and power consumption ($UA/\dot{W}$) can be expressed through the target exergy efficiency and the exergy load of the natural gas ($\psi_{target} \cdot UA/\Delta\dot{E}_{NG}$).

In addition to serving as a trade-off parameter between operating and investment cost, Wahl et al. (2013) pointed out that the minimum temperature difference may also serve as a safety margin for the thermodynamic models. The temperature driving forces in LNG heat exchangers are very small, and accurate thermodynamic modelling is required to ensure feasibility in practical designs. It may, therefore, still be advantageous to include a minimum temperature difference constraint when other problem formulations based on mean logarithmic temperature difference, heat exchanger conductance or total annual cost are employed. The value of the minimum temperature difference may, however, be smaller than when used as a trade-off parameter.

Proper formulation of constraints would lead to better distribution of the temperature driving forces and thereby the utilization of heat exchanger area in the perspective of exergy of heat. A simplified heat exchanger model based on composite curves does, however, not take into account the effects of pressure drop and variations in heat transfer characteristics of the fluids.

7.5.2 Pressure drop

The importance of taking into consideration pressure drop in heat exchangers was pointed out by Del Nogal et al. (2008) and Zhu and Nie (2002) among others. Neglecting pressure drop in process design could lead to inaccurate prediction of the temperature profiles, with a non-optimal or practically infeasible design as a result (Del Nogal et al., 2008). In addition, pressure drop in heat exchangers contributes to exergy destruction.

Auracher (1984) found that exergy losses due to flow friction increase with decreasing temperature level. Hence, minimization of pressure losses is of particular importance in low-temperature applications and could be important for the optimal trade-off between capital and operating costs. In general, pressure drop and thereby the cost of pumps and compressors is reduced for increasing values of the minimum temperature difference (Zhu and Nie, 2002). Thus, when pressure drop is considered in the design trade-off in addition to heat exchanger area and utility consumption, a larger optimal minimum temperature difference is expected. This may lead to significantly different network structures and costs (Zhu and Nie, 2002).

Cornelissen and Hirs (1997) pointed out the trade-off between exergy savings in operation of a heat exchanger and the exergy required for construction. Manjunath and Kaushik (2014) provided a review of thermodynamic studies of heat exchangers

considering exergy losses due to heat transfer, fluid friction, materials and manufacturing. Agrawal and Woodward (1991) found the exergy loss due to pressure drop to be larger than the losses due to heat transfer in the main heat exchanger of a cryogenic nitrogen generator.

In a short-cut solution used by Del Nogal et al. (2008), the pressure drop was estimated by a pre-defined fixed value and modelled as a linear function of the hot stream temperature in the heat exchanger. A similar approach was taken by Aspelund et al. (2010). According to Del Nogal et al. (2008), accurate pressure drop estimation would require use of detailed heat exchanger models. This is essential also in order to account for variations in heat transfer characteristics.

7.5.3 Rigorous heat exchanger modelling

As pointed out by Haug-Warberg (2000), Xu (1997) and Chang et al. (2011) among others, differences in heat transfer properties must also be taken into account when determining the temperature profile for minimum irreversibilities in heat transfer.

Altering the temperature profiles in a heat exchanger leads to changes in the heat transfer coefficient of the heat exchanger, which may drastically change entropy production (Balkan, 2005). If the difference in inlet and outlet temperature for a stream in the heat exchanger is reduced, a higher flow rate is required to provide the same heat transfer. With a higher flow rate, the heat transfer coefficient is improved, especially if fluid resistance dominates the heat transfer rate (Balkan, 2005). Hence, the temperature driving forces and thereby the entropy production can be reduced. The opposite holds if the temperature range is increased (Balkan, 2005). When altering the design of a two-stream heat exchanger to obtain equipartition of entropy production, assuming that both streams can be changed, Balkan (2005) proposed to make the changes for the stream that will experience an increase in the flow rate.

Chang et al. (2012) found the assumption of a uniform temperature profile for the hot and cold streams of a multi-stream heat exchanger to be hard to realize in practice. A simplified heat exchanger model assuming identical temperature profiles for the two hot streams was compared with a model in which the overall heat transfer coefficients were assumed different (but constant) for the two streams. The simplified model represents an upper limit on performance (exergy efficiency). Chang et al. (2012) argue, however, that this limit can be closely approached with proper heat exchanger design.

More advanced heat exchanger models have also been applied for different LNG applications. Afrianto et al. (2014) presented a computational fluid dynamics study of a shell and tube heat exchanger for LNG regasification. Based on operational data,

Hasan et al. (2009) proposed a mixed-integer nonlinear programming (MINLP) approach to predict the operational performance of multi-stream heat exchangers. According to the authors, the model is independent of the heat exchanger type, and therefore applicable for both plate-fin, spiral-wound and shell-and-tube heat exchangers. Kamath et al. (2012) used an equation-oriented approach for the modelling of the heat exchanger.

Skaugen et al. (2010, 2013) have presented a modelling framework for multi-stream heat exchangers. Applied to the heat exchanger in a single mixed-refrigerant LNG process, the results indicated large variations in local heat transfer coefficients and thereby variation in the temperatures of the two hot streams (Skaugen et al., 2013). Skaugen et al. (2010) found an LNG process design based on simplified heat exchanger models to be prone to unstable operation, and that measures reducing the risk of Ledinegg instability would inevitably lead to increased power consumption.

The drawback of rigorous heat exchanger modelling is increased computational effort and increased complexity of the optimization problem (Del Nogal et al., 2008). Hence, the accuracy and complexity of both process and unit models must be weighed against each other. A simplified optimization problem may be solved to global optimality, but this is insignificant if a non-optimal solution found for an advanced model turns out to provide better performance in the real application.

7.6 Conclusions

The results presented in this work illustrate the importance of optimal utilization of heat exchanger area in low-temperature applications. Comparison of various proposed design principles indicates that for optimal distribution of the temperature driving forces, the temperature difference should be proportional to the absolute temperature at which heat is transferred. This is equivalent to a uniform distribution of entropy production per unit of area. The importance of optimal distribution of temperature driving forces increases with decreasing temperature level and increasing temperature range of operation.

Four different constraint formulations were tested and compared as trade-off parameter to balance investment and operating cost in LNG process design. The commonly used minimum temperature approach is found not to be a suitable since it leads to non-optimal utilization of the heat exchanger conductance. Three reasons have been identified explaining the inadequacy of $\Delta T_{\min}$ as a trade-off parameter; (1) distribution of driving forces with respect to temperature level, (2) nonlinearity of composite curves, and (3) trade-off between driving forces and heat load. The last point applies to process concepts where the refrigerant itself is cooled and the total cooling load

therefore is a function of the design. Only a specification based on a maximum *UA* value was found to accommodate all these three aspects.

A simple heat exchanger model assuming uniform heat transfer properties and temperature profiles does not account for the characteristics of multi-stream heat exchangers. Hence, for more accurate design, rigorous heat exchanger models are required. The accuracy of complex heat exchanger models comes with an increased computational effort and increased complexity of the optimization problem. A simple heat exchanger model may therefore be useful in the initial design phase locating promising starting points for optimization of the rigorous model.

7.7 References

Afrianto H, Tanshen MR, Munkhbayar B, Suryo UT, Chung H, Jeong H. A numerical investigation on LNG flow and heat transfer characteristic in heat exchanger. *International Journal of Heat and Mass Transfer* 2014;68:110-118.

Agrawal R, Woodward DW. Efficient cryogenic nitrogen generators: An exergy analysis. *Gas Separation and Purification* 1991;5(3):139-150.

Ahmad S, Linnhoff B, Smith R. Cost optimum heat exchanger networks – 2. Targets and design for detailed capital cost models. *Computers and Chemical Engineering* 1990;14(7):751-767.

Alabdulkarem A, Mortazavi A, Hwang Y, Radermacher R, Rogers P. Optimization of propane pre-cooled mixed refrigerant LNG plant. *Applied Thermal Engineering* 2011;31(6-7):1091-1098.

Aspelund A, Gundersen T, Myklebust J, Nowak MP, Tomasgard A. An optimization-simulation model for a simple LNG process. *Computers and Chemical Engineering* 2010;34(10):1606-1617.

Auracher H. Fundamental Aspects of Exergy Application to the analysis and optimization of energy processes. *Heat Recovery Systems* 1984;4(5):323-327.

Balkan F. Comparison of entropy minimization principles in heat exchange and a short-cut principle: EoTD. *International Journal of Energy Research* 2003;27(11):1003-1014.

Balkan F. Application of EoEP principle with variable heat transfer coefficient in minimizing entropy production in heat exchangers. *Energy Conversion and Management* 2005;46(13-14):2134-2144.

Bejan A. A General Variational principle for thermal insulation system design. *International Journal of Heat and Mass Transfer* 1979;22(2):219-228.

Bejan A. Method of entropy generation minimization, or modeling and optimization based on combined heat transfer and thermodynamics. *Revue Generale de Thermique* 1996;35(418-419):637-646.

Bejan A. *Advanced Engineering Thermodynamics*. 2nd ed. New York: John Wiley & Sons; 1997.

Castillo L, Dorao CA. Consensual decision-making model based on game theory for LNG processes. *Energy Conversion and Management* 2012;64:387-396.

Chang H-M, Chung MJ, Lee S, Choe KH. An efficient multi-stage Brayton-JT cycle for liquefaction of natural gas. *Cryogenics* 2011;51(6):278-286.

Chang H-M, Lim HS, Choe KH. Effect of multi-stream heat exchanger on performance of natural gas liquefaction with mixed refrigerant. *Cryogenics* 2012;52(12):642-647.

Colberg RD, Morari M. Area and Capital Cost Targets for Heat Exchanger Network Synthesis with Constrained Matches and Unequal Heat Transfer Coefficients. *Computers and Chemical Engineering* 1990;14(1):1-22.

Cornelissen RL, Hirs GG. Exergetic optimisation of a heat exchanger. *Energy Conversion and Management* 1997;38(15-17):1567-1576.

Del Nogal F, Kim J-K, Perry S, Smith R. Optimal design of mixed refrigerant cycles. *Industrial and Engineering Chemistry Research* 2008;47(22):8724-8740.

Del Nogal FL, Kim J-K, Perry S, Smith R. Synthesis of mechanical driver and power generation configurations, Part 2: LNG applications. *AIChE Journal* 2010;56(9):2377-2389.

Fodor Z. Klemeš JJ, Varbanov PS, Walmsley MRW, Atkins MJ, Walmsley TG. Total site targeting with stream specific minimum temperature difference. *Chemical Engineering Transactions* 2012;29:409-414.

Fodor Z, Varbanov PS, Klemeš JJ. Total site targeting accounting for individual process heat transfer characteristics. *Chemical Engineering Transactions* 2010;21:49-54.

Fraser DM. The use of minimum flux instead of minimum approach temperature as a design specification for heat exchanger networks. *Chemical Engineering Science* 1989;44(5):1121-1127.

Fredheim AO. *Thermal Design of Coil-Wound LNG Heat Exchangers – Shell-Side Heat Transfer and Pressure Drop* [dissertation]. Trondheim, Norway: The University of Trondheim, The Norwegian Institute of Technology, Department of Refrigeration Engineering; 1994.

Hall SG, Ahmad S, Smith R. Capital cost targets for heat exchanger networks comprising mixed materials of construction, pressure ratings and exchanger types. *Computers and Chemical Engineering* 1990;14(3):319-335.

Hasan MMF, Jayaraman G, Karimi IA. Synthesis of heat exchanger networks with nonisothermal phase changes. *AIChE Journal* 2010;56(4):930-945.

Hasan MMF, Karimi IA, Alfadala HE, Grootjans H. Operational modeling of multistream heat exchangers with phase changes. *AIChE Journal* 2009;55(1):150-171.

Hatcher P, Khalilpour R, Abbas A. Optimisation of LNG mixed-refrigerant processes considering operation and design objectives. *Computers and Chemical Engineering* 2012;41:123-133.

Haug-Warberg T. Comments on "Equipartition of forces: A new principle for process design and optimization". *Industrial and Engineering Chemistry Research* 2000;39(11):4431-4433.

He T, Ju Y. Design and optimization of a novel mixed refrigerant cycle integrated with NGL recovery process for small-scale LNG plant. *Industrial and Engineering Chemistry Research* 2014;53(13):5545-5553.

Jacobsen MG, Skogestad S. Active constraint regions for a natural gas liquefaction process. *Journal of Natural Gas Science and Engineering* 2013;10:8-13.

Jegede FO, Polley GT. Capital cost targets for networks with non-uniform heat exchanger specifications. *Computers and Chemical Engineering* 1992;16(5):477-495.

Jensen JB, Skogestad S. Problems with specifying ΔT_{min} in the design of processes with heat exchangers. *Industrial and Engineering Chemistry Research* 2008;47(9):3071-3075.

Jin Z-L, Chen X-T, Wang Y-Q, Liu M-S. Heat exchanger network synthesis based on environmental impact minimization. *Clean Technologies and Environmental Policy* 2014;16(1):183-187.

Johannessen E, Nummedal L, Kjelstrup S. Minimizing the entropy production in heat exchange. *International Journal of Heat and Mass Transfer* 2002;45(13):2649-2654.

Kamath RS, Biegler LT, Grossmann IE. Modeling multistream heat exchangers with and without phase changes for simultaneous optimization and heat integration. *AIChE Journal* 2012;58(1):190-204.

Kemp IC. *Pinch Analysis and Process Integration: a user guide on process integration for the efficient use of energy*. 2nd ed. Oxford: Butterworth-Heinemann; 2007.

Khan MS, Lee M. Design optimization of single mixed-refrigerant natural gas liquefaction process using the particle swarm paradigm with nonlinear constraints. *Energy* 2013;49(1):146-155.

Khan MS, Lee S, Lee M. Optimization of single mixed refrigerant natural gas liquefaction plant with nonlinear programming. *Asia-Pacific Journal of Chemical Engineering* 2012;7(Suppl. 1):S62-S70.

Kjelstrup S, Bedeaux D, Sauar E. Minimum entropy production by equipartition of forces in irreversible thermodynamics. *Industrial and Engineering Chemistry Research* 2000;39(11):4434-4436.

Kjelstrup S, Sauar E, Lien KM. Equipartition of forces: Review of a new principle for process design and optimization. *Periodica Polytechnica: Chemical Engineering* 1998;42(2):103-114.

Kotas TJ. *The Exergy Method of Thermal Plant Analysis*. Malabar: Krieger Publishing Company; 1995.

Lee I, Tak K, Kwon H, Kim J, Ko D, Moon I. Design and optimization of a pure refrigerant cycle for natural gas liquefaction with subcooling. *Industrial and Engineering Chemistry Research* 2014;53(25):10397-10403.

Lee S, Long NVD, Lee M. Design and optimization of natural gas liquefaction and recovery processes for offshore floating liquefied natural gas plants. *Industrial and Engineering Chemistry Research* 2012;51(30):10021-10030.

Li Y, Motard RL. Optimal pinch approach temperature in heat-exchanger networks. *Industrial and Engineering Chemistry Fundamentals* 1986;25(4):577-581.

Linnhoff B, Ahmad S. Cost optimum heat exchanger networks – 1. Minimum energy and capital using simple models for capital cost. *Computers and Chemical Engineering* 1990;14(7):729-750.

Linnhoff B, Flower JR. Synthesis of heat exchanger networks: I. Systematic generation of energy optimal networks. *AIChE Journal* 1978;24(4):633-642.

Linnhoff B, Hindmarsh E. The pinch design method for heat exchanger networks. *Chemical Engineering Science* 1983;38(5):745-763.

Linnhoff B, Mason DR, Wardle I. Understanding heat exchanger networks. *Computers and Chemical Engineering* 1979:3(1-4):295-302.

Manjunath K, Kaushik SC. Second law thermodynamic study of heat exchangers: A review. *Renewable and Sustainable Energy Reviews* 2014;40:348-374.

Morin A, Wahl PE, Mølnvik M. Using evolutionary search to optimise the energy consumption for natural gas liquefaction. *Chemical Engineering Research and Design* 2011;89(11):2428-2441.

Nishimura H. A Theory of the optimal synthesis of heat-exchanger systems. *Journal of Optimization Theory and Applications* 1980;30(3):423-450.

Nummedal L, Kjelstrup S. Equipartition of forces as a lower bound on the entropy production in heat exchange. *International Journal of Heat and Mass Transfer* 2001;44(15):2827-2833.

Rev E, Fonyo Z. Diverse pinch concept for heat exchange network synthesis: The case of different heat transfer conditions. *Chemical Engineering Science* 1991;46(7):1623-1634.

Saboo AK, Morari M. Design of resilient processing plants – IV. Some new results on heat exchanger network synthesis. *Chemical Engineering Science* 1984;39(3):579-592.

Sauar E, Kjelstrup S, Lien KM. Rebuttal to Comments on "Equipartition of forces: A new principle for process design and optimization". *Industrial and Engineering Chemistry Research* 1997;36(11):5045-5046.

Sauar E, Ratkje SK, Lien KM. Equipartition of forces: A new principle for process design and optimization. *Industrial and Engineering Chemistry Research* 1996;35(11):4147-4153.

Shah NM, Hoadley AFA, Rangaiah GP. Inherent safety analysis of a propane precooled gas-phase liquified natural gas process. *Industrial and Engineering Chemistry Research* 2009;48(10):4917-4927.

Shirazi MMH, Mowla D. Energy optimization for liquefaction process for natural gas in peak shaving plant. *Energy* 2010;35(7):2878-2885.

Skaugen G, Gjøvåg, GA, Nekså P, Wahl PE. Use of sophisticated heat exchanger simulation models for investigation of possible design and operational pitfalls in LNG processes. *Journal of Natural Gas Science and Engineering* 2010;2(5):235-243.

Skaugen G, Kolsaker K, Walnum HT, Wilhelmsen Ø. A flexible and robust modelling framework for multi-stream heat exchangers. *Computers and Chemical Engineering* 2013;49:95-104.

Smith R. *Chemical Process Design and Integration*. Chichester: John Wiley & Sons; 2005.

Taal M, Bulatov I, Klemeš J, Stehlík P. Cost estimation and energy price forecasts for economic evaluation of retrofit projects. *Applied Thermal Engineering* 2003;23(14):1819-1835.

Taleshbahrami H, Saffari H. Optimization of the C3MR Cycle with genetic algorithm. *Transactions of the Canadian Society for Mechanical Engineering* 2010;34(3-4):433-448.

Thiel GP, McGovern RK, Zubair SM, Lienhard V, JH. Thermodynamic equipartition for increased second law efficiency. *Applied Energy* 2014;118:292-299.

Tondeur D. Equipartition of entropy production: A design and optimization criterion in chemical engineering. In: Sieniutycz S, Salamon P, editors. Finite-Time Thermodynamics and Thermoeconomics. New York: Taylor & Francis; 1990. p. 175-208.

Tondeur D, Kvaalen E. Equipartition of entropy production. An optimality criterion for transfer and separation processes. *Industrial and Engineering Chemistry Research* 1987;26(1):50-56.

Trivedi KK, O'Neill BK, Roach JR, Wood RM. A new dual-temperature design method for the synthesis of heat exchanger networks. *Computers and Chemical Engineering* 1989;13(6):667-685.

Varbanov PS, Fodor Z, Klemeš JJ. Total Site targeting with process specific minimum temperature difference (ΔT_{min}). *Energy* 2012;44(1):20-28.

Wahl PE, Løvseth SW, Mølnvik MJ. Optimization of a simple LNG process using sequential quadratic programming. *Computers and Chemical Engineering* 2013;56:27-36.

Wang M, Khalilpour R, Abbas A. Operation optimization of propane precooled mixed refrigerant processes. *Journal of Natural Gas Science and Engineering* 2013;15:93-105.

Wang M, Zhang J, Xu Q. Optimal design and operation of a C3MR refrigeration system for natural gas liquefaction. *Computers and Chemical Engineering* 2012;39:84-95.

Wang M, Zhang J, Xu Q, Li K. Thermodynamic-analysis-based energy consumption minimization for natural gas liquefaction. *Industrial and Engineering Chemistry Research* 2011;50(22):12630-12640.

Wen Y, Shonnard DR. Environmental and economic assessments of heat exchanger networks for optimum minimum approach temperature. *Computers and Chemical Engineering* 2003;27(11):1577-1590.

Xu J. Comments on "Equipartition of forces: A new principle for process design and optimization". *Industrial and Engineering Chemistry Research* 1997;36(11):5040-5044.

Xu X, Liu J, Cao L. Optimization and analysis of mixed refrigerant composition for the PRICO natural gas liquefaction process. *Cryogenics* 2014;59:60-69.

Xu X, Liu J, Jiang C, Cao L. The correlation between mixed refrigerant composition and ambient conditions in the PRICO LNG process. *Applied Energy* 2013;102:1127-1136.

Yoon S, Cho H, Lim D-H, Kim J-K. Process design and optimization of natural gas liquefaction processes. *Chemical Engineering Transactions* 2012;29:1585-1590.

Zhu XX, Nie XR. Pressure drop consideration for heat exchanger network grassroots design. *Computers and Chemical Engineering* 2002;26(12):1661-1676.

8 Design Strategy

The challenge of LNG process optimization increases with the complexity of the process. When the optimization method used in this work is applied to more complex process concepts, the success rate drops while the search time increases. Therefore, in this chapter, measures are proposed for possible simplification and improvement of the optimization approach.

For a given load distribution, the characteristics of cascade LNG processes indicate that the operating conditions of a vertical stage is independent of the configurations of all vertical stages operating at higher temperature levels. Based on this, an approach has been proposed for optimization of cascade processes where the load distribution is optimized in an outer loop and the different refrigeration cycles are optimized sequentially in an inner loop, starting with the cycle operating at the lowest temperature level. Due to the interaction between the vertical stages, the operating conditions of preceding refrigeration cycles (i.e. cycles at higher temperatures) should be taken into account when optimizing the different cycles. A case study has been performed for a dual mixed-refrigerant process to illustrate the framework of the suggested procedure.

In processes with multi-stage compression with intercooling, the number of decision variables could be reduced by using heuristic rules to estimate optimal intermediate pressure levels. The common approach of using the geometric mean for intermediate pressure levels has been found to give increased power consumption when the suction temperature of the different compression stages is different. For compression with constant isentropic efficiency, a new approach for estimation of the optimal intermediate pressure levels has been proposed, based on the results presented in Chapter 5. For optimization of the sub-cooling cycle in a dual-mixed refrigerant process, the new estimate resulted in a penalty in compression power smaller than 0.01 % for the cases where the underlying assumptions hold.

8.1 Introduction

As was discussed in Chapter 2, relatively few studies on optimization of complex process concepts for liquefaction of natural gas are available in the literature. Except for single-stage processes such as PRICO®, most optimization studies related to LNG involves different propane-precooled mixed-refrigerant processes. These processes use two vertical stages, yet the number of horizontal stages varies between the different studies. In Chapter 6, it was indicated that pure-refrigerant processes are simpler than mixed-refrigerant processes, in the sense that the number of degrees of freedom is smaller and the complex thermodynamic characteristics of evaporation and condensation of a mixed-refrigerant is avoided. Hence, propane-precooled mixed-refrigerant processes may be considered to be easier to optimize than cascade processes using mixed-refrigerants in more than one vertical stage.

Alabdulkarem et al. (2011) minimized the power consumption of a propane-precooled mixed-refrigerant process using a sequential approach. In the first step, the compression power in the mixed-refrigerant cycle was minimized subject to a maximum cooling load in the propane cycle (the heat removed from the mixed-refrigerant by the propane refrigeration cycle varies with the design). The choice of value for this maximum cooling load was not given. Nor was the load division between the two refrigeration cycles (intermediate natural gas temperature) discussed. The power consumption of the propane cycle was minimized in the second step, with the conditions of the mixed-refrigerant cycle given as the best solution found in the first step.

Wang et al. (2011) also performed optimization of a propane-precooled mixed-refrigerant process. From the description, it seems like only the pressure ratio for each of the compressors in the process were used as decision variables. A simultaneous approach to optimization of a propane-precooled mixed-refrigerant was taken by Wang et al. (2013), considering all decision variables at the same time.

Hatcher et al. (2012) and Wang et al. (2012) optimized only the mixed-refrigerant cycle in a propane-precooled process. As was discussed in Chapter 6, Mortazavi et al. (2010, 2012), Castillo and Dorao (2013), Castillo et al. (2013) and Lee et al. (2014) studied different alternatives for the precooling cycle in cascade refrigeration processes. Taleshbahrami and Saffari (2010) performed optimization of a process with three vertical stages, a propane-precooling stage followed by two mixed-refrigerant cycles. The composition of the two mixed-refrigerants (with three components each) and the flow rate of the three refrigerants were optimized using a genetic algorithm.

Optimization studies of different process concepts with two vertical stages using mixed-refrigerants have also been presented. Morin et al. (2011) and Hwang et al.

(2013a, 2013b) performed optimization of dual mixed-refrigerant concepts considering all decision variables simultaneously. In order to identify interesting regions of the search space, Hwang et al. (2013a, 2013b) used a stochastic search method (genetic algorithms) in the initial phase of the optimization search.

In this work, different approaches have been proposed for simplification of the optimization problem, with the purpose of enabling design optimization of more complex process concepts.

8.2 Cascade process design

Based on the results obtained for the pure-refrigerant cascade processes in Chapter 6, a design strategy for sequential design of the different vertical stages in cascade refrigeration process has been developed.

8.2.1 Optimization search performance

In order to motivate the use of simplified design approaches, the performance of the NLPQLP search is compared for mixed-refrigerant processes with one, two and three vertical stages. Each process was modelled with one horizontal stage in each vertical stage, and optimized with different variable bounds to study the effect of limiting the search space. All processes were modelled in Aspen HYSYS® using the Soave-Redlich-Kwong equation of state.

Properties for the natural gas stream are given in Table 8.1, again based on the case study presented by Aspelund et al. (2010). The target temperature is given such that after throttling to the product pressure 1.05 bar, the natural gas stream will be saturated liquid. The throttling of the natural gas stream is not included in the flowsheet drawings. Optimization was performed assuming a constant isentropic efficiency $\eta_s = 0.80$ for all compressors and a minimum temperature difference $\Delta T_{\min} = 2$ K.

Table 8.1. Natural gas properties.

Property	Unit	Value
Molar flow rate	kmol/s	1.00
Feed temperature	K	293.15
Target temperature	K	109.10
Molar composition:		
Methane	-	0.9589
Ethane	-	0.0296
Propane	-	0.0072
N-butane	-	0.0006
Nitrogen	-	0.0037

Each of the processes has been optimized with four different choices for the variable bounds. Since the wide variable bounds require little or no knowledge of the location of the optimal solution, the search region is relatively large. Another set of variable bounds has been used, with the same bounds but only the components present in the best known solution used as decision variables. The narrow variable bounds suggested are based on the best known solution. A set of medium variable bounds, somewhere in between the wide and narrow bounds, has also been tested.

The medium and narrow variable bounds are both based on the best known solution and therefore require knowledge of the process characteristics. Notice, however, that the best known solution, around which the narrow variables bounds have been set, is not guaranteed to be the global optimal solution. This especially applies to the processes with three vertical stages, where the best known solution has been found by gradually refining the search by trial and error.

Wider bounds for the pressure levels could have been achieved by replacing the variables used for the high pressure levels (or the low pressure levels for that matter) with variables for the pressure ratios of the two compressors. In order to avoid the possibility of zero refrigerant flow rate, which would cause problems for the process simulation, the lower bound on one of the refrigerant component flow rates in each cycle was set to a value larger than zero. This was done for refrigerant components likely to be present in the mixtures.

One vertical stage

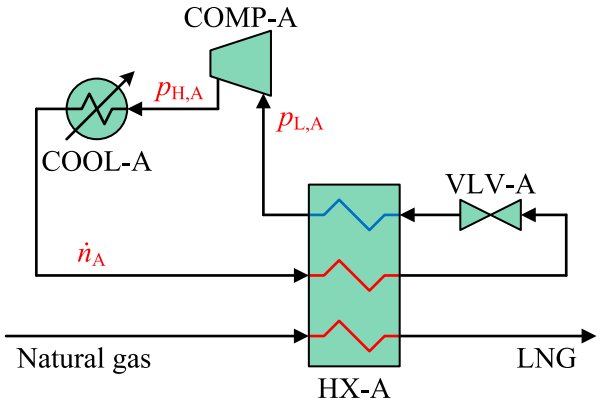

Figure 8.1. Mixed-refrigerant process with one vertical stage.

A flowsheet for a mixed-refrigerant process with one vertical stage (the PRICO® process) is given in Fig. 8.1. The decision variables used for this process are, as before, the low and high pressure levels of the refrigerant and the component flow rates. The

variables (eight in total), sets of variable bounds and the best known solution are listed in Table 8.2.

Table 8.2. Decision variables for optimization of mixed-refrigerant process with one vertical stage with different choices of variables bounds and best known solution.

		Wide		Component		Medium		Narrow		
Variable	Unit	LB	UB	LB	UB	LB	UB	LB	UB	Best
$p_{L,A}$	bar	1.0	7.0	1.0	7.0	1.0	5.0	1.0	5.0	3.46
$p_{H,A}$	bar	8.0	50.0	8.0	50.0	8.0	30.0	10.0	20.0	15.50
$\dot{n}_{A,C1}$	kmol/s	0.00	2.00	0.00	2.00	0.50	1.50	0.75	1.25	0.932
$\dot{n}_{A,C2}$	kmol/s	0.10	2.00	0.10	2.00	0.50	1.50	1.00	1.50	1.236
$\dot{n}_{A,C3}$	kmol/s	0.00	2.00	-	-	0.00	1.00	-	-	-
$\dot{n}_{A,nC4}$	kmol/s	0.00	2.00	0.00	2.00	0.50	1.50	0.75	1.25	0.940
$\dot{n}_{A,iC4}$	kmol/s	0.00	2.00	-	-	0.00	1.00	-	-	-
$\dot{n}_{A,N2}$	kmol/s	0.00	2.00	0.00	2.00	0.00	1.00	0.10	0.50	0.334

Two vertical stages

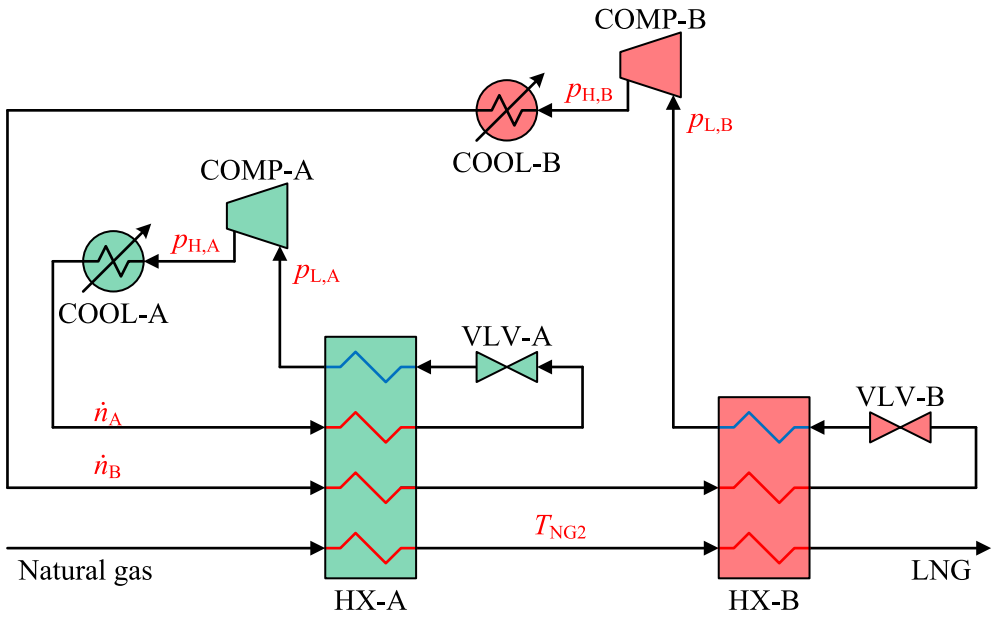

Figure 8.2. Mixed-refrigerant cascade process with two vertical stages.

A process with two vertical stages (DMR) is illustrated in Fig. 8.2. In total, there are 17 degrees of freedom left for the optimization. Here, the low and high pressure level for each of the refrigerants, the molar flow rates of each refrigerant component in each

cycle (six potential components in each refrigerant mixture) and the intermediate temperature level of the natural gas stream were used as decision variables. The decision variables are given in Table 8.3 for different choices of variable bounds, with the best known solution in the rightmost column. Since it cannot be guaranteed that the best known solution is the global optimal solution, there is no guarantee that the global optimum is located within the variable bounds.

Table 8.3. Decision variables for optimization of a mixed-refrigerant process with two vertical stages with different choices of variable bounds and best known solution.

		Wide		Component		Medium		Narrow		
Variable	Unit	LB	UB	LB	UB	LB	UB	LB	UB	Best
T_{NG2}	K	140	270	140	270	220	250	230	240	236.3
$p_{L,A}$	bar	1.0	3.0	1.0	3.0	1.0	3.0	1.5	2.5	2.25
$p_{H,A}$	bar	4.0	50.0	4.0	50	4.0	10.0	4.0	6.0	5.04
$p_{L,B}$	bar	1.0	5.0	1.0	5.0	1.0	3.0	1.0	2.0	1.00
$p_{H,B}$	bar	6.0	50.0	6.0	50	8.0	20.0	10.0	15.0	12.52
$\dot{n}_{A,C1}$	kmol/s	0.00	2.00	0.00	2.00	0.00	0.50	0.00	0.10	0.005
$\dot{n}_{A,C2}$	kmol/s	0.10	2.00	0.10	2.00	0.10	1.00	0.30	0.50	0.400
$\dot{n}_{A,C3}$	kmol/s	0.00	2.00	0.00	2.00	0.10	1.00	0.20	0.40	0.318
$\dot{n}_{A,nC4}$	kmol/s	0.00	2.00	0.00	2.00	0.50	1.50	0.85	1.05	0.951
$\dot{n}_{A,iC4}$	kmol/s	0.00	2.00	-	-	0.00	1.50	-	-	-
$\dot{n}_{A,N2}$	kmol/s	0.00	2.00	-	-	0.00	0.20	-	-	-
$\dot{n}_{B,C1}$	kmol/s	0.00	2.00	0.00	2.00	0.20	1.00	0.30	0.50	0.428
$\dot{n}_{B,C2}$	kmol/s	0.10	2.00	0.10	2.00	0.20	1.00	0.35	0.55	0.461
$\dot{n}_{B,C3}$	kmol/s	0.00	2.00	0.00	2.00	0.10	0.50	0.10	0.30	0.200
$\dot{n}_{B,nC4}$	kmol/s	0.00	2.00	-	-	0.00	0.50	-	-	-
$\dot{n}_{B,iC4}$	kmol/s	0.00	2.00	0.00	2.00	0.00	0.50	0.05	0.25	0.180
$\dot{n}_{B,N2}$	kmol/s	0.00	2.00	0.00	2.00	0.01	0.20	0.05	0.15	0.065

Three vertical stages

A mixed-refrigerant cascade process with three vertical stages (similar to MFC) is given in Fig. 8.3. Each vertical stage here only contains one horizontal stage. The decision variables are illustrated in red, including low and high pressure levels for each refrigeration cycle, three refrigerant compositions and flow rates and two intermediate natural gas temperatures. In total, there are 26 degrees of freedom available for the process optimization.

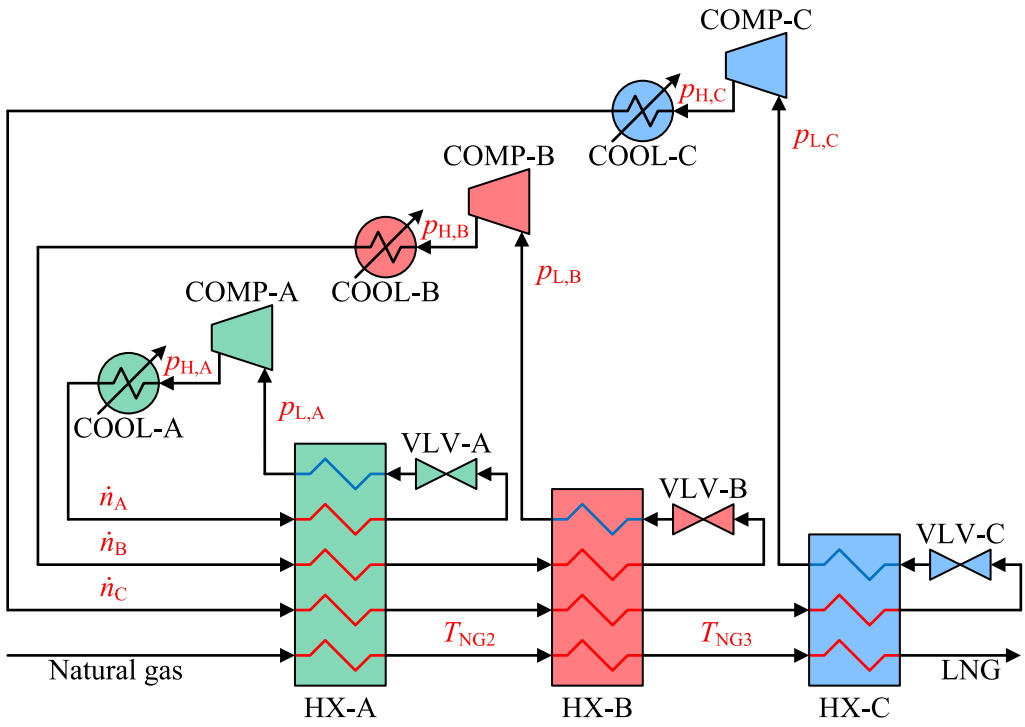

Figure 8.3. Mixed refrigerant cascade process with three vertical stages.

The decision variables used for the design and different choices of bounds are given in Table 8.4, together with the best known solution. This solution has been obtained by gradual confinement of the variable bounds around the best solution. There is no guarantee that this solution is the global optimal.

The power consumption of the optimized process with one vertical stage (Fig. 8.1) was 16.383 MW for the given operating conditions. As expected, the power consumption was reduced when two vertical stages were used. In the dual mixed-refrigerant process (Fig. 8.2) the best solution obtained had a total power consumption of 13.858 MW, about 15.4 % less than the single mixed-refrigerant process.

Further reduction in the energy use was observed for the optimized process with three vertical stages (Fig. 8.3). A power consumption of 13.118 MW was found to be equivalent to a reduction of around 19.9 % compared to the single mixed-refrigerant process and about 5.3 % compared to the dual mixed-refrigerant process. One may notice that a smaller reduction in power consumption was observed when moving from two to three vertical stages than when increasing the number of vertical stages from one to two.

Table 8.4. Decision variables for optimization of a mixed-refrigerant process with three vertical stages with different choices of variable bounds and best known solution.

		Wide		Component		Medium		Narrow		
Variable	Unit	LB	UB	LB	UB	LB	UB	LB	UB	Best
T_{NG2}	K	210	280	210	280	230	270	245	255	250.9
T_{NG3}	K	160	200	160	200	170	210	185	195	190.9
$p_{L,A}$	bar	1.0	3.0	1.0	3.0	1.0	3.0	2.0	3.0	2.60
$p_{H,A}$	bar	4.0	10.0	4.0	10.0	4.0	8.0	4.0	6.0	4.87
$p_{L,B}$	bar	1.0	5.0	1.0	5.0	1.0	3.0	1.0	2.0	1.00
$p_{H,B}$	bar	8.0	30.0	8.0	30.0	10.0	20.0	10.0	12.0	11.13
$p_{L,C}$	bar	1.0	5.0	1.0	5.0	1.0	3.0	1.0	2.0	1.30
$p_{H,C}$	bar	8.0	30.0	8.0	30.0	10.0	25.0	15.0	20.0	19.35
$\dot{n}_{A,C1}$	kmol/s	0.00	1.50	-	-	0.00	0.20	-	-	-
$\dot{n}_{A,C2}$	kmol/s	0.10	1.50	0.10	1.50	0.10	0.50	0.20	0.30	0.256
$\dot{n}_{A,C3}$	kmol/s	0.00	1.50	0.00	1.50	0.00	0.20	0.00	0.10	0.043
$\dot{n}_{A,nC4}$	kmol/s	0.00	1.50	-	-	0.00	0.20	-	-	-
$\dot{n}_{A,iC4}$	kmol/s	0.00	1.50	0.00	1.50	0.50	1.50	0.90	1.10	1.056
$\dot{n}_{A,N2}$	kmol/s	0.00	1.50	-	-	-	-	-	-	-
$\dot{n}_{B,C1}$	kmol/s	0.00	1.50	0.00	1.50	0.00	0.20	0.00	0.10	0.020
$\dot{n}_{B,C2}$	kmol/s	0.10	1.50	0.10	1.50	0.20	0.80	0.40	0.50	0.427
$\dot{n}_{B,C3}$	kmol/s	0.00	1.50	0.00	1.50	0.00	0.50	0.15	0.25	0.200
$\dot{n}_{B,nC4}$	kmol/s	0.00	1.50	0.00	1.50	0.00	0.20	0.05	0.15	0.100
$\dot{n}_{B,iC4}$	kmol/s	0.00	1.50	0.00	1.50	0.00	0.20	0.00	0.10	0.076
$\dot{n}_{B,N2}$	kmol/s	0.00	1.50	-	-	-	-	-	-	-
$\dot{n}_{C,C1}$	kmol/s	0.00	1.50	0.00	1.50	0.10	0.60	0.30	0.40	0.329
$\dot{n}_{C,C2}$	kmol/s	0.10	1.50	0.10	1.50	0.10	0.60	0.25	0.35	0.319
$\dot{n}_{C,C3}$	kmol/s	0.00	1.50	0.00	1.50	0.00	0.20	0.00	0.10	0.005
$\dot{n}_{C,nC4}$	kmol/s	0.00	1.50	-	-	-	-	-	-	-
$\dot{n}_{C,iC4}$	kmol/s	0.00	1.50	-	-	-	-	-	-	-
$\dot{n}_{C,N2}$	kmol/s	0.00	1.50	0.00	1.50	0.00	0.20	0.02	0.10	0.051

Optimization results

The performance of a multi-start search with the sequential quadratic programming algorithm NLPQLP for optimization of mixed-refrigerant processes with one to three vertical stages is given in Table 8.5. In each case, 100 runs from randomly generated starting points (not necessarily feasible) were performed. This was done since the probability of finding a feasible solution by random generation was found to be very small for the processes with two and three vertical stages. The success rate given in Table 8.5 indicates the number of searches for which the best solution fulfils a given criteria, while the number of evaluations listed reflects the total number of flowsheet evaluations. This is given for the average of all runs performed and the average of all runs returning a feasible solution.

The search performance is likely to be influenced by the settings of the search algorithm (i.e. step length for estimation of derivatives and weighting of objective and constraints). Hence, it may be that the settings used benefit one of the processes more than others and that the performance in general could be improved by changing the settings. Nevertheless, the results give an indication of the influence of the size of the search space and the complexity of the process flowsheet.

As can be observed in Table 8.5, the success rate was found to increase when the search space was reduced for all the three processes studied. Still, the success rate was highest for the process with one vertical stage and lowest for the process with three vertical stages. With wide variable bounds, a solution within 0.1 % of the best known solution was obtained in 49 % of the searches for the process with one vertical stage. For the process with three vertical stages, however, no solution was obtained within 10 % of the best known and only 4 % of the runs ended up identifying a feasible solution. The results obtained for the process with two vertical stages lie somewhere in between, with 9 % of the final solutions within 10 % of the best known but no solutions within 1 %.

Table 8.5. Optimization search performance for mixed-refrigerant processes with 1-3 vertical stages.

	Success rate (%)					Evaluations	
Case	Feasible	100 %	10 %	1 %	0.1 %	Avg.	Feasible
1 vertical stage							
Wide	83	69	66	59	49	762	898
Component	83	72	72	72	67	427	498
Medium	92	90	86	83	70	562	604
Narrow	100	100	99	99	90	312	312
2 vertical stages							
Wide	50	33	9	0	0	1718	3027
Component	52	44	9	0	0	1605	2886
Medium	66	66	39	11	4	2564	3729
Narrow	93	93	93	90	79	1583	1631
3 vertical stages							
Wide	4	4	0	0	0	434	5054
Component	7	7	1	0	0	555	4552
Medium	35	33	24	2	0	2063	4757
Narrow	58	57	56	41	19	2802	4057

With narrow variable bounds, 90 % of the runs end up with a solution with power consumption within 0.1 % of the best known for the process with one vertical stage. For the process with two vertical stages, this number is 79 %, while for the most

complex process, 19 % of the solutions end up within 0.1 % of the best known solution.

Due to increased number of decision variables, the average number of evaluations in each run increases considerable with increasing number of vertical stages. Since some of the runs fail within relatively few iterations, the average number of flowsheet evaluations is higher for the runs that end up identifying a feasible solution than for the ones that do not. In case of searches that end up in the feasible region, the number of evaluations required typically reduces when the variables bounds are tightened and the number of decision variables reduced. As can be observed from the results obtained for the formulations with the same bounds as the wide variables bounds but only components present in the best known solution included as variables, the success rate is similar but the number of evaluations smaller than for the formulations with wide variable bounds.

As one would expect, the process simulation time increases with increasing process complexity. The average computational time required for each function evaluation was around 0.14-0.19 s for the process with one vertical stage, around 0.31-0.34 s for the process with two vertical stages and around 0.45-0.47 s for the process with three vertical stages. Again, most of the computational time is used for the process simulation in Aspen HYSYS®.

Even though no conclusion can be drawn based on the case studies presented here, the results presented in Table 8.5 indicate that the performance of optimization of complex process concepts could be improved by taking advantage of the fact that the success rate increases with tighter variable bounds. In order to obtain these narrow variable bounds, one could utilize the fact that success rate for optimization cycles with one vertical stage is significantly higher, even with relatively wide variable bounds.

8.2.2 Sequential optimization

As can be observed from the flowsheets for the cascade processes in Figs. 8.2 and 8.3, the different refrigeration cycles are separated by the intermediate temperatures of the natural gas stream (stage temperatures). These temperature levels determine the load division between the vertical stages.

For fixed stage temperatures, the operating conditions and behaviour of any given vertical stage is not affected by changes in preceding vertical stages (stages operating at higher temperature). Since the refrigerants operating at lower temperature levels are precooled in preceding stages, however, the opposite does not hold. If the high pressure level, refrigerant flow rate or composition of refrigerant B changes for the process given in Fig. 8.2, the operating conditions of refrigeration cycle A changes. No

changes in refrigeration cycle A will, however, affect the operating conditions of cycle B. This suggests an opportunity to optimize the different vertical stages sequentially, starting with the stage operating at the lowest temperature level.

When optimizing the whole cycle simultaneously, minimizing irreversibilities is equivalent to minimizing power consumption, since by definition

$$\dot{W}_{\text{tot}} = \Delta\dot{E}_{\text{NG}} + \sum \dot{I} \,. \tag{8.1}$$

Here, $\Delta\dot{E}_{\text{NG}}$ is the change in exergy for the natural gas stream from inlet to outlet. Since the inlet and outlet conditions are given, the exergy load associated with cooling the natural gas is fixed.

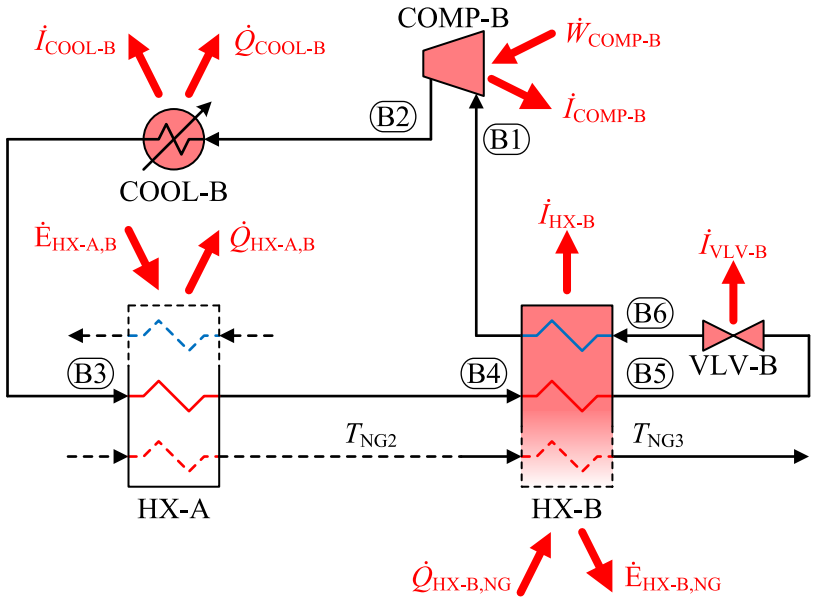

Figure 8.4. Energy and exergy balance for the sub-cooling cycle in a mixed-refrigerant process with two vertical stages and one horizontal stage each.

As was discussed in Chapter 6, the operating conditions providing the smallest power consumption within a given vertical stage may not coincide with the operating conditions that gives the smallest power consumption for the overall process. This is due to the interaction between the refrigeration cycles. If all irreversibilities in HX-A are assigned to refrigeration cycle A, the exergy balance for refrigerant cycle B can be expressed as

$$\dot{W}_{\text{B}} + \Delta\dot{E}_{\text{HX-A,B}} = \Delta\dot{E}_{\text{HX-B,NG}} + \sum \dot{I}_{\text{B}} \,, \tag{8.2}$$

where $\Delta\dot{E}_{\text{HX-A,B}}$ is the exergy change of refrigerant B passing through HX-A and $\sum\dot{I}_{\text{B}}$ is the sum of irreversibilities in refrigeration cycle B,

$$\sum\dot{I}_{\text{B}} = \dot{I}_{\text{COMP-B}} + \dot{I}_{\text{COOL-B}} + \dot{I}_{\text{HX-B}} + \dot{I}_{\text{VLV-B}}\,. \tag{8.3}$$

Here, energy and exergy stream are assumed positive when supplied to the system. Energy and exergy flows to and from refrigeration cycle B in Fig. 8.2 are illustrated in Fig. 8.4. As given by Eq. (8.3) the irreversibilities in the different unit operations represents a loss of exergy. One may notice that above ambient temperature (COOL-B) exergy is rejected from the system when heat is rejected. Below ambient, however, heat rejected from the system is associated with exergy supplied to the system. Hence, for refrigeration cycle B, exergy is supplied to the system in the form of work in COMP-B and in the form of heat in HX-A.

As can be observed from Fig. 8.4 and Eq. (8.2), minimizing the irreversibilities in refrigeration cycle B is not equivalent to minimizing the compression power in the cycle. Since the exergy supplied to refrigerant B in HX-A must be removed by refrigeration cycle A, increased cooling load in HX-A (or rather increased exergy load) generally leads to increased power consumption in refrigeration cycle A.

These findings suggest that the total irreversibilities in refrigeration cycle B should be minimized rather than the compression power in order to find the solution that gives the smallest power consumption for the overall process. This is equivalent to minimizing the sum of compression power in COMP-B and exergy supplied to refrigerant B in HX-A (see Eq. (8.2)). This will provide the solution with the highest rational exergy efficiency for refrigeration cycle B.

The extra exergy load in refrigeration cycle A caused by cooling of refrigerant B, will be provided with a rational efficiency smaller than unity. Hence, the increase in power consumption in refrigeration cycle A will be larger than the increase in exergy load when the cooling load in HX-A increases. This may indicate that the exergy load associated with the precooling of refrigerant B in HX-A should be emphasized more than the power supply in COMP-B when optimizing refrigeration cycle B. Assuming the rational exergy efficiency of refrigeration cycle A to be around 0.5, would suggest that the exergy load could be weighted by a factor of two in order to find the design that gives the smallest overall power consumption.

The influence of precooling of refrigerant B in refrigeration cycle A could alternatively be accounted for by minimizing the sum of power consumption in COMP-B and the cooling load associated with refrigerant B in HX-A. This is, however, expected to put

too much or too little attention on the refrigerant precooling, depending on the temperature level at which the heat is rejected.

In total, four different objective function formulations have been tested and compared for optimization of refrigeration cycle B:

O1: Minimization of compression power:

$$\min_{\mathbf{x}_B} \quad \dot{W}_{\text{COMP-B}}\left(\mathbf{x}_B\right) \tag{8.4}$$

O2: Minimization of the sum of compression power and exergy load:

$$\min_{\mathbf{x}_B} \quad \dot{W}_{\text{COMP-B}}\left(\mathbf{x}_B\right) + \Delta\dot{E}_{\text{HX-A,B}}\left(\mathbf{x}_B\right) \tag{8.5}$$

O3: Minimization of a weighted sum of compression power and exergy load:

$$\min_{\mathbf{x}_B} \quad \dot{W}_{\text{COMP-B}}\left(\mathbf{x}_B\right) + 2 \cdot \Delta\dot{E}_{\text{HX-A,B}}\left(\mathbf{x}_B\right) \tag{8.6}$$

O4: Minimization of the sum of compression power and cooling load:

$$\min_{\mathbf{x}_B} \quad \dot{W}_{\text{COMP-B}}\left(\mathbf{x}_B\right) + \dot{Q}_{\text{HX-A,B}}\left(\mathbf{x}_B\right) \tag{8.7}$$

In Eqs. (8.4)-(8.7), $\mathbf{x}_B$ is a vector containing the decision variables for refrigeration cycle B. These are the low and high pressure levels, and the component flow rates for refrigerant B. For all formulations, the objective function has been minimized subject to a minimum superheating of 10 K for the compressor suction streams and 2 K minimum temperature in the heat exchangers (similar to the case study in Section 8.2.1).

Irreversibilities (and exergy associated with heat transfer) have been calculated assuming the ambient temperature to be equal to the external cooling temperature, $T_0 = 293.15$ K. This was done in order to make sure that the heat removed from refrigerant B in HX-A represents exergy transferred from the cold stream (refrigerant A) to the hot stream (refrigerant B). As previously discussed, heat rejection below ambient temperature is associated with exergy supply, while heat rejection above ambient temperature means that exergy is also rejected.

Since there are no refrigeration cycles operating above refrigeration cycle A, the only external exergy input to this cycle is the compression power in COMP-A. The objective is therefore, for all the problem formulations suggested, to minimize the

power consumption in this compressor. This is done with the best known solution for refrigeration cycle B for each of the four objective function formulations ($\mathbf{x}_B^*$):

$$\min_{\mathbf{x}_A} \quad \dot{W}_{\text{COMP-B}}\left(\mathbf{x}_A, \mathbf{x}_B^*\right). \tag{8.8}$$

In Eq. (8.8), $\mathbf{x}_A$ is a vector containing the decision variables for refrigeration cycle A, while $\mathbf{x}_B^*$ is a vector containing the variable values providing the best solution for refrigeration cycle B with any of the four objective formulations. The decision variables for refrigeration cycle A include the low and high pressure levels, and the component flow rates for refrigerant A.

8.2.3 Case study – dual mixed-refrigerant process

In order to illustrate the proposed strategy for design optimization, the vertical stages in the dual mixed-refrigerant process illustrated in Fig. 8.2 has been optimized sequentially for different values of the intermediate natural gas temperature (load distribution). The intermediate natural gas temperature was formulated as

$$T'_{\text{NG2}} = \frac{T_{\text{NG2}} - T_{\text{NG3}}}{T_{\text{NG1}} - T_{\text{NG3}}}. \tag{8.9}$$

Refrigeration cycle B

The compression power in refrigeration cycle B is plotted in Fig. 8.5 (a) for different values of the stage temperature for the best solution found with each of the four objective function formulations. As one would expect, the power consumption is smallest when minimization of power consumption is used directly as objective (O1). A slight increase in power consumption is observed with the sum of compression power and exergy load used as objective (O2). Somewhat higher again is the power consumption of the solutions obtained with a weighted sum of compression power and exergy load as objective function (O3). Using the sum of compression power and cooling load as objective function (O4) gives a significant increase in power consumption in refrigeration cycle B. The exception is for small values of the stage temperature, where the largest compression power is observed for objective function O3.

When the stage temperature is equal to the inlet temperature of the natural gas ($T'_{\text{NG2}} = 1$), there is no precooling of refrigerant B in HX-A. Hence, all four objective formulations give the same optimal solution (equal to the power consumption of a single mixed-refrigerant process). Since the temperature range covered by refrigeration cycle B decreases with decreasing stage temperature, the compression power is reduced. As can be observed in Fig. 8.5 (a), the difference in compression power for

the different formulations generally increases with decreasing stage temperature T'_{NG2}. For low values of the intermediate temperature level, the difference in power consumption between O1 and O4 actually decreases.

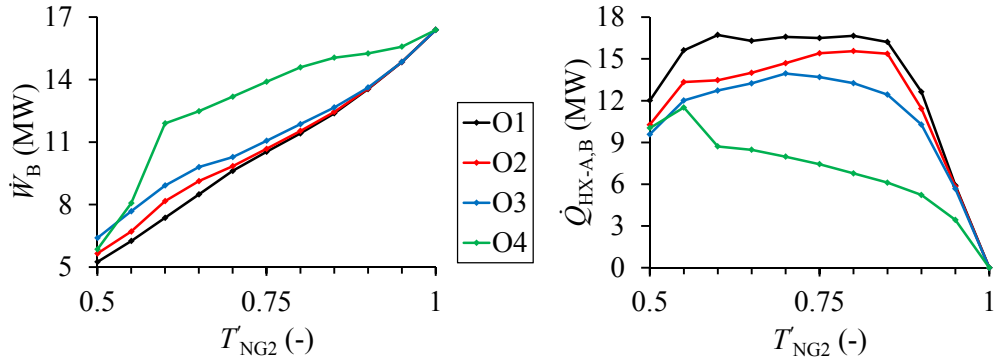

(a) (b)

Figure 8.5. (a) Compression power in refrigeration cycle B as function of the natural gas stage temperature for four different objective function formulations; (b) Heat removed from refrigerant B in HX-A.

As can be observed in Fig. 8.5 (b), a consequence of the small compression power in refrigeration cycle B obtained for objective function O1 is a higher cooling load in HX-A. The results indicate that the cooling is smallest for the solutions with the highest compression power. Even though the temperature range covered by refrigeration cycle A increases with decreasing stage temperature, the cooling load associated with precooling refrigerant B decreases with O1, O2 and O3 for small values of the stage temperature. This is found to be related to changes in refrigerant phase envelope and flow rate.

The vapour fraction of stream B3 (i.e. refrigerant B entering HX-A) is plotted as function of the stage temperature for the four different objective function formulations in Fig. 8.6 (a), while the vapour fraction of stream B4 (refrigerant B exiting HX-A) is plotted in Fig. 8.6 (b). For O1, O2 and O3, the vapour fraction of stream B3 increases with decreasing stage temperature. With O4, the vapour fraction of stream B3 decreases with decreasing stage temperature for large values of the stage temperature, while the behaviour is similar to solutions obtained for the other formulations for $T'_{NG2} < 0.85$.

Since the temperature of refrigerant B entering HX-A is the same for all cases where the compressor discharge temperature is higher than the ambient cooling temperature, the changes in vapour fraction for stream B3 is related to changes in the refrigerant composition and high pressure level. With decreasing stage temperature, refrigeration cycle B covers a smaller temperature range and the composition is generally shifted towards lower volatility. Only in one of the cases studied, it was observed a

compressor discharge temperature smaller than the ambient cooling temperature (objective O1 for $T'_{NG2} = 0.90$). As can be observed from Fig. 8.6 (a), the cases where refrigerant B enters HX-A as superheated vapour corresponds with the cases where the cooling load in HX-A is observed to decrease (or the increase is very small) with decreasing stage temperature (Fig. 8.5 (b)).

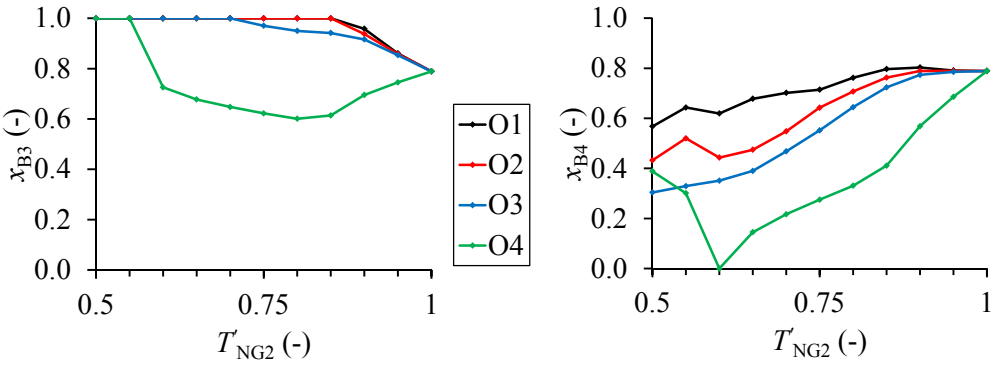

(a) (b)

Figure 8.6. (a) Vapour fraction in stream B3 as function of the natural gas stage temperature for four different objective function formulations; (b) Vapour fraction in stream B4.

Since the exit temperature of refrigerant B from HX-A decreases with decreasing stage temperature T'_{NG2}, the vapour fraction of stream B4 is generally also reduced. Exceptions can be observed in Fig. 8.6 (b) for small stage temperatures, and for O1, O2 and O3 at high stage temperatures. One may observe that for the same stage temperature, the vapour fraction in stream B4 is actually smallest for the design with the largest cooling load in HX-A and opposite. Among other factors, this is related to differences in refrigerant flow rate.

Refrigerant flow rate and pressure ratio of the best solutions obtained for the four objective function formulations are given in Fig. 8.7 (a) and (b), respectively, for different values of the stage temperature. When effects of refrigerant precooling in HX-A is considered in the objective (O2, O3 and O4), the best solution is shifted towards smaller flow rate and higher pressure ratio. The more effort is put on limiting the cooling load in HX-A or the exergy supply associated with this heat transfer, the more the trade-off between refrigerant flow rate and pressure ratio is shifted. Hence, in general, objective function formulation O1 gives the solution with the largest flow rate but smallest pressure ratio, while objective function formulation O4 gives the solution with the smallest flow rate and highest pressure ratio.

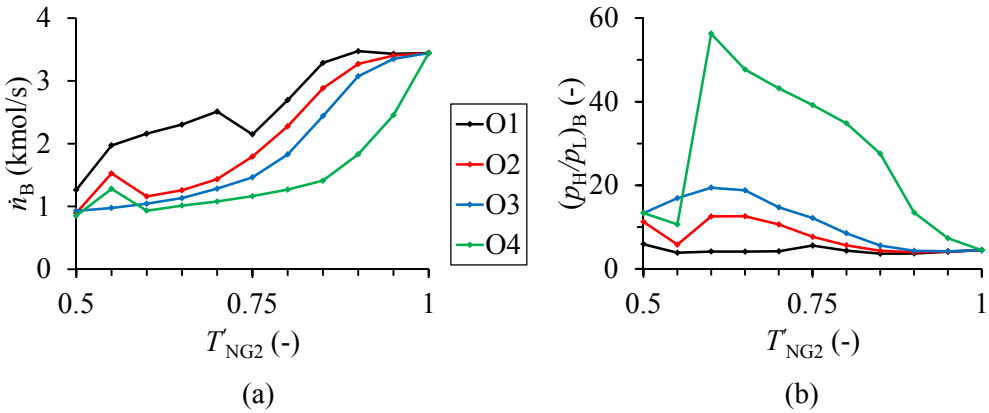

(a) (b)

Figure 8.7. (a) Refrigerant flow rate in refrigeration cycle B as function of the natural gas stage temperature for four different objective function formulations; (b) Pressure ratio for refrigerant B.

In addition to smaller cooling load in HX-A, the design solutions with smaller refrigerant flow rate naturally also gives a smaller exergy load in refrigerant cycle A. As can be observed from Fig. 8.8 (a), due to the fact that more heat must be removed in HX-A, the exergy load associated with the cooling in HX-A, and thereby also the minimum work requirement in cycle A, is higher for the solutions obtained with objective function O1. By comparing Fig. 8.5 (b) with Fig. 8.8 (a), it is, of course, apparent that the design with the smallest cooling load also is the design with smallest exergy load (the distribution of heat with respect to temperature is similar for the four design solutions). Since the exergy of heat increases with decreasing temperature below ambient, the ratio of exergy load to cooling load does, however, increase with decreasing stage temperature.

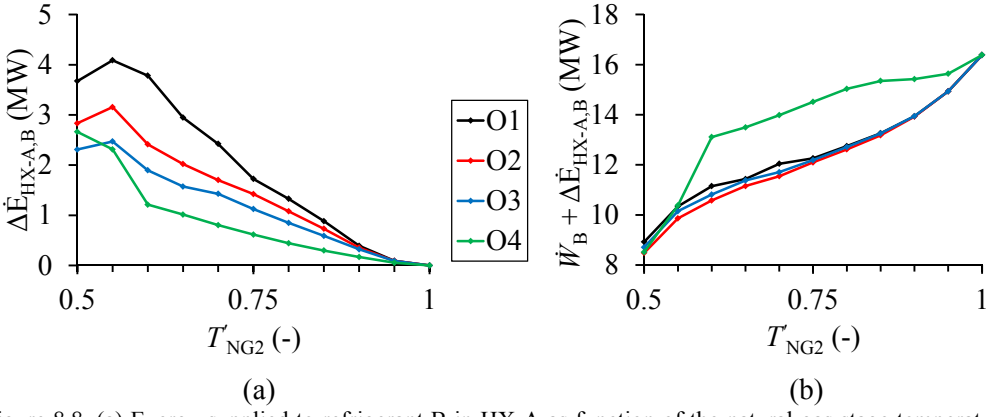

(a) (b)

Figure 8.8. (a) Exergy supplied to refrigerant B in HX-A as function of the natural gas stage temperature for four different objective function formulations; (b) Sum of compression power and supplied exergy.

The sum of compression power in refrigeration cycle B and the exergy load associated with the cooling of refrigerant B in HX-A is plotted as function of the stage temperature in Fig. 8.8 (b). Since this is the same as the objective function O2, the

smallest values are observed for the solutions obtained with this formulation. This also means that the irreversibilities in refrigeration cycle B are smallest for objective function formulation O2. The values are slightly larger for the formulations C1 and C3. Except for the smallest stage temperature values, the irreversibilities in refrigeration cycle B are significantly larger for the solutions obtained with objective function formulation O4, which indicates that too much attention may have been put on limiting the load in refrigeration cycle A.

In Fig. 8.9 (a), the optimization results are plotted in terms of objective function O3 ($\dot{W}_B + 2\cdot\Delta\dot{E}_{HX\text{-}A,B}$) for the best solution obtained for each of the four formulations. As expected, the smallest values are observed for the solutions obtained with O3. A similar plot is given in Fig. 8.9 (b) for the value of objective function O4 ($\dot{W}_B + 2\cdot\dot{Q}_{HX\text{-}A,B}$). Correspondingly, the smallest values are obtained for the constraint formulation O4.

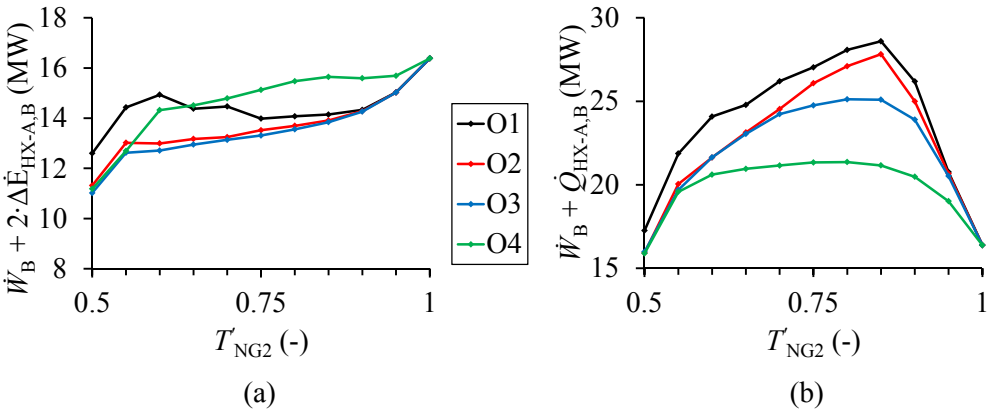

(a) (b)

Figure 8.9. (a) Weighted sum of compression power in refrigeration cycle B and exergy supplied to refrigerant B in HX-A as function of the natural gas stage temperature for four different objective function formulations; (b) Sum of compression power and heat removed from refrigerant B in HX-A.

Refrigeration cycle A

The power consumption in refrigeration cycle A has been minimized for different values of the stage temperature, given the solutions obtained with the different formulations for refrigeration cycle B. Due to the fact that different values of the decision variables are found to be best for refrigeration cycle B with the different objective function formulations, optimization of refrigerant cycle A will give different results even though the objective function is the same. The refrigeration flow rate and pressure ratio of refrigerant A are plotted as functions of the stage temperature in Fig. 8.10, with operating conditions given by the four different objective function formulations used for optimization of cycle B.

As can be observed in Fig. 8.10 (a), the refrigerant flow rate is smallest for the formulations with the smallest cooling load induced by refrigerant B (see Fig. 8.5 (b)). Hence, the refrigerant flow rate is generally largest for the solutions based on objective function formulation O1 and smallest for O4. From Fig. 8.10 (b), one may observe that the pressure ratio of refrigerant A is similar for the four different formulations.

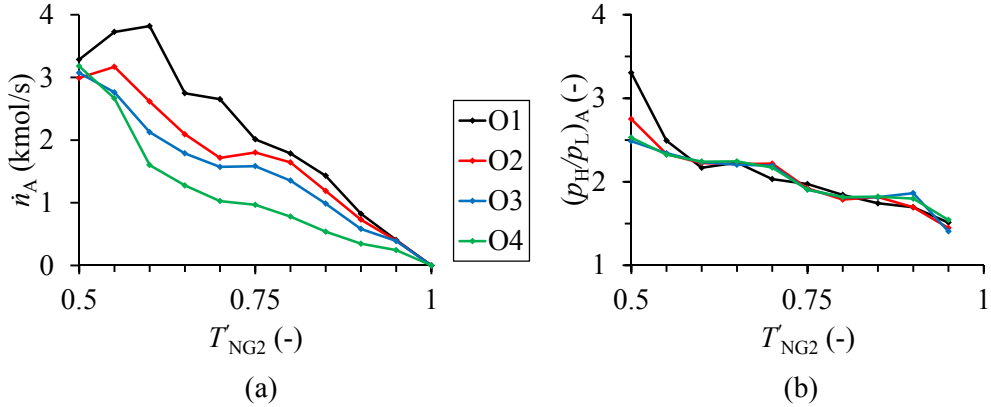

Figure 8.10. (a) Refrigerant flow rate in refrigeration cycle A as function of the natural gas stage temperature with settings in cycle B given by the four different objective function formulations; (b) Pressure ratio for refrigerant A.

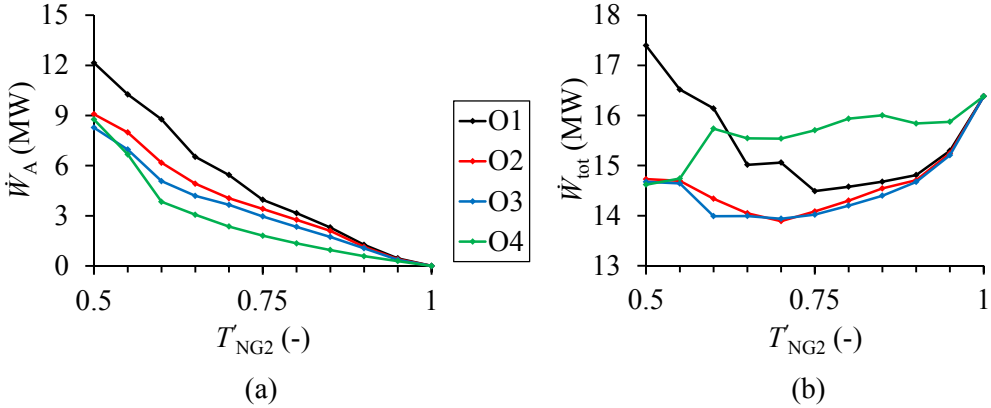

Figure 8.11. (a) Compression power in refrigeration cycle A as function of the natural gas stage temperature with settings in cycle B given by the four different objective function formulations; (b) Total power consumption.

Since the pressure ratios of the different formulations are similar, the compression power in refrigeration cycle A has a similar behaviour as the refrigerant flow rate. As can be observed from Fig. 8.11 (a), the power consumption in cycle A is generally largest when formulation O1 is used for optimization of cycle B and smallest formulation O4 is used. As expected, since the operating range and cooling load increase, the compression power in cycle A increases with decreasing stage temperature for all the formulations. Recalling the results obtained for the compression power in refrigeration cycle B (see Fig. 8.5 (a)), the behaviour is opposite for

refrigeration cycle A. In general, the problem formulation that gives the smallest compression power in cycle B gives the largest power consumption in cycle A, and opposite.

Overall process

The compression power in the two refrigeration cycles, the total power consumption, is plotted as function of the stage temperature in Fig. 8.11 (b). As can be observed, the smallest total power consumption is observed for objective the function formulations O2 and O3. For most values of the stage temperature, formulation O3 gives the smallest power consumption. An exception is observed for $T'_{NG2} = 0.70$, where the solution obtained for O2 provides the smallest total power consumption. This is actually also the solution that provides the smallest overall power consumption of all the cases studied.

Compared to the formulations O2 and O3, the best solution found for formulation O1 is observed at a higher stage temperature. One may also notice that the best solution obtained for formulation O1 has a higher total power consumption than the solutions obtained for O2 and O3 for all values of the stage temperature (except for the case where only one refrigeration cycle is used and all the formulations give the same result). In general the difference in power consumption between the best solutions obtained for formulations O1 and the formulations O2 and O3 increases with decreasing stage temperature.

For the smallest values of the stage temperature tested, the results obtained for formulation O1 gives a power consumption larger than what has been observed for a single-stage process. The results obtained indicate that the influence of precooling of refrigerant B in HX-A is underestimated when objective function formulation O1 is used for refrigeration cycle B. In fact, formulation O1 does not take this effect into account at all, which is why the deviation from the best known solutions increases with decreasing stage temperature (and thereby increased precooling in HX-A).

The results obtained using objective function formulation O4 when optimization refrigeration cycle B indicate that the influence of precooling of refrigerant B in HX-A is overestimated. This is because the exergy change of refrigerant B in HX-A is smaller than the amount of heat removed (see Figs. 8.5 (b) and 8.8 (a)). This is particularly evident for large values of the stage temperature, since the exergy content of heat increases with decreasing temperature level. Hence, for large values of the stage temperature, formulation O4 gives significantly larger power consumption than O2 and O3.

For formulation O4, the smallest power consumption is actually observed for the lowest stage temperature tested, and it could be that solutions with even smaller power consumption is found for an even lower stage temperature. For the two smallest values of the stage temperature tested, the solutions obtained with objective function O4 used for optimization of refrigeration cycle B are similar to those obtained for O2 and O3, which would indicate that the solutions would be similar also for smaller values of the stage temperature.

The rational exergy efficiencies of the two refrigeration cycles are indicated in Fig. 8.12. Again, notice that all irreversibilities in HX-A have been allocated to refrigeration cycle A and that the ambient temperature is assumed to be equal to the cooling temperature.

The exergy input in refrigeration cycle B is, as previously discussed, the sum of compression power in COMP- B and the exergy supplied to refrigerant B in HX-A, while the exergy load is constant for all the formulations given by cooling requirement of the natural gas stream. Hence, since the sum of exergy supplied is minimized in objective function formulation O2, the highest rational efficiency is observed for this formulation (see Fig. 8.12 (b)).

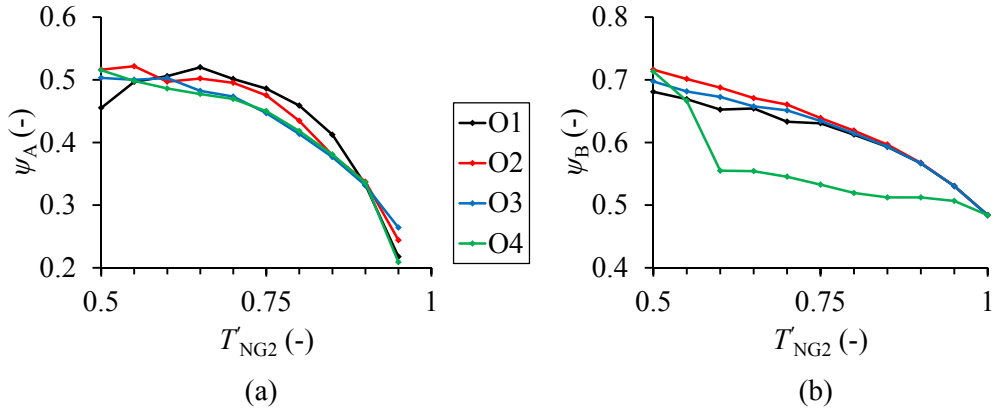

Figure 8.12. (a) Rational efficiency of refrigeration cycle A as function of the natural gas stage temperature with settings in cycle B given by the four different objective function formulations; (b) Rational efficiency of refrigeration cycle B.

With objective function formulation O1, a peak is observed for the exergy efficiency of refrigeration cycle A around $T'_{NG2} = 0.65$. For the other formulations, the rational exergy efficiencies of both refrigeration cycles generally increase with decreasing stage temperature. One may therefore assume that the overall exergy efficiency would benefit from smaller stage temperatures. Notice, however, that refrigeration cycle B has a higher exergy efficiency than refrigeration cycle A for all the stage temperatures

studied. This indicates that natural gas cooling load shifted to cycle A when the stage temperature is reduced will be supplied with a smaller exergy efficiency. In addition, the total exergy load of the process (cooling of natural gas and precooling of refrigerant B in HX-A) increases with decreasing stage temperature. The optimal stage temperature is found for the optimal trade-off between rational exergy efficiencies of the two refrigeration cycles and the exergy load.

Objective function formulation O3 is based on the assumption that the rational efficiency of refrigeration cycle A is around 50 %, which would indicate that this exergy supply should be weighted more than the exergy supplied as power in refrigeration cycle B. As can be observed from Fig. 8.12 (a), this assumption is close to fulfilled for the best known solution. Due to the weighting of the exergy supplies, however, the exergy efficiency of refrigeration cycle B will be smaller than if the actual exergy supply is minimized (see Fig. 8.12 (b)).

With objective function formulation O2, the exergy supplied is minimized and the rational exergy efficiency of refrigeration cycle B maximized. This formulation does, however, not take into account the fact that the exergy load caused by precooling of refrigerant B in HX-A is supplied with an exergy efficiency smaller than unity. The optimal weighting of the two exergy supplies in refrigeration cycle B may therefore be somewhere in between O2 and O3. By using a factor of 1.5, more focus is put on the exergy efficiency of refrigeration cycle B than in O3. At the same time, the exergy supply in HX-A is given more attention than in O2.

Comparison with simultaneous optimization

The power consumption of the best solution found in the sequential design approach (obtained for O2 with $T'_{NG2} = 0.70$) was 13.9 MW, about 0.25 % higher than the best known solution found through simultaneous optimization of all process variables (see Table 8.3). The variable values are also similar to the best known solution. A local optimization search (using all decision variables) initialized from the best solution obtained through the sequential design approach was found to end up in the best known solution.

Taking into account that the case study was performed for discretized values of the intermediate natural gas temperature, these results clearly indicates that the sequential design approach is capable of identifying interesting regions of the search space. As an alternative to use of a stochastic search, a sequential design approach could therefore be used in the initial phase of a search strategy used for optimization of complex LNG process concepts.

One may also notice that, even though minimizing the power consumption in the low-temperature cycle does not give the optimal solution for the overall process, it gives a lower bound on the power consumption in this cycle for a given load distribution (stage temperature).

8.2.4 Proposed design strategy

As can be observed in Figure 8.11 (b), the total power consumption of the dual mixed-refrigerant process seems to be a (close to) unimodal function of the intermediate natural gas temperature (when problem formulation O2 or O3 is used to provide the power consumption for each value of the natural gas temperature). This may not hold when the discretization is refined, yet still indicates that the optimization problem could potentially be solved in a nested loop, where the load division (intermediate natural gas temperature) is optimization in an outer loop and the two mixed-refrigerant cycles could then be optimized sequentially in an inner loop, starting at the lowest temperature level.

The inner optimization loop could be organized in different ways. The simplest alternative would be to follow the approach used for the case study in Section 8.2.3, where the solution is returned to the outer loop directly after sequentially optimizing the vertical stages. Alternatively, an extra iteration could be added where the two vertical stages are optimized simultaneously for the given load distribution before the solution is returned to the outer loop. In any case, the sequential design approach would be followed by a full optimization search taking all decision variables into account, starting from the optimization result from the nested loop design approach.

An alternative use of sequential optimization could be to generate feasible starting points for optimization, without necessarily using the full optimization strategy. As previously discussed, obtaining a feasible solution by random generation of values for the different decision variables is very time consuming (if at all possible in reasonable time) even for the dual mixed-refrigerant process (likely to be even harder with three vertical stages). For the single mixed-refrigerant process, this can, however, usually be obtained within quite short time.

The results presented in this work therefore suggests that generation of feasible starting points for complex process concepts could possibly be done in a sequential way as well. First, random values would be generated for the variables describing the load distribution between the different vertical stages in the process. Second, sets of random values would be generated for the variables describing the vertical stage operating at the lowest temperature level until a feasible solution is obtained (satisfying the constraints concerning this vertical stage). Further, with this solution fixed, the same approach would be used for the vertical stage operating at the second lowest

temperature level. This would be continued until feasible solutions have been found for all the vertical stages in the process.

The suggested design approach could also be used for optimization of cascade processes with three (or more vertical stages). In this case, there would be two variables to be optimized in the outer loop and three refrigeration cycles to be optimized sequentially in the inner loop. The complexity of the optimization problem would, of course, increase. The suggested approach does only apply to the vertical stages in a cascade. Hence all the horizontal stages within a vertical stage would need to be optimized simultaneously. The proposed strategy would also apply to other cascade LNG processes such as pure-refrigerant cascade processes, propane-precooled mixed-refrigerant processes and the AP-X® process.

Finally, one should notice that the proposed design strategy for optimization of cascade refrigeration processes has not been implemented and tested in this work. It is therefore not possible to conclude on its applicability or performance.

8.3 Multi-stage compression

In order to reduce the number of decision variables (at least in the initial phase of the optimization search), heuristic rules could be used to set the value of intermediate pressure levels in multi-stage compression. For a complex process concept with several instances of multi-stage compression with intercooling, a decent estimate for the optimal intermediate pressure levels could potentially give a considerable reduction in search time with little loss in solution quality.

As discussed in Chapter 5, the geometric mean gives a good prediction of the optimal intermediate pressure when the compressor suction temperature is close to equal for all compressors. In other situations, however, this may not be the case. As long as a refrigeration cycle operates close to ambient temperature, the suction temperature of the first compression stage is likely to be close to the intermediate cooling temperature. In cascade processes, however, this does not hold for stages operating at lower temperature levels.

In the following, different estimates for the optimal intermediate pressure level have been compared with the results obtained when the intermediate pressure is used as a decision variable. This has been done for the sub-cooling stage (refrigeration cycle B) in the dual mixed-refrigerant process illustrated in Fig. 8.2. The effect of difference in compressor suction temperatures has been studied by varying the operating range of the refrigeration cycle (different stage temperatures).

8.3.1 Formulation of intermediate pressure

If all the intermediate pressure levels in a multi-stage compression series are to be specified individually, accurate estimates of the optimal solution must be available in order to set the bounds for each pressure level narrow enough to avoid crossing (pressure reduction in compression stage). It may therefore be an alternative, at least in the initial phase of optimization search, to specify only the lowest and highest pressure levels and let the intermediate pressure levels be dependent upon these.

Fig. 8.13 illustrates a series of n stages of compression with intercooling. A constant isentropic efficiency has been assumed for all compression stages. The pressure level of the stream entering the first compression stage is equal to the low pressure level ($p_1 = p_L$), while the pressure of the stream exiting the last compression stage is equal to the high pressure level ($p_{n+1} = p_H$). In between each stage the compressed stream is cooled to the ambient cooling temperature (T_{cool}) if the temperature is high enough:

$$T_i = \min\left\{T_{(i-1)b}, T_{cool}\right\}, \qquad i = 2,...,n+1. \tag{8.10}$$

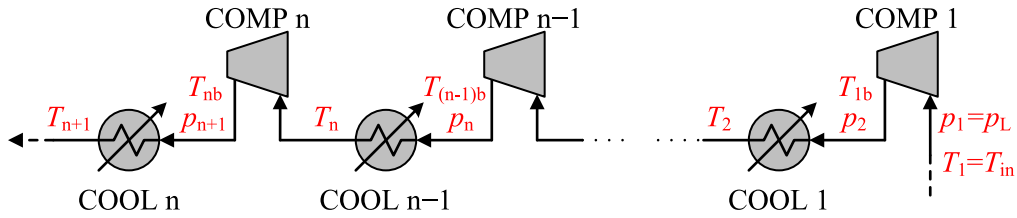

Figure 8.13. Multi-stage compression with intercooling.

8.3.2 Two-stage compression

First, the performance of different estimates for the optimal intermediate pressure level was compared with a formulation using the intermediate pressure level as a degree of freedom. This was done for the sub-cooling cycle in a two-stage mixed-refrigerant process illustrated in Fig. 8.14. Cooling is applied in COOL-B1 only if the discharge temperature from COMP-B1 is higher than the ambient cooling temperature T_{cool} = 293.15 K. Refrigerant component flow rates and pressure levels were used as decision variables. In this case study, the superheating constraint for the second compression stage was not considered.

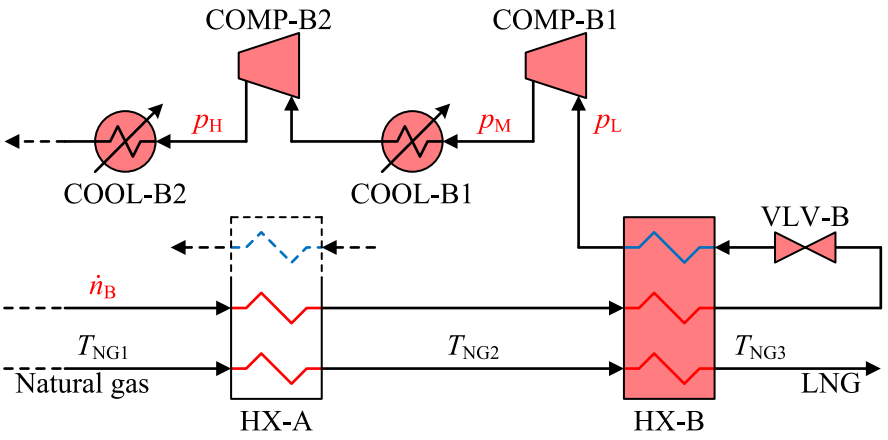

Figure 8.14. Mixed-refrigerant sub-cooling cycle with two-stage compression.

Estimates for the optimal intermediate pressure level

Three different estimates have been compared for prediction of the optimal intermediate pressure level in two-stage compression. First, using the geometric mean, the optimal intermediate pressure level would be given as

$$p_{M,GEO} = \sqrt{p_L \cdot p_H} \,. \tag{8.11}$$

The geometric mean has been proven to provide decent estimates for the optimal intermediate pressure levels in multi-stage compression of real gases when the suction temperatures of the different stages are similar.

Based on the results obtained in Chapter 5, a second estimate for the optimal intermediate pressure level could be expressed as

$$p_{M,OPT} = \sqrt{p_L \cdot p_H} \cdot \left(\frac{T_{cool}}{T_{in}} \right)^{c_{p,MR}/(2 \cdot R)} , \tag{8.12}$$

where T_{in} and T_{cool} are the suction temperatures of the first and second compression stage, respectively. Since the refrigerant does not behave like a perfect gas, a value for the specific heat capacity must be estimated. This could simply be taken as the specific heat capacity of the inlet stream for the first compression stage, $c_{p,MR1}$, or alternatively as the average of the specific heat at the compressor inlet and after the after-cooler ($c_{p,MR} = (c_{p,MR1} + c_{p,MR5})/2$). Both of these streams are defined irrespective of the value of the intermediate pressure level. Corrections are made to the estimate in the possible case that the suggested intermediate pressure level is smaller than the low pressure level or higher than the high pressure level.

As was discussed in Chapter 5, the optimal intermediate pressure level for perfect gas compression is equivalent to having the same isentropic discharge temperature in each compression stage. Assuming that this holds also for real gas compression with constant isentropic efficiency, a third estimate for the optimal intermediate pressure level can be derived from entropy considerations.

In the case of isentropic compression, the specific entropy of the refrigerant would, of course, be constant throughout each compression stage. Hence, an estimate for the optimal intermediate pressure level can be given by the geometric mean of the high pressure level and the pressure of the refrigerant with the same specific entropy as the inlet stream of the first compression stage and the same temperature as the refrigerant after intercooling:

$$p_{\mathrm{M,ENT}} = \sqrt{p\left(T_{\mathrm{cool}}, s_{\mathrm{in}}\right) \cdot p_{\mathrm{H}}} \tag{8.13}$$

If the inlet temperature of the first compression stage is very low compared to the intercooling temperature, it may be that the intermediate pressure levels suggested by Eqs. (8.12) and (8.13) are higher than the high pressure level. In this case, the power consumption will be minimized if the compression takes place in a single stage. The intermediate pressure is therefore set equal to the high pressure level.

Results

In Table 8.6, optimization results obtained using the three different estimates have been compared with the best solution obtained with all degrees of freedom used in the optimization. The power consumption has been minimized for different values of the intermediate natural gas temperature (T_{NG2}). Results are given for the pressure ratio, the isentropic discharge temperature of the two compressors and the total power consumption. The values of the different decision variables are not given, but the values will, of course, be different for the four formulations.

For the formulations where the intermediate pressure is estimated by use of heuristic guidelines, the deviation in power consumption compared to the case of using the intermediate pressure level as a design variable is also given. Again, there are neither guarantees that global optimal solutions have been found nor certain that the degree of optimality is the same for the different cases. Anyway, the results give indications of the behaviour of the different problem formulations.

For the best solutions found using $p_{\mathrm{M,GEO}}$ for the intermediate pressure level, the power consumption is from 0.8 % to 2.8 % higher than for the best known solution. This clearly indicates that the geometric mean is not a suitable estimate for the intermediate

pressure level in two-stage compression when the suction temperatures of the two compression stages are different.

Table 8.6. Optimization results for sub-cooling cycle with two-stage compression for different formulations of the intermediate pressure level assuming constant isentropic efficiency.

		$(T_{NG2} - T_{NG3})/(T_{NG1} - T_{NG3})$								
Property	Unit	0.60	0.65	0.70	0.75	0.80	0.85	0.90	0.95	1.00
VAR										
p_M/p_L	-	4.16	3.82	3.59	4.42	3.42	2.81	2.54	3.04	2.90
p_H/p_M	-	1.00	1.09	1.19	1.44	1.43	1.46	1.59	1.70	1.80
$T_{s,B1}$	K	284.9	298.3	303.5	310.5	310.2	312.4	317.0	332.3	340.7
$T_{s,B2}$	K	-	298.0	303.1	310.4	310.5	312.1	317.1	311.5	313.2
$\dot{W}_{tot}$	kW	7 366	8 476	9 568	10 412	11 264	12 145	13 154	14 046	15 099
GEO										
p_M/p_L	-	2.04	2.01	2.01	2.33	2.26	2.03	2.02	2.10	2.20
p_H/p_M	-	2.04	2.01	2.01	2.33	2.26	2.03	2.02	2.10	2.20
$T_{s,B1}$	K	244.6	262.3	271.1	281.1	290.6	296.4	306.2	317.0	327.4
$T_{s,B2}$	K	284.8	301.7	309.7	319.6	329.7	328.4	329.0	330.6	331.8
$\dot{W}_{tot}$	kW	7 506	8 637	9 783	10 702	11 521	12 328	13 257	14 252	15 375
Penalty	%	1.90	1.90	2.25	2.79	2.28	1.51	0.78	1.47	1.83
OPT										
p_M/p_L	-	4.16	4.09	3.83	4.54	3.53	2.88	2.59	2.80	2.74
p_H/p_M	-	1.00	1.00	1.10	1.39	1.37	1.42	1.55	1.93	1.97
$T_{s,B1}$	K	284.9	302.3	307.1	311.7	311.7	313.7	318.1	328.3	326.9
$T_{s,B2}$	K	-	-	298.8	308.5	308.5	310.7	315.7	316.5	316.1
$\dot{W}_{tot}$	kW	7 366	8 488	9 578	10 413	11 265	12 146	13 155	14 090	15 249
Penalty	%	0.00	0.15	0.10	0.01	0.01	0.01	0.00	0.31	1.00
ENT										
p_M/p_L	-	4.16	3.80	3.56	4.37	3.40	2.78	2.50	2.72	2.66
p_H/p_M	-	1.00	1.09	1.19	1.44	1.43	1.47	1.60	2.00	2.03
$T_{s,B1}$	K	284.9	298.1	302.9	309.9	309.9	311.9	316.3	327.1	325.9
$T_{s,B2}$	K	-	298.2	303.1	310.3	310.3	312.5	317.3	320.7	317.4
$\dot{W}_{tot}$	kW	7 366	8 476	9 569	10 412	11 264	12 145	13 155	14 127	15 279
Penalty	%	0.00	-0.00	0.00	0.00	-0.00	0.00	0.00	0.58	1.19

As can be observed from Table 8.6, the power consumption of the solutions obtained with the intermediate pressure level given by $p_{M,ENT}$ is within 0.01 % of the best known solution found when all degrees of freedom are used. The exception is when the inter-stage temperature is high (0.95 and 1.00). The reason for this is the fact that the refrigerant will be two-phase vapour-liquid after intercooling. In this case, the optimal intermediate pressure level was found to be higher than the one suggested by the heuristics. Compression (or rather pumping) of liquid is more efficient than compression of gas, hence the optimal pressure level is shifted to a higher level to

increase the liquid formation in the intercooler. The estimate given by $p_{M,OPT}$ generally provides solutions with slightly larger penalties in the power consumption compared to $p_{M,ENT}$.

Ideally, the problem should be formulated such that the intercooling was limited to avoid liquid formation (and fulfil the minimum superheating requirement). Since the intercooling temperature then would be a function of the design, iterations would be required when using the heuristic estimates $p_{M,OPT}$ and $p_{M,ENT}$. Even though the results are not given here, this has been tested and found to give only a small increase in the evaluation time for the process flowsheet.

Even though this could be accounted for by iteration, the estimates for the optimal intermediate pressure level may not provide the optimal solution when the intercooling is limited by the dew point temperature of the refrigerant. This is because the dew point temperature is a function of the pressure level (increasing with increasing pressure). Hence, by reducing the intermediate pressure level (beyond what is suggested by the estimate), a lower intercooling temperature and thereby also a lower suction temperature could be obtained and the total power consumption potentially reduced.

An alternative design solution when full intercooling results in formation of liquid would be to separate the liquid from the vapour and pump it to the required outlet pressure. Since pumping in general has a higher efficiency than compression, this may give a reduction in power consumption that can compensate the investment cost required. Anyway, the optimal intermediate pressure level will be altered.

In the cases where the refrigeration cycle operates on low temperature levels, the discharge temperature of the first compression stage may not reach the ambient temperature level even though all compression takes place in this stage. In this case, there is no intercooling between the compression stages irrespective of the intermediate pressure level. One may therefore assume that the power consumption would be independent of the intermediate pressure level. However, as was discussed in Chapter 3, the preheating effect will influence the operating conditions of the second compression stage.

As a consequence of the problem formulation with a constant isentropic efficiency in the compressors, the power consumption is therefore minimized when the compression is carried out in a single stage. Two effects influence the total power consumption when the intermediate pressure level changes. On the one hand, the preheating increases with increasing intermediate pressure level since the pressure ratio in the first compression stage increases. On the other hand, the pressure ratio in the second compression stage decreases and a smaller part of the total compression process will be

influenced by the preheating effect. The smallest power consumption is therefore found when the intermediate pressure is equal to the low or high pressure level. Maximum power consumption is obtained for an intermediate pressure level close to the geometric mean. For the case of perfect gas compression it would actually be exactly equal to the geometric mean.

In Table 8.6, it can be observed that the isentropic discharge temperatures are close to equal for the best solutions found for the different values of T_{NG2}, which confirms that the findings in Chapter 5 give a reasonable measure for optimal intermediate pressure levels also for real gases. This also confirms why $p_{M,ENT}$ gives performance very close to the best observed. Except for the cases where the intercooling is limited, the resulting isentropic discharge temperature is slightly higher for the first compression stage than for the second compression stage. This would suggest that $p_{M,ENT}$ slightly underestimates the optimal intermediate pressure level. The difference in isentropic discharge temperature decreases for decreasing values of the stage temperature T_{NG2}.

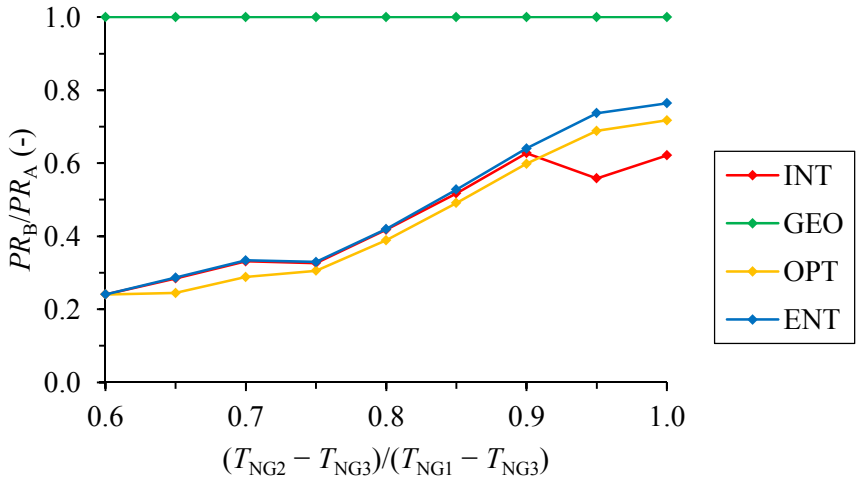

Figure 8.15. Ratio between the pressure ratios in the two compressors with constant isentropic efficiency.

As can be observed from Table 8.6, the first compression stage has a higher discharge temperature in the first compression stage than in the second stage, which would indicate that $p_{M,OPT}$ overestimates the optimal intermediate pressure. This is confirmed by the results given Fig. 8.15, where the ratio of the pressure ratio in COMP-B to the pressure ratio in COMP-A are plotted for the four different formulations for different values of the natural gas stage temperature. With $p_{M,OPT}$, the value is smaller than the optimal value (higher intermediate pressure), while with $p_{M,ENT}$, the value is slightly higher than the optimal. Exceptions are observed for the two cases where liquid is formed in the intercooler.

For solutions with the intermediate pressure given by $p_{M,GEO}$, the ratio of the pressure ratios is, of course, equal to unity. As can be observed in Fig. 8.15, the geometric mean therefore underestimates the optimal intermediate pressure level. Disregarding the two cases where full intercooling is not available without entering the two-phase region at the suggested intermediate pressure levels, the optimal ratio PR_B/PR_A generally decreases with decreasing natural gas stage temperature. This is as expected, since the difference between the suction temperatures of the two compressors increase.

The results obtained for the different heuristic guidelines for the optimal intermediate pressure level indicate that $p_{M,ENT}$ provides better performance than $p_{M,OPT}$. It may be that the latter could be improved by a better estimate for the average specific heat capacity of the refrigerant. The estimate based on entropy consideration does, however, seem to be simpler in nature and therefore more easily applicable in different situations.

Polytropic efficiency

As was discussed in Chapter 3, the optimal design of a refrigeration process will change if a constant polytropic efficiency is assumed for the compression process rather than a constant isentropic efficiency. This also applies to the optimal intermediate pressure level. In Table 8.7, results are given for optimization of the same sub-cooling cycle (Fig. 8.14) with a constant polytropic efficiency $\eta_p = 0.80$ for both compression stages. Otherwise, the conditions are the same as for the results obtained in Table 8.6.

Due to the fact that the isentropic efficiency of a compressor with constant polytropic efficiency decreases with increasing pressure ratio, the optimal intermediate pressure level is shifted closer to the geometric mean. Hence, the penalty associated with estimating the intermediate pressure level by the geometric mean is smaller than in the case of constant isentropic efficiency (2.18 % in the worst case).

The optimal intermediate pressure is overestimated by the estimates $p_{M,OPT}$ and $p_{M,ENT}$, leading to a penalty in power consumption. As for the case of constant isentropic efficiency, $p_{M,OPT}$ gives a higher intermediate pressure level than $p_{M,ENT}$. Therefore, the former leads to a slightly larger total compression power. Still, the power consumption is smaller than for the case of $p_{M,GEO}$.

With the exception of the two cases where complete intercooling between the compressors gives condensation of liquid, the penalty obtained with $p_{M,ENT}$ as the intermediate pressure level is smaller than 0.25 %. The ratio of the pressure ratios in the two compression stages is plotted as function of the stage temperature for the four different formulations in Fig. 8.16.

Table 8.7. Optimization results for sub-cooling cycle with two-stage compression for different formulations of the intermediate pressure level assuming constant polytropic efficiency.

		$(T_{NG2} - T_{NG3})/(T_{NG1} - T_{NG3})$								
Case	Unit	0.60	0.65	0.70	0.75	0.80	0.85	0.90	0.95	1.00
VAR										
p_M/p_L	-	3.67	3.42	3.25	3.92	3.15	2.65	2.38	2.92	2.74
p_H/p_M	-	1.10	1.21	1.30	1.54	1.51	1.53	1.61	1.73	1.80
$\eta_{s,B1}$	%	77.3	77.5	77.7	77.9	78.2	78.4	78.6	78.3	78.5
$\eta_{s,B2}$	%	79.8	79.6	79.5	79.3	79.3	79.3	79.2	79.3	79.3
$\dot{W}_{tot}$	kW	7 636	8 730	9 821	10 658	11 487	12 353	13 359	14 294	15 336
GEO										
p_M/p_L	-	1.99	1.99	2.00	2.26	2.22	2.02	1.98	2.09	2.16
p_H/p_M	-	1.99	1.99	2.00	2.26	2.22	2.02	1.98	2.09	2.16
$\eta_{s,B1}$	%	78.5	78.6	78.6	78.7	78.8	78.8	78.9	78.8	78.9
$\eta_{s,B2}$	%	78.6	78.7	78.7	78.8	78.8	78.9	78.9	78.8	78.8
$\dot{W}_{tot}$	kW	7 659	8 803	9 963	10 890	11 705	12 507	13 446	14 466	15 606
Penalty	%	0.30	0.83	1.44	2.18	1.90	1.25	0.65	1.20	1.77
OPT										
p_M/p_L	-	3.97	3.96	3.82	4.51	3.49	2.87	2.51	2.72	2.49
p_H/p_M	-	1.00	1.00	1.10	1.38	1.36	1.41	1.53	1.88	1.95
$\eta_{s,B1}$	%	77.1	77.3	77.4	77.7	78.0	78.3	78.5	78.4	78.6
$\eta_{s,B2}$	%	-	-	79.8	79.5	79.5	79.4	79.3	78.9	79.2
$\dot{W}_{tot}$	kW	7 651	8 793	9 875	10 677	11 506	12 367	13 367	14 348	15 481
Penalty	%	0.20	0.73	0.55	0.18	0.17	0.12	0.06	0.37	0.95
ENT										
p_M/p_L	-	3.95	3.80	3.57	4.33	3.36	2.77	2.43	2.69	2.52
p_H/p_M	-	1.00	1.09	1.20	1.43	1.41	1.46	1.58	1.97	2.03
$\eta_{s,B1}$	%	77.1	77.3	77.5	77.8	78.1	78.3	78.6	78.4	78.6
$\eta_{s,B2}$	%	-	79.8	79.7	79.4	79.4	79.4	79.2	78.8	79.1
$\dot{W}_{tot}$	kW	7 650	8 750	9 836	10 667	11 495	12 357	13 361	14 383	15 508
Penalty	%	0.19	0.24	0.15	0.08	0.07	0.04	0.01	0.62	1.13

As one would expect, the isentropic efficiency of the two compression stages is close to equal when the intermediate pressure level is given by the geometric mean. The slight differences are likely to be caused by the variation in thermodynamic properties throughout the compression process. As can be observed for the best known solutions obtained with the intermediate pressure level used as decision variable, the isentropic efficiency of both compressors are smaller than the isentropic efficiency of the compressors used to generate the results in Table 8.6. The power consumption is therefore higher than when a constant isentropic efficiency of 80 % was assumed. As expected the isentropic efficiency is highest for the compressor with the smallest pressure ratio.

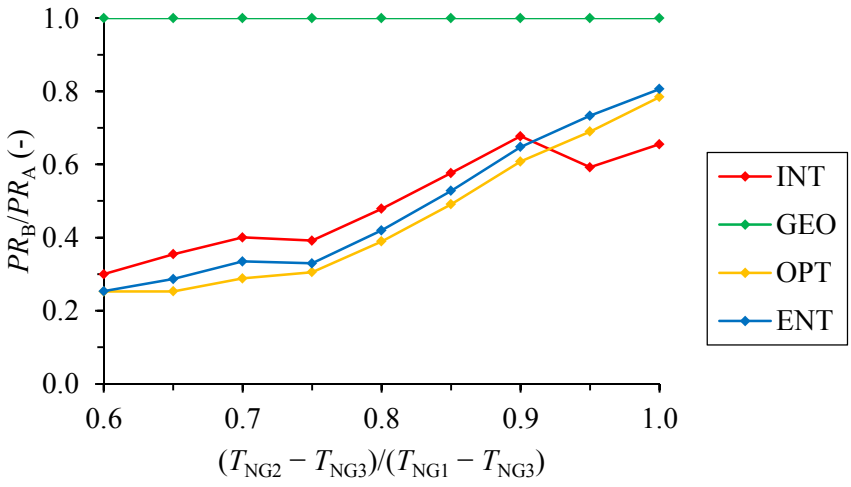

Figure 8.16. Ratio between the pressure ratios in the two compressors with constant polytropic efficiency.

As can be observed in Table 8.7, the solutions obtained using $p_{M,OPT}$ and $p_{M,ENT}$ for the intermediate pressure level have a lower isentropic efficiency for the first compression stage but higher for the second stage. Since the pressure ratio is larger in the first compression stage than in the second stage, the lower efficiency in the first compression stage has a larger influence on the overall compression power than the higher efficiency in the second stage.

Compared to the case of constant isentropic efficiency, the optimal intermediate pressure level is shifted to a smaller value to increase the isentropic efficiency of the compressor operating with the largest pressure ratio. This is also why the total pressure ratio (p_H/p_L) is smaller for the case of constant polytropic efficiency than for constant isentropic (in accordance with the results in Chapter 3). The optimal intermediate pressure level is given by the optimal trade-off between two opposing guidelines. On the one hand, the isentropic efficiency is maximized when the pressure ratios are similar for both stages. The effect of intercooling, on the other hand, is maximized when the pressure ratio of the first compression stage is higher.

In general, the penalty associated with the estimate given by $p_{M,ENT}$ increases with decreasing stage temperature. This is related to the fact that the ratio between the pressure ratios of the two compressors increase when the stage temperature decrease. With larger difference in the pressure ratios, the difference in isentropic efficiency also increases, as can be observed in Table 8.7. The shift from the estimated optimal intermediate pressure level towards the geometric mean is therefore larger. For the

smallest stage temperature tested, the penalty is smaller again, due to the fact that $p_{M,ENT}$ in this case gives a solution where the compression takes place in a single stage (the intermediate pressure level cannot be shifted any higher).

Comparison

In Fig. 8.17, the total power consumption of the refrigeration cycle is plotted as function of the intermediate pressure level for the case with $(T_{NG2} - T_{NG3})/(T_{NG1} - T_{NG3}) = 0.70$. Except for the intermediate pressure level, the decision variables were set equal to the optimal solution given in Tables 8.6 and 8.7, respectively. The power consumption is given relative to the power consumption of the best known solution for each case.

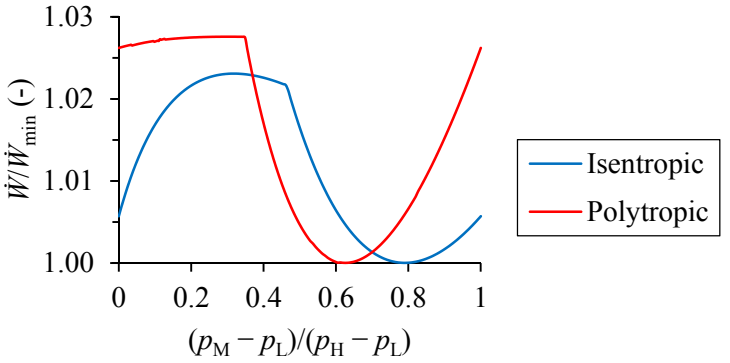

Figure 8.17. Total power consumption as function of intermediate pressure in two-stage compression.

A non-differentiable point is observed for the case of constant polytropic efficiency for $(p_M - p_L)/(p_H - p_L) \approx 0.35$, and for the case of constant isentropic efficiency for $(p_M - p_L)/(p_H - p_L) \approx 0.46$. For intermediate pressure levels smaller than these values, the discharge temperature of the first compressor is smaller than the ambient cooling temperature and there is therefore no cooling in between the two compressors. The point at which the compressor discharge temperature reaches the ambient cooling temperature is different for the two formulations due to the fact that the optimal solution is different and because the efficiency affects the compressor discharge temperature.

Due to the preheating effect (discussed in Chapter 3), the power consumption increases with increasing intermediate pressure level when the isentropic efficiency is constant and there is no intercooling. For the case of constant isentropic efficiency, the geometric mean actually provides the highest power consumption. The preheating effect continues to grow when the pressure is increased above the geometric mean, but the since the pressure ratio in the second compression stage decreases, the preheat will

affect a smaller part of the compression path. Hence, opposite to the intention, the total power consumption is maximized when the intermediate pressure level is given by the geometric mean when the isentropic efficiencies are constant and the discharge temperature of the first compression stage is smaller than the ambient cooling temperature.

From the definition of polytropic efficiency, one would expect that the total power consumption would be independent of the intermediate pressure level when the there is no cooling in between the compression stages. As can be observed from Fig. 8.17, below the non-differentiable point there is a small increase in the power consumption with increasing intermediate pressure. This is likely to be caused by variations in thermodynamic properties. In both cases (isentropic and polytropic), the power consumption is, of course, the same when the intermediate pressure level is equal to the low pressure level and the high pressure level.

8.3.3 Four-stage compression

In order to study the influence of estimating the optimal intermediate pressure levels on the optimization search performance, a case study was performed with four compression stages as illustrated in Fig. 8.18. This was done for the sub-cooling cycle of the two-stage process illustrated in Fig. 8.2 with $T'_{NG2} = 0.70$. Again, the isentropic efficiency of all compression stages was assumed constant $\eta_s = 0.80$. The intercoolers were operated such that the exit temperature was given by the smallest of the preceding compressor discharge temperature and the available external cooling temperature.

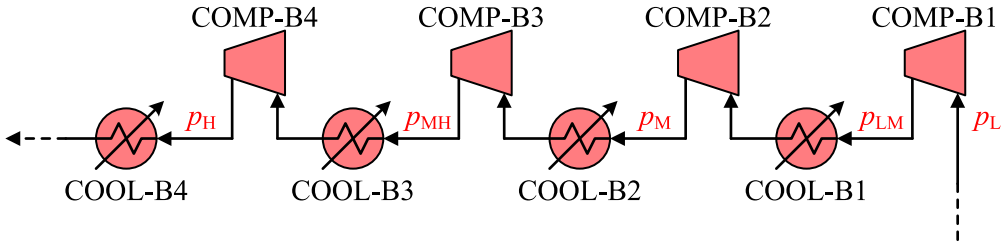

Figure 8.18. Four-stage compression with intercooling.

Five different formulations were compared. In the first approach all the intermediate pressure levels were used as decision variables. As previously discussed, this requires narrow variable bounds and therefore a priori knowledge of the approximate location of the optimal solution. In the second approach, the pressure ratios of the compression stages were used as decision variables, in addition to the low pressure level. In this case, the high pressure level depends on the four variables used for the pressure ratios.

The third approach was based on using the low and high pressure levels as variables and distributing the intermediate pressure levels within the interval given by these. For n compression stages this can be formulated as

$$p_{\mathrm{i}} = p_{\mathrm{i\text{-}1}} + x_{\mathrm{i}} \cdot \left(p_{\mathrm{H}} - p_{\mathrm{i\text{-}1}} \right) \qquad i = 2,...,n \,. \tag{8.14}$$

Here, $n - 1$ variables x_{i} bounded between zero and unity were used to distribute the intermediate pressure levels.

Using the geometric mean, the intermediate pressure levels could be expressed as

$$p_{\mathrm{i}} = p_{\mathrm{L}}^{(n-i)/n} \cdot p_{\mathrm{H}}^{(i-1)/n} \qquad i = 2,...,n \,. \tag{8.15}$$

The final approach used was based on the entropy considerations. The intermediate pressure levels would then be given as

$$p_{\mathrm{i}} = p_{\mathrm{ENT}}^{(n-i)/n} \cdot p_{\mathrm{H}}^{(i-1)/n} \qquad i = 2,...,n \,, \tag{8.16}$$

where

$$p_{\mathrm{ENT}} = \min \left\{ p\left(T_{\mathrm{cool}}, s_{\mathrm{in}} \right), p_{\mathrm{H}} \right\} . \tag{8.17}$$

This estimate is based on the assumption that the refrigerant would be cooled to the same ambient cooling temperature T_{cool} in between all the compression stages. One could also have taken into account the fact that a suction temperature in first stage higher than the ambient cooling temperature would give p_{ENT} smaller than p_{L}. Such a temperature would, however, also mean that the minimum temperature difference constraint would be violated in the hot end of the heat exchanger HX-B and the solutions would anyway be infeasible.

The best solutions obtained for formulations where the intermediate pressure levels are estimated by heuristics are compared with the best known solution with all degrees of freedom utilized in Table 8.8. As can be observed, the power consumption is comparable for the best solution obtained with all degrees of freedom used and the heuristics based on equal isentropic discharge temperatures. As expected, using the geometric mean to determine intermediate pressure levels give a higher power consumption. Compared to the best known solution, the pressure ratio is too small in the first compression stage and too large in the remaining three.

One may notice, however, that the values for the decision variables otherwise are quite close to the best known solution for this case. The results therefore indicate that the

geometric mean potentially could be used as an estimate in the initial phase of an optimization search, before switching to another formulation to refine the solution at a later stage. Overall, comparing the solution obtained using the proposed heuristics with best known solution indicate a very close resemblance, both with respect to variable values and objective function value.

Table 8.8. Best known solution for different constraint formulations with four-stage compression.

Variable	Unit	Variable	Geometric	Entropy
p_{L}	bar	1.000	1.000	1.000
PR_{B1}	-	4.821	1.779	4.789
PR_{B2}	-	1.274	1.779	1.271
PR_{B3}	-	1.268	1.779	1.271
PR_{B4}	-	1.261	1.779	1.271
$\dot{n}_{\mathrm{B,C1}}$	kmol/s	0.480	0.473	0.480
$\dot{n}_{\mathrm{B,C2}}$	kmol/s	0.511	0.510	0.512
$\dot{n}_{\mathrm{B,C3}}$	kmol/s	0.199	0.195	0.199
$\dot{n}_{\mathrm{B,nC4}}$	kmol/s	0.000	0.000	0.000
$\dot{n}_{\mathrm{B,iC4}}$	kmol/s	0.230	0.229	0.230
$\dot{n}_{\mathrm{B,N2}}$	kmol/s	0.066	0.066	0.066
$\dot{W}_{\mathrm{best}}$	kW	9 515	9 745	9 515

In Table 8.9, the performance of the different problem formulations are compared with respect to the number of successful runs and the number of evaluations required. One may notice that the number of evaluations refers to the total number of evaluations used in a given search, not the number of evaluations required to reach a given state. The success rate of each search has been evaluated with respect to the deviation of the final result from best known solution. 100 runs were performed for each formulation.

As can be observed, the success rates are fairly similar for the different formulations, with the exception of the formulation based on using all pressure levels as variables. One should, however, notice that the variable bounds for the pressure levels are narrower in this case. As expected, no solutions within 1.0 % of the best known is obtained when the geometric mean is used to specify the pressure levels.

Similar success rate is observed for the formulations based on pressure ratios, distribution of intermediate pressure levels and the heuristics based on entropy considerations when it comes to identification of solutions within 10 % or 100 % of the best known and the feasible region. The estimate based on entropy considerations did, however, provide slightly more solutions within 0.1 % and 1.0 % of the best known.

Table 8.9. Optimization search performance for different problem formulations with four-stage compression.

	Criteria					
Formulation	0.1 %	1.0 %	10 %	100 %	Feasible	Total
Pressure levels						
Success rate	37	40	47	47	47	100
Evaluations	1140	1262	1226	1226	1226	795
Pressure ratios						
Success rate	4	18	47	57	61	100
Evaluations	1565	2478	2633	2520	2369	1717
Distribution						
Success rate	7	23	51	54	57	100
Evaluations	1575	1601	1865	1791	1707	1036
Geometric						
Success rate	0	0	47	55	57	100
Evaluations	-	-	1456	1393	1369	785
Entropy						
Success rate	14	38	47	55	56	100
Evaluations	966	1432	1461	1352	1329	795

The main advantage of the formulations where the intermediate pressure levels are estimated based on heuristic rules is a reduction in the number of evaluations. Since derivatives are estimated by finite difference, more evaluations are required per iteration when the number of decision variables is higher. The search time per run depends on the computer load and variations in convergence properties in different search regions, but average time required per evaluation was found to be around 0.20-0.25 seconds (similar for the different formulations).

8.4 Conclusions

In this work, two approaches have been proposed for simplification of the search procedure for optimization of complex LNG process concepts. In the first approach, a strategy for sequential design of the different refrigeration cycles in a cascade process has been suggested, based on the characteristics of the process. The second measure suggested for simplification of the optimization search is based on reducing the number of decision variables in processes with multi-stage compression, by using accurate heuristics for intermediate pressure levels.

8.4.1 Optimization of cascade processes

The challenge associated with optimization of processes for liquefaction of natural gas increase with increasing complexity of the process flowsheet. With increasing complexity of the process, the success rate of the optimization approach used in this

search has been found to decrease. At the same time, both the number of evaluations required in each search and the simulation time increase.

The characteristics of cascade LNG processes (both with pure refrigerants and mixed refrigerants) enable the different vertical stages to be designed one by one for given load distribution (intermediate natural gas temperatures). Since the operating conditions of a vertical stage are independent of the configuration of stages operating at higher temperature levels, an approach where the different vertical stages are designed sequentially starting from the lowest temperature level has been proposed. This could be done in an inner loop, while the variables determining the load distribution are optimized in an outer loop.

Due to precooling of refrigerants, the configuration of a vertical stage has significant influence on the operating conditions of preceding stages. For this reason, case studies of a dual mixed-refrigerant process indicated that the formulation of the objective function is of considerable influence when the vertical stage are designed sequentially. Even though the overall objective is to minimize the total power consumption in the process, minimizing the power consumption in the sub-cooling cycle alone gives excessive cooling loads in the precooling cycle. The objective should therefore be to minimize the exergy supplied to the refrigeration cycle (or alternatively a weighted sum of different exergy inputs), which in addition to the compression power includes the exergy required to precool the refrigerant in preceding cycles.

The efficiency of the proposed strategy for optimization of cascade processes has not been tested. Hence, no conclusions can be made concerning its practical feasibility. Regardless, in the case that a feasible solution is required as starting point for an optimization search, sequential design starting from the lowest temperature level could be used to locate such an initial solution.

8.4.2 Multi-stage compression

Heuristics for estimation of optimal intermediate pressure levels in multi-stage compression with constant isentropic efficiencies have been proposed in order to reduce the number of degrees of freedom in optimization. Case studies of the low-temperature cycle in a dual mixed-refrigerant process proved inadequacy of the geometric mean as an estimate for the optimal intermediate pressure level when the suction temperatures of the different compression stages are different.

Based on the findings in Chapter 5, which concluded that the isentropic discharge temperature of the different compression stages should be equal to minimize the total power consumption, an estimate for the optimal intermediate pressure level have been proposed. For cases where there are no restrictions on the intercooling (no refrigerant

condensation), the design solutions obtained with the proposed heuristics gave results within 0.01 % of the best solution found when the intermediate pressure is used as a decision variable. Larger errors were observed when maximum intercooling would give liquid formation.

Since the optimization approach used in this work is dependent upon derivatives estimated by finite differences, the number of evaluations (process simulations) in each iteration of the optimization search increases with increasing number of variables. Hence, using heuristics for the intermediate pressure levels could give a reduction in the number of process evaluations required, with negligible loss in solution quality. For a case study with four-stage compression (three intermediate pressure levels), optimization using the heuristics based on equal isentropic discharge temperatures gave similar success rates but fewer evaluations, compared to formulations using decision variables to determine the intermediate pressure levels.

Even though the suggested approach may not give the optimal solution for all cases, the estimates may still be used in the initial phase of an optimization search in order to allocate interesting regions of the search space. More degrees of freedom can be introduced at a later stage in the optimization search in order to refine the solution.

Since the conditions are different, the proposed heuristic estimate does not provide the same solution quality when constant polytropic efficiency is assumed. In general the optimal intermediate pressure level is overestimated in this situation. For a case study, the solutions were still better than what is found using the geometric mean for the intermediate pressure levels. However, further development of the approach would be required in order to give an accurate estimate of the optimal intermediate pressure level also for polytropic compression.

8.5 References

Alabdulkarem A, Mortazavi A, Hwang Y, Radermacher R, Rogers P. Optimization of propane pre-cooled mixed refrigerant LNG plant. *Applied Thermal Engineering* 2011;31(6-7):1091-1098.

Aspelund A, Gundersen T, Myklebust J, Nowak MP, Tomasgard A. An optimization-simulation model for a simple LNG process. *Computers and Chemical Engineering* 2010;34(10):1606-1617.

Castillo L, Dahouk MM, Di Scipio S, Dorao CA. Conceptual analysis of the precooling stage for LNG processes. *Energy Conversion and Management* 2013;66:41-47.

Castillo L, Dorao CA. On the conceptual design of pre-cooling stage of LNG plants using propane or an ethane/propane mixture. *Energy Conversion and Management* 2013;65:140-146.

Hatcher P, Khalilpour R, Abbas A. Optimisation of LNG mixed-refrigerant processes considering operation and design objectives. *Computers and Chemical Engineering* 2012;41:123-133.

Hwang J-H, Ku N-K, Roh M-I, Lee K-Y. optimal design of liquefaction cycles of liquefied natural gas floating, production, storage, and offloading unit considering optimal synthesis. *Industrial and Engineering Chemistry Research* 2013a;52(15):5341-5356.

Hwang J-H, Roh M-I, Lee K-Y. Determination of the optimal operating conditions of the dual mixed refrigerant cycle for the LNG FPSO topside liquefaction process. *Computer and Chemical Engineering* 2013b;49:25-36.

Lee I, Tak K, Kwon H, Kim J, Ko D, Moon I. Design and optimization of a pure refrigerant cycle for natural gas liquefaction with subcooling. *Industrial and Engineering Chemistry Research* 2014;53(25):10397-10403.

Morin A, Wahl PE, Mølnvik M. Using evolutionary search to optimise the energy consumption for natural gas liquefaction. *Chemical Engineering Research and Desisgn* 2011;89(11):2428-2441.

Mortazavi A, Somers C, Alabdulkarem A, Hwang Y, Radermacher R. Enhancement of APCI cycle efficiency with absorption chillers. *Energy* 2010;35(9):3877-3882.

Mortazavi A, Somers C, Hwang Y, Radermacher R, Rodgers P, Al-Hashimi S. Performance enhancement of propane pre-cooled mixed refrigerant LNG plant. *Applied Energy* 2012;93:125-131.

Taleshbahrami H, Saffari H. Optimization of the C3MR Cycle with genetic algorithm. *Transactions of the Canadian Society for Mechanical Engineering* 2010;34(3-4):433-448.

Wang M, Khalilpour R, Abbas A. Operation optimization of propane precooled mixed refrigerant processes. *Journal of Natural Gas Science and Engineering* 2013;15:93-105.

Wang M, Zhang J, Xu Q. Optimal design and operation of a C3MR refrigeration system for natural gas liquefaction. *Computers and Chemical Engineering* 2012;39:84-95.

Wang M, Zhang J, Xu Q, Li K. Thermodynamic-analysis-based energy consumption minimization for natural gas liquefaction. *Industrial and Engineering Chemistry Research* 2011;50(22):12630-12640.

9 Conclusions and Future Work

The main objective of this work has been to make use of thermodynamic analysis and insight in LNG process optimization. A commercial process simulation tool, Aspen HYSYS®, has been used for process modelling, while the sequential quadratic programming algorithm NLPQLP has been used for optimization. Adaptive Simulated Annealing, a stochastic search method, has also been tested. Processes studied include single and dual mixed-refrigerant processes, single and dual nitrogen expander processes and simple and complex pure-refrigerant cascade processes.

In the following, the most important observations from the work are given, together with suggestions for future work. More detailed conclusions are given at the end of each chapter.

9.1 Conclusions

9.1.1 Literature review

A review of literature relevant to LNG process optimization was carried out in order to evaluate the current status of the field, which has received increased attention during the past decades. In the majority of the studies, local deterministic search methods (typically sequential quadratic programming), stochastic search methods (typically genetic algorithms) or hybrids of the two have been used. Use of global deterministic optimization has not been observed for process flowsheet optimization. Typically, commercial sequential modular simulators have been used to model the processes using cubic equations of state.

The majority of the studies on LNG process optimization have considered relatively simple process concepts such as single mixed-refrigerant processes and propane-precooled mixed-refrigerant processes. In recent years, studies concerned with dual mixed-refrigerant processes have also been published. There are, however, very few studies available on optimization of more complex process concepts.

9.1.2 Problem characteristics

Optimization of natural gas liquefaction processes has been found to be a challenging non-convex optimization problem. In order to get familiar with the challenges in LNG process optimization, sensitivity analyses and parameter studies were performed for a single mixed-refrigerant process. Numerical noise (non-differentiable points) related to phase change for different refrigerant streams and changes in heat exchanger temperature profiles was found to be present close to the best known solution of the optimization problem. Hence, the optimization search must be able to handle the challenges posed by this behaviour.

Confinement of variable bounds has been found to improve the performance of the optimization search. Parameter studies did, however, reveal that changes in process parameters and operating conditions give considerable changes in the best known solution. This would indicate that the prevailing conditions should be taken into account when setting the variable bounds for optimization.

9.1.3 Optimization search methods

Multi-start local optimization by use of a sequential quadratic programming algorithm from randomly generated starting points was found to provide a high success rate for the single mixed-refrigerant process, even with quite wide variable bounds. These results indicate that the non-convexities of the optimization problem may be less influential for such simple process concepts. For more complex process concepts, however, the success rate of this search method was found to be significantly reduced.

An alternative optimization approach using an implementation of the stochastic search method Adaptive Simulated Annealing was also tested. Since the optimal solution is expected to be located on or close to the boundary of the feasible region, constraint handling methods based on process characteristics were proposed for better improved search performance near the feasible boundary. These were compared with conventional static penalty functions for optimization of a single mixed-refrigerant process.

The results indicated that the stochastic search method was able to identify a solution close to the best obtained with the local search method. Compared to the standard settings of the algorithm, the annealing schedule was reduced to improve the search performance. For the case studied, the choice of constraint handling method was found to be of little importance.

Even though similar solutions were obtained, the computational time required for the stochastic search was found to be significantly longer than for the multi-start local deterministic search. Stochastic search methods could, however, serve as an interesting

alternative for optimization of complex process concepts, for which low performance is observed for local search methods. This should, however, be done in a hybrid approach. Due to their random nature, stochastic search methods are not suitable for refinement of local solutions. In a hybrid approach, stochastic search methods should be used to identify interesting regions of the search space, while local deterministic search methods should be used to refine the objective in these regions. This was not tested in this work.

9.1.4 Process modelling

Energy efficient LNG processes are operated with small driving forces in the heat transfer process. Hence, in order to ensure practical feasibility of the process models used in design and optimization, rigorous thermodynamic models should be used. Rigorous process models do, however, lead to more complex optimization problems. The choice of thermodynamic models is therefore a trade-off between accuracy and complexity. A simplified process model may be easier to optimize, but the optimal solution may not necessarily correspond to the optimal solution in practice.

In order to study the influence of the thermodynamic model, nitrogen expander processes were optimized using both a simplified and a rigorous process model. Nitrogen expander processes were chosen for this study due to the refrigerants near-ideal behaviour. A single and a dual expander process were optimized for different values of the minimum temperature difference and the isentropic efficiency of compressors and expanders.

The simplified process model was modelled assuming perfect gas behaviour (ideal gas with constant specific heat capacity) for the refrigerant and constant specific heat for the natural gas stream. Based on thermodynamic analysis, the number of degrees of freedom was reduced to one. For a single expander process, the optimization problem was solved analytically. The rigorous process model was simulated using the Soave-Redlich-Kwong equation of state and optimized using the previously discussed approach based on multi-start local deterministic search.

For the single expander process, two local solutions were observed for the rigorous process model. One of these was found to be in close agreement with the optimal solution of the simplified model. In the majority of the cases studied, however, the other local solution was found to provide smaller net power consumption. Taking into account the non-ideal behaviour of nitrogen at higher pressure levels, this solution provided a reduction in the net power consumption compared to the simplified model.

For the dual expander process, little agreement was found between the optimization results obtained for the two process models. In this case, the assumption of constant

heat capacity for the natural gas was found to influence the accuracy of the simplified process model. The performance of the simplified model could potentially be improved by modelling the natural gas cooling curve as a piecewise linear function, dividing it into intervals with constant heat capacity.

For both process models, significant savings in energy used were observed when the two-stage compression was introduced. Even larger savings were found for the dual expander process. In conclusion, the simplified process model was found not to provide accurate estimates for the rigorous process model.

9.1.5 Multi-stage compression with intercooling

Studies on multi-stage compression with intercooling indicated that the widely used estimate based on the geometric mean (uniform pressure ratios) does not give optimal performance when the suction temperatures of the different compression stages are different. An expression was derived for determination of the optimal intermediate pressure in two-stage compression of a perfect gas with constant isentropic efficiency and different suction temperatures.

The results indicated that the pressure ratio should be higher in compression stages with low suction temperatures. Rather than uniform pressure ratios, the optimal intermediate pressure levels were found to be characterized by uniform isentropic discharge temperatures (discharge temperature in the case of fully isentropic compression). For the special case of uniform suction temperatures, this was found to be equivalent to the geometric mean.

Based on the results found for perfect gas compression, a heuristic rule was proposed for the optimal intermediate pressure levels in real-gas compression. For optimization of a single mixed-refrigerant process, this estimate was found to provide negligible penalty in the power consumption compared to optimization with the intermediate pressure levels used as decision variables. Hence, the number of degrees of freedom and thereby also the search time could potentially be reduced by applying this heuristic rule in optimization of complex process concepts with several instances of multi-stage compression (with the optimization methods used in this work, one flowsheet evaluation must be performed for each variable in each iteration in order to estimate the derivatives).

The proposed heuristic rule was, however, found not to provide accurate estimates for the optimal intermediate pressure levels in cases where the intercooling is limited by the requirement of superheated vapour in all compressor suction streams. In addition, the proposed heuristic rule does not apply when constant polytropic efficiency is assumed for the compressors.

9.1.6 Decision variables and bounds

Optimization studies of pure-refrigerant cascade processes were used to illustrate the influence of choice of decision variables and variable bounds. Based on thermodynamic analysis, a set of easily bounded decision variables was proposed. Compared to a fairly intuitive choice of decision variables, considerable improvement in optimization search performance was observed.

Both for a simple and a complex cascade process, minimum total power consumption was observed with no refrigerant sub-cooling, maximum utilization of refrigerant superheating and temperature differences in the cold end of all heat exchangers equal to the minimum required.

Exergy analyses of the processes illustrated the fact that the design solution that provides the minimum power consumption of the overall process not necessarily corresponds to the solution that provides the smallest compression power in the individual stages. This is related to the fact that the refrigerant is precooled in preceding vertical stages (cycles operating at higher temperature). Exergy is supplied to the refrigerant not only through the compressor but also through this sub-ambient cooling.

9.1.7 Complex process optimization

The performance of the optimization approach based on multi-start local deterministic search was found to decrease drastically with increasing process complexity. Narrow variables bounds, which would require detailed insight in the process characteristics, were found to be required in order to increase the success rate for optimization of mixed-refrigerant cascade processes with two or three vertical stages. As an alternative to simultaneous optimization of all decision variables, the characteristics of cascade refrigeration processes indicate that the different cycles of the process could be optimized sequentially.

For a given load distribution between the refrigeration cycles, cascade process are connected such that the operating conditions of each vertical stage are independent of the preceding stages (refrigeration cycles operating at higher temperature). Hence, the different vertical stages could be optimized sequentially starting with the cycle operating at lowest temperature level. In accordance with the results obtained for the pure-refrigerant cascade process, the interaction between the vertical stages should, however, be taken into account. Even though the objective was to minimize the overall power consumption, the results indicated that when optimizing the individual refrigeration cycles, the irreversibilities associated with the cycle should be minimized rather than the compression power.

Instead of optimizing the complete cascade process simultaneously, series of simpler optimization problems could be solved in a nested approach. In an outer loop, variables describing the load distribution between the vertical stages in the cascade are optimized, while the vertical stages are optimized sequentially (taking the interaction into account) in an inner loop. This could be used to narrow the variables bounds within which the optimal solution is expected to be found and provide a starting point for simultaneous optimization of the overall process.

The suggested approach has not been implemented in this work, but the principle was illustrated for a case study where a dual mixed-refrigerant process was optimized. For the given case study, a solution close to the best known was obtained. In addition, the results indicate that the total power consumption may be close to a unimodal function of the variable used in the outer loop (load distribution).

9.1.8 Constraint formulation

Due to lack of cost data, the optimization objective for conceptual process design is often simplified. In LNG process optimization, the objective is typically taken to be minimization of power consumption, which is of major influence for the operating cost of the process. Constraints are usually added to the optimization problem to account for the investment cost. In LNG processes, energy use and heat exchanger investment cost are conflicting, since reduced energy use typically results in increased heat exchanger size. Similar to heat exchanger network design, a minimum temperature difference in the heat exchangers is often used as a trade-off parameter in order to limit the heat exchanger size.

This constraint was, however, found to give non-optimal utilization of the heat exchanger area. In order to minimize the irreversibilities in a heat exchanger with fixed size, the temperature driving forces should be distributed such that the temperature difference between the composite curves is a linear function of the temperature at which the heat is transferred. Optimal distribution of driving forces was found to be of increasing influence when the temperature span of the cooling load increases and/or the temperature level is reduced, which is the case for natural gas liquefaction.

Four different constraint formulations were compared for minimization of the power consumption in a single mixed-refrigerant process subject to a given heat exchanger size. Significant savings in power consumption, increasing with decreasing size of the heat exchanger, were identified when a maximum heat exchanger conductance was used as constraint rather than a minimum temperature difference. The inadequacy of the minimum temperature difference constraint was found to be related to non-optimal distribution of driving forces with respect to temperature level, non-optimal adaption to

the non-linear temperature-enthalpy relations of the composite curves, and non-optimal trade-off between refrigeration flow rate and pressure ratio.

9.1.9 Summary

The main findings of this work are related to the impact of the problem formulation in LNG process optimization. Based on thermodynamic insight and analysis, potential improvements in choice of decision variables and bounds, formulation of optimization objective and formulation of constraints have been proposed. Combined with improvements in optimization methods, these findings could lead to more energy efficient, environmentally friendly and cost effective LNG processes.

9.2 Future work

In this work, only the refrigeration process has been considered, and all natural gas pre-treatment and conditioning have been assumed done prior to liquefaction. Process integration within the LNG plant may enable savings in energy use beyond what can be achieved through optimization of the liquefaction process alone. Of particular interest is integrated heavy hydrocarbon extraction. Since this complicates the optimization problem, it has received little attention in the literature up until now.

This work has been concerned with minimization of power consumption subject to limitations in heat exchanger size (measured through a minimum temperature difference or a maximum heat exchanger conductance). In floating LNG operations, objectives other than minimization of cost are also of importance. In order to account for properties such as environmental impact, safety and compactness, different objectives should be translated to a common measure (cost) or the optimization problem should be formulated with multiple objectives.

The simplified heat exchanger models used in this work are based entirely on energy balances. These do, however, not consider variations in heat transfer properties and pressure drop. All hot and cold streams, respectively, are assumed to follow the same temperature profile, which is likely not to be obtainable in practical design. Hence, by introduction of heat exchanger models taking these effects into account, more accurate process models can be obtained. The complexity of the optimization problem would, of course, also increase.

The heuristics for optimal intermediate pressure levels proposed in this work do not apply when constant polytropic efficiencies are assumed. Nor are the estimates accurate when the intercooling between compressors is limited by the superheating constraint. Hence, more work should be put into these estimates in order to make them applicable for a wider range of cases.

In this work, only local deterministic optimization methods and stochastic search methods have been applied. Even though consistency in the results obtained suggests that global optimal solutions are obtained, no guarantees can be made. By use of global deterministic optimization methods this could be obtained. Still, the problem formulation is of significant importance for the performance of such methods. Further development of the ideas proposed in this work could perhaps lead to improved problem formulations for global optimization of liquefaction processes for natural gas.

In order to be applied, the ideas proposed for sequential optimization of cascade refrigeration processes should be further developed and implemented in a simulation-optimization framework. The underlying principles of interaction between the different cycles in a cascade may also apply to other processes, such as other low-temperature refrigeration systems and distillation.